THE JOURNAL
OF
CHEMICAL PHYSICS

VOLUME 19, NUMBER 3 MARCH, 1951

Spectroscopic Moment: A Parameter of Substituent Groups Determining Aromatic Ultraviolet Intensities

JOHN R. PLATT
Physics Department, University of Chicago, Chicago, Illinois
(Received October 31, 1950)

By the theory of Sklar and Förster, the added intensity produced in the benzene 2600A transition by monosubstitution is proportional to the square of a transition moment or "spectroscopic moment" induced by the substituent. The sign of the moment may be positive or negative. On disubstitution, *para* intensities are greater than *meta* and *ortho* if both signs are the same, less if they are opposite. The theory is used with available data to determine the relative spectroscopic moment for 25 different substituents. This moment is closely related to the "mesomeric moment" and to directing power, but the correlation is not perfect.

The theory is extended to account for intensity changes in the weak long-wavelength transitions ($^1A-{}^1L_b$) of derivatives of other cata-condensed ring systems, such as naphthalene, phenanthrene, 1,2-benzanthracene, etc. The increases of intensity produced by substituents, and their spectroscopic moments, appear to be almost identical with those found in benzene.

INTRODUCTION

SKLAR showed how to predict the intensities in the weak 2600A transitions of polysubstituted benzene derivatives from the intensities in the monosubstituted compounds.[1] He accounted quantitatively for the intensities in all the methylbenzenes, all the chlorobenzenes, and in the methyl benzonitriles. Förster later arrived at essentially the same theory, apparently independently, and went on to predict wavelength shifts in these transitions as well.[2] He applied his predictions to the chlorobenzenes in detail.

According to the results of these authors, the intensity of the 2600A transition in a benzene derivative can be divided into two parts. One part is attributed to vibrational interaction with stronger transitions at higher energies. This part is taken as approximately equal to the intensity in benzene itself, where the 2600A transition is symmetry forbidden and would have no dipole intensity in the absence of vibrations.

The second part of the intensity is that which concerns us here. It is attributed to a transition moment, "migration moment" (Sklar), or "spectroscopic moment" (as we shall call it), induced in the ring by the presence of any substituent which destroys the symmetry. The purpose of the present paper is not to predict the intensity, as Sklar and Förster did, but rather to turn the theory around, applying it to the available intensity data in order to determine the spectroscopic moment of different substituents, and to examine whether these moments are indeed correlated with the directing effects of these substituents, as Sklar assumed.

SUMMARY OF THEORY

The top part of Fig. 1(a) is taken from an earlier paper.[3] It shows the "polarization diagram" for the 2600A transition in benzene. This transition is presumed to be of type $^1A_{1g}-{}^1B_{2u}$, in the usual symmetry notation. The polarization diagram is also shown for the corresponding weak transition in naphthalene. This is of type $^1A-{}^1L_b$ in the notation of reference 3.

These diagrams give the simplest classical distribution of charge having the necessary symmetry characteristics of the total upper state wave function and having the number of nodes required for this wave function when configuration interaction is taken into account. Since the ground-state wave function is totally symmetrical, these are also diagrams of the oscillating classical charge corresponding to the transition, at one instant of the oscillation. The dipole moment of these charge distributions, properly normalized, is roughly

[1] A. L. Sklar, J. Chem. Phys. **10**, 135 (1942); Revs. Modern Phys. **14**, 232 (1942).
[2] Th. Förster, Z. Naturforsch. **2a**, 149 (1947).
[3] J. R. Platt, J. Chem. Phys. **17**, 484 (1949).

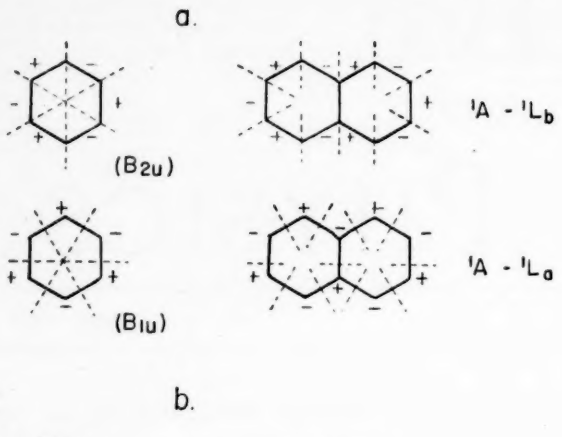

FIG. 1. (a) Equivalent distribution of oscillating classical charge in $^1A-^1L_b$ and $^1A-^1L_a$ transitions. (b) Vectorial contribution to the transition moment produced by substituents at each position.

proportional to the transition moment integral. It is seen to vanish exactly for benzene and approximately for naphthalene in the absence of vibrational distortion.

Polarization diagrams for some other cata-condensed ring systems may be found in reference 3. With the help of these diagrams, the Sklar-Förster theory may be extended to derivatives of these other aromatics in the same way that it will be extended in the present paper to the naphthalenes.

A local perturbation by a substituent will enhance or reduce some of the oscillating charges in the polarization diagram in an unsymmetrical way. This may give rise to a resultant finite transition moment vector. If the charges are enhanced near the substituent, and if the vector direction is taken as from + to −, the moment vectors induced by a given substituent at different positions are as shown at the top of Fig. 1(b) for the instant of oscillation depicted in Fig. 1(a). If the charges are reduced near the substituent, the direction of the vectors will be reversed. The sign of a moment may thus be positive or negative with respect to the sign of the moment of some particular substituent chosen as positive for reference.

For polysubstitution, in first approximation, the sum of the vectors from each substituent will give the resultant transition moment vector. Resultants are shown in Fig. 2 for disubstitution with two different substituents, (a) when both moments have the same sign, and (b) when they have opposite signs. In the first case, the *para* moment is greater, in the second case it is less than the other two moments

The induced intensity in the transition will be proportional to the square of the transition moment integral.

$$I-I_0=Km^2. \tag{1}$$

For monosubstitution, then, the square root of the intensity increment (above the unsubstituted intensity) will be proportional to the spectroscopic moment, m. For disubstitution, as seen from Fig. 2,

$$I-I_0=K(m_a^2+m_b^2+2m_am_b), \quad (para) \tag{2}$$

$$=K(m_a^2+m_b^2-m_am_b). \quad (ortho,\ meta) \tag{3}$$

In Eqs. (1)–(3), I_0 is the vibrational intensity, approximately the intensity of benzene itself; I is the intensity in the derivative; m, m_a, and m_b are the moments of the substituents separately; and K is a proportionality factor. For disubstitution, two intensity values, the *para* and the *meta* (or *ortho*), suffice to determine the relative moments, including sign, of both substituents. They determine two independent values of the moment if the two substituents are the same. For polysubstitution, the corresponding formulas may be easily obtained from a vector diagram. Diagrams for certain AB_2 substitutions are shown in Fig. 3.

One of the triumphs of the theory, as pointed out by Sklar, is that it predicts zero moment for 1,2,3-trisubstitution by the same substituent, in spite of the lack of symmetry. Intensities about as low as that of benzene itself are indeed observed in these tri-chloro and tri-methyl compounds. Similar zero moments should be observed in many other unsymmetrical trisubstituted aromatics, if the extension of these arguments to the larger ring systems given here is valid. Data seem to be available only for 1,2,8-trimethyl phenanthrene, where the expected low intensity is found (Table II, below).

Other Transitions

The lower parts of Figs. 1(a) and 1(b) show the polarization diagram and the moment vectors for the other forbidden transition in benzene at 2100A. This transition is assumed to be $^1A_{1g}-^1B_{1u}$. The diagram and vectors for the corresponding transition in naphthalene, $^1A-^1L_a$, are also shown. The diagrams may be easily drawn for $^1A-^1L_a$ in the other cata-condensed ring systems.

For the instants of oscillation depicted in Fig. 1(a),

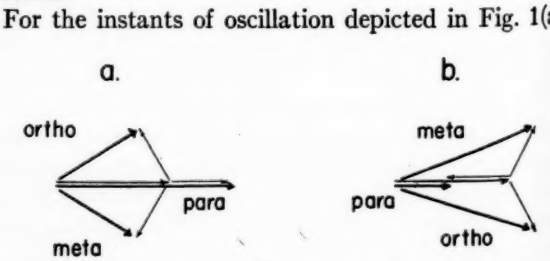

FIG. 2. Resultant transition moments for two different substituents with separate transition moments (a) of the same sign; (b) of opposite signs.

these ^1L_a moment vectors are all rotated 90 degrees clockwise from the ^1L_b vectors. Except for this rotation, the vector diagrams for polysubstitution in ^1L_a will be identical with those for ^1L_b. As a result, it is not possible, from examination of the intensities under different substitutions, to distinguish the transitions with the $^1B_{1u}(^1L_a)$ and the $^1B_{2u}(^1L_b)$ upper states in benzene or the other aromatics. This intensity data is therefore of no help in the current debates over classification of some of these transitions.

In spite of this expected similarity in behavior between the 2600A and the 2100A transitions, the latter transitions and their analogs in the other aromatics will not be discussed here. For benzene the available data on these transitions are less abundant. For all the aromatics, these transitions are so strong that the intensity variations under substitution are relatively small. These variations may be due as much to changes in the vibrational contributions to the intensity under substitution as to the induced transition moments. It seemed better in a first examination of spectroscopic moments to confine attention to the relatively weak 2600A bands where the relatively large intensity changes permit accurate determination of the moments. Later, it may be instructive to compare these with the moments from the other transitions, if they can be evaluated.

Wavelength Shifts

Förster showed that the wavelength shift of the 2600A transition under polysubstitution was proportional to the intensity increment plus another term involving an additional parameter.[4] No doubt the shift of the 2100A transition would follow a similar formula. These shifts will not be treated here because of the complications introduced by the second parameter. Again it will be instructive later to compare this parameter with the moments determined from intensity changes.

CHOICE AND TREATMENT OF DATA

Only substituents with relatively weak effects on the transitions are discussed here, since we are dealing with first-order perturbation theory. The effects are weak (a) if the transition is close enough in position to the benzene 2600A transition (or its analog in the other ring systems) to be certainly related, and (b) if the intensity is still small compared to that of the allowed transitions (ϵ_{max} of 15,000 or more). This rule permits inclusion of a surprising number of double-bonded substituents, and even permits treatment of the aza nitrogen atom in pyridine as a perturbation of the same type. It excludes such strong substituents as $-NH_2$ and $-NO_2$; these may be examined later.

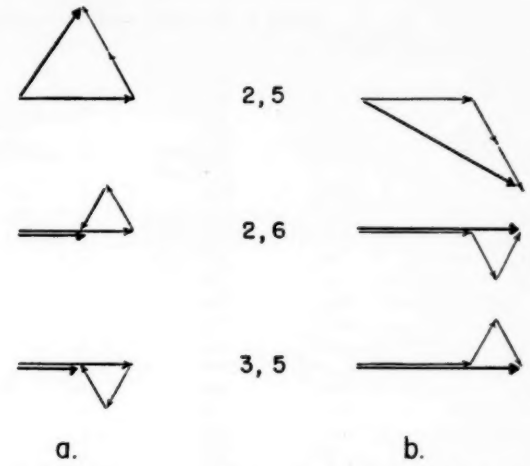

FIG. 3. Transition moments for pyridine dihalides if halogen and aza moments are (a) of same sign; (b) of opposite signs.

The intensity data used for the determination of the spectroscopic moments are shown in Table I for benzenes and in Table II for the larger cata-condensed aromatics and for pyrenes. (The pyrene data were included because there is some reason to believe that the weak long-wavelength transition of pyrene may be similar in its properties to the $^1A-{}^1L_b$ transitions in the cata-condensed ring systems.[3]) The references on each compound are not exhaustive, as the aim was only to get sufficient data to establish the spectroscopic moment.

For the same reason, no poly-substituted benzenes are included in Table I except for the dihalopyridines, which are needed to determine the signs of the Br and I moments. Sklar and Förster have treated adequately the poly-substituted compounds; and probably, these compounds are less reliable for our purpose of determining the moments of substituents, since unknown second-order and *ortho* effects may come in to complicate the simple theory.

Molar extinction values are given in the tables instead of oscillator strengths because they were easier to obtain. Smooth curves were drawn by eye through the extinction curves in the literature so as to average out the vibrational structure. The maximum extinctions so obtained, $\epsilon_{max}(sm)$, are good measures of the transition intensities and are listed in Table I. They would be exactly proportional to the oscillator strengths, f, if the smoothed curve had the same shape and half-width in all compounds. They are found to be almost proportional, as shown by comparison with a list of six f-values of simple benzene derivatives given by Sponer and

[4] H. Conrad-Billroth, in Z. physik. Chem. **B25**, 139 (1934); **B33**, 133 (1936); and other papers, devised some empirical vector rules for predicting wavelength shifts in benzenes, naphthalenes, and anthracenes. From monosubstitution data, he obtained a quantity ("Q^1" in his notation) which was analogous to our spectroscopic moment, and which was apparently correlated with the dipole moment. However, he did not understand the full importance of the signs. His rules for disubstitution have no theoretical foundation, and they fail when the signs of the moments are opposite.

Similar remarks apply to the qualitative results of H. Schüler, Z. Naturforsch. **3a**, 313 (1948); but here additional problems arise in the assignments and in the appearance or concealment of certain transitions.

TABLE I. Smoothed peak extinctions of 2600A transitions of benzene derivatives.

Subs.	Pos.	$\epsilon_{max}(sm)$*	Ref.†
none		*110*(205)	a, b, c, d, e
F		*670*	f
Cl		*180*(190)	a, d, e, f, g
Br		*175*(190)	a, f
I		*670*	f
OH		*1320*(1450)	a, d, e, h
OCH_3		1650(1480)	a, d
CH_3		*205*(225)	a, b
C_2H_5		*180*	i, j
$i-C_3H_7$		*170*	i, j
$t-C_4H_9$		*150*	i, j
CH_2F		*190*	f
CHF_2		*240*	f
CF_3		*360*	f, k
CH_2Cl		*190*	f
$CHCl_2$		*305*	f
CCl_3		*440*	f
$CHBr_2$		*ca 800*	f
CBr_3		*ca 1260*	f
CN		*490*(1000)	a, l, m
NC		190	m
COOH		*990*(970)	a, n, o
(N)		*1800*(1800)	p, q, r, s
SO_2NH_2		(740)	a
F, CH_3	*o*	660	k
	m	500	k
	p	750	k
F, CF_3	*m*	1020	k
	p	160	k
Cl, Cl	*o*	250	c, d
	m	250	c, d
	p	400	c, d
Cl, OH	*o*	2100	d
	p	1950(1600)	a, d
Cl, CH_3	*o*	*280*	d, g
	m	*240*	d, g
	p	*390*	d, g
Cl, CN	*o*	970	m
	m	760	m
	p	380(820)	a, m
Cl, NC	*o*	500	m
	m	440	m
	p	300	m
Cl, COOH	*m*	(1080)	a
OH, OH	*o*	2000	e, t
	m	1500	e, t
	p	2300	e, t
OH, CH_3	*o*	1800	d
	m	1600	d
	p	1950 *1840*	d, u
OH, $t-C_4H_9$	*p*	*1680*	v
OH, COOH	*o*	3700	w
	m	2600(2500)	a, w
	p	*ca* 2000	w
OCH_3, OCH_3	*o*	2450	d
	m	2200	d
	p	3000	d
CH_3CH_3	*o*	*235*	b, d, j
	m	*230*	b, d, j
	p	*400*	b, d, j
CH_3, $t-C_4H_9$	*m*	*220*(300)	a, x
	p	*310*	x
CH_3, CN	*o*	*1000*	l, m
	m	*830*(1280)	a, l
	p	*360*(750)	a, l, m
CH_3, NC	*o*	950	m
	p	245	m
CH_3, SO_2NH_2	*p*	(540)	a
CH_3, SO_3H	*p*	*1200*	z
COOH, COOH	*m*	(950)	a
CH_3, (N)	2	*2400*	p, y
(N), COOH	3	*4200*(2500)	r
(N), (N)	1, 2	690	aa
	1, 3	(2350)	aa
	1, 4	6350	aa
(N), Cl	2	2350	s
	3	2350‡	s
(N), Br	2	2200‡	s
	3	1900§	s
(N), I	2	3500	s
	3	3700	s
(N), Cl, Cl	2, 5	2900	s
	2, 6	4400	s
(N), Br, Br	2, 5	3100	s
	2, 6	4800	s
	3, 5	2900	s
(N), I, I	2, 5	3600	s

* Italicized figures are from API data; bracketed, for polar solvents (usually water).

† Abbreviations used in references:

API—Catalog of Ultraviolet Spectrograms (American Petroleum Institute Research Project 44, National Bureau of Standards, 1945–1950). The name of the contributing laboratory is given with each reference.

ICT—V. Henri, *Ultraviolet Spectra of Organic Compounds*, ICT (McGraw-Hill Book Company, Inc., New York, 1929), Vol. V, p. 359.

‡ Beer's law violated.

§ Uncertain.

[a] L. Doub and J. M. Vandenbelt, J. Am. Chem. Soc. **69**, 2714 (1947); **71**, 2414 (1949).

[b] API 40, 42–5 (Shell Development Company).

[c] H. Conrad-Billroth, Z. physik Chem. **B19**, 76 (1932).

[d] K. L. Wolf and W. Herold, Z. physik Chem. **B13**, 201 (1931).

[e] ICT 1, 5, 7.

[f] API 296–308 (Duke University).

[g] API 115–8 (California Research Corporation).

[h] API 99 (California Research Corporation).

[i] API 6, 20, 22 (Ethyl Corporation).

[j] API 54–7, 69, 70 (Texas Company).

[k] C. H. Miller and H. W. Thompson, J. Chem. Phys. **17**, 845 (1949).

[l] API 227–30 (Socony-Vacuum Laboratory).

[m] K. L. Wolf and O. Strasser, Z. physik Chem. **B21**, 389 (1933).

[n] ICT 27.

[o] API 354 (Shell Development Company).

[p] API 34–7 (Union Oil Company).

[q] API 108, 110 (California Research Corporation).

[r] ICT 47.

[s] C. W. F. Spiers and J. P. Wibaut, Rec. trav. Chim. **56**, 573 (1937).

[t] Kiss, Molnar, and Sandorfy, Bull. soc. chim. France, 275 (1949).

[u] API 322 (Shell Development Company).

[v] API 267 (Gulf Research and Development Company).

[w] ICT 13.

[x] API 196–7, 276–7 (National Advisory Committee for Aeronautics).

[y] API 213 (Mellon Institute of Industrial Research).

[z] API 114 (California Research Corporation).

[aa] F. Halverson and R. C. Hirt, J. Chem. Phys. **17**, 1165(L) (1949).

Lowe,[5] which fit the equation

$$f = 1.5 \times 10^{-5}\, \epsilon_{max}(sm), \qquad (4)$$

within about 20 percent.

The $\epsilon_{max}(sm)$ for the compounds of Table II were hard to determine accurately because of the interference of nearby stronger transitions. Instead, $\epsilon_{1st\ pk}(sm)$, the value of the smoothed curve at the position of the first vibrational peak, is tabulated there. The values are more uncertain than those of Table I and become unreliable as measures of the transition intensity if the vibrational envelope changes its shape markedly. Some of the data of Table II were available only from tables of ϵ_{max} in the literature. These values were corrected by a constant factor to conform as well as possible to the smoothed-curve values of the rest of the table.

The data in Tables I and II are taken from extinction curves in nonpolar solvents as far as possible. Some data from water and alcohol solutions are included

[5] H. Sponer and D. S. Lowe, J. Opt. Soc. Am. **39**, 840 (1949).

TABLE II. Smoothed extinctions of first ^1L_b vibrational peak in derivatives of larger ring systems.

Subs.	Pos.	$\epsilon_{1st\ pk}(sm)$	Ref.**
	Naphthalenes		
none		*150*(140)	bb, cc, dd, ee
Br	1	*ca* 165	dd
	2	200	dd
OH	1	*1500*	dd, ff
	2	*1430*	dd, ff
CH_3	1	*240*	bb, dd
	2	*235*	bb, cc, dd, gg
CN	1	1400	dd
	2	700	dd
COOH	2	1800	dd
(N)	1	2000(1600)	hh, dd
	2	*1700*(2000)	ii, dd
Cl, Cl	1, 2	220	jj
	1, 3	320	jj
	1, 4	570	jj
	1, 5	500	jj
	1, 6	200	jj
	1, 7	280	jj
	1, 8	900	jj
	2, 3	350	jj
	2, 6	500	jj
	2, 7	250	jj
CH_3, CH_3	1, 2	*405*	kk
	1, 3	*290*	kk
	1, 4	(*270*+?)	kk
	1, 5	(*280*+?)	kk
	1, 6	*420*	kk
	1, 7	*300*	kk
	1, 8	*600*	kk
	2, 3	*260*	kk
	2, 6	*670*	kk
	2, 7	*170*	kk
$(CH_2)^2$ace	1, 8	1000	ll
	Phenanthrenes		
none		125(90)	gg, mm, nn
Cl	2	170	gg
Br	2	220	gg
OH	9	1500	mm
CH_3, CH_3	1, 2	185	nn
$(CH_3)_3$	1, 2, 8	135	nn
	1.2-Benzanthracenes		
none		500	gg, oo, pp
OH	3	1750	gg, qq
OCH_3	3	1250	gg, qq
	10	970	gg
CH_3	1′	660††	oo
	4	790††	oo
	5	740††	oo
	6	240	pp
	7	620	pp
	8	710††	oo
	9	660††	oo
	10	700	gg, oo
OCH_3, CH_3	9, 10	2000, 820††	gg, qq
CH_3, CH_3	5, 8	790††	oo
	5, 10	950††	oo
	8, 10	820	gg, oo
	6, 7	490	pp
$(CH_2)^2$ ace (cholanthrene)	5, 10	2100	rr
	4, 10	2100	ss
	Chrysenes		
none		340	tt, uu
CH_3	1	460	uu
	3	440††	uu
	4	530	uu
	5	460	gg, uu, vv
	6	540††	uu
COOH	5	620	gg
CH_3, CH_3	5, 6	480	vv, ww
	1,2,5,6-Dibenzanthracenes		
none		350	gg
OH, OH	4′, 8′	4000	gg
	Pyrenes		
none		140	gg, pp
Cl	3	400	xx
OH	3	4000	gg, xx
	4	4000, 1250	gg, xx
OCH_3	3	3200	gg
CH_3	2	140	pp
	3	250	gg, xx
	4	160	xx
CN	3	3000	xx
COOH	3	1000	xx

** See footnotes to Table I for references.
†† Estimated smoothed extinction from table of peak values.
bb API 130–2 (Sun Oil Company).
cc API 87–8 (California Research Corporation).
dd ICT 14–19, 21.
ee ICT 78.
ff API 244, 246 (Universal Oil Products Company).
gg R. N. Jones, J. Am. Chem. Soc. **67**, 2127 (1945).
hh ICT 26.
ii API 214 (Mellon Institute of Industrial Research).
jj H. de Laszlo, Compt. rend. **185**, 599 (1927).
kk API 215–24 (Trinidad Leaseholds, Ltd.).
ll M. Pestemer and F. Manchen, Monatsh. **68**, 92 (1936).
mm Ramart-Lucas, Matti, and Guilmart, Bull. soc. chim. France, 1215 (1948).
nn F. A. Askew, J. Chem. Soc. 509 (1935).
oo R. N. Jones, J. Am. Chem. Soc. **62**, 148 (1950).
pp W. V. Mayneord and E. M. F. Roe, Proc. Roy. Soc. (London) **A152**, 299 (1935).
qq R. N. Jones, J. Am. Chem. Soc. **63**, 151 (1941).
rr W. V. Mayneord and E. M. F. Roe, Proc. Roy. Soc. (London) **A158**, 634 (1937).
ss L. F. Fieser and F. Novello, J. Am. Chem. Soc. **64**, 802 (1942).
tt Nichol, Thorn, Jones, and Sandin, J. Am. Chem. Soc. **69**, 376 (1947).
uu W. R. Brode and J. W. Patterson, J. Am. Chem. Soc. **63**, 3252 (1941).
vv R. N. Jones, J. Am. Chem. Soc. **63**, 313 (1941).
ww R. N. Jones, J. Am. Chem. Soc. **65**, 1815 (1943).
xx G. Förster and J. Wagner, Z. physik Chem. **B37**, 353 (1937).

in brackets in the tables. These values lie within the range of the nonpolar values taken from different authors, except in the case of the nitriles and of nicotinic acid, which also shows other anomalies. (Because of these peculiarities, the isomers of nicotinic acid, whose spectra are available in alcohol solution, are not included here.) Later it may be instructive to examine in detail the effect of solvent, of association and complex formation, of *p*H, of proton addition, etc., upon the spectroscopic moments of particular groups.

The data from the API curves are given in the tables in italics. They are modern measurements, usually taken with analytical accuracy on compounds of known purity. They are usually consistent among themselves within 10 percent. They are more consistent with the Sklar-Förster theory than are the older data of other authors. Where available, they were preferred for determining the spectroscopic moments. In the older data, disagreements by 20 percent are common and by factors of 2, occasional. Simple averages of these meas-

urements are given in the tables except where it seemed important for self-consistency to use the data from a single laboratory on a large group of compounds.

DETERMINATION OF MOMENTS

The moment for a particular substituent was determined by use of Eqs. (1)–(3) for every compound in Table I in which that substituent was present. If the intensity parameter is taken as $\epsilon_{max}(sm)$, and if the constant K of Eqs. (1)–(3) is set equal to unity, the spectroscopic moments, m, are found in units of (cm moles/liter)$^{-\frac{1}{2}}$. The transition moment integral Q is then given approximately by

$$Q=6\times10^{-3}\,m,$$

in angstrom units, assuming the transition is near 2800A.[6]

In the disubstituted compounds, the *para* and *meta* data were used for determining moments in preference to the *para* and *ortho* data, so as to avoid possible *ortho* effects. In finding the average moments, the monosubstituted values were weighted more heavily than the disubstituted values because of some systematic deviations from the theory which appeared in the latter as described below. The disubstituted values were used to determine the signs of the moments with respect to the methyl moment, which was arbitrarily taken as positive.

TABLE III. Determination of spectroscopic moments for F, CH_3, and CF_3 with other substituent.

Substituent		None	F	CH_3	CF_3	Average
F	*a*	23.7	—	21.4	20.8	22.0
	b	22.8	—	20.4	18.6	20.6
CH_3	*a*	9.8	3.9	$\begin{Bmatrix}11.0m\\8.5p\end{Bmatrix}$	—	8.3
	b	7.4	4.1	$\begin{Bmatrix}4.5m\\7.9p\end{Bmatrix}$	—	6.0
CF_3	*a*	−15.8	−13.7	—	—	−14.8
	b	−14.5	−15.5	—	—	−15.0

a—assuming vibrational contribution to ϵ of 110.
b—assuming vibrational contribution to ϵ of 150.

Signs of Halogen Moments

The signs for Br and I had to be determined from the halopyridines. The 2- and 3-monohalo-, and the 2, 5-, 2, 6-, and 3, 5-dihalopyridines will all have intensities greater than pyridine itself if the signs of the halogen moments are opposite to that of (N). [See Figs. 2(b) and 3.] This is found to be the case. Since the sign for (N) is established by other evidence as negative, the halogen signs must all be positive.[7] The dihalo- intensities should be almost constant, according to the theory, but the observed intensities for the 2- and 6-substituted compounds are excessive. Probably *ortho* effects are involved.

Averaging of Moments. Vibrational Effects

Table III shows how the different moment values for each substituent were compared and averaged. It contains all the moment values found for F and CF_3 from the compounds of Table I, and some of the best values found for CH_3. The line marked *a* for each substituent gives the moments found under the assumption that the vibrational contribution, ϵ_0, to the intensity is simply 110, the intensity given for benzene itself in Table I.

There are two reasons for believing this is not the best assumption. First, as seen in Sklar's diagrams, the predicted *meta* intensities are then too low (or the computed moments too high), and the predicted *para* intensities are too high (or the computed moments too low). This is apparent in the CH_3, CH_3 values (line *a*) of Table III. With two different substituents, the computed moment of the weak substituent appears to be much too low (CH_3 with F, line *a*, in Table III); the moment of the strong substituent is less affected, but tends to be too high.

Increasing ϵ_0, as in lines *b* of Table III, improves this situation and may even reverse the direction of the deviations.

The second reason for discarding $\epsilon_0=110$ is that each of the three series CH_3, CH_2X, CHX_2, CX_3, with $X=$F, Cl, and Br, might be expected to have an orderly sequence of moments with, say, almost constant second differences.[8] Such orderly sequences are obtained for all three series if, and only if, ϵ_0 is raised to about 190. Unfortunately, this value is now too high to fit the alkylbenzenes.

The best compromise value of ϵ_0, if we are to retain the simplicity of the original idea and not compute a separate value for each compound or group of compounds, seems to be about 150. This value is used in lines *b* of Table III and the adopted moments given in Table IV are based on it. Since it is only a compromise, some systematic errors remain in the individual moment values but are averaged out in Table IV.

Possible Disagreements with Theory

Except for one compound, every intensity value in Table I can be predicted, with an accuracy almost as high as the experimental accuracy, from the adopted moments in Table IV. Even *ortho* intensities are usually close to those of the *meta* isomers, as expected.

The one exception is nicotinic acid, with (N) and

[6] From Eq. (4), and from Eq. (4) of R. S. Mulliken and C. A. Rieke, Rep. Prog. Phys. 8, 231 (1941).

[7] The data of Conrad-Billroth in Reference 4 on the halobenzenes and halotoluenes give the same qualitative result. They were not included here because his intensity values, even though they agree well with the A.P.I. values for the chloro compounds, are larger than the latter values for some of the fluoro and iodo compounds by factors of over two.

[8] W. F. Hamner and F. A. Matsen, J. Am. Chem. Soc. **70**, 2482 (1948) discuss the variation and the change of sign of the moments along these sequences, but not quantitatively.

COOH *meta* to each other. The signs of both moments must be negative to fit intensities in several other compounds. Therefore, from Fig. 2, the nicotinic acid intensity ought to be less than the pyridine intensity. It is observed to be considerably greater, in both paraffin and water solutions.

The explanation of this apparent exception is that a "zwitter-ion" is formed by nicotinic acid. The proton is attached to the nitrogen instead of to the carboxyl group. The intensity should be derived not from the moments of (N) and COOH but from those of $(N)H^+$ and COO^-. Later these relations may be studied in detail.

The apparent exception thus turns out instead to be evidence of the real chemical change in the structure of the molecule from the supposed form.

Adopted Moments

The adopted moments for the 24 substituents of Table I are shown in Table IV. The signs of some moments are uncertain, where no disubstituted data were available. The probable signs are put in brackets. They were determined partly from the requirement that homologous sequences be orderly and parallel. Partly, they were chosen to fit in with the known dipole moments and directing effects of these substituents, since the latter parameters seem to be correlated with the better established spectroscopic moments, as described below. In one case, CH_2Br, the value of $\epsilon_{max}(sm)$ was not certain; but a moment could be estimated from the other moments in its sequence, and this moment has also been included in Table IV.

Some idea of the uncertainties in the values in Table IV may be obtained from the variations in the moments for any substituent in Table III. Variations for other substituents were, in some cases, considerably larger than those shown. But some of these variations were systematic and could be roughly corrected, since they represented the influence of other effects rather than an uncertainty in the moments. For some substituents, also, the uncertainty in the moments was reduced by having several independent determinations—from 4 to 12 for OH, CH_3, Cl, CN, and (N). The values in Table IV are therefore believed to have an absolute accuracy of about ± 3 units; and, in the moments from $+7$ to $+2$, a relative accuracy of about half this.

It should be noted that in averaging and selecting the values, care was taken to preserve the order in the sequences: OH, OCH_3; CH_3, Cl, Br; $CH_n(CH_3)_{3-n}$; and CH_nX_{3-n}. This order was sometimes indicated only by single measurements.

MOMENTS FOR OTHER AROMATIC DERIVATIVES

In considering derivatives of other aromatics, three questions must be answered. First: in monosubstitution, is the change of intensity (and the spectroscopic moment) induced by a given substituent almost independent of the kind of ring system and of position? Second: is the change of intensity (and the moment) similar to that for the same substituent in benzene? Third: in di- and polysubstitution, do the rules hold for vector addition of moments as indicated in Fig. 1 and the accompanying discussion?

Values of Moments

The answer to the first question is: only approximately. For, if we assume that the intensity of the unsubstituted aromatic gives us ϵ_0, then the values of the CH_3 moments from the monosubstitution data of Table II range from 8 to 14 except for one imaginary moment in benzanthracene. The values of the OH moments range from 33 to 37 except for two very high values in the pyrenes which are contradicted by measurements from another laboratory. The COOH values spread very widely: 18, 30, 41. These differences seem to be too large to be experimental error, but they may indicate that $\epsilon_{1st\ pk}(sm)$ is not a very good measure of transition intensity rather than that the assumptions underlying the theory are wrong.

TABLE IV. Adopted spectroscopic moments.

Substituent	Spectro. moment (cm m/l)$^{-1}$	Substituent	Spectro. moment (cm m/l)$^{-1}$
OH	34	NC	−6
OCH_3	31	CHF_2	(−) 9
F	21	$CHCl_2$	(−)11
I	21	CH_2Br	(−12?)
CH_3	7	CF_3	−15
Cl	6	SO_2NH_2	−15
C_2H_5	5	CCl_3	(−)17
Br	4	CN	−19
$i-C_3H_7$	3.5	$CHBr_2$	(−)25
$t-C_4H_9$	2	COOH	−28
H	—0—	CBr_3	(−)33
CH_2F	(−) 2	(N)(aza)	−38
CH_2Cl	(−) 3	SO_3H	(−)42

The worst deviations of the intensities from the expected values occur in the pyrenes. There is evidence that some of this is experimental error; but possibly the theory is not applicable to peri-condensed compounds; or possibly the moments of substituents are simply much larger than in the cata-condensed compounds. Further measurements are needed to decide among these possibilities.

As for question two, the moment values for the substituents of Table II, OH, OCH_3, CH_3, Cl, Br, CN, COOH, and (N), seem to be the same as the values given in Table IV within the wide variance described above; and where substituents at the same position on the same ring system are compared, the order of the moments, as given in Table IV, seems to be preserved.

Vector Addition

The best material for examination of the third question is: (a) the datum on 1,2,8-trimethylphenanthrene (where the intensity should be, and is, approximately ϵ_0), which has already been cited in support of the ex-

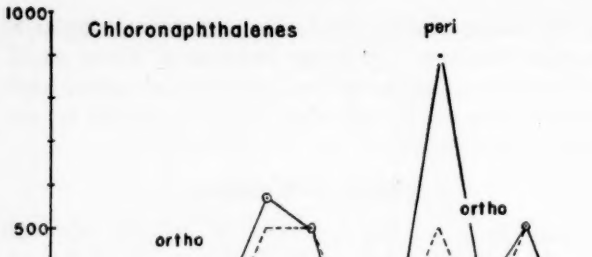

FIG. 4. Computed (- - - -) and observed (——) values of $\epsilon_{1st\ pk}(sm)$ for chloronaphthalenes; $\epsilon_0=180$, Cl moment=9.

tended theory; and (b) the data on all the dichloro- and dimethylnaphthalenes. The latter data are plotted in Figs. 4 and 5 in diagrams similar to Sklar's. The theoretical values are given by the dashed lines, assuming a Cl moment of 9 and a CH_3 moment of 10, with $\epsilon_0=180$ in both cases. The high values of the 1, 4; 1, 5; 1, 8; and 2, 6 derivatives are seen to be accounted for by the theory. The 1, 4 and 1, 5 dimethyl compounds do not have the high values of the dichloro compounds; but they have unusual vibrational envelopes with a weak first band, so that $\epsilon_{1st\ pk}(sm)$ is obviously not a good measure of transition intensity. The fit in Fig. 4 is about as good as in Sklar's benzene diagrams; in Fig. 5 it is appreciably poorer.

Qualitatively, the other compounds of Table II also behave as expected by the vector rules. Unfortunately, no clear-cut data are available in these larger ring systems for determining the signs of the moments.

The evidence seems to be that the vector addition rules are approximately correct but that the intensities again show a wide variance, as in the monosubstituted compounds. The study of the disubstituted naphthalenes with a stronger substituent might provide a more satisfactory test of the theory.

It is worth noting that dimethylene substitution (leading to *ace* compounds) has much stronger effects than two methyl substituents at the same positions. Some tabulated data on substituted cholanthrenes were examined to see if the vector rules continue to apply in this case, but the evidence was scanty and conflicting; examination of the original spectral curves might be more profitable.

COMPARISON WITH MESOMERIC MOMENTS AND DIRECTING POWERS

We now compare the spectroscopic moments determined here with some older parameters which also measure the disturbance of the symmetry of the benzene ring electrons by a substituent.

One of these parameters is $\Delta\sigma$, the differential "substituent constant" of Hammett. This quantity is a measure of the directing power of the substituent, or difference in chemical reactivity at the *meta* and *para* positions. A table of $\Delta\sigma$ values was given by Price.[9]

Another important parameter is the "electromeric" or "mesomeric" moment, μ_e. This is measured by the difference in the permanent dipole moments of the phenyl derivative and of the corresponding aliphatic derivative. Values of μ_e were given by Sutton[10] and later by Watson.[11]

In Fig. 6, these parameters, $\Delta\sigma$ and μ_e, are compared with the spectroscopic moments. In Fig. 6, values for a given substituent are connected by straight lines. If the correlation among the parameters were perfect, these lines for different substituents would not cross.

A strong but not a perfect correlation is seen. Part of the crossing may be due to the uncertainties, but probably not all of it. The spectroscopic moments appear to be intermediate in their behavior between the dipole moments and the directing powers. This is shown by the halogens; fluorine induces less mesomeric moment than iodine, but is more *op*-directing, while their spectroscopic moments are about the same.

The spectroscopic moments of the various alkylbenzenes in Table IV follow the same sequence as the directing powers, as was shown by Matsen and coworkers, but an opposite sequence to the dipole moments.[12]

The spectroscopic moments for CH_2X, which have been tentatively assigned negative values here so as to make certain sequences orderly, would have positive signs if the moments behaved like the other parameters in Fig. 6. Hamner and Matsen pointed this out for CH_2Cl.[8] It would be important to obtain disubstitution data for these substituents so as to determine the signs of their moments unambiguously.

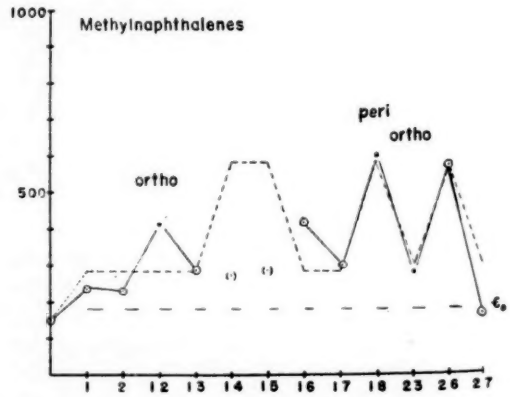

FIG. 5. Computed (- - - -) and observed (——) values of $\epsilon_{1st\ pk}(sm)$ for methylnaphthalenes; $\epsilon_0=180$, CH_3 moment=10.

[9] C. C. Price, Chem. Revs. **29**, 37 (1941).
[10] L. E. Sutton, Proc. Roy. Soc. (London) **133A**, 668 (1931).
[11] H. B. Watson, *Modern Theories of Organic Chemistry* (Oxford University Press, New York, 1941), second edition, pp. 60–62.
[12] Matsen, Robertson, and Chuoke, Chem. Revs. **41**, 273 (1947).

A perfect correlation among these three quantities should not be expected. Each involves different properties of the ring electrons. The dipole moment involves perturbation of the ground state of the ring. The directing power involves, in addition, the effect of the substituent on the ground state of some intermediate reaction complex, and the spectroscopic moment involves perturbation of both the ground and excited states of the ring by the substituent.

The fact that there is a correlation simply shows that strong substituents affect the ring electrons strongly, weak ones weakly; but there are evidently differences in detail. Similarly, Matsen and Robertson[13] have expressed the resonance energy, the mesomeric moment, the directing power (qualitatively), and the frequency and intensity shift of the 2600A transition in monosubstituted benzenes in terms of a single electronegativity or resonance parameter, δ; but they had to introduce a second inductive parameter, δ_1, to account for the intensities in the halobenzenes. The separation of inductive and resonance effects did not seem necessary for the purposes of the present paper and was not attempted; it may not be feasible from intensity data alone.

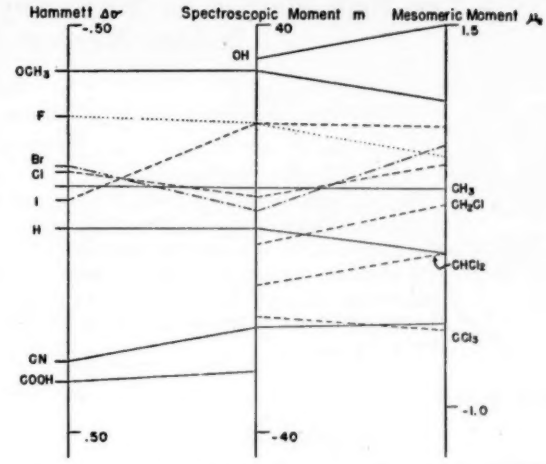

FIG. 6. Correlation among three parameters. Spectroscopic m in (cm mole/liter)$^{-1}$; mesomeric moment in 10^{-18} esu.

Note added in proof: The vector rules are also confirmed by the relative strength of the first transitions (^1L_b) of the 2-, 3-, 6-, and 7-fluoroquinolines [Miller, Knight, and Roe, J. Am. Chem. Soc. **72**, 1629 (1950)] and of the same quinolinols and amino-quinolines [Ewing and Steck, J. Am. Chem. Soc. **68**, 2181 (1946); **70**, 3397 (1948)], though for these last two groups the 4-, 5-, and 8- comparison transitions are weak and hidden.

[13] F. A. Matsen and W. W. Robertson, "Molecular orbital theory and spectra of monosubstituted benzenes. I–IV," J. Am. Chem. Soc. (to be published).

A Two-Path Method for Measuring Flame Temperatures and Concentrations in Low Pressure Combustion Chambers*

S. S. PENNER
Jet Propulsion Laboratory, California Institute of Technology, Pasadena, California
(Received October 30, 1950)

The two-path method for flame-temperature determinations has been extended to discrete radiators observed with instruments of arbitrary resolving power. Representative calculations of radiant intensity have been carried out for low pressure combustion flames in order to ascertain the feasibility of experimental study with standard spectroscopic instruments. It is shown how experimentally determined temperatures and emissivities can be utilized to calculate the concentrations of emitters, provided the emitting species is known and the radiation emitted corresponds to the thermodynamic equilibrium for the local conditions of temperature and pressure.

I. INTRODUCTION

THE two-path method for the determination of flame temperatures was apparently invented by Hottel and Broughton in 1932.[1] Recent applications of this technique have been made to flame-temperature measurements on pulse jets by Hett and Gilstein.[2] All of these discussions of the two-path method, as well as a critical analysis of the technique included in a recently published comprehensive review of optical methods for flame-temperature determinations,[3] have been restricted to the use of this method with optical instruments of infinite resolving power or to radiators, the emissivity of which is independent of wavelength in the resolved spectral range. Application of the results obtained previously, therefore, involves an undetermined error in any given practical problem.

It is the purpose of this article to show how the two-path method may be applied to actual investigations involving the use of instruments of limited resolving power, such as an infrared spectrometer or a visible and ultraviolet spectrograph. The present analysis was stimulated by current spectroscopic studies of a low pressure combustion flame in an apparatus constructed by M. Gilbert.[4] However, the discussion which is given in this paper is of general validity and is in no sense restricted to a specific problem. In fact, it is quite obvious how the calculations should be modified for applications to flames burning at intermediate and elevated pressures.

In addition to extending the analysis of the two-path method to instruments of arbitrary resolving power, it will be shown how the results obtained by the use of the two-path method, i.e., the measured spectral emissivities and vibration-rotation temperatures, can be utilized to determine the concentrations of the emitting species, provided the nature of the emitting species is known and the radiation emitted is the radiation emitted at thermodynamic equilibrium for the local conditions of temperature and pressure. The use of measured emissivities and flame temperatures for the calculation of concentrations of emitters is a difficult computational problem which does not appear to have been either suggested or attempted in the past. Nevertheless, as the result of theoretical studies of gaseous emissivities,[5,6] a sufficient backlog of detailed information has been accumulated to permit the inversion of theoretical emissivity studies, at least for simple diatomic molecules such as carbon monoxide. No attempt will be made to present in this article detailed numerical results for practical calculations. Instead, the principles of the procedure will be outlined briefly. For a more detailed discussion of the fundamental theoretical problems involved in radiant-heat-transfer calculations, reference should be made to the published work on radiant heat transfer.[5–9] The numerical results for carbon monoxide, which are of immediate practical value for the calculation of concentrations of this molecule from emissivity and temperature measurements on flames, will be published in a forthcoming report on radiant heat transfer.

Since the present discussion of temperature and concentration measurements is predicated on the assumption that isothermal flame zones can be isolated, it appears appropriate to describe how a suitable experimental arrangement can be obtained, for example, for a low pressure combustion flame. On the basis of available thermocouple explorations of the low pressure combustion flame,[4] it appears likely that rather well-defined isothermal regions exist in the two-dimensional flame. A region of known path length can be defined between a sapphire window (which transmits infrared radiation to about 6.5 microns) and an opposite enclo-

* This paper presents the results of one phase of research carried out at the Jet Propulsion Laboratory, California Institute of Technology, under U. S. Army Ordnance Department Contract No. W-04-200-ORD-455 and U. S. Air Forces Contract No. W-33-038-ac-4320.

[1] H. C. Hottel and F. P. Broughton, Ind. Eng. Chem., Anal. Ed. 4, 166 (1932).
[2] J. H. Hett and J. B. Gilstein, J. Opt. Soc. Am. 39, 909 (1949).
[3] S. S. Penner, Am. J. Phys. 17, 422, 491 (1949).
[4] M. Gilbert, Report No. 4–54 (Jet Propulsion Laboratory, Pasadena, 1949).
[5] S. S. Penner, J. Appl. Phys. 21, 685 (1950).
[6] L. E. Benitez and S. S. Penner, J. Appl. Phys. 21, 907 (1950).
[7] W. M. Elsasser, Phys. Rev. 54, 126 (1938).
[8] W. M. Elsasser, Harvard Meteorological Studies No. 6 (Blue Hill Observatory, 1942).
[9] Matossi, Mayer, and Rauscher, Phys. Rev. 76, 760 (1949).

sure which acts either as a cool blackbody or as a mirror. The window and reflecting surfaces can be protected by infrared inactive gas shields such as argon or helium. The experimental arrangement is sketched in Fig. 1.

If probe 2 in Fig. 1 can be made to act either as a mirror or as a cool blackbody, it is possible to make two independent radiant-intensity determinations, one with probe 2 acting as an absorber and one with probe 2 acting as a reflector. From these two independent experimental results, it is possible to determine two unknowns, namely, the temperature of the emitters between the probes and the spectral emissivity of the emitters. With an instrument of low resolving power, an average emissivity over a small wavelength region will be determined rather than a spectral emissivity. The assumption that a nearly isothermal flame zone has been isolated between the probes can be checked experimentally by repeating the measurements for different distances between probes 1 and 2. If the calculated flame temperatures and emissivities are independent of the positions of the probes for appreciable distances between the probes, then a nearly isothermal region of nearly constant composition must have been isolated. By the use of probes of different sizes, it may also be possible to estimate the effect of the probes in disturbing the flame pattern.

For purposes of exposition the application of the two-path method will first be described for an instrument of infinite resolving power (see Section II).[10] Measurements of the vibration-rotation temperature with an instrument of low resolving power are described in Section III. Finally, the calculation of concentrations of diatomic emitters from observed emissivities and temperatures is considered in Section IV.

II. THE TWO-PATH METHOD FOR MEASURING FLAME TEMPERATURES

The following summary of the two-path method for flame-temperature measurements utilizes the same notation employed in a previous publication.[3]

The intensity of radiation $J(\lambda, T)$ emitted by a blackbody per unit area of emitter per unit time, in the wavelength range between λ and $\lambda+d\lambda$, into a solid angle of 2π steradians, is given by Planck's equation:

$$J(\lambda, T)d\lambda=\frac{c_1}{\lambda^5}\frac{1}{[\exp(c_2/\lambda T)]-1}d\lambda. \quad (1)$$

Here, T=absolute temperature of emitter; c_1=first radiation constant, which has the numerical value $2\pi c^2h=3.740\times10^{-5}$ erg cm^2 sec^{-1}; c_2=second radiation constant, which has the numerical value $ch/k=1.436$ cm°K; c=velocity of light; h=Planck constant; and

[10] A microwave spectrometer may approach the requirements of an instrument of infinite resolving power for the present purposes. The requirements on resolving power are merely that the instrument must be capable of isolating spectral intervals which are so narrow that the gaseous emissivity does not vary appreciably in the spectral interval resolved.

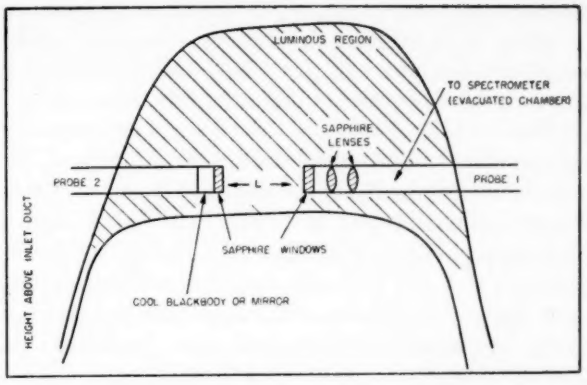

FIG. 1. Schematic diagram of experimental arrangement for emission studies on isothermal flames.

k=Boltzmann constant. The brightness temperature T_{Br} of a non-black radiator, whose true temperature is T, is defined as the temperature of a blackbody emitting the same intensity of radiation as the non-black radiator under study, i.e.,

$$J(\lambda, T_{Br})d\lambda=\epsilon(\lambda, T)J(\lambda, T)d\lambda. \quad (2)$$

Here, the spectral emissivity of the non-black radiator is designated as $\epsilon(\lambda, T)$ in order to emphasize the fact that the emissivity is a function of wavelength and temperature.

The emissivity $\epsilon(\lambda, T)$ is well known[5,8] to depend on the optical density X through a relation of the form

$$\epsilon(\lambda, T)=1-\exp[-P(\lambda, T)X], \quad (3)$$

where $P(\lambda, T)$ is the spectral absorption coefficient. The optical density is equal to the product of the partial pressure p of emitter and the path length L.

Let T_{Br1} represent the brightness temperature of the flame when probe 2 acts as a cool blackbody; let T_{Br2} be equal to the brightness temperature when probe 2 acts as a mirror with reflectivity R_λ. Then,[11]

$$J(\lambda, T_{Br1})=J(\lambda, T_F)\{1-\exp[-P(\lambda, T)pL]\}, \quad (4)$$

and

$$J(\lambda, T_{Br2})=J(\lambda, T_F)\{1-\exp[-P(\lambda, T)pL]\}\times\{1+R_\lambda\exp[-P(\lambda, T)pL]\}, \quad (5)$$

where the pathlength L is the distance between the probes. Dividing Eq. (5) by Eq. (4), it follows that

$$[J(\lambda, T_{Br2})]/[J(\lambda, T_{Br1})]=1+R_\lambda\exp[-P(\lambda, T)pL]. \quad (6)$$

But from Eq. (4)

$$\exp[-P(\lambda, T)pL]=1-[J(\lambda, T_{Br1})/J(\lambda, T_F)]. \quad (7)$$

Hence, Eq. (6) can be written in the form

$$1-[J(\lambda, T_{Br2})/J(\lambda, T_{Br1})]=-R_\lambda\{1-[J(\lambda, T_{Br1})/J(\lambda, T_F)]\}. \quad (8)$$

[11] All operational factors such as absorption and reflection of light by windows are neglected in the present discussion for the sake of simplicity. They must, of course, be included in applications of the two-path method to concrete problems.

The only unknown in Eq. (8) is the flame temperature T_F which is, therefore, determined from the experimental measurements of $J(\lambda, T_{Br1})$ and $J(\lambda, T_{Br2})$. If the measured intensities of radiation refer to a part of a vibration-rotation spectrum, then T_F will represent the corresponding vibration-rotation temperature of the emitters independently of the existence or nonexistence of statistical equilibrium in the flame. If T_F is known, it is evidently possible to calculate the spectral absorption coefficient $P(\lambda, T)$, and, hence, the spectral emissivity $\epsilon(\lambda, T)$ by the use of Eqs. (7) and (3), respectively. It should, perhaps, be emphasized that, although the measured vibration-rotation flame temperatures and the measured vibration-rotation emissivities are uniquely determined by the experimental results, considerable caution should be exercized in associating, for example, vibration-rotation temperatures with local translational temperature, etc. This particular problem has been dealt with in a previous publication.[3]

III. THE TWO-PATH METHOD APPLIED TO AN INSTRUMENT OF FINITE RESOLVING POWER

Although the following discussion is restricted to application of the two-path method to flames burning at sufficiently low total pressures to prevent overlapping of individual rotational lines, extension of the treatment can be made without difficulty to arbitrary values of the total pressure. In this connection reference should be made to the work of Elsasser[7,8] and Matossi *et al.*[9] as well as to the vast literature concerned with theoretical and experimental studies of the pressure broadening of spectral lines.[12–18]

For an instrument of resolving power[19] $\Delta\nu$, Eqs. (4) and (5) take the form

$$\int_{\Delta\nu} J(\nu, T_{Br1})d\nu = \int_{\Delta\nu} J(\nu, T_F)\{1-\exp[-P_\nu(T)pL]\}d\nu, \quad (9)$$

and

$$\int_{\Delta\nu} J(\nu, T_{Br2})d\nu = \int_{\Delta\nu} J(\nu, T_F)\{1-\exp[-P_\nu(T)pL]\} \times\{1+R_\nu \exp[-P_\nu(T)pL]\}d\nu, \quad (10)$$

where the wavelength λ has been replaced as variable by the wave number $\nu=1/\lambda$. It is apparent that Eqs. (9) and (10) are substantially equivalent to Eqs. (4) and (5) only if $\Delta\nu$ is so narrow that both $J(\nu, T)$ and $P_\nu(T)$ are nearly constant in the interval $\Delta\nu$. This condition can be realized in practice, at least approximately, by the use of a microwave spectrometer ($\Delta\nu$ very small) or at high pressures for moderate value of $\Delta\nu$ [$P_\nu(T)$ and $J(\nu, T)$ nearly constant]. For a low pressure combustion flame, $\Delta\nu$ can be chosen small enough so that $J(\nu, T)$ is nearly constant. However, for the resolving power attainable with an infrared prism spectrometer or even with a good grating instrument, $P_\nu(T)$ is a rapidly varying function of ν in the spectral interval $\Delta\nu$. It is therefore necessary to evaluate the integrals given in Eqs. (9) and (10) for the case of rapidly varying $P_\nu(T)$.

The exact dependence of $P_\nu(T)$ on ν is not known at the high temperatures and low pressures of a low pressure combustion flame. On the basis of available theoretical and experimental information,[12–18] it appears reasonable to consider the rotational lines of a simple diatomic molecule such as CO as being composed of the contributions resulting from Doppler and from collision broadening, since the natural half-width of the rotational lines is negligibly small ($\sim 10^{-6}$ cm^{-1}). The Doppler contribution leads to the result that $P_\nu(T)$ as a function of ν follows an error curve, whereas collision broadening produces the dispersion formula for $P_\nu(T)$.[16] The superposition of Doppler and collision broadening results in asymmetries which are difficult to treat.[16] Furthermore, the contributions to line shape resulting from van der Waals' broadening, electric fields, etc. cannot be estimated reliably, but these effects are probably unimportant at very low pressures. Since the principal contribution to $P_\nu(T)$ in the wings of the rotational lines results from the dispersion representation of collision broadening, it is not unreasonable to assume a dispersion formula for $P_\nu(T)$. For the sake of simplicity the Doppler contribution may be included by increasing the half-width resulting from collision broadening by an appropriate amount. If the half-widths are merely added, the contributions of Doppler broadening are underestimated near the line centers and overestimated in the wings.† The following discussion will be restricted to a dispersion representation for $P_\nu(T)$. For applications to concrete problems it may

[12] J. H. Van Vleck and V. F. Weisskopf, Revs. Modern Phys. **17**, 227 (1945).
[13] P. W. Anderson, Phys. Rev. **76**, 647 (1949).
[14] E. Lindholm, dissertation (Uppsala, 1942).
[15] E. B. Wilson, Jr., and A. J. Wells, J. Chem. Phys. **14**, 578 (1946).
[16] H. Margenau, and W. W. Watson, Revs. Modern Phys. **8**, 22 (1936).
[17] S. D. Cornell, Phys. Rev. **51**, 739 (1937).
[18] D. M. Dennison, Phys. Rev. **31**, 503 (1928).
[19] The term resolving power is used somewhat loosely in the present discussion. For the sake of simplicity, it will be assumed that the term resolving power $=\Delta\nu$ implies that the instrument used for measurements responds to 100 percent of the radiation in the spectral interval $\Delta\nu$ and does not respond at all to any radiation lying outside of the indicated spectral range. For practical applications this statement should be replaced by a careful analysis of slit corrections, etc. [see reference 18 and J. C. Slater, Phys, Rev. **25**, 783 (1925)].

† In this connection see also R. Minkowski and H. Bruck, Z. Physik **95**, 274, 284 (1935).

prove to be desirable to replace the dispersion representation by a more nearly correct description of line shape resulting from appropriate superposition of Doppler and collision broadening. For this more realistic description of the rotational lines, it is no longer possible to evaluate the integrals of Eqs. (9) and (10) in closed form. Hence, it will be necessary to take recourse to numerical integrations.

For a representative diatomic molecule such as carbon monoxide, the individual rotational lines are, in general, so narrow that overlapping of rotational lines can be neglected at sufficiently low total pressures. This statement is supported by the numerical calculations on carbon monoxide described in Appendix I. To summarize, therefore, the evaluation of the integrals appearing in Eqs. (9) and (10) will be carried out for nonoverlapping rotational lines described by the dispersion formula. Furthermore, the spectral intervals $\Delta\nu$ will be assumed to have been chosen as sufficiently narrow to permit replacement, without appreciable error, of $J(\nu, T)$ by $\langle J(\nu, T)\rangle_{\Delta\nu} \simeq J(\bar{\nu}, T)$, where $\bar{\nu}$ is the average wave number included in the resolved spectral range.

According to the dispersion formula, the spectral absorption coefficient associated with the vibrational transition $n\rightarrow n+1$ and the rotational transition $j\rightarrow j\pm 1$ is given by a relation of the form[8]

$$[P_\nu(T)]_{j\rightarrow j\pm 1}^{n\rightarrow n+1} = \frac{S_{j\rightarrow j\pm 1}^{n\rightarrow n+1}}{\pi} \frac{\alpha}{(\nu-\nu_{j\rightarrow j\pm 1}^{n\rightarrow n+1})^2+\alpha^2}, \quad (11)$$

where $S_{j\rightarrow j\pm 1}^{n\rightarrow n+1}$ = integrated absorption for the indicated transition under the given conditions of temperature and pressure; α = rotational half-width of the spectral lines, i.e., the half-width at which $P_\nu(T)$ has fallen to one-half of its maximum value; and $\nu_{j\rightarrow j\pm 1}^{n\rightarrow n+1}$ = wave number of the line center. Only the vibrational transitions $n\rightarrow n+1$ are considered in the present discussion since, in general, only the emission intensity of the fundamental vibration-rotation band will be sufficient for quantitative study. Extension of the treatment to other spectral regions can be made without difficulty.

Replacing $J(\nu, T)$ by the constant value $J(\bar{\nu}, T)$ in Eqs. (9) and (10) leads to the following results for nonoverlapping rotational lines:

$$J(\bar{\nu}, T_{Br1})\Delta\nu = J(\bar{\nu}, T_F) \sum_{j \text{ for } \nu_{j\rightarrow j+1}^{n\rightarrow n+1} c\Delta\nu} \times \int_{-\infty}^{\infty} \{1-\exp[-(P_\nu)_{j\rightarrow j\pm 1}^{n\rightarrow n+1} pL]\}\, d\nu, \quad (12)$$

and

$$J(\bar{\nu}, T_{Br2})\Delta\nu = J(\bar{\nu}, T_F) \sum_{j \text{ for } \nu_{j\rightarrow j+1}^{n\rightarrow n+1} c\Delta\nu} \times \int_{-\infty}^{\infty} \{1-\exp[-(P_\nu)_{j\rightarrow j\pm 1}^{n\rightarrow n+1} pL]\} \times \{1+\bar{R}\exp[-(P_\nu)_{j\rightarrow j\pm 1}^{n\rightarrow n+1} pL]\}\, d\nu. \quad (13)$$

Here, the symbol $\nu_{j\rightarrow j\pm 1}^{n\rightarrow n+1} c\Delta\nu$ means that the summation is extended only over the rotational lines whose centers lie within $\Delta\nu$. Edge effects, resulting from the presence of rotational lines very close to the limits of $\Delta\nu$, are thereby neglected but can readily be included in a more detailed discussion. Each of the integrals appearing in Eqs. (12) and (13) should have been extended over an appropriate interval $\Delta\nu_{j\rightarrow j\pm 1}^{n\rightarrow n+1}$. However, as is well known,[8] the limits of integration for widely spaced spectral lines, obeying the dispersion formula of Eq. (11), may be extended to $\pm\infty$ without sensible error. Finally, the spectral reflectivity R_ν has been replaced by an appropriate average value $\bar{R}$ in Eq. (13).

Infinite integrals of the type appearing in Eqs. (12) and (13) have been evaluated by Ladenburg and Reiche for P_ν given by Eq. (11).[20] Details of the integration are described in Appendix II, where the method which Elsasser[8] used to evaluate the integral of Eq. (12) is employed for the determination of the integrals in Eqs. (12) and (13). The results of the integrations are

$$\int_{-\infty}^{\infty} \{1-\exp[-(P_\nu)_{j\rightarrow j\pm 1}^{n\rightarrow n+1} pL]\}\, d\nu = 2\pi\alpha x_j[\exp(-x_j)][J_0(ix_j)-iJ_1(ix_j)], \quad (14)$$

and

$$\int_{-\infty}^{\infty} \{1-\exp[-(P_\nu)_{j\rightarrow j\pm 1}^{n\rightarrow n+1} pL]\} \times \{1+\bar{R}\exp[-(P_\nu)_{j\rightarrow j\pm 1}^{n\rightarrow n+1} pL]\}\, d\nu = 2\pi\alpha x_j[\exp(-x_j)](1-\bar{R})[J_0(ix_j)-iJ_1(ix_j)] + 4\pi\alpha\bar{R}x_j[\exp(-2x_j)][J_0(2ix_j)-iJ_1(2ix_j)], \quad (15)$$

where

$$x_j = S_{j\rightarrow j\pm 1}^{n\rightarrow n+1} pL/2\pi\alpha, \quad (16)$$

and J_0 and J_1 are Bessel functions of order zero and order one, respectively. Hence, Eqs. (12) and (13) become

$$J(\bar{\nu}, T_{Br1})\Delta\nu = J(\bar{\nu}, T_F) \sum_{j \text{ for } \nu_{j\rightarrow j+1}^{n\rightarrow n+1} c\Delta\nu} \times \{2\pi\alpha x_j[\exp(-x_j)][J_0(ix_j)-iJ_1(ix_j)]\}, \quad (17)$$

[20] R. Ladenburg and F. Reiche, Ann. Physik 42, 181 (1913).

and

$$J(\bar{\nu}, T_{Br2})\Delta\nu = J(\bar{\nu}, T_F) \sum_{j \text{ for } \nu_{j\to j\pm1}}^{n\to n+1} c\Delta\nu \times\{2\pi\alpha x_j[\exp(-x_j)](1-\bar{R})[J_0(ix_j)-iJ_1(ix_j)] +4\pi\alpha\bar{R}x_j[\exp(-2x_j)][J_0(2ix_j)-iJ_1(2ix_j)]\}. \quad (18)$$

Equations (17) and (18) represent the general results from which flame temperatures and spectral emissivities can be calculated for a given set of measured values of $J(\bar{\nu}, T_{Br1})$ and $J(\bar{\nu}, T_{Br2})$. Representative calculations, involving the use of Eqs. (17) and (18), are given in Section IV.

Reference to the defining equation for x_j, given in Eq. (16), shows that this quantity depends on the integrated absorption, the partial pressure of the emitter, the total pressure, and the optical path length. The optical path length and the total pressure are defined unambigously by the experimental conditions. Hence, since the $S_{j\to j\pm1}^{n\to n+1}$ can be calculated for a given emitter by use of the method outlined in Section IV, Eqs. (17) and (18) involve only two unknowns, namely, the rotation-vibration temperature T_F and the partial pressure p of the emitting species. It is, therefore, evident that the two-path method is capable, in principle, of yielding not only the temperature but also the concentration of the emitter. This fact has not been utilized in the past, although it is of obvious importance in connection with optical studies of kinetic processes.

Equations (16)–(18) can be used to obtain definite results for two special cases without requiring detailed knowledge of integrated absorption. For the sake of simplicity it will be assumed that $\bar{R}=1$, a result which can be approached very closely for infrared radiation. Furthermore, it will be assumed that all of the rotational lines in the interval $\Delta\nu$ have the same value for the integrated absorption. This condition will obtain, approximately, at moderate temperatures for the rotational lines near the emission peaks for simple molecules such as carbon monoxide. Let $n_{\Delta\nu}$ represent the number of equally intense rotational lines in the spectral range $\Delta\nu$. Then, Eqs. (17) and (18) become, respectively,

$$J(\bar{\nu}, T_{Br1})\Delta\nu = J(\bar{\nu}, T_F)n_{\Delta\nu} \cdot 2\pi\alpha x[\exp(-x)][J_0(ix)-iJ_1(ix)] \quad (19)$$

and

$$J(\bar{\nu}, T_{Br2})\Delta\nu = J(\bar{\nu}, T_F)n_{\Delta\nu} \cdot 4\pi\alpha x[\exp(-2x)][J_0(2ix)-iJ_1(2ix)], \quad (20)$$

where $x=SpL/2\pi\alpha$ is determined by the constant value of S for given partial pressure of emitter, fixed total pressure, and given optical path length. Dividing Eq. (20) by Eq. (19) leads to the relation

$$\frac{J(\bar{\nu}, T_{Br2})}{J(\bar{\nu}, T_{Br1})} = 2[\exp(-x)]\frac{J_0(2ix)-iJ_1(2ix)}{J_0(ix)-iJ_1(ix)}. \quad (21)$$

Equation (21) can be used to obtain asymptotic limiting forms for small and for large values of x. The Bessel function $J_n(z)$ can be written[21] as a power series in $z/2$ as follows:

$$J_n(z)=\frac{(z/2)^n}{0!n!}=\frac{(z/2)^{n+2}}{1!(n+1)!}+\frac{(z/2)^{n+4}}{2!(n+2)!}\cdots.$$

Hence,

$$\lim_{x\to0}\left\{[\exp(-x)]\frac{J_0(2ix)-iJ_1(2ix)}{J_0(ix)-iJ_1(ix)}\right\}=2. \quad (22)$$

Similarly, for large values of x,

$$\lim_{x\to\infty}J_n(ix)=\frac{(i)^n\exp(x)}{(2\pi x)^{\frac{1}{2}}}$$

whence

$$\lim_{x\to\infty}\left\{[\exp(-x)]\frac{J_0(2ix)-iJ_1(2ix)}{J_0(ix)-iJ_1(ix)}\right\}=\sqrt{2}. \quad (23)$$

Hence, the conclusion is reached that

$$\sqrt{2}\leq J(\bar{\nu}, T_{Br2})/J(\bar{\nu}, T_{Br1})\leq 2. \quad (24)$$

The result given in Eq. (24) can be shown to follow immediately from Elsasser's study of absorption coefficients for equally intense and equally spaced[22] rotational lines.[7,8] It is gratifying to note that for nonoverlapping lines the observed radiant intensity will be increased at least by $\sqrt{2}$ when the optical path length is doubled by the use of a mirror. This conclusion is different from the result which would have been obtained if the variation of P_ν with ν had been neglected. In particular, it is apparent by reference to Eq. (6) that the condition given in Eq. (24) would be replaced by the relation

$$1\leq J(\bar{\nu}, T_{Br2})/J(\bar{\nu}, T_{Br1})\leq 2, \quad (25)$$

if an average absorption coefficient $\bar{P}$ had been used for the spectral range $\Delta\nu$. The discrepancy between Eqs. (24) and (25) is illusory in so far as it is impossible to retain nonoverlapping rotational lines in the limiting case as $x\to\infty$. However, again on the basis of Elsasser's theoretical studies,[8] it is apparent that even for moderate values of the optical density,

$$J(\bar{\nu}, T_{Br2})/J(\bar{\nu}, T_{Br1})\sim\sqrt{2}.$$

This last result is also verified by numerical calculations for the special case considered in Section IV.

As was pointed out earlier in this section, the complete utilization of the results embodied in Eqs. (16), (17), and (18) requires detailed knowledge of the integrated absorption $S_{j\to j\pm1}^{n\to n+1}$. Accordingly, the calculation of $S_{j\to j\pm1}^{n\to n+1}$ for diatomic molecules is considered in Section IV.

[21] Gray, Mathews, and MacRobert, *A Treatise on Bessel Functions* (Macmillan Company, Ltd., London, 1931).

[22] The spacing of the rotational line centers is unimportant for the present analysis as long as overlapping of rotational lines does not occur.

IV. CALCULATIONS OF INTEGRATED ABSORPTION OF ROTATIONAL LINES FOR DIATOMIC MOLECULES

The following outline of the calculation of integrated absorption for diatomic molecules is valid for emitters which are in thermodynamic equilibrium for the local conditions of temperature and pressure.

The integrated absorption for transitions from the ground vibrational level for the rotational lines of a diatomic molecule, in the region of the fundamental vibration-rotation spectrum, is given by Oppenheimer's equation.[18,23] Thus,

$$S^{0\to1}_{j\to j-1}=\frac{N_T\pi\epsilon^2}{3\mu c}\frac{\nu^{0\to1}_{j\to j-1}}{\nu_{0\to1}}\times\frac{j\exp(-E_{0,j}/kT)}{\sum_n\sum_j(2j+1)\exp(-E_{n,j}/kT)}FG, \quad (26)$$

and

$$S^{0\to1}_{j-1\to j}=\frac{N_T\pi\epsilon^2}{3\mu c}\frac{\nu^{0\to1}_{j-1\to j}}{\nu_{0\to1}}\times\frac{j\exp(-E_{0,j-1}/kT)}{\sum_n\sum_j(2j+1)\exp(-E_{n,j}/kT)}F'G'. \quad (27)$$

Here, N_T = total number of emitting molecules per unit volume per unit of total pressure; μ = reduced mass of the diatomic molecule under discussion; c = velocity of light; ϵ = effective charge, which must be determined empirically;[15,17,18,24,25] $\nu_{0\to1}$ = wave number corresponding to the (forbidden) transition $j=0\to j=0$ and $n=0\to n=1$; $E_{n,j}$ = energy of the n'th vibrational and j'th rotational level;

$$F=1+4\gamma j[1+(5\gamma j/8)-(3\gamma/8)];$$
$$F'=1-4\gamma j[1-(5\gamma j/8)-(3\gamma/8)];$$

$\gamma=h/4\pi^2I\nu_{0\to1}$, where I represents the moment of inertia of the emitting molecule; $G=1-\exp(-hc\nu^{0\to1}_{j\to j-1}/kT)$; and $G'=1-\exp(hc\nu^{0\to1}_{j-1\to j}/kT)$.

The wave numbers $\nu^{n\to n'}_{j\to j'}$ are determined by the use of Planck's equation from the expression for $E_{n,j}$, i.e.,

$$E_{n,j}=(n+\tfrac{1}{2})hc\nu_e-(n+\tfrac{1}{2})hcx_e\nu_e+j(j+1)hc\beta_e-j^2(j+1)^2hcD_e-(n+\tfrac{1}{2})j(j+1)hc\alpha', \quad (28)$$

where ν_e, x_e, β_e, D_e, and α' are empirical constants which are usually known with a high degree of accuracy.[26,27]

[23] J. R. Oppenheimer, Proc. Cambridge Phil. Soc. **23**, 327 (1926).
[24] E. Bartholomé, Z. Physik **B23**, 131 (1933).
[25] Thorndike, Wells, and Wilson, Jr., J. Chem. Phys. **15**, 157 (1947).
[26] G. Herzberg, *Molecular Spectra and Molecular Structure. I, Diatomic Molecules* (Prentice-Hall, Inc., New York, 1939, or D. Van Nostrand Company, Inc., New York, 1950).
[27] H. Sponer, *Molekülspektren* (Verlag. Julius Springer, Berlin, 1935).

The integrated absorption for transitions from vibrational levels above the ground level is not known accurately since a complete solution, taking account of vibration-rotation interactions, does not appear to have been obtained for this problem. As a first approximation the following relation, which can be shown to be valid for the integrated absorption over the entire vibration-rotation band of a harmonic oscillator, may be used:

$$\frac{S^{n\to n'+1}_{j\to j'}}{S^{0\to1}_{j\to j'}}=(n+1)\frac{\nu^{n\to n+1}_{j\to j'}}{\nu^{0\to1}_{j\to j'}}\{\exp[-(E_{n,j}-E_{0,j})/kT]\}\times[1-\exp(-hc\nu^{n\to n+1}_{j\to j'}/kT)]\times[1-\exp(-hc\nu^{0\to1}_{j\to j'}/kT)]^{-1}. \quad (29)$$

A somewhat more satisfactory relation than Eq. (29) is obtained from the analysis of Scholz[28] for a diatomic molecule whose interatomic interaction is described by a Morse potential. The treatment of Scholz can be shown to lead to the conclusion that for arbitrary vibrational transitions $n\to n'$

$$\frac{S^{n\to n'}_{j\to j'}}{S^{0\to1}_{j\to j'}}=f(n,n')\frac{\nu^{n\to n'}_{j\to j'}}{\nu^{0\to1}_{j\to j'}}\{\exp[-(E_{n,j}-E_{0,j})/kT]\}\times[1-\exp(-hc\nu^{n\to n'}_{j\to j'}/kT)]\times[1-\exp(-hc\nu^{0\to1}_{j\to j'}/kT)]^{-1}, \quad (30)$$

where

$$f(n,n')=[(k'-3)/(k'-2)^2]^{-1}\times\frac{1}{(n-n')^2}\frac{(k'-1-2n)(k'-1-2n')}{(k'-1-n-n')^2}\times\frac{n!}{(n-n')!n'!}\frac{(k'-n-1)!(n-n')}{(k'-n'-1)!}. \quad (31)$$

Here, k' is the nearest integer less than $4D/hc\nu_{0\to1}$, where D represents the dissociation energy of the molecule under discussion. For transitions of the type $n\to n+1$, it is readily seen that $f(n,n')\simeq n+1$ for small values of n and that, therefore, Eq. (29) will lead to results which are nearly identical with those obtained from Eqs. (30) and (31).

By the use of Eqs. (26), (27), and (29) or of Eqs. (30) and (31), it is possible to calculate, probably with adequate precision, the values of the integrated absorption for diatomic molecules at any desired temperature.

[28] K. Scholz, Z. Physik **78**, 751 (1932).

TABLE I. Integrated absorption of rotational lines for carbon monoxide at 2000°K, for 0→1 vibrational transitions.

Rotational transitions $j \to j-1$	$\frac{3\mu cQ(T)}{N_T\pi\epsilon^2} S^{0\to1}_{j\to j-1}$	Rotational transitions $j-1 \to j$	$\frac{3\mu cQ(T)}{N_T\pi\epsilon^2} S^{0\to1}_{j-1\to j}$
1→ 0	0.3617	0→ 1	0.3594
2→ 1	0.7227	1→ 2	0.7135
4→ 3	1.4301	3→ 4	1.3940
6→ 5	2.0997	5→ 6	2.0197
8→ 7	2.7077	7→ 8	2.6034
10→ 9	3.2380	9→10	3.0356
12→11	3.6752	11→12	3.4014
14→13	4.0108	13→14	3.6637
16→15	4.2392	15→16	3.8220
18→17	4.3616	17→18	3.8814
20→19	4.3820	19→20	3.8492
22→21	4.3318	21→22	3.7363
24→23	4.1597	23→24	3.5573
26→25	3.9412	25→26	3.3252
28→27	3.6711	27→28	3.0555
30→29	3.3643	29→30	2.7626
32→31	3.0357	31→32	2.4585
34→33	2.6691	33→34	2.1558
36→35	2.3650	35→36	1.8624
38→37	2.0436	37→38	1.5864
40→39	1.7410	39→40	1.3331
42→41	1.4641	41→42	1.1048
44→43	1.2149	43→44	0.9036
46→45	0.9954	45→46	0.7293
48→47	0.8051	47→48	0.5812
50→49	0.6432	49→50	0.4572
52→51	0.5075	51→52	0.3554
54→53	0.3956	53→54	0.2728
56→55	0.3077	55→56	0.2068
58→57	0.2327	57→58	0.1550
60→59	0.1746	59→60	0.1147
62→61	0.1298	61→62	0.0839
64→63	0.0955	63→64	0.0607
66→65	0.0694	65→66	0.0435
68→67	0.0499	67→68	0.0306
70→69	0.0355	69→70	0.0214
72→71	0.0249	71→72	0.0148
74→73	0.0173	73→74	0.0101
76→75	0.0119	75→76	0.0068
78→77	0.0081	77→78	0.0045
80→79	0.0055	79→80	0.0030
85→84	0.0019	85→86	0.0008
90→89	0.0006	90→91	0.0003
95→94	0.0002	95→96	0.0001

Hence, the quantities x_j, defined by Eq. (16), can be expressed as a given number multiplying the partial pressure or number density of the emitter. The rotational half-width, which appears to be the least reliably known quantity entering into the calculation of x_j, is evaluated by use of the method described in Appendix I.

The quantities $[3\mu cQ(T)/N_T\pi\epsilon^2]S^{0\to1}_{j\to j-1}$ and $[3\mu cQ(T)/N_T\pi\epsilon^2]S^{0\to1}_{j-1\to j}$ appearing in Eqs. (26) and (27) have been calculated for carbon monoxide over a wide range of temperatures by use of the spectroscopic constants of Sponer.[27] The results of these calculations at 2000°K are reproduced in Table I.

The numerical value of the effective charge ϵ must be determined from quantitative infrared absorption measurements.[29] The value for CO is 3.14×10^{-10} esu.[30] For ideal gases N_T is given by the relation

$$N_T = 7.34\times10^{21}/T \text{ (molecules/cc}\times\text{atmos)}.$$

The reduced mass μ of the emitter is readily calculated, and the partition function $Q(T)$ can be determined by standard statistical methods.[31] For CO at 2000°K it is found that

$$\frac{N_T\pi\epsilon^2}{3\mu cQ(T)} = 0.0888 \text{ cm}^{-1}\times(\text{cm atmos})^{-1}. \quad (32)$$

By use of the numerical constant for $N_T\pi\epsilon^2/3\mu cQ(T)$ given in Eq. (32), it is a simple matter to convert the values given in Table I to absolute values for the integrated absorption for each of the indicated transitions. The absolute values of integrated absorption for transitions from excited energy levels may then be determined by the use of Eq. (29) or of Eqs. (30) and (31).

In order to illustrate the method used for practical calculations, it will now be shown that the intensity output from CO at 2000°K in a representative interval $\Delta\nu$ which is 20-cm^{-1} wide should be adequate for quantitative detection with a standard infrared spectrometer.

In order to calculate the intensity of radiation emitted from carbon monoxide radiators in the wave number range between 2080 and 2100 cm^{-1} the contributions from each of the radiating rotational lines must be included. Preliminary estimates based on statistical equilibrium calculations indicate that the population densities of molecules in vibrational energy levels above the fourth is negligibly small. For transitions originating in the first four vibrational energy levels, the rotational lines listed in Table II must be included in the wave number range 2080 to 2100 cm^{-1}. The line centers given in Table II were obtained by use of Sponer's spectroscopic constants.[27] These wave number values may require slight revision in absolute value as the result of more recent work by Lagemann *et al.*[32] and by Herzberg and Rao.[33] However, if Sponer's spectroscopic data are used for calibration of the spectrometer, as well as for flame emission studies, no corrections for new wave number assignments will be required. Included in Table II are absolute values for the integrated absorption which were computed from the data given in Table I by the use of Eqs. (30), (31), and (32).

The data listed in Table II permit the calculation of $J(\bar{\nu}, T_{Br1})\Delta\nu$ and $J(\bar{\nu}, T_{Br2})\Delta\nu$ from Eqs. (17) and (18) for given values of p, L, and α. In particular, for $p=20$

[29] L. A. Matheson, Phys. Rev. **40**, 813 (1932).

[30] This value for the effective charge is based on extensive infrared absorption measurements on CO carried out by the author and D. Weber. Details concerning this work will be described in a forthcoming publication. It should be noted that the value $\epsilon=3.14\times10^{-10}$ esu compares favorably with the result $\epsilon=3.18\times10^{-10}$ esu based on Havens infrared dispersion measurements (see R. J. Havens, dissertation, University of Wisconsin, Madison, 1938) although it is considerably smaller than the effective charge $\epsilon=3.9\times10^{-10}$ esu calculated from Matheson's measurements (see reference 29).

[31] J. E. Mayer and M. G. Mayer, *Statistical Mechanics* (John Wiley & Sons, Inc.) New York, 1946).

[32] Lagemann, Nielsen, and Dickey, Phys. Rev. **72**, 284 (1947).

[33] K. N. Rao, J. Chem. Phys. **18**, 213 (1950).

mm of mercury, $L=10$ cm, and $\alpha=10^{-2}$ cm^{-1}, i.e., $pL/2\pi\alpha=4.188$ cm$\times$(cm atmos), it is found that

$$J(\bar{\nu}, T_{Br1})\Delta\nu=0.340J(\bar{\nu}, 2000) \text{ ergs/cm}^2 \times\sec\times 2\pi \text{ steradians},$$

and, for $\bar{R}=1$,

$$J(\bar{\nu}, T_{Br2})\Delta\nu=0.526J(\bar{\nu}, 2000) \text{ ergs/cm}^2 \times\sec\times 2\pi \text{ steradians}.$$

Reference to the preceding results shows that, for the particular problem under discussion, introduction of a reflecting mirror should increase the observed radiant intensity by a factor of 1.55. Furthermore, the absolute value of $J(\bar{\nu}, T_{Br1})\Delta\nu$ is 1.74×10^4 ergs/cm$^2\times\sec\times 2\pi$ steradians.

In practice it should be possible to focus 1 percent of the radiant intensity emitted into a solid angle of 2π-steradians on a thermopile. If the radiating surface has an area of 0.1 cm^2 (preferably in the shape of a rectangle, 1X0.1 cm), it is apparent that the thermopile would receive about 18 ergs/sec. In a Model 12C Perkin-Elmer infrared spectrometer, the thermopile will develop an emf of 6 to 10 microvolts per microwatt. Hence, the output of the thermopile should be of the order of 10 microvolts, i.e., 100 times the output necessary to produce a deflection of several inches on the recording system. Therefore, for the indicated conditions, it should be possible to detect as little as 1 percent of CO radiating at 2000°K in the flame, provided the CO emission bands are not masked by stronger bands such as CO_2 emission bands.

V. CONCLUSIONS

On the basis of the discussion presented in Sections II through IV, it appears justifiable to arrive at the following conclusions:

1. The two-path method can be used with an instrument of limited resolving power for simultaneous temperature and concentration measurements of emitters in combustion flames.

2. For diatomic emitters the calculation of concentration and temperature can be carried out readily, if the dispersion formula is used to represent the absorption coefficient for individual rotational lines. For more general types of line shape it is still possible to carry through the necessary numerical calculations.

3. The intensity output from an emitter such as carbon monoxide in a combustion flame, burning at a total pressure of about 20 mm, should be adequate for detection with standard infrared instruments.

4. The experimental problems involved in realizing spatial resolution of the flame, as well as intensity output sufficient for quantitative analysis of concentrations, appear to be of considerable complexity for a number of reasons. Among the important problems which remain to be settled experimentally are those concerned with isolation of isothermal regions and disturbances of the combustion pattern by the probes. Furthermore, it is apparent that the sensitivity of detection and, therefore, the ultimate limits of spatial analysis will be greatly improved by replacing the infrared spectrometer with its thermopile receiver by a suitable combination of filters and a photo-conducting cell. Whether or not this refinement in technique is warranted cannot be said until current experimental work on the low pressure combustion flame has been completed.

APPENDIX I. NUMERICAL CALCULATIONS OF LINE WIDTHS AND LINE SPACING FOR CARBON MONOXIDE

The Doppler half-width α_D of rotational lines is given by the relation[16]

$$\alpha_D=(\log 2)^{\frac{1}{2}}(2RT/Mc^2)^{\frac{1}{2}}\nu_0, \qquad \text{(A-1)}$$

where R is the gas constant per mole, M represents the molecular weight of the emitter, and ν_0 is the wave number at the center of the rotational line. For CO at 2000°K with ν_0 set equal to 2500 cm^{-1}, it is found that

$$\alpha_D\sim5\times10^{-3} \text{ cm}^{-1}.$$

The half-width α_c, resulting from collision broadening, can be calculated from the relation

$$\alpha_c=(1/\pi)(2\pi kT)^{\frac{1}{2}}N_T\rho^2[(m_1+m_2)/m_1]^{\frac{1}{2}}, \qquad \text{(A-2)}$$

where ρ is the empirically determined optical collision diameter, and m_1 and m_2 represent, respectively, the masses of the perturbing and absorbing molecules. Since the value of α_c for CO at room

TABLE II. Line centers and integrated absorption at 2000°K of rotational lines of carbon monoxide in the wave number interval 2080 to 2100 cm^{-1}.

Vibrational transition	Rotational transition	Line center, cm^{-1}	$S_{j\to j\pm1}^{n\to n+1}$ (cm^{-2}-atmos^{-1})
$n=0\to n=1$	$j=15\to j=14$	2080.7	0.366
	$j=14\to j=13$	2085.0	0.357
	$j=13\to j=12$	2089.3	0.341
	$j=12\to j=11$	2093.6	0.327
	$j=11\to j=10$	2097.9	0.307
$n=1\to n=2$	$j=9\to j=8$	2080.1	0.112
	$j=8\to j=7$	2084.2	0.102
	$j=7\to j=6$	2088.3	0.091
	$j=6\to j=5$	2092.3	0.079
	$j=5\to j=4$	2096.2	0.066
$n=2\to n=3$	$j=2\to j=1$	2081.6	0.0082
	$j=1\to j=0$	2085.4	0.0041
	$j=0\to j=1$	2093.0	0.0041
	$j=1\to j=2$	2096.7	0.0081
$n=3\to n=4$	$j=4\to j=5$	2080.9	0.0055
	$j=5\to j=6$	2084.4	0.0065
	$j=6\to j=7$	2087.9	0.0074
	$j=7\to j=8$	2091.4	0.0084
	$j=8\to j=9$	2094.8	0.0091
	$j=9\to j=10$	2098.2	0.0097
$n=4\to n=5$	$j=12\to j=13$	2081.2	0.0030
	$j=13\to j=14$	2084.4	0.0032
	$j=14\to j=15$	2087.6	0.0032
	$j=15\to j=16$	2090.7	0.0033
	$j=16\to j=17$	2093.8	0.0033
	$j=17\to j=18$	2096.8	0.0034
	$j=18\to j=19$	2099.9	0.0034

temperature and atmospheric pressure is known to be[34] approximately 0.1 cm^{-1}, it follows that at 2000°K and a pressure of 20 mm of mercury

$$\alpha_c \sim 7\times 10^{-3}\ cm^{-1}.$$

Here, it has been assumed that the factor $[(m_1+m_2)/m_1]^{\frac{1}{2}}$ will have approximately the same value in the low pressure flame as in room temperature absorption measurements. This assumption seems to be reasonable, since the molecular weights of CO, O_2, N_2, OH, CO_2, etc. do not differ greatly and since, in any event, α_c does not vary rapidly with m_2.

From the preceding calculations, it is evident that the rotational half-width of CO at 2000°K and 20 mm of mercury pressure will be of the order of 10^{-2} cm^{-1} unless abnormal and unpredictable broadening effects occur. Since the rotational spacing for CO is approximately 4 cm^{-1}, and since at 2000°K the equilibrium population densities of CO molecules in vibrational levels above the fourth or fifth are negligibly small, it may be concluded that, on the average, a rotational line of half-width 10^{-2} cm^{-1} will be found in a spectral range 1 cm^{-1} wide. Thus, the narrow rotational lines are well separated, and very little overlapping of rotational lines should occur.

APPENDIX II. EVALUATION OF INTEGRALS

It is desired to evaluate the infinite integrals

$$I_1=\int_{-\infty}^{\infty}\{1-\exp[-(P_\nu)_{j\to j\pm 1}^{n\to n+1}pL]\}d\nu \qquad \text{(A-3)}$$

and

$$I_2=\int_{-\infty}^{\infty}\{1-\exp[-(P_\nu)_{j\to j\pm 1}^{n\to n+1}pL]\}\times\{1+\bar{R}\exp[-(P_\nu)_{j\to j\pm 1}^{n\to n+1}pL]\}d\nu, \qquad \text{(A-4)}$$

where

$$(P_\nu)_{j\to j\pm 1}^{n\to n+1}=\frac{S_{j\to j\pm 1}^{n\to n+1}}{\pi}\,\frac{\alpha}{(\nu-\nu_{j\to j\pm 1}^{n\to n+1})+\alpha^2}. \qquad \text{(A-5)}$$

Introducing Eq. (A-5) into Eq. (A-3) and making the substitutions used by Elsasser,[8]

$$x_j=S_{j\to j\pm 1}^{n\to n+1}pL/2\pi\alpha \qquad \text{(A-6)}$$

and

$$(\nu-\nu_{j\to j\pm 1}^{n\to n+1})/\alpha=\tan(S/2) \qquad \text{(A-7)}$$

leads to the result

$$I_1=\alpha\int_{-\pi}^{\pi}[1-\exp(-x_j\cos S-x_j)]d[\tan(S/2)]. \qquad \text{(A-8)}$$

Integration by parts of Eq. (A-8) leads to the relation

$$I_1=\alpha\left|[1-\exp(-x_j\cos S-x_j)]\Big/\cot(S/2)\right|_{-\pi}^{\pi}+\alpha\int_{-\pi}^{\pi}x_j\sin S[\exp(-x_j\cos S-x_j)]\tan(S/2)dS.$$

The first term on the right-hand side of the preceding expression can be shown to vanish at $+\pi$ and at $-\pi$ by application of l'Hospital's rule. Hence,

$$I_1=\alpha x_j\exp(-x_j)\int_{-\pi}^{\pi}(1-\cos S)[\exp(-x_j\cos S)]dS. \qquad \text{(A-9)}$$

The Bessel functions of order n are $J_n(z)$ and may be defined (see p. 64 of reference 21) by the relation

$$J_n(z)=[(-i)^n/\pi]\int_0^{\pi}[\exp(iz\cos S)]\cos(nS)dS. \qquad \text{(A-10)}$$

Since the cosine is an even function, it is evident that

$$J_n(z)=[(-i)^n/2\pi]\int_{-\pi}^{\pi}[\exp(iz\cos S)]\cos(nS)dS. \qquad \text{(A-11)}$$

Hence, in particular,

$$J_0(ix_j)=(1/2\pi)\int_{-\pi}^{\pi}[\exp(-x_j\cos S)]dS \qquad \text{(A-12)}$$

and

$$iJ_1(ix_j)=(1/2\pi)\int_{-\pi}^{\pi}[\exp(-x_j\cos S)]dS. \qquad \text{(A-13)}$$

Comparison of Eq. (A-9) with Eqs. (A-12) and (A-13) leads to the result

$$I_1=2\pi\alpha x_j[\exp(-x_j)][J_0(ix_j)-iJ_1(ix_j)]. \qquad \text{(A-14)}$$

The integral I_2 defined by Eq. (A-4) is evaluated by the same procedure which was used to obtain Eq. (A-14) for I_1. Introduction of Eqs. (A-5), (A-6), and (A-7) into Eq. (A-4) leads to the relation

$$I_2=\alpha\int_{-\pi}^{\pi}[1-\exp(-x_j\cos S-x_j)]d[\tan(S/2)]+\alpha\bar{R}\int_{-\pi}^{\pi}[1-\exp(-x_j\cos S-x_j)]\times[\exp(-x_j\cos S-x_j)]d[\tan(S/2)]. \qquad \text{(A-15)}$$

The first integral on the right-hand side of Eq. (A-15) is evidently equal to I_1. The second integral in Eq. (A-15) can again be integrated by parts. Proceeding as before leads to the result

$$I_2=I_1(1-\bar{R})+4\pi\alpha x_j[\exp(-2x_j)][J_0(2ix_j)-iJ_1(2ix_j)]. \qquad \text{(A-16)}$$

[34] L. A. Matheson, Phys. Rev. **40**, 813 (1932). Recent infrared absorption measurements carried out by the author and D. Weber indicate that the rotational half-width for CO broadened by H_2 is only about 0.08 cm^{-1} $atmos^{-1}$. The effect of the choice of a somewhat smaller rotational half-width on the present calculations is of minor importance and will, therefore, be ignored.

The Visco-Elastic Properties of Solutions of Rod-Like Macromolecules

JOHN G. KIRKWOOD AND PETER L. AUER
*Gates and Crellin Laboratories of Chemistry, California Institute of Technology, Pasadena, California**
(Received December 4, 1950)

The general theory of irreversible processes in solutions of macromolecules is employed to investigate the visco-elastic behavior of solutions of rod-like macromolecules. It is found that rotatory diffusional torques are responsible for three-fourths of the stationary intrinsic viscosity. Under the action of periodic shear waves, the rotatory diffusional contribution to the stress exhibits relaxation phase lag and imparts a rigidity to the solution. As the frequency is increased, the intrinsic viscosity drops to one-fourth of its stationary value and the rigidity modulus increases to an asymptotic value of $3RT/5$ per mole/cm³ of solute.

A GENERAL theory of the visco-elastic properties of solutions of macromolecules has been developed in a previous article.[1] In the present article, we shall apply the methods of the general theory to a detailed investigation of the visco-elastic behavior of solutions of rod-like macromolecules, supplementing the theory of the intrinsic viscosity of such molecules developed by Riseman and Kirkwood.[2]

It has been shown that in order to take proper account of brownian motion, the hydrodynamic torques exerted by the solvent on a macromolecule must be equated not to zero, as is customarily done, but to the rotatory diffusional torques arising from the statistical orientation of the molecules in the velocity field of the solvent. It is then found that the rotatory diffusional torques contribute a term linear in the rate of shear to the stress and thus to the newtonian part of the viscosity. This term exhibits relaxation phase lags in the nonstationary case, imparting a rigidity to the solution, as observed by Mason and Baker and collaborators in the propagation of shear waves through solutions of macromolecules.[3] In the stationary case, the rigidity modulus vanishes, but the rotatory diffusion torques then make an important contribution to the intrinsic viscosity.

The necessity of introducing rotatory diffusion corrections into the theory of intrinsic viscosity was recognized by Simha[4] and Kuhn,[5] although their methods differ somewhat from our own. In a later part of the paper, we shall compare our results with those of Simha and show that they agree in the static limiting intrinsic viscosity.

Our model of the rod-like macromolecule is a rigid array of $2n+1$ groups, each with a friction constant, ζ, spaced at equal intervals b on a linear axis of length L. The internal coordinates of the molecule are therefore two in number, the polar angle ϑ and azimuthal angle φ specifying the orientation of the axis relative to an external coordinate system. We suppose the molecule to be bathed in solvent, in which the unperturbed velocity at a point $\mathbf{R}$ from the position of the center of mass of the molecule is given by

$$\mathbf{V}^0=\dot{\epsilon}(\mathbf{e}_y\cdot\mathbf{R})\mathbf{e}_x \qquad \dot{\epsilon}=i\omega\epsilon_0 e^{i\omega t}, \tag{1}$$

where $\dot{\epsilon}$ is the rate of strain in a periodic shear wave, propagated in the z-direction, and $\mathbf{e}_x$ and $\mathbf{e}_y$ are unit vectors in the x and y directions. By Eqs. (I24), (I25), and (I26) of our article on the general theory of visco-elastic properties,[1] which will here be designated as I, the intrinsic viscosity $[\eta]$ and intrinsic rigidity $[\mu]$ of the solution are,

$$[\eta]=N\zeta G'/100M\eta_0$$
$$[\mu]=N\zeta G''/100M$$
$$[\eta]=\lim_{c\to 0}\eta-\eta_0/\eta_0 c \qquad [\mu]=\lim_{c\to 0}\mu/c, \tag{2}$$

where η_0 is the viscosity coefficient of the solvent, N Avogadros number, M the molecular weight, c the concentration of the macromolecular sepcies in grams per 100 grams of solvent, and G' and $-G''$ are the real and imaginary parts of the velocity perturbation function G, given by

$$G=G'-iG''$$
$$G=-\frac{1}{\zeta\dot{\epsilon}}\sum_{l=-n}^{+n}\langle(\mathbf{e}_x\cdot\mathbf{F}_l)(\mathbf{e}_y\cdot\mathbf{R}_{0l})\rangle_{Av}, \tag{3}$$

where the sum extends over all groups of the molecule, $-n\leq l\leq+n$, $\mathbf{R}_{0l}$ is the position of group l relative to the molecular center of mass, and $\mathbf{F}_l$ is the hydrodynamic resistance exerted by group l on the surrounding solvent. The average is to be taken in the space of the internal coordinates ϑ and φ with a probability distribution function $f(\vartheta,\varphi)$ determined by the equation of rotatory diffusion. Since the $\mathbf{F}_l$ are proportional to $\dot{\epsilon}$ in the limit of low rates of shear, the averages may be calculated with the unperturbed uniform distribution in the space of the internal coordinates, if only Newtonian terms in the stress are desired. However, the forces $\mathbf{F}_l$ depend, in an important manner, on the gradients of

* Contribution No. 1502.
[1] J. G. Kirkwood, Rec. trav. chim. **68**, 649 (1949).
[2] J. Riseman and J. G. Kirkwood, J. Chem. Phys. **18**, 512 (1950).
[3] Mason, Baker, McSkemin, and Heiss, Phys. Rev. **73**, 1074 (1948).
[4] R. Simha, J. Phys. Chem. **44**, 25 (1940); J. Research. Nat. Bur. Standards **42**, 409 (1949).
[5] W. Kuhn, Helv. Chim. Acta **28**, 97 (1945).

$f(\vartheta, \varphi, t)$ produced by the statistical orientation of the molecules in the velocity field of the solvent, which are also linear in $\dot{\epsilon}$ for small rates of shear and thus affect the linear terms in the $\mathbf{F}_l$, contributing to newtonian terms in the stress.

Equations (I29), determining the hydrodynamic forces $\mathbf{F}_l$ assume the following form for the present model,

$$\mathbf{F}_l+\lambda_0 \sum_{\substack{s=-n \\ \neq l}}^{+n} \frac{(\mathbf{1}+\mathbf{e}_R\mathbf{e}_R)}{|l-s|}\cdot\mathbf{F}_s=-\zeta lb\Big\{\dot{\epsilon}\sin^2\vartheta\sin2\varphi\mathbf{e}_R/2 + D^{\vartheta\vartheta}\frac{\partial \log f}{\partial\vartheta}\mathbf{e}_\vartheta+D^{\varphi\varphi}\sin\vartheta\frac{\partial \log f}{\partial\varphi}\mathbf{e}_\varphi\Big\}$$

$$\lambda_0=\zeta/8\pi\eta_0 b, \tag{4}$$

where $D^{\vartheta\vartheta}$ and $D^{\varphi\varphi}$ are the rotatory diffusion constants associated with the coordinates ϑ and φ, $\mathbf{1}$ is unit tensor, and $\mathbf{e}_\vartheta$, $\mathbf{e}_\varphi$, $\mathbf{e}_R$ are the unit vectors associated with ϑ and φ, and with the direction of the molecular axis. Equation (I14) yields for the diffusion constants,

$$D^{\vartheta\vartheta}=kT(1+\gamma)/\zeta\sigma b^2,$$

$$D^{\varphi\varphi}=\frac{kT}{\zeta\sigma b^2}\frac{(1+\gamma)}{\sin^2\vartheta},$$

$$\sigma=\sum_{l=-n}^{+n} l^2=n(n+1)(2n+1)/3,$$

and

$$\gamma=\frac{2\lambda_0}{\sigma}\sum_{\substack{l'=-n \\ l'<l}}^{+n}\frac{ll'}{|l-l'|}. \tag{5}$$

With the use of the rotatory diffusion constants of Eq. (5), Eq. (I17), determining the distribution function $f(\vartheta, \varphi, t)$, becomes,

$$\frac{1}{\sin\vartheta}\frac{\partial}{\partial\vartheta}\left(\sin\vartheta\frac{\partial f}{\partial\vartheta}\right)+\frac{1}{\sin^2\vartheta}\frac{\partial^2 f}{\partial\varphi^2}-6\tau\frac{\partial f}{\partial t} =6i\omega\tau\epsilon_0 e^{i\omega t}\Big\{-\tfrac{3}{2}\sin^2\vartheta\sin2\varphi f + \tfrac{1}{4}\sin2\vartheta\sin2\varphi\frac{\partial f}{\partial\vartheta}-\sin^2\varphi\frac{\partial f}{\partial\varphi}\Big\}$$

$$\tau=\frac{\sigma b^2\zeta}{6(1+\gamma)kT}. \tag{6}$$

When the distribution function $f(\vartheta, \varphi, t)$ is expanded in powers of the amplitude ϵ_0 of the shear wave, Eq. (1) is in the form

$$f(\vartheta, \varphi, t)=\frac{1}{4\pi}+\frac{i\omega\epsilon_0 e^{i\omega t}}{4\pi}f_1(\vartheta, \varphi)+0(\epsilon_0^2). \tag{7}$$

Equation (6) yields for the function $f_1(\vartheta, \varphi)$,

$$f_1(\vartheta, \varphi)=\frac{3}{2}\frac{\tau}{1+i\omega\tau}\sin^2\vartheta\sin2\varphi, \tag{8}$$

which is sufficient for determining the terms in $\mathbf{F}_l$ of Eqs. (4), linear in the rate of strain. In the static case, with $\omega=0$ and $\dot{\epsilon}=\lim_{\omega\to0} i\omega\epsilon_0$, $f_1(\vartheta, \varphi)$ also determines the flow birefringence of the solution arising from statistical orientation of the macromolecules.

Expansion of the right-hand sides of Eqs. (4) in powers of ϵ_0, and substitution of $f_1(\vartheta, \varphi)$ from Eq. (8) leads to the following expressions for the hydrodynamic forces $\mathbf{F}_l$, to terms linear in the rate of strain,

$$\mathbf{F}_l\cdot\mathbf{e}_R=-\frac{\zeta\dot{\epsilon}b}{2}\psi_l(2\lambda_0)\sin^2\vartheta\sin2\varphi,$$

$$\mathbf{F}_l\cdot\mathbf{e}_\vartheta=-\frac{\zeta\dot{\epsilon}b}{4}\psi_l(\lambda_0)\frac{\sin2\vartheta\sin2\varphi}{1+i\omega\tau},$$

and

$$\mathbf{F}_l\cdot\mathbf{e}_\varphi=-\frac{\zeta\dot{\epsilon}b}{2}\psi_l(\lambda_0)\frac{\sin\vartheta\cos2\varphi}{1+i\omega\tau}, \tag{9}$$

where the functions $\psi_l(\lambda)$ satisfy the system of equations,

$$\psi_l+\lambda\sum_{\substack{s=-n \\ \neq l}}^{+n}\frac{\psi_s}{|l-s|}=l;\quad -n\le l\le+n \tag{10}$$

which for large n are asymptotically approximated by the integral equation of Kirkwood and Riseman,[2]

$$\psi(x)=nx-\lambda\int_{-1}^{+1}K(x, y)\psi(y)dy$$

$$x=l/n;\quad y=s/n$$

$$K(x, y)=1/(x-y);\quad -1\le y\le x-1/n$$

$$=0;\qquad x-1/n<y<x+1/n$$

$$=1/(y-x);\quad x+1/n\le y\le+1. \tag{11}$$

The integral equation (11) has been solved by Kirkwood and Riseman in the form,

$$\psi(x)=\frac{2n}{\pi}\sum_{k=1}^{\infty}\frac{(-1)^{k+1}}{k}\frac{\sin kx}{1-2\lambda Ci[\pi k/n]}$$

$$Ci(x)=\int_{\infty}^{x}\frac{\cos u}{u}du. \tag{12}$$

Substitution of Eqs. (9) and (12) into Eq. (3), and replacing the summation in the expression for G by an integration over the variable x, leads to the following expressions for the intrinsic viscosity and intrinsic

rigidity of the solution of Eq. (2),

$$[\eta]=\frac{N\zeta L^2}{18000M_0\eta_0}\left\{F(2\lambda_0, L)+\frac{3}{2}\frac{F(\lambda_0, L)}{1+\omega^2\tau^2}\right\},$$

$$[\mu]=\frac{N\zeta L^2}{12000M_0\tau}\frac{\omega^2\tau^2}{1+\omega^2\tau^2}F(\lambda_0, L),$$

$$F(\lambda, L)=\frac{6}{\pi^2}\sum_{k=1}^{\infty}\frac{1}{k^2}\frac{1}{1-2\lambda Ci[2\pi kb/L]},$$

$$L=(2n+1)b; \quad M_0=M/(2n+1), \tag{13}$$

where L is the length of the molecule, and M_0 is the molecular weight of each of the $2n+1$ elements or monomer units.

Before discussing the significance of the results of Eq. (13), we present the following asymptotic expressions for the function $F(\lambda, L)$ and for the relaxation time τ:

$$F(\lambda, L)=1/2\lambda\log(L/b),$$

and

$$\tau=\pi\eta_0L^3/18kT\log(L/b). \tag{14}$$

The first Part of Eq. (14) is obtained with the use of the asymptotic expression $\log x$ for $Ci(x)$, valid for very small x, and the second is obtained by approximating the sum defining γ of Eqs. (5) and (6) by an integral. Introducing the expressions of Eq. (14) into Eq. (13), we obtain the asymptotic formulas,

$$[\eta]=\frac{\pi NL^2}{9000M_0\log(L/b)}\left\{1+\frac{3}{1+\omega^2\tau^2}\right\},$$

and

$$[\mu]=\frac{6NkT}{1000M}\frac{\omega^2\tau^2}{1+\omega^2\tau^2}. \tag{15}$$

The static value of the intrinsic viscosity, for $\omega=0$, is given by

$$[\eta]_0=\frac{4\pi NL^2}{9000M_0\log(L/b)}. \tag{16}$$

This value is in agreement with the asymptotic form of Simha's formula for the prolate ellipsoid for very large semi-major axis, $L/2$, with the neglect of terms of the order $[\log(a/b)]/[\log(L/b)]$ if M_0 is taken as $\pi\rho a^2L/3n$, where a is the semi-minor axis of the ellipsoid and ρ the density. It differs from the value of Riseman and Kirkwood[2] by a factor 8/15, due to the inadequate treatment of brownian motion and other approximations in the earlier theory.

We remark from Eq. (15) that with increasing frequency, the intrinsic viscosity decreases from $[\eta]_0$ to an asymptotic value $[\eta]_\infty$ equal to one quarter of $[\eta]_0$, while the intrinsic rigidity $[\mu]$ increases from zero to an asymptotic value $6RT/1000M$. The rigidity of the solution, therefore, approaches the value $3RT/5$ per mole/cm^3 of the macromolecular solute. These predictions are in qualitative agreement with published measurements of the velocity and attenuation of shear waves in liquid high polymers by Mason, Baker, and collaborators[3] and with unpublished measurements in dilute polymer solutions, which they have kindly communicated to us. Quantitative agreement is not to be expected, since the rod-like molecular model is not appropriate for the substances investigated. Explicit application of the general theory to the random coil molecular model, with a distribution in relaxation times, necessary for a detailed interpretation of the results of Mason and Baker, is impeded by purely mathematical obstacles which have not yet been overcome.

Wall Reactions and Diffusion in Static and Flow Systems

ROBERT GOMER
Institute for the Study of Metals, The University of Chicago, Chicago, Illinois
(Received November 22, 1950)

The distribution of radicals at steady state has been computed for simple systems subject to heterogeneous and homogeneous reactions. Sample distributions are given. Expressions for two non-steady-state situations are derived for the case of a first-order gas and first- or second-order wall reaction. The effect of expansion and longitudinal diffusion on radical concentration in flow systems is discussed. Equations governing the former are derived and a method of estimating its effect rapidly is given. Expressions giving the upper limit of the latter are presented. It is shown that expansion may simulate a first-order reaction, and may be of considerable importance in fast flow.

ATTEMPTS to elucidate in detail processes occurring on surfaces require a knowledge of the concentration of the reacting species at the surface. For instance, it is impossible to determine the mechanism of wall reactions when diffusion of active species to the surface is rate controlling. It is obvious that much valuable information could be obtained if diffusion could be eliminated or if the concentration of active species at the surface could be calculated. In many cases, the situation is complicated by reaction in the gas (or liquid) phase. The present paper discusses some of these effects for simple systems. Since it will be seen that recourse must be had to flow systems in many cases, the effect of expansion and longitudinal diffusion on concentration in such systems will also be discussed, although these factors are of importance whether there is wall reaction or not.

I. DIFFUSION IN SYSTEMS AT STEADY STATE

The case of a single reactive species, present in very small mole fraction, will be considered. We shall allow this species, R, to disappear by homogeneous and wall reactions. We shall limit ourselves to the one-dimensional case. In practice this may be realized for reactions at catalyst surfaces, mirror removal by free radicals, and so on. The conclusions will apply qualitatively to two-dimensional cases. The condition of steady state is:

$$D\frac{d^2c}{dx^2}-f_g(c)+I=0; \tag{1}$$

x represents distance from the origin, D the diffusion coefficient (assumed constant), c concentration of R, I its rate of formation, and $f_g(c)$ its rate of removal by homogeneous reactions. It is assumed that production of R is uniform throughout the vessel. We shall consider the gas phase bounded by two planes $2l$ cm apart and choose the origin midway between them. Reaction is assumed to occur equally on both walls. This model is equivalent to taking the origin at one of the planes and assuming that plane to be inactive. The boundary conditions are:

$$(dc/dx)_{x=0}=0, \tag{2}$$

$$-(dc/dx)_{x=l}=(1/D)f_w(c_2), \tag{3}$$

$$Il=\int_0^l f_g(c)dx+f_w(c_2); \tag{4}$$

$f_w(c)$ represents the rate of wall reaction, c_2 the concentration of R at either wall.

Case 1–1

$f_g(c)=k_1\cdot c$; $f_w(c)=k_2\cdot c$. Solution of Eq. (1) and application of Eqs. (2) and (3) yields:

$$c(x)=c_0(1-b\cosh(k_1/D)^{\frac{1}{2}}x), \tag{5}$$

where b is given by:

$$b=k_2/((k_1D)^{\frac{1}{2}}\sinh m+k_2\cosh m), \tag{6}$$

and c_0 is the steady-state concentration of R in the absence of wall reaction:

$$c_0=I/k_1; \tag{7}$$

m is given by:

$$m=(k_1/D)^{\frac{1}{2}}l. \tag{8}$$

It will be noted that $c(x)/c_0$ is independent of I. It is of interest to evaluate the average concentration, $\bar{c}$:

$$\bar{c}/c_0=1-1/l(k_1/k_2+(k_1/D)^{\frac{1}{2}}\coth m). \tag{9}$$

Case 1–2

$f_g(c)=k_1\cdot c$; $f_w(c)=k_2'c^2$. The solution has the form of Eq. (5), with b given by:

$$b=\frac{(k_1D)^{\frac{1}{2}}\tanh m}{2k_2'\cosh m}\times\left\{1+\frac{2Ik_2'}{(k_1^3D)^{\frac{1}{2}}}\coth m-\left[1+\frac{4Ik_2'}{(k_1^3D)^{\frac{1}{2}}}\coth m\right]^{\frac{1}{2}}\right\}. \tag{10}$$

The average concentration is found from:

$$\bar{c}=c_0(1-(b/l)(D/k_1)^{\frac{1}{2}}\sinh m). \tag{12}$$

Case 2–1

$f_g(c)=k_1'\cdot c^2$; $f_w(c)=k_2\cdot c$. In this case $c_0=(I/k_1)^{\frac{1}{2}}$. Series solution of Eq. (1) yields:

$$c(x)=c_1-a_2x^2-a_4x^4-a_6x^6\cdots-a_{2n}x^{2n}-\cdots. \quad (13)$$

The coefficients of x^{2n} are given by:

$$\begin{aligned} a_2&=(I-k_1'c_1^2)/2!D,\\ a_4&=2\cdot k_1'c_1(I-k_1'c_1^2)/4!D^2,\\ a_6&=2\cdot k_1'(I-k_1'c_1^2)(5k_1'c_1^2-3I)/6!D^3, \end{aligned} \quad (14)$$

up to a_6. The constant of integration c_1 has the physical significance of being the concentration of R at the origin. For small values of c_1, powers higher than the second may be neglected and under these conditions:

$$c_1=[-B+(B^2+4I\cdot A^2/k_1')^{\frac{1}{2}}]/2A, \quad (15)$$

where A and B are given by:

$$\begin{aligned} A&=(k_1'/2D)(2D+k_2l),\\ B&=(k_2/l)-(k_1'\cdot Il^2/3D)-(k_1'\cdot k_2\cdot Il^3/12D^2). \end{aligned} \quad (16)$$

The average concentration is readily seen to be:

$$\bar{c}=c_1-a_2l^2/3-a_4l^4/5-\cdots. \quad (17)$$

Case 2–2

$f_g(c)=k_1'\cdot c^2$; $f_w(c)=k_2'c^2$. $c(x)$ is given by Eqs. (13) and (14) where c_1 is:

$$c_1=[B+(B^2+4AC)^{\frac{1}{2}}]/2A, \quad (18)$$

where:

$$\begin{aligned} A&=D/Il^2-\frac{2}{3}\cdot\frac{k_1'l^2}{D}-\frac{43}{360}\cdot\frac{k_1'^2Il^6}{D^3}+\frac{k_1'D}{Ik_2'l},\\ B&=1+\frac{k_1'l}{3k_2'}-\frac{1}{10}\cdot\frac{k_1'Il^4}{D^2},\\ C&=\frac{D}{k_2'l}-\frac{Il^2}{4D}-\frac{1}{20}\cdot\frac{k_1'Il^3}{k_2'D}. \end{aligned} \quad (19)$$

Powers of c_1 higher than the second have again been neglected. $\bar{c}$ is given by Eq. (17) with the appropriate value of c_1.

It is instructive to apply these results to some hypothetical but reasonable cases. For this purpose we shall consider that R represents CH_3 radicals and that k_1 refers to the reaction:

(Reaction 1) $CH_3+(CH_3)_2CO\rightarrow CH_4+CH_2COCH_3$,

and that k_1' refers to recombination of CH_3 radicals:

(Reaction 1′) $CH_3+CH_3\rightarrow C_2H_6$.

If we consider the radicals to be produced photochemically, it is always possible to adjust light intensities in such a way that reaction 1 or 1′ predominates. Hence, no great loss of generality results by considering these reactions separately. While the second-order homogeneous reaction will predominate as the light intensity is increased, the opposite is true of the heterogeneous reaction. If the latter proceeds for instance by the following mechanism:

(Reaction 2a) $CH_3+M\rightarrow MCH_3$,
(Reaction 2b) $MCH_3\rightarrow M+CH_3$,
(Reaction 2c) $MCH_3+CH_3+M(CH_3)_2\uparrow$,

where M might represent a metal atom on a mirror surface, it will readily be seen that the high intensity limiting rate is:

$$R_{M(CH_3)_2}=k_{2a}\cdot CH_3\cdot M, \quad (20)$$

whereas the low intensity limiting rate is:

$$R_{M(CH_3)_2}=(k_{2a}\cdot k_{2c}/k_{2b})\cdot CH_3^2\cdot M. \quad (21)$$

It follows that the cases of greatest interest would, therefore, be 1–2 and 2–1. We shall, nevertheless, consider only Cases 1–1 and 2–1, since we are chiefly interested here in finding the upper limit of nonuniformity in radical distribution throughout the cell. It is obvious that this will occur when every collision of a radical with the wall leads to its eventual disappearance; this implies a first-order wall reaction.

The following numerical values have been used: $k_1\simeq 10^{10}\times e^{-9500/RT}$ (acetone) sec^{-1}; $k_1'\simeq 10^{14}$ (mole/cc)$^{-1}$ sec^{-1}. These are taken from a recent determination of these constants in the photo-decomposition of acetone.[1] k_2 is equal to the number of effective impacts per cm^2 per sec per unit concentration and is $k_2=1.9\times 10^4\alpha$ cm/sec, α being the ratio of effective to total collisions. The diffusion coefficient for CH_3 radicals in acetone is estimated as $10^2\cdot p^{-1}$ cm^2/sec, p being the total pressure in mm of Hg. All the calculations have been carried out for a cell of half-width $l=0.5$ cm and at 400°K. For Case 2–1 the rates of formation I are indicated on the figures.

Case 1–1

A typical distribution is shown in Fig. 1. Figures 2 and 3 summarize some of the results, which will now be discussed.

$\bar{c}/c_0$—Figure 2 shows that this quantity is least when D is greatest and largest when D is least. For a given value of D, $\bar{c}/c_0$ is largest when k_1 is largest. It will also be noticed from Fig. 1 that $c(x)$ varies very little from $\bar{c}$ over most of the cell, except very close to the wall, even when α is large. Nevertheless, it is seen that even for $\alpha=10^{-4}$, where $c(x)$ is almost uniform up to the wall, $\bar{c}/c_0$ is still only of the order of 10^{-2} for $k_1=10^{-2}$ and of the order of 10^{-1} for $k_1=10^{-1}$. Figure 2 shows the interesting result that $\bar{c}/c_0$ is a very slowly changing function of α for $\alpha>10^{-2}$. The function varies most rapidly in the region $10^{-2}>\alpha>10^{-5}$ and then approaches 1 asymptotically. Figure 2 shows only the lower halves of what are really S-shaped curves.

[1] R. Gomer and G. B. Kistiakowsky, J. Chem. Phys. **13**, 85 (1951).

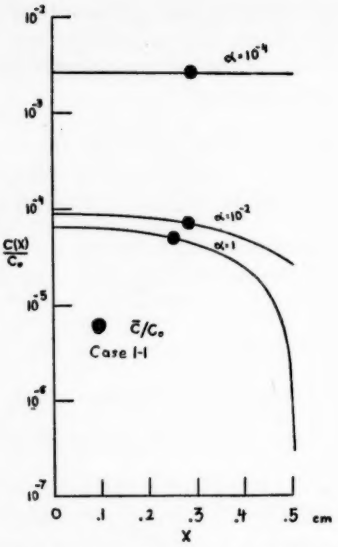

FIG. 1. Distribution of CH_3 concentration with distance for Case 1-1. Acetone pressure 5 mm Hg, $k_1=10^{-2}$ sec^{-1}. $D=20$ cm^2/sec.

$c_2/\bar{c}$—A plot of this quantity *vs* α for various conditions is shown in Fig. 3 and is a measure of conditions at the wall relative to those in the bulk of the gas. It will be seen that D is the critical parameter, $c_2/\bar{c}$ being almost insensitive to a 10-fold increase in k_1 at constant D. It will be seen that for $\alpha>10^{-2}$, c_2 and $\bar{c}$ differ by powers of ten.

Case 2-1

A representative distribution is shown in Fig. 4. It is to be expected that increase in intensity will have the same effect here as an increase in k_1 in Case 1-1. This is seen from Fig. 5, which shows a plot of $\bar{c}/c_0$ *vs* α. The S-shape of the curves is already apparent for the high intensity case. The conclusions drawn for Case 1-1 apply here also. It is interesting to note, however, that a 100-fold increase in I (and, hence, a 10-fold increase in c_0), increases c_2 only very slightly when α is large, so that $c_2/\bar{c}$ is actually less at the higher intensity. This may be seen from Fig. 6. It follows that c_2 is proportional to $\bar{c}$ only for values of α for which the curves of Fig. 6 coincide.

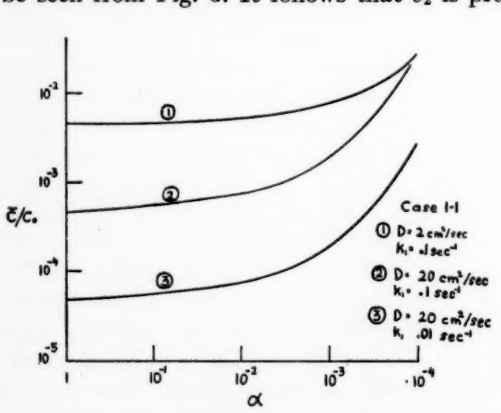

FIG. 2. Mean concentration/unperturbed concentration *vs* α for Case 1-1.

The results just discussed show that the concentration of active species at the wall differs widely from that in the bulk of the gas; there is not even the assurance that a given change in mean gas phase concentration will result in a proportional change in concentration at the wall. Since the evaluation of the detailed mechanism of any surface reaction requires at least a knowledge of relative wall concentrations, it is seen that the use of static systems makes it difficult to draw quantitative conclusions about mechanism, since only the mean gas phase concentration or a ratio of these is usually susceptible to measurement. It is, therefore, of interest to get an idea of the speed with which a reactive surface must move relative to the gas phase to keep c_2 at some desired fraction of c_0. This reduces to a time dependent diffusion problem.

II. TIME DEPENDENT DIFFUSION

The problem just outlined is solved as follows. Imagine that the cell of the preceding section is supplied with a pair of shutters covering the reactive walls. The cell is illuminated for a sufficiently long time to allow R to attain its steady-state concentration c_0. At the instant of counting time, the shutters are removed so that wall reaction now starts to occur. The equation governing concentration as a function of x and t is:

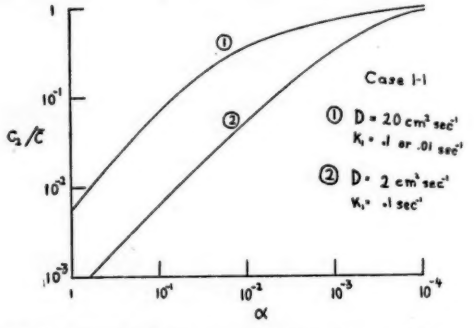

FIG. 3. Wall concentration/mean concentration *vs* α for Case 1-1.

$$D(\partial^2 c/\partial x^2)-(\partial c/\partial t)-f_g(c)=-I. \qquad (22)$$

The general solution of Eq. (22) for Case 1-1 takes the form:

$$c(x,t)=I/k_1+\sum_{a'} g(a')\exp(a'x)\cdot\exp[(a'^2D-k_1)t]. \qquad (23a)$$

Since $c(x,\infty)=c(x)$ as given by Eq. (5), a' must be imaginary, $a'=ia$. Equation (23a) then reduces to the steady state solution Eq. (5) at $t=\infty$, since any assignment of a, other than $a=\pm i(k_1/D)^{\frac{1}{2}}$, leads to terms vanishing at $t=\infty$ The latter values of lead to the term $-b\cosh(k_1/D)^{\frac{1}{2}}x$, so that the initial condition, $c(x,0)=c_0=I/k_1$ requires that

$$\sum_{a\neq\pm i(k_1/D)^{\frac{1}{2}}} g(a)e^{iax}=b\cosh(k_1/D)^{\frac{1}{2}}x.$$

This is accomplished by Fourier expansion of $\cosh(k_1/D)^{\frac{1}{2}}x$ in terms of the orthogonal set $A_n \cos a_n x$, leading to the final result:

$$c(x,t)=c(x)+b\sum_n \frac{a_n \cos a_n x}{k_1/D+a_n^2} \cdot \frac{\exp\{+(k_1/D)^{\frac{1}{2}}l\}[(k_1/D)^{\frac{1}{2}}\cos a_n l+a_n \sin a_n l]-\exp\{-(k_1/D)^{\frac{1}{2}}l\}[(k_1/D)^{\frac{1}{2}}\cos a_n l-a_n \sin a_n l]}{\sin a_n l \cdot \cos a_n l+a_n l} \times \exp[-(Da_n^2+k_1)t]. \quad (23)$$

The a_n's are found from the boundary condition $-D(\partial c/\partial x)_{\substack{t \\ x=l}}=k_2 c(l,t)$ and are given by:

$$a_n=(k_2/D)\cot a_n l. \quad (24)$$

We are now able to find $c(l,t)$ and, hence, the speed at which a surface of given width must travel through the gas stream.

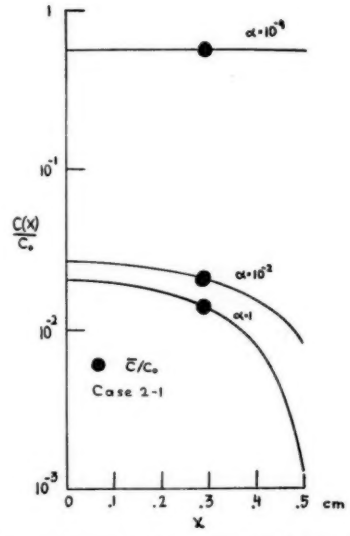

FIG. 4. Distribution of CH_3 concentration with distance for Case 2-1. Acetone pressure 5 mm Hg, $D=20$ cm²/sec, $I=10^{-13}$ mole/cc/sec.

It is also of interest to find out at what rate decay occurs if $I=0$ and if the concentration of R has some value c' at the instant of shutter removal. This is, of course, the problem encountered in mirror removal experiments of the Paneth type, where the assumption is generally made that the rate of mirror removal is proportional to the radical concentration in the gas stream. This assumption is valid only if the wall reaction is first order and if $c(l,t)$ is proportional to c'. For Case 1–1 the solution is:

$$c(x,t)=4c'\sum_n \frac{\sin a_n l}{2a_n l+\sin 2a_n l} \cdot \exp[-(Da_n^2+k_1)t]\cdot \cos a_n x, \quad (25)$$

where a_n is given by Eq. (24). It is seen that for the case of a first-order gas and first-order wall reaction only, there is a linear relation between c' and $c(l,t)$. The two-dimensional case has been worked out for a cylindrical cell by Herzfeld[2] on the assumption of no gas reaction at all and first-order wall reaction. If α is large and k_1 small this will generally be adequate if D is also large. It should be noted, however, that experimental proof is lacking that mirror removal by free radicals proceeds by a first-order reaction. A mechanism similar to the one outlined in the preceding section is actually more likely. Furthermore it must be noted that application of Eq. (25) or Herzfeld's formula should take into account the fact that D is a function of pressure and should, hence, be computed from Eq. (40) as shown in the next section.

The values of a_n to be used in Eqs. (23) and (25) are obtained by bringing Eq. (24) into the form:

$$x=K\cot x; \quad K=k_2 l/D. \quad (26)$$

The roots of Eq. (26) are well known.[3]

III. EXPANSION AND LONGITUDINAL DIFFUSION IN FLOW SYSTEMS

Usually the decrease in concentration of active species due to the expansion in a flow system is neglected. With fast flows the effect is often appreciable, as will be seen.

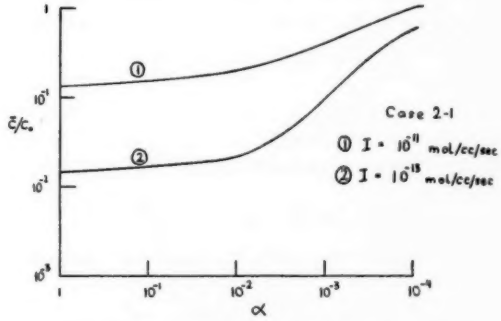

FIG. 5. Mean concentration/unperturbed concentration *vs* α for Case 2-1 $D=20$ cm²/sec.

[2] F. Paneth and K. Herzfeld, Z. Elektrochem. **37**, 577 (1931). The authors replace $\partial c/\partial t$ by $v_0(\partial c/\partial t)$; an error of two or less would result from this.

[3] H. S. Carslaw and J. C. Jaeger [*Conduction of Heat in Solids* (Clarendon Press, Oxford, 1947), p. 377] give the first six roots for values of K up to 100. Equation (26) may also be solved graphically by finding the intersections of the curves $y=\cot x$ and $y=x/K$.

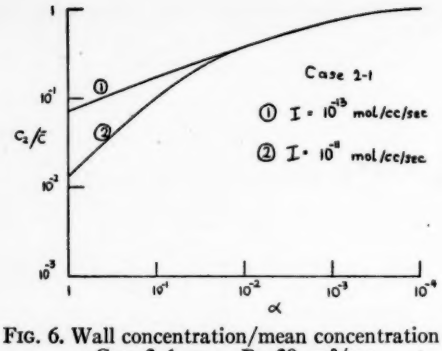

FIG. 6. Wall concentration/mean concentration for Case 2-1. *vs* α. $D=20$ cm²/sec.

We assume that the rate of disappearance of active species due to reaction is given by $-f(c)$; this includes homogeneous and heterogeneous processes. The total rate of change of concentration with time is then given by:

$$\frac{dc}{dt}=\left(\frac{\partial c}{\partial t}\right)_x+\left(\frac{\partial c}{\partial x}\right)_t\frac{dx}{dt}. \tag{27}$$

If a linear pressure gradient is assumed:

$$\left(\frac{\partial c}{\partial x}\right)_t=-c_0/l_0, \tag{28}$$

and

$$dx/dt=v_0/(1-x/l_0). \tag{29}$$

c_0 is the concentration of R at the source, v_0 the linear flow velocity at the source, x the distance from the source at time t, and l_0 that distance from the source at which the total pressure would be zero. Equation (29) follows from conservation of matter, since the mole fraction of R in the gas stream is taken to be small. Integration of Eq. (29) yields:[4]

$$x=l_0\{1-[1-2(v_0/l_0)t]^{\frac{1}{2}}\}. \tag{30}$$

It may be pointed out in passing that it follows from Eq. (30) that $\bar{v}=2v_0$. Equation (27), therefore, becomes:

$$dc/du=f(c)\cdot l_0/2v_0+u^{-\frac{1}{2}}\cdot c_0/2, \tag{31}$$

where:

$$u=(1-2(v_0/l_0)t). \tag{32}$$

Equation (31) can also be expressed in terms of c and x:

$$-dc/dx=f(c)\cdot(l_0-x)/l_0v_0+c_0/l_0. \tag{33}$$

We shall integrate Eq. (33) for the case $f(c)=k_1c$. The result is:

$$c(x)=\frac{c_0\exp[a(l_0-x)^2]}{l_0a^{\frac{1}{2}}}\cdot\left[\int_0^{a^{\frac{1}{2}}(l_0-x)}e^{-n^2}dn-\int_0^{a^{\frac{1}{2}}l_0}e^{-n^2}dn\right]+c_0\exp[+a(x^2-2xl_0)], \tag{34}$$

with a given by:

$$a=k_1/2v_0l_0. \tag{35}$$

The integral occurring in Eq. (34) is the error integral, available in tabular form.[5] If it is desired to evaluate k_1 rather than $c(x)$, Eq. (33) can be rewritten in terms of c_0/c and solved for k_1;

$$k_1=(-d(c/c_0)/dx-1/l_0)(c_0/c)(l_0v_0)/(l_0-x). \tag{33a}$$

Equation (33a) may be solved by finding $d(c/c_0)/dx$ graphically or numerically if a plot of c/c_0 *vs* x can be constructed.

While Eq. (33) may be solved numerically for any given case, if $f(c)$ is a known function of c, this is tedious and a rapid method of estimating the effect of expansion is desirable. This may be done by integrating the terms in Eq. (31) separately. The decrease in concentration due to expansion is:

$$-\Delta c_{\text{exp}}=c_0\cdot(1-u^{\frac{1}{2}}). \tag{36}$$

Equation (36) must be compared with:

$$-\Delta c_{\text{reaction}}=c_0(1-e^{-k_1t}), \tag{37}$$

for the first-order case, and with:

$$-\Delta c_{\text{reaction}}=k_1'c_0^2t/(1+k'c_0t), \tag{38}$$

for the second-order case. Since expansion will tend to make $|\Delta c_{\text{reaction}}|$ smaller than the value given by Eqs. (37) or (38), the sum of Eqs. (36) and (37) or (38) gives an upper limit to the effect.

It is interesting to estimate the magnitude of the expansion effect for a plausible case. If $v_0=10$ m/sec, $l_0=1$ m (the range of Paneth type experiments), it can be seen that a first-order rate constant would have to be of the order of 10 sec^{-1} to give concentration decreases of the same order of magnitude as the expansion effect; for a second-order rate constant of magnitude 10^{13} (mole/cc)$^{-1}$ sec^{-1} c_0 would have to be equal to $c_0=10^{-11}$ mole/cc to compete with expansion. It should also be mentioned that a plot of $\log(c_0/c)$ *vs* time, based on only the expansion effect, gives a curve whose deviation from linearity is easily blurred by wishful thinking and leads to a first-order rate constant of 23 sec^{-1}.

An effect generally neglected is that of diffusion in the direction of flow. At very low pressures this effect can become appreciable. An upper limit can be calculated with relative ease by assuming that the concentration gradient is sufficiently represented by the unperturbed gradient and can be written as:

$$-dc/dx=(1/v_0)\cdot f(c). \tag{39}$$

[4] This is essentially the formula given by F. Paneth and W. Lautsch, Ber. deut. chem. Ges. **64**, 2708 (1931).

[5] The most recent, extensive table commonly available is the Works Project Administration Table of the Probability Function, New York (1941). Shorter tables may be found, for instance, in Jahnke-Emde, *Tables of Higher Functions*, p. 23. (B. G. Teubner Verlagsgesellschaft, Leipzig, 1948), fourth edition.

In addition, it will be assumed that the diffusion coefficient at any point x is given by:

$$D=D_0\cdot l_0/(l_0-x), \tag{40}$$

D_0 being the diffusion coefficient at the source. Then, Δc_{diff}, the change in concentration at any point x due to diffusion (considered as having occurred along the unperturbed concentration gradient for the length of time it takes an element of gas to reach x from the source), is:

$$\Delta c_{\text{diff}}=\frac{k_1^2 D_0 l_0 c_0}{v_0^3}\cdot\exp[-k_1 l_0/v_0]$$
$$\times\left[\ln\left(1-\frac{v_0 t}{l_0}\right)-k_1 t+\frac{k_1^2}{2\cdot 2!}\left(t^2-2\frac{l_0 t}{v_0}\right)\right.$$
$$\left.+\frac{k_1^3}{3\cdot 3!}\left((l_0/v_0-t)^3-\left(\frac{l_0}{v_0}\right)^3\right)+\cdots\right], \tag{41}$$

for a first-order gas reaction of rate $-k_1 c$ and:

$$\Delta c_{\text{diff}}=\frac{2D_0 l_0 k_1'^2 c_0^3}{(l_0 c_0 k_1'+v_0)v_0^2}\cdot\left[\frac{1-(1+k_1' c_0 t)^2}{2(1+k_1' c_0 t)^2}+\frac{v_0}{(l_0 c_0 k_1'+v_0)}\right.$$
$$\left.\cdot\left(\frac{-k_1' c_0 t}{1+k_1' c_0 t}+\frac{v_0}{(l_0 c_0 k_1'+v_1)}\cdot\ln\frac{1-v_0 t/l_0}{1+k_1' c_0 t}\right)\right], \tag{42}$$

for a second-order reaction of rate $k_1'\cdot c^2$. t in Eqs. (41) and (42) is given by:

$$t=x/v_0, \tag{43}$$

x being the distance from the source. It will be seen that Eq. (43) is not strictly correct, a maximum error of 2 resulting from its use rather than Eq. (29).

ACKNOWLEDGMENT

The author wishes to thank Drs. Zener and Walnut for valuable help with the solution of Eqs. (23) and (25) and Drs. Nachtrieb and Brooks for stimulating discussions throughout this work.

THE JOURNAL OF CHEMICAL PHYSICS VOLUME 19, NUMBER 3 MARCH, 1951

Exchange between N_2^{30} and N_2^{28} over Iron Catalysts

J. T. KUMMER AND P. H. EMMETT
Gulf Research and Development Company's Multiple Fellowship, Mellon Institute, Pittsburgh, Pennsylvania
(Received November 13, 1950)

The rates of exchange between N_2^{28} and N_2^{30} obtained on doubly- and singly-promoted iron catalysts is of the right order to be accounted for by assuming that all nitrogen evaporating from the surface of the catalyst is completely equilibrated with respect to the nitrogen isotope exchange. Large concentrations of hydrogen (50 percent H_2 in N_2) markedly accelerate the reaction. Small traces of surface oxides poison the iron catalysts severely for the isotope exchange.

A NUMBER of years ago Joris and Taylor[1] made the surprising observation that a good doubly-promoted and a singly-promoted iron synthetic ammonia catalyst when reduced and degassed at 500°C were incapable of rapidly catalyzing the reaction

$$N^{14}N^{14}+N^{15}N^{15}=2N^{14}N^{15} \tag{1}$$

at temperatures in the range 450° to 500°C. This result was especially puzzling in view of the fact that it was known to be possible to readily adsorb nitrogen on these catalysts and to desorb it from them in this temperature range, and that apparently the nitrogen was dissociatively adsorbed to form atoms on the catalyst surface. It did not seem reasonable that the isotope exchange should fail to take place rapidly unless some such surface structure, as suggested by Kobosev,[2] existed on the catalyst surface. He concluded that the surface of an iron synthetic ammonia catalyst consisted of an "ensemble of iron atoms" (usually about 3 in number), completely surrounded by and isolated from other ensembles by promoter molecules. It would be understandable how such ensembles could adsorb nitrogen, synthesize ammonia, and yet not permit nitrogen atoms from one molecule to come in contact with those from another and, thus, not catalyze the isotope exchange. Accordingly, it seemed desirable to re-measure the rate of reaction (1) over iron synthetic ammonia catalysts in order to ascertain whether any unusual surface conformation was needed to explain the observed reaction rate.

EXPERIMENTAL

Unfortunately, neither catalyst 931 nor 954, used by Joris and Taylor, was available in sufficient quantity to warrant their being used for most of the experiments. However, in place of 931, doubly-promoted catalyst 435 containing 0.8 percent Al_2O_3 and 0.25 percent K_2O was employed. Two catalysts containing irreducible oxide promoters but no alkali were used in place of singly-promoted catalyst 954; they were catalyst 423 con-

[1] G. J. Joris and H. S. Taylor, J. Chem. Phys. 7, 893 (1939).
[2] N. I. Kobosev, Acta Physicochim. U.R.S.S. 9, 805 (1938).

TABLE I. $N_2^{28}-N_2^{30}$ exchange rate at 500°C and 60-mm pressure* over a 3.2 g sample of doubly-promoted iron synthetic ammonia catalyst No. 435 (contained 0.8 percent Al_2O_3 and 0.25 percent K_2O as promoters).

Time (hr)	0	0.5†	3.3†	16.5†	74†
N_2^{29}/N_2^{30}	1.21	1.35	2.09	17.0	17.0
% N^{15} in gas phase	11.09	11.05	11.67	10.39	10.23
$K=$	0.119	0.142	0.302	3.92	3.86

* Approximately 0.5 cc gas was adsorbed and 5 cc was in the gas phase throughout this experiment.
† These were run in the order 16.5, 74 hr, 3.3, and 0.5 hr with an accidental heating to 562° during the 74-hr run. Between each run the catalyst was evacuated at 500°C for ½ to 1 hr.

taining 2.26 percent Al_2O_3, 0.62 percent SiO_2, 0.21 percent ZrO_2, and catalyst 422 containing 1.55 percent Al_2O_3 and 0.58 percent ZrO_2. The principal component of the unreduced catalyst was an iron oxide approximating Fe_3O_4 in composition. These catalysts were reduced at 500°C for several days in pure dry hydrogen at a space velocity of about 1000, the hydrogen passing through a vertical bed of the catalyst. After being reduced, the sample was evacuated overnight with mercury diffusion pumps.

Heavy nitrogen was obtained from a sample of NH_4NO_3 in which 62 percent of the nitrogen in the ammonium group was N^{15} but substantially all of the nitrate nitrogen was N^{14}. The nitrate sample was purchased from the Eastman Kodak Company.

A gas rich in N_2^{30} was obtained by adding the NH_4NO_3 to alkali and distilling off the NH_3. The hydrogen was removed from the ammonia by hot CuO to form free nitrogen. The nitrogen obtained in this way was rich in N_2^{30}, since the nitrogen in the ammonium group was 62 percent N^{15}.

The final gas to be used in the exchange experiments was made up by suitable combinations of ordinary nitrogen with portions obtained from the reaction of ammonia with CuO. The gas used in most of the runs contained initially 84.7 percent N_2^{28}, 8.3 percent N_2^{29}, and 7.0 percent N_2^{30}. In each run a known amount of this gas was added, until the pressure was about 70 mm, and circulated by means of an all-glass circulating pump[3] over the catalyst and through a trap cooled in liquid nitrogen to −195°C. It was assumed that the circulation rate was sufficiently fast so as not to control the rate of approach of the gas phase to equilibrium. All analyses of gases were made by a mass spectrometer.

RESULTS AND DISCUSSION

The results of the present experiments are shown in Table I for catalyst 435 and in Table II for catalyst 423. It is at once evident that a fairly rapid exchange occurs over both catalysts. On the doubly-promoted catalyst, the exchange was complete in 16 hours using the same ratio of gaseous nitrogen to weight of catalyst that was used by Joris and Taylor. If one assumes that all nitrogen desorbing from the surface is at statistical equi-

[3] Porter, Bardwell, and Lind, Ind. Eng. Chem. 18, 1086 (1926).

TABLE II. $N_2^{28}-N_2^{30}$ exchange rate at 500°C and 70-mm pressure* over 30 g of iron catalyst No. 423 (contained 1.55 percent Al_2O_3 and 0.58 percent ZrO_2 as promoters).

Time (min)	0	5†	10†	15†
N_2^{29}/N_2^{30}	1.19	9.65	17.0	17.05
% N^{15} in gas	11.17	8.09	9.97	10.49
Calc K	0.117	1.52	3.73	4.0

* Approximately 6 cc of nitrogen was adsorbed and 6 cc was in the gas phase throughout these runs.
† Separate successive runs in the order shown with evacuation at 500°C for 24 hr between the 5- and 10-min run and 1 hr between the 10- and 15-min run.

librium with respect to the three molecular forms, one can then set up the following equation to express the amount of exchange that would be expected after time t

$$t=\frac{A}{V}\ln\frac{c-x_0}{c-x} \qquad (2)$$

where A is the total number of cc (S.T.P.) of nitrogen in the gas phase, V is the rate of desorption of nitrogen from the surface, x is the mole fraction of N_2^{29} in the gas phase at time t, x_0 the corresponding value at the start of the run, and c the value at statistical equilibrium. The value of V calculated from the amount of exchange that had occurred in the 30-minute run, shown in Table I, was 0.00925 and that calculated from the 200-minute run was 0.011. If one compares this with the rate of desorption of N_2 that can be calculated from the equation of Brunauer, Love, and Keenan[4] using an energy of activation of 51,000 calories per mole for the desorption, one finds that the observed rate of desorption is about one-tenth as fast as the estimated rate of desorption, the latter being 0.099 cc per minute. This presumably means that the rate of equilibration of the nitrogen isotopes is within one order of magnitude of that which one would expect from the rate of desorption of nitrogen from the catalyst surface.

On catalyst 423 the exchange was even faster than on catalyst 435. In Table II are shown the results of three runs in which samples were taken at the end of 5, 10, and 15 minutes. Evidently, nearly complete equilibrium was obtained in 10 minutes. In these runs the volume of gas to weight of catalyst had a ratio of about 0.45, whereas on catalyst 435, as in the experiments of Joris and Taylor, the gas to weight ratio was about 3. Since the equation of Brunauer, Keenan, and Love was derived for a doubly-promoted catalyst, it did not seem wise to use it to calculate the rate of desorption from the singly-promoted catalyst. Accordingly, measurements were actually made for the rate of desorption at various pressures at 500°C. It was found that the observed rate of desorption was 2.9 cc per minute at the pressure of 70 mm* used in the exchange runs. The values for V

[4] Brunauer, Love, and Keenan, J. Am. Chem. Soc. 64, 751 (1942).
* The rates of desorption per minute are approximate in that they represent twice the volume of nitrogen escaping in 30 seconds from the catalyst into a large charcoal trap cooled in liquid nitro-

calculated by the above-mentioned equation for the 5- and 10-minute runs were 1.9 and 2.6 respectively. It, thus, appears that the rate of exchange on this catalyst also is about that which would be expected from the observed rate of desorption of nitrogen, if the desorbed gas is at statistical equilibrium with respect to reaction (1).

Although these runs made it clear that isotope exchange between the two nitrogen isotopes was rapid, they did not necessarily show that all of the surface was participating in the reaction. To obtain information as to the rate of mixing of the nitrogen on the surface, two additional experiments were made at 500°C. These are shown in Table III. In the first of the two runs, 7.6 cc of normal nitrogen was added to a catalyst that had equilibrated with 6.8 cc of a sample containing heavy nitrogen. The resulting gas pressure was 74 mm. After 14 minutes circulation, the gas from the gas phase and from the catalyst were pumped off separately and analyzed. The percentage of N^{15} in the two samples was practically identical (6.2 and 6.15 percent N^{15} respectively). In the second experiment, very little gas phase was present; 1.91 cc of heavy nitrogen was first added to the catalyst and allowed to distribute itself at a pressure of a fraction of a millimeter. Then 1.96 cc of normal nitrogen was added, yielding a total pressure of only 5 mm (0.2 cc in the gas phase). After 5 minutes, the gas was removed from the catalyst in two portions, the first requiring 63 minutes of pumping, the second 16 hours. Both samples were again identical in N^{15} content within experimental error (5.70 and 5.74 percent N^{15} respectively). These two runs show that not only does gaseous N_2^{30} react rapidly with gaseous N_2^{28} in the presence of the catalyst, but that the heavy and light nitrogen atoms on the surface mix rapidly and completely to yield a homogeneous adsorbed phase.

In concluding the work with nitrogen isotopes, a few additional runs were made on another singly-promoted iron catalyst, No. 422. The results are given in Table IV. First, a standard run was made at 500°C, showing an expected high conversion in 15-minutes time of contact, the $N_2^{29}:N_2^{30}$ ratio being 20.5 at the end of the run. Next, after an intervening reduction and thorough evacuation at 500°C, a run was made at 450°C. The conversion in one hour was about the same in this run ($N_2^{29}:N_2^{30}=18.7$) as in 15 minutes at the higher temperature; even in one-half hour this ratio had reached a value of 6.4. Then, two runs were made to show the effect of added hydrogen and the effect of added oxygen poison. When 50 percent hydrogen was present with the nitrogen over catalyst 422 at 450°C, practically complete conversion (the $N_2^{29}:N_2^{30}$ ratio was 22.5), was obtained in one-half hour, showing a marked accelerating effect of the added hydrogen. In the poisoning run 25 cc of water vapor mixed with hydrogen at one atmosphere was permitted to react with the surface of the iron catalyst. The actual final residual amount of water vapor was not determined except to note that there was no longer any water condensed in a trap at room temperature. Accordingly, the ratio of water vapor to hydrogen in the final mixture was less than 0.03. This poisoned surface in two hours yielded a $N_2^{29}:N_2^{30}$ ratio of only 3:1 at 450°C. This is considerably less conversion in 2 hours than was obtained in 0.5 hour in the absence of any poison.

In agreement with the work of Joris and Taylor, we have observed that the N^{15} content of the gas phase is frequently lower than one would expect from the composition of the added nitrogen. For example, in Table II the percent N^{15} drops from 11.17 percent to 8.09 percent in the first run. Also, in Table IV, experiments done at *lower* temperatures than those in Table II show that the percent N^{15} in the gas phase is lower over the catalyst than in the original gas. Furthermore, in the runs in Table IV the total percent N^{15} in the gas phase remains lower than that of the original gas after even 1 to 2 hours' circulation over the catalyst. One might expect to find N_2^{29} or N_2^{30} to be adsorbed slightly slower than N_2^{28} because of an isotope effect, but one would not expect the final steady-state or equilibrium value for N^{15} in the gas phase at these temperatures to be appreciably lower than that of the adsorbed gas.[5] In agreement with this conclusion, it is to be noted in Table III that the percent of N^{15} in the gas phase is substantially equal to that of

TABLE III. Rate of surface equilibration of nitrogen isotopes on the surface of a 30 g sample of Fe catalyst No. 423 at 500°C.

First fraction added		Second fraction added			Analysis	
Volume added	% N^{15} in added sample	Volume of second fraction	% N^{15} in second fraction	Time of mixing	Volume of sample	% N^{15} in sample
6.8 cc[a]	13[a]	7.63 cc	Normal (0.38%)	14 min	6.2 cc from gas phase	6.2
					6.58 cc from surface	6.15
1.91 cc[b]	11.17	1.96 cc	Normal	5 min[c]	first 2.6 cc	5.70
					second 1.9 cc	5.74

[a] At the end of the 15-min run (Table II), the gas phase pressure was reduced, leaving about 6.0 cc of gas adsorbed and 0.8 cc in the gas phase. Since the inlet gas was 11.17 percent N^{15} and the gas removed was 10.49 N^{15} (see Table II) the N^{15} content of the 6.8 cc left was originally calculated to be 13 percent. Actually, after completion of the experiments in this table, it was realized that the gas phase at the end of the 15-min run of Table II was probably identical in composition with the adsorbed phase and, hence, contained 10.49 percent N^{15} rather than 13 percent. However, it is also certain that the evacuation for one hour between the 10- and 15-min runs in Table II must have left considerable adsorbed nitrogen containing about 10 percent N^{15} on the surface. Hence, the figure 6.8 in the first column of Table III is probably too low and the 13 percent figure in column two is too high. Fortunately, these uncertainties have no influence on the conclusion to be drawn from Table III to the effect that the nitrogen adsorbed on the surface rapidly equilibrates to an adsorbed phase of constant and uniform isotopic composition.

[b] Sample evacuated overnight after above run before adding this gas.

[c] Collection of the first sample of the gas from the sample that was started 5 min after the second fraction of the nitrogen was added. However, the removal of the 2.6 cc of gas in the first sample required 63 min. The second sample required an additional 15 hr for removal.

gen. During the 30 seconds about 10 percent of the adsorbed nitrogen escaped from the surface. It is estimated the rate might have been higher by a factor of two if the catalyst had been covered during the entire 30 seconds to the same extent to which it was covered when in equilibrium with 70 mm of nitrogen.

[5] H. Urey, J. Chem. Soc. 562 (1947).

TABLE IV. Rate of exchange of nitrogen isotopes over 25 g of iron synthetic ammonia catalyst No. 422.

Temperature (°C)	Time of circulation (min)	Volume of N_2 gas phase (cc)	Volume of N_2 adsorbed (cc)	Analysis $\%N_2^{28}$	Analysis $\%N_2^{29}$	Analysis $\%N_2^{30}$	$\%N^{15}$ in gas phase (cc)	K	Remarks
—	0	—	—	84.7	8.3	7.0	11.15	0.12	Original nitrogen gas sample.
500	15	6.5	4.6	84.9	14.4	0.7	7.9	3.48	Freshly reduced and evacuated. 0.08%[a] H_2 reported present in gas phase.
450	28	8.3	5.3	84.6	13.3	2.1	8.75	1.0	Freshly reduced and evacuated. 0.08%[a] H_2 reported present in gas phase. Gas sample withdrawn after 28 min and after 60 min.
450	60	6.3	4.3	83.6	15.6	0.8	8.6	3.64	
450	30	~9.0	~6.0	84.8	14.5	0.7	7.95	3.54	Freshly reduced and evacuated. 50% H_2 present in gas phase. Gas sample withdrawn after 30 min and after 57 min.
450	57	~9.0	~6.0	84.5	14.8	0.7	8.1	3.70	
450	15	8.8	1.8	84.6	8.6	6.8	11.1	0.13	Sample reduced and evacuated and poisoned with 18 mg of O_2 as water. Gas sample withdrawn after 15 min and 125 min.
450	125	7.68[b]	—	85.8	10.8	3.4	8.8	0.4	

[a] By mass spectrographic analysis.
[b] Gas phase and adsorbed phase.

the adsorbed gas. It is possible that the lowering of the N^{15} content at the start of a run is due to dilution by normal nitrogen chemisorbed on the sample from the nitrogen in the hydrogen used for reduction. Some of this nitrogen might be left even after 24 hours' pumping at 500°C. As a matter of fact, experimental evidence that nitrogen is left on the surface of a catalyst during reduction by hydrogen was obtained.[6] A sample of catalyst 423 was reduced for 100 hours with tank hydrogen at 450°C. After being subjected to evacuation for a few minutes to remove the gas phase, the catalyst was pumped off for 16 hours at 500°C. The effluent gas was collected and found to contain 34 percent N_2. The total nitrogen in this sample of gas (1.7 cc) was equal to 15 to 20 percent of the volume that would be adsorbed at 1-atmos pressure of N_2 at 450°C. This same result was obtained in several different runs. Presumably, the nitrogen was picked up from the small nitrogen content (probably about 0.1 percent N_2), that may be present in tank hydrogen. Calculations from the data of Emmett and Brunauer[7] for the adsorption of nitrogen make it reasonable to expect the observed amount of nitrogen to be taken up during reduction by hydrogen containing as much as 0.1 percent N_2.

The marked poisoning effect of a small amount of surface oxide, as revealed by the last two experiments in Table IV, suggests that the failure of Joris and Taylor to obtain satisfactory rates of exchange was probably due to traces of oxygen poison that may not have been completely removed from their catalysts during reduction.† At any rate, the work here reported shows that over both singly- and doubly-promoted iron catalysts the rate of reaction (1) is of the same order as one would predict from the rates of desorption of N_2 from the same iron catalysts. Furthermore, rapid mixing of the two isotopic forms of nitrogen seems to take place on the catalysts. Accordingly, no special assumption as to the nature of the catalyst surface (such as, for example, the "ensemble theory" of Kobosev) is required to explain the behavior of the surface toward mixtures of N_2^{28} and N_2^{30}.

[6] J. T. Kummer and P. H. Emmett (to be published).
[7] P. H. Emmett and S. Brunauer, J. Am. Chem. Soc. **56**, 35 (1934).

† H. S. Taylor (Discussion of the Faraday Soc. No. 8, 1950, pp. 9–18) and McGeer (thesis, Princeton University, 1949) have recently confirmed the extreme sensitivity of the nitrogen isotope exchange reaction to traces of surface oxide on the iron catalysts.

The Rotation-Vibration Spectrum of Methyl Cyanide in the Region 1.6μ–20μ

PUTCHA VENKATESWARLU*
Division of Physics, National Research Council of Canada,† Ottawa, Canada
(Received October 16, 1950)

The infrared spectra of gaseous and liquid CH_3CN have been investigated in the region 1.6μ–20μ with a Perkin-Elmer spectrometer using LiF, NaCl, and KBr prisms. The parallel type bands show, in general, a sharp Q branch and broad but more intense P and R branches. The perpendicular type bands are well resolved and show the expected intensity alternation "strong, weak, weak, strong . . ." of the subbands (Q branches).

All the fundamentals, except $\nu_8(e)$, which is beyond the region investigated, have been definitely established and vibrational assignments have been made for all the observed bands.

Values for the rotational constants from microwave data have been used to obtain the Coriolis interaction constants, ζ_i, from the observed separations of the subbands of the ⊥ bands. The following values have been obtained: $\zeta_5=0.10$, $\zeta_6=-0.44$, and $\zeta_7=0.41$.

A. INTRODUCTION

THE infrared spectrum of liquid methyl cyanide, (CH_3CN), has been investigated under low dispersion by a number of earlier workers.[1–5] The Raman spectrum has also been studied by a number of investigators, notably Reitz and Skrabal;[6] but there are no polarization data available for the observed Raman bands. Except for some bands in the photographic infrared,[5] there are no data available for the infrared absorption of gaseous CH_3CN. Therefore, the investigation of the infrared spectrum of both gaseous and liquid CH_3CN was undertaken, and the results obtained are discussed in this paper.

B. EXPERIMENTAL

The spectra of liquid and gaseous CH_3CN were recorded with a Perkin-Elmer infrared spectrometer using KBr, LiF, and NaCl prisms. In the case of the vapor, absorption paths of 10 cm and 100 cm were used with varying pressures (1 mm–100 mm), and in the case of the liquid, the Perkin-Elmer sealed liquid cell of 1/10-mm column was used. The same method of calibration as was described in an earlier paper[7] was used.

The methyl cyanide was obtained from Eastman Kodak Company and used without further purification.

C. THE OBSERVED SPECTRUM

The spectrum of CH_3CN vapor, as determined from the recordings obtained with the Perkin-Elmer spectrometer, is shown in Fig. 1. The wave numbers of the bands of both gaseous and liquid CH_3CN are listed in Table I. The accuracy of the measurements for sharp peaks is ±0.5 cm^{-1} from 700 to 3200 cm^{-1}, ±1 cm^{-1} from 3200 to 5000 cm^{-1}, and ±2 cm^{-1} from 5000 to 6000 cm^{-1}. The relative intensities of the bands, which are obtained in the same way as described in the previous paper,[7] are also included in Table I.

The bands obtained are of three kinds. (1) Those that show the fine structure with the alternation of intensity "strong, weak, weak, strong . . ." for the constituent subbands. Since this feature is expected for the ⊥ bands of a symmetric top molecule like CH_3CN, these bands will be classified as ⊥ bands. (2) The bands that show a weak but sharp Q branch with more intense and broader P and R branches. These bands are of the parallel type. Under low dispersion, these bands show only the P and R branches; the Q branch, which is weaker, being unobservable. (3) The bands that show a strong central maximum corresponding to the Q branch, and weaker humps or peaks on either side which correspond to the P and R branches. These bands, as will be discussed later, are of the ⊥ type. In the case of the liquid, all the || and ⊥ bands show, as expected, only broad maxima without any structure.

D. THE ASSIGNMENT OF FUNDAMENTALS

The molecule CH_3CN belongs to the point group C_{3v}. It has four totally symmetric (||) vibrations (species A_1) and four degenerate (⊥) vibrations (species E). All these vibrations are active both in infrared absorption and in the Raman effect.

The frequencies of the fundamentals, and the description of their respective modes of vibration, are shown in Table II. The Raman data for the liquid are also included for comparison. Seven fundamentals have been observed in the present recordings. The eighth fundamental, $\nu_8(e)$, has been observed in the Raman spectrum[6] of liquid CH_3CN at 380 cm^{-1}. It falls beyond the region investigated here.

* National Research Laboratories Postdoctorate Fellow.
† Contribution No. 2324 from the National Research Council, Ottawa, Canada.

[1] W. W. Coblentz, *Investigation of Infrared Spectra* (Carnegie Inst., Washington, D. C., 1905).
[2] F. K. Bell, J. Am. Chem. Soc. **57**, 1023 (1935).
[3] W. Gordy and D. Williams, J. Chem. Phys. **3**, 664 (1935) and **4**, 85 (1936).
[4] P. Barchewitz and M. Parodi, Compt. rend. **209**, 30 (1939).
[5] R. M. Badger and S. H. Bauer, J. Am. Chem. Soc. **59**, 303 (1937).
[6] A. W. Reitz and R. Skrabal, Monatsh. Chem. **70**, 398 (1937). References to earlier work are given in this paper.
[7] P. Venkateswarlu, J. Chem. Phys. **19**, 298 (1951).

TABLE I. Infrared absorption bands of CH_3CN from 600–6100 cm^{-1}.

Experimental data for the vapor					Experimental data for the liquid
ν_{vac}(obs) cm^{-1}	Band type[a]	Intensity[d]	Assignment	ν_{vac}(calc)[e] cm^{-1}	ν_{vac}(obs) cm^{-1}
701.7	b P				
712.6	s [b]		$3\nu_8-\nu_8$		
717.0	s Q	151	$2\nu_8(A_1)$	760	749
728.5	b R				
907.6	b P				
919.1	s Q	159	$\nu_4(a_1)$		917
924.6	s [b]		$\nu_4+\nu_8-\nu_8$		
932.1	b R				
1059.0	resolved	185	$\nu_7(e)$		1047
1204.0	s P				
1217.0	s Q	30	$\nu_4+\nu_8(E)$	1299.1	
1228.5	s R				
1377.5	b P				
1388.0	s Q[c]	754	$\nu_3(a_1)$		1376
1400.5	R				
1412.6	resolved	1000	$\nu_6(e)$		1443
2062	b P				
2084	b R	15	$2\nu_7(A_1)$	2118.0	2074
...			$2\nu_4+\nu_8$	2218.2	2204
2254.5	b P				
2261.2	s [b]		$\nu_2+\nu_8-\nu_8$		
2267.0	s Q	151	$\nu_2(a_1)$		2254
2279.0	b R				
2291.5	h P				
2306.0	s Q	131	$\nu_3+\nu_4(A_1)$	2307.1	2293
2317.5	b R				
2417.4	resolved	57	$\nu_3+\nu_7(E)$	2447.0	2411
2486.8	resolved	33	$\nu_6+\nu_7(E)$	2471.6	2482
2609.8	h P				
2620.5	s Q	82	$\nu_2+\nu_8(E)$	2647.0	2628
2633.7	h R				
2663.0		11	$\nu_3+\nu_4+\nu_8(E)$	2687.1	2674
2731.4	P	23	$2\nu_3(A_1)$	2776.0	
2755.0	R				
2793.5	subbands				
2808.2	of a ⊥				
2821.0	band	11	$\nu_3+\nu_6(E)$	2800.6	
2837.6					
2852.0	b P				
2867.9	s Q	82	$2\nu_6(A_1)$	2825.2	2859
2877.6	b R				
2902.0		6[g]	$2\nu_4+\nu_7(E)$	2897.2	
2942.8	b P				
2954.0	s Q	250	$\nu_1(a_1)$		2944
2966.7	b R				
3009.6	resolved	100	$\nu_5(e)$		3002
3166.8	b P				
3179.0	s Q	84	$\nu_2+\nu_4(A_1)$	3186.1	3165
3192.0	b R				
...	P				
3220.7	s Q[f]	15[g]	$2\nu_4+\nu_3(A_1)$	3226.2	3203
3227.5	b R				
3978.0	subbands				
3994.5	of a ⊥				
4010.0	band with	15	$\nu_5+\nu_7(E)$		3976
4022.0	origin at				
4041.3	3999.2				
4085.0	b P				
4103.0	b R	15	$\nu_5+\nu_7(A_1)$	4068.6	4027
			$\nu_1+\nu_3(A_1)$	4342.0	4332
4392.9	b	71	$\nu_1+\nu_6(E)$	4366.6	4375
			$\nu_3+\nu_5(E)$	4397.6	4402
4442.5	h P?				
4453.7	b Q?	69	$\nu_5+\nu_6(A_1, E)$	4422.2	4445
4474.6	h R?				
5701	b	6.7	$\nu_1+2\nu_3(A_1)$	5730.2	5701
5851	b	33	$2\nu_1(A_1)$	5908	5832
5972	b	20	$2\nu_5(A_1, E)$	6019.2	5965

[a] Abbreviations: s = sharp, b = broad, h = hump (i.e., no distinct maximum). P, Q, and R refer to peaks that are P, Q, and R branches, respectively. "Resolved" means the band is a ⊥ band that has been resolved. The wave number value that has been given corresponds to the origin of the band.

[b] These bands are those that were explained in the text as hot bands of the type $\nu_i+\nu_8-\nu_8$.

[c] This band is overlapped by the band envelope of the 1412.6 cm^{-1} band.

[d] The intensity of the strongest band at 1412.6 cm^{-1} is assumed to be 1000, and the intensities of the other bands are calculated with the assumption that the intensity is proportional to $(1/pl)\log(I_0/I)$, where p and l are pressure and path lengths and where I_0 and I are the incident and transmitted intensities, respectively. These values are necessarily rough.

[e] Based on harmonic oscillator approximation.

[f] The P branch of this band is probably completely overlapped by the R branch of the adjacent strong band 3179 cm^{-1}.

[g] These bands are measured on the background of a large slope.

E. FINE STRUCTURE

In the case of a symmetric top molecule like CH_3CN, the origins of the subbands of a || band are given by[8]

$$\nu_o^{sub}=\nu_o+[(A_v'-A_v'')-(B_v'-B_v'')]K^2, \quad (1)$$

where A_v', B_v' and A_v'', B_v'' are the rotational constants for the upper and lower states, respectively, and K is the quantum number of the component of angular momentum about the figure axis. The spacing of the successive lines in the P and R branches of a subband of a parallel band is approximately $2B$. As long as the coefficient of K^2 in Eq. (1) is small compared with $2B$, the whole || band will appear to consist, under medium dispersion, of a sharp Q branch and broader P and R branches. The resolution of the instrument used is not high enough to show the fine structure of the || bands.

The formula[8] for the Q branches of the subbands of a ⊥ band is

$$\nu_o^{sub}=\nu_o+[A_v'(1-2\zeta_i)-B_v'] \pm 2[A_v'(1-\zeta_i)-B_v']K + [(A_v'-B_v')-(A_v''-B_v'')]K^2, \quad (2)$$

TABLE II. Fundamentals of CH_3CN.

Description	Designation	Present infrared work: vapor ν_{vac} cm^{-1}	Present infrared work: liquid ν_{vac} cm^{-1}	Raman effect in liquid[9] ν_{vac} cm^{-1}
Symmetric C−H stretching	$\nu_1(a_1)$	2954.0	2943.9	2942
Symmetric C≡N stretching	$\nu_2(a_1)$	2267.0	2253.5	2249
Symmetric CH_3 deformation	$\nu_3(a_1)$	1388.0	1375.5	1376
Symmetric C−C stretching	$\nu_4(a_1)$	919.1	917.4	918
Degenerate C−H stretching	$\nu_5(e)$	3009.6	3001.5	2999
Degenerate CH_3 deformation	$\nu_6(e)$	1412.6	1443.0	1440
Degenerate CH_3 rocking	$\nu_7(e)$	1059.1 or 1041.9	1047.3	
Degenerate C−C≡N bending	$\nu_8(e)$			380

[8] G. Herzberg, *Infrared and Raman Spectra of Polyatomic Molecules* (D. Van Nostrand, Inc., New York, 1945).

where ζ_i is the Coriolis interaction constant. The positive sign in the third term at the right of the above formula applies to the R branch ($\Delta K=+1$), and the negative sign to the P branch ($\Delta K=-1$).

As CH_3CN has three identical nuclei of non-zero spin, an intensity alternation of the type "strong, weak, weak, strong . . ." is expected[8] among the subbands. Further, as the spin of the identical nuclei is $\frac{1}{2}$, one would expect the intensity ratio of the strong to the weak subbands to be 2:1. In the series of the Q branches (subbands), the first ^RQ branch, i.e., $^RQ_0$, forms a strong "line," and the first ^PQ branch, i.e., $^PQ_1$, forms a weak "line." The origin of the band is between $^RQ_0$ and $^PQ_1$.

The fine structure of the $\perp$ bands 3009.6 and 1412.6 cm^{-1}, which correspond to $\nu_5(e)$ and $\nu_6(e)$, respectively, can be seen in Fig. 1. The wave numbers and the assignment of the subbands (Q branches) of the band 3009.6 cm^{-1} are given in Table III. The subbands can all be represented by the formula

$$\nu_0^{\text{sub}}=3013.5\pm 8.84K, \tag{3}$$

TABLE III. Wave numbers of the subbands in the fundamental $\nu_5(e)$ at 3009.6 cm^{-1}.

Assignment	ν_{vac}[a]	$\Delta\nu$	Assignment	ν_{vac}[a]	$\Delta\nu$
$^RQ_{12}$	3119.6 s		$^RQ_3$	3040.2 s	9.6
$^RQ_{11}$	3110.1 w	9.5	$^RQ_2$	3031.2 w	9.0
$^RQ_{10}$	3102.0 w	8.1	$^RQ_1$	3022.5 w	8.7
$^RQ_9$	3093.2 s	8.8	$^RQ_0$	3013.5 s	9.0
$^RQ_8$	3084.0 w	9.2	$^PQ_1$	3003.9 w	9.6
$^RQ_7$	3075.3 w	8.7	$^PQ_2$	2995.0 w	8.9
$^RQ_6$	3067.0 s	8.3	$^PQ_3$	2985.5 s	9.5
$^RQ_5$	3058.1 w	8.9	$^PQ_4$	2977.2 w	8.3
$^RQ_4$	3049.8 w	8.3			

[a] In the table, "s" stands for "strong," "w" for "weak."

which is similar to Eq. (2) except that the quadratic term is omitted. The ^PQ branches of this band are overlapped by the band 2954 cm^{-1}.

The subbands of the band 1412.6 cm^{-1}, which are given in Table IV, can be represented by the formula

$$\nu_0^{\text{sub}}=1422.2\pm 14.6K+0.07K^2. \tag{4}$$

The fine structure of the band $\nu_7(e)$ is shown separately in Fig. 2. The subbands 1059.7 and 1042.5 cm^{-1} are the strongest of the subbands of $\nu_7(e)$, the first being slightly more intense than the second. If 1059.7 cm^{-1} is taken as $^RQ_0$, the subbands can all be represented by the equation

$$\nu_0^{\text{sub}}=1059.7\pm 5.67K+0.02K^2. \tag{5a}$$

If, however, 1042.5 cm^{-1} is taken as $^RQ_0$, the subbands can be represented by

$$\nu_0^{\text{sub}}=1042.5\pm 5.57K+0.015K^2. \tag{5b}$$

The wave numbers of the subbands and the numberings according to the above two assignments are given in Table V. The first assignment (Eq. (5a)) is to be preferred, as the subband at 1059.7 cm^{-1} is slightly more intense than the one at 1042.5 cm^{-1}.

TABLE IV. Wave numbers of the subbands in the fundamental $\nu_6(e)$ at 1412.6 cm^{-1}.

Assignment	ν_{vac} cm^{-1}[a]	$\Delta\nu$	Assignment	ν_{vac} cm^{-1}[a]	$\Delta\nu$
$^RQ_6$	1515.4 s		$^PQ_5$	1352.1 w	13.0
$^RQ_5$	1498.2 w	17.2	$^PQ_6$	1338.6 s	13.5
$^RQ_4$	1482.6 s	15.6	$^PQ_7$	1325.0 w	13.6
$^RQ_3$	1465.8 w	16.8	$^PQ_8$	1311.0 w	14.0
$^RQ_2$	1450.4 w	15.4	$^PQ_9$	1296.9 s	14.1
$^RQ_1$	1436.5 w	13.9	$^PQ_{10}$	1283.2 w	13.7
$^RQ_0$	1422.0 s	14.5	$^PQ_{11}$	1270.0 w	13.2
$^PQ_1$	1408.3 w	13.7			
$^PQ_2$	1395.7 bl.	12.6			
$^PQ_3$	··· bl.				
$^PQ_4$	1365.1 bl. w				

[a] Bands marked bl. are overlapped by the || band $\nu_8(a_1)$ at 1388.0 cm^{-1}. "s" and "w" stand for "strong" and "weak," respectively.

Kessler, Ring, Trambarulo, and Gordy,[9] from a study of the microwave spectrum of CH_3CN, obtained $I_B^0=91.20\times10^{-40}$ g cm^2 and $B_0=0.3068$ cm^{-1}. By investigating various isotopic molecules, they obtained the molecular dimensions for CH_3CN as $r_0(C-H)=1.092A$, $r_0(C-C)=1.460A$, $r_0(C\equiv N)=1.158A$, and $\angle HCH=109°8'$. Using these values, one can obtain the moment of inertia $I_A^0=4r_0^2(C-H)M_H\sin^2\frac{1}{2}\angle HCH=5.30\times10^{-40}$ g cm^2. From this value of I_A^0, the rotational constant A_0 is found to be 5.28 cm^{-1}.

Considering Eq. (2), it is seen that the coefficient of the linear term in any of Eqs. (3)–(5) is equal to $2[A_v'(1-\zeta_i)-B_v']$. Using as an approximation the above values of A_0 and B_0 for A_v' and B_v', one obtains the Coriolis interaction constants $\zeta_5=0.10$, $\zeta_6=-0.44$, and $\zeta_7=0.41$.

Subtracting $[A(1-2\zeta_i)-B]$ from the constant terms in Eqs. (3)–(5), the origins of the $\perp$ bands are found to be $\nu_5=3009.6$, $\nu_6=1412.6$, and $\nu_7=1059.1$ (or 1041.9) cm^{-1}.

TABLE V. Wave numbers of the subbands in the fundamental $\nu_7(e)$ at 1059.1 cm^{-1}.

Assignment a	Assignment b	ν_{vac} cm^{-1}[a]	$\Delta\nu$	Assignment a	Assignment b	ν_{vac} cm^{-1}[a]	$\Delta\nu$
$^RQ_9$	$^RQ_{12}$	1112.7 s		$^PQ_3$	$^RQ_0$	1042.5 s	5.9
$^RQ_8$	$^RQ_{11}$	1106.4 w	6.3	$^PQ_4$	$^PQ_1$	1037.1 w	5.4
$^RQ_7$	$^RQ_{10}$	1100.4 w	6.0	$^PQ_5$	$^PQ_2$	1031.5 w	5.6
$^RQ_6$	$^RQ_9$	1094.3 s	6.1	$^PQ_6$	$^PQ_3$	1026.2 s	5.3
$^RQ_5$	$^RQ_8$	1088.4 w	5.9	$^PQ_7$	$^PQ_4$	1020.3 w	5.9
$^RQ_4$	$^RQ_7$	1082.8 w	5.6	$^PQ_8$	$^PQ_5$	1015.2 w	5.1
$^RQ_3$	$^RQ_6$	1076.9 s	5.9	$^PQ_9$	$^PQ_6$	1009.8 s	5.4
$^RQ_2$	$^RQ_5$	1071.0 w	5.9	$^PQ_{10}$	$^PQ_7$	1005.0 w	5.8
$^RQ_1$	$^RQ_4$	1065.2 w	5.8	$^PQ_{11}$	$^PQ_8$	999.6 w	5.4
$^RQ_0$	$^RQ_3$	1059.7 s	5.5	$^PQ_{12}$	$^PQ_9$	994.6 s	5.0
$^PQ_1$	$^RQ_2$	1053.9 w	5.8	$^PQ_{13}$	$^PQ_{10}$	989.0 w	5.6
$^PQ_2$	$^RQ_1$	1048.4 w	5.5	$^PQ_{14}$	$^PQ_{11}$	983.5 w	5.5

[a] In the table, "s" and "w" stand for "strong" and "weak," respectively.

[9] Kessler, Ring, Trambarulo, and Gordy, Phys. Rev. **79**, 54 (1950).

TABLE VI. Wave numbers of the subbands of $\nu_6+\nu_7(E)$ and $\nu_3+\nu_7(E)$ at 2486.8 and 2417.4 cm^{-1}, respectively.

2486.8 cm^{-1} band			2417.4 cm^{-1} band		
Assignment	ν_{vac} cm^{-1} [a]	$\Delta\nu$	Assignment	ν_{vac} cm^{-1}	$\Delta\nu$
$^RQ_8$	2574.1 w		$^RQ_5$	2448.4 w	
$^RQ_7$	2564.0 w	10.1	$^RQ_4$	2443.4 w	5.0
$^RQ_6$	2554.0 s	10.0	$^RQ_3$	2438.0 s	5.4
$^RQ_5$	2543.0 w	11.0	$^RQ_2$	2430.0 w	8.0
$^RQ_4$	2533.0 w	10.0	$^RQ_1$	2424.0 w	6.0
$^RQ_3$	2523.0 s	10.0	$^RQ_0$	2418.5 s	5.5
$^RQ_2$	2513.3 w	9.7	$^PQ_1$	2413.0 w	5.5
$^RQ_1$	2502.8 w	10.5	$^PQ_2$	2407.0 w	6.0
$^RQ_0$	2492.0 s	10.8	$^PQ_3$	2401.2 s	5.8
$^PQ_1$	2482.5 w	9.5	$^PQ_4$	2395.0 w	6.2
$^PQ_2$	2472.8 w	9.7	$^PQ_5$	2388.5 w	6.5
$^PQ_3$	2463.5 s	9.3			
	2457.5 bl.				
	2455.5 bl.				

[a] The subbands marked bl. could not be assigned, as they are the resultant of the overlapping of the band envelopes of 2486.8 and 2417.4 cm^{-1}. "s" and "w" stand for "strong" and "weak," respectively.

Johnston and Dennison[10] have derived a sum rule for the ζ_i values of an axially symmetric XYZ_3 molecule. Cowan[11] has recently extended the calculation to an axial $WXYZ_3$ molecule and obtained the relation

$$\zeta_5+\zeta_6+\zeta_7+\zeta_8=(B/2A)+1. \quad (6)$$

From the known values for ζ_5, ζ_6, ζ_7, B, and A in the above equation, the value of ζ_8 is found to be 0.95. Therefore, it can be expected that the spacing of the subbands of the fundamental $\nu_8(e)$ will be very small; and its band envelope will show, under medium dispersion, a strong central maximum corresponding to the Q branch. Similar spacing of the subbands and similar band envelope can be expected for the combination bands like $\nu_i(a_1)+\nu_8(e)$, which involve $\nu_8(e)$, since the ζ of such combination bands will be ζ_8 itself (see below).

F. OVERTONE AND COMBINATION BANDS

In addition to the fundamentals, a large number of overtone and combination bands have been observed. They are included in Table I. The overtone $2\nu_8(A_1)$ is at 717.0 cm^{-1} and is very strong. Its band envelope shows a subsidiary peak besides the usual PQR peaks. This extra peak, at 712.6 cm^{-1}, probably corresponds to the difference band $3\nu_8-\nu_8$. Each of the band envelopes of the fundamentals $\nu_2(a_1)$ and $\nu_4(a_1)$ also show a subsidiary peak besides the P, Q, and R peaks. These extra peaks, at 2261.2 and 924.6 cm^{-1}, will probably correspond to the difference bands $\nu_2+\nu_8-\nu_8$ and $\nu_4+\nu_8-\nu_8$, respectively.

TABLE VII.

Assignment	Band origin cm^{-1}	ζ computed	$\Delta\nu$ cm^{-1} computed from ζ	$\Delta\nu$ cm^{-1} observed
$\nu_3+\nu_7$	2417.4	0.41	5.67	6.0
$\nu_6+\nu_7$	2486.8	0.03	9.6	10.2
$\nu_3+\nu_6$	2827.9	−0.44	14.6	14.7
$\nu_5+\nu_7$	3999.2	−0.51	15.3	15.8

The combination band $\nu_3+\nu_4(A_1)$ at 2306.0 cm^{-1} is quite strong because of the Fermi resonance with the fundamental $\nu_2(a_1)$. This band, as well as the overtone $2\nu_6(A_1)$ at 2867.9 cm^{-1} and the combination band $\nu_2+\nu_4(A_1)$ at 3179.0 cm^{-1}, all show peaks similar to those of the || type fundamentals.

The parallel bands $2\nu_7(A_1)$, $2\nu_3(A_1)$, and $\nu_6+\nu_7(A_1)$ are weak and show only P and R branches but no central Q branches. The overtones $2\nu_1(A_1)$ and $2\nu_5(A_1, E)$ lie at 5851 and 5972 cm^{-1}, respectively; but their structure could not be observed, as the resolution of the instrument in that region is not high enough.

The perpendicular bands $\nu_3+\nu_7(E)$ and $\nu_6+\nu_7(E)$ are well resolved but overlap mutually to some extent. Their origins are at 2417.4 cm^{-1} and 2486.8 cm^{-1}, respectively. The wave numbers and the assignments of their subbands are given in Table VI. These subbands can be represented by the following formulas

$$\nu_o^{sub}=2418.5\pm 6.0K \quad (7)$$

$$\nu_o^{sub}=2492.0\pm 10.2K. \quad (8)$$

The four weak peaks between 2790 and 2840 cm^{-1} (Table I), which have the intensity alternation expected for the subbands of a ⊥ band, can be represented by the equation

$$\nu_o^{sub}=2837.6\pm 14.7K. \quad (9)$$

This band, whose origin is at 2827.9 cm^{-1}, corresponds to the combination $\nu_3+\nu_6(E)$.

There are five weak peaks at about 4000 cm^{-1} (Table I) for which the successive separations are somewhat irregular. They may be considered as the subbands of a perpendicular band which probably corresponds to $\nu_5+\nu_7(E)$. These subbands can be roughly represented by the equation

$$\nu_o^{sub}=4010.0\pm 15.8K. \quad (10)$$

The origin of this band is at 3999.2 cm^{-1}.

The band 2620.5 cm^{-1} shows a strong central maximum which corresponds to the Q branch and two shoulders which correspond to the P and R branches. This cannot be a || band as the other || bands of CH_3CN in this region show a weak Q branch and stronger P and R branches. This band is most probably the combination band $\nu_2+\nu_8(E)$, which is expected to show a strong unresolved Q branch, since the spacing of its successive subbands, as mentioned above, will be very small. Incidentally, it may be pointed out that the envelope of the band 2620.5 cm^{-1} is similar to that of a CH_3I band at 7505 cm^{-1} obtained by Herzberg and Herzberg,[12] which they classified as a ⊥ band. Another

[10] M. Johnston and D. M. Dennison, Phys. Rev. **48**, 868 (1935).

[11] R. D. Cowan, J. Chem. Phys. **18**, 1101 (1950).

[12] G. Herzberg and L. Herzberg, Can. J. Research **B27**, 332 (1949).

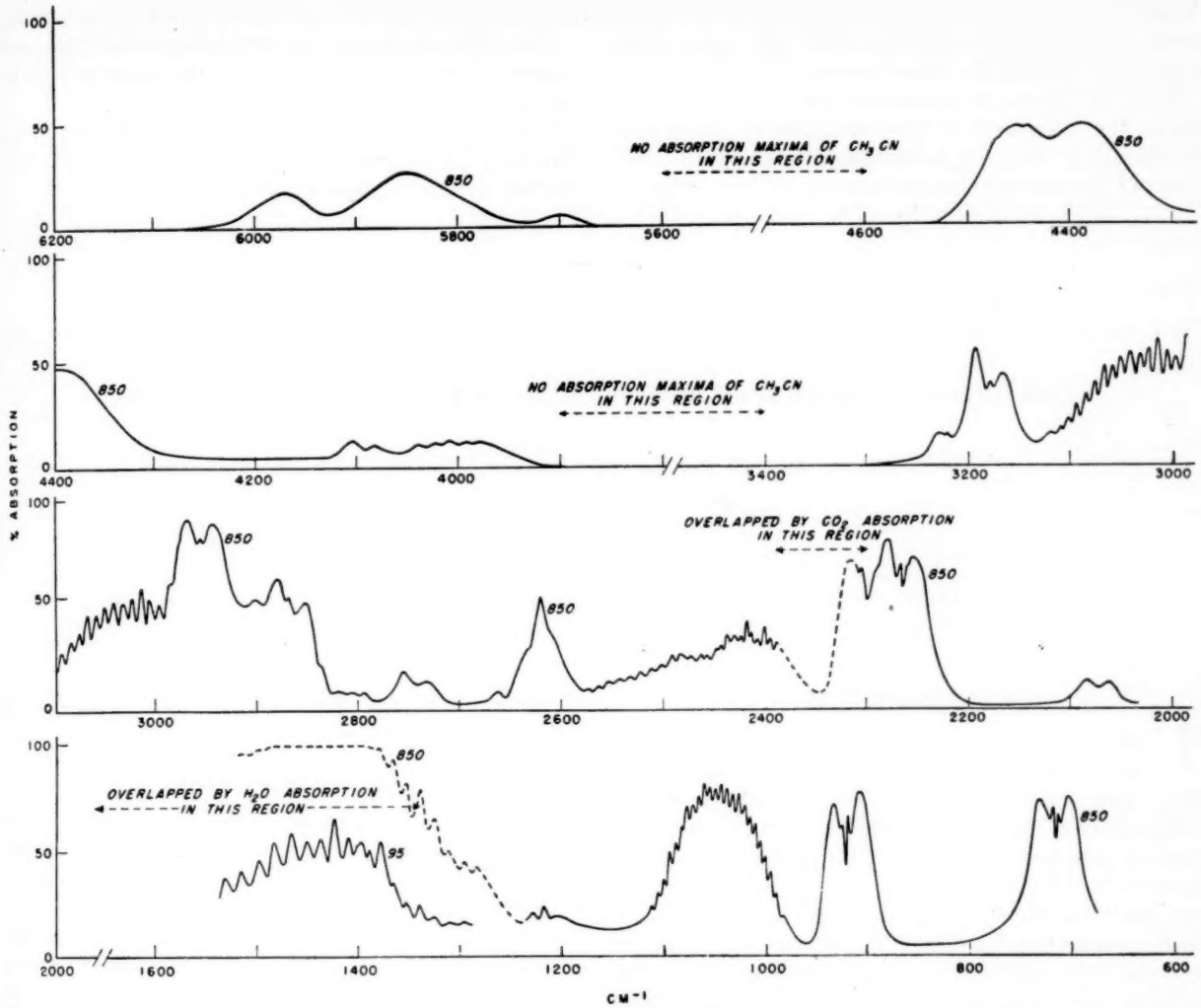

FIG. 1. The infrared absorption spectrum of methyl cyanide vapor from 6100 to 600 cm^{-1}. The italic numbers written on the curves refer to the products of the pressure and the absorbing path length both in cm.

binary $\perp$-type combination band, which involves $\nu_8(e)$, is found at 1217.0 cm^{-1}. This is the band $\nu_4+\nu_8(E)$ and shows the expected strong Q peak and weaker P and R peaks. The fact that $\nu_2+\nu_8(E)$ and $\nu_4+\nu_8(E)$ show the unresolved strong Q peaks supports the value 0.95 obtained above for ζ_8.

The remaining bands are also easily interpreted as binary and ternary combinations as indicated in Table I. The calculated wave numbers for all the overtone and combination bands, neglecting anharmonicity, are included in Table I.

The values of ζ_i of the fundamentals can be used to calculate the expected separations of the subbands of the perpendicular type combination bands $\nu_3+\nu_7$, $\nu_6+\nu_7$, $\nu_3+\nu_6$, and $\nu_5+\nu_7$ (Table I). Johnston and Dennison[11] computed the ζ's for the overtone and combination bands for molecules of threefold axis of symmetry in terms of ζ's of the fundamentals. Neglecting the anharmonicity, they obtained

$$\zeta_{2\nu_i}=-2\zeta_i, \quad \zeta_{3\nu_i}=\zeta_i, \quad \zeta_{\nu_k+\nu_i}=\zeta_i,$$

if ν_k is a $\|$-type vibration and ν_i is a $\perp$-type, and

$$\zeta_{\nu_k+\nu_i}=-(\zeta_k+\zeta_i)$$

if ν_k and ν_i are both $\perp$-type. Using these relations, the

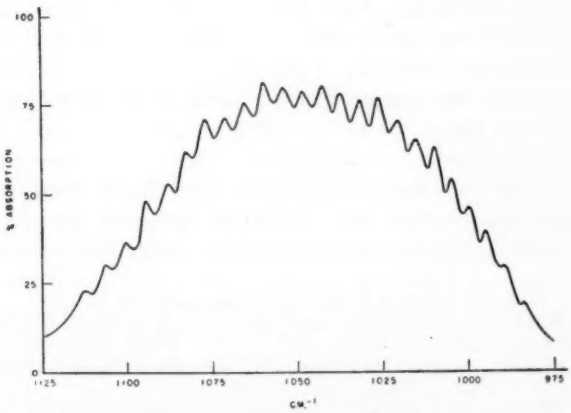

FIG. 2. Fine structure of the fundamental band $\nu_7(e)$ of methyl cyanide at 1059.0 cm^{-1}.

ζ's have been computed for the observed combination bands, and have been used to give the separations of successive subbands [linear term of Eq. (2)].

Table VII shows the observed and computed values of $\Delta\nu$. The agreement is very satisfactory taking into consideration that the anharmonicity has been neglected in the above computations for ζ. This supports well the values of the ζ's obtained for the fundamentals.

The band origins for the combination bands given in Table VII have been obtained in the same way as for the fundamentals.

The author wishes to express his thanks to Dr. G. Herzberg for suggesting the problem, and for his kind interest during the course of the work.

THE JOURNAL OF CHEMICAL PHYSICS VOLUME 19, NUMBER 3 MARCH, 1951

The Infrared Spectrum of Methyl Chloroform in the Region 1.6μ–20μ

PUTCHA VENKATESWARLU*
Division of Physics, National Research Council of Canada,† Ottawa, Canada
(Received September 14, 1950)

The infrared spectrum of methyl chloroform has been investigated in the region 1.6μ–20μ with a Perkin-Elmer spectrometer using LiF, NaCl, and KBr prisms. Vibrational assignments are given to all the bands observed, and all fundamentals except the torsional vibration have been fairly definitely established. Most of the bands, whether perpendicular or parallel type, show the same kind of *PQR* structure.

A. INTRODUCTION

THE infrared spectrum of methyl fluoroform was investigated by Cowan, Herzberg, and Sinha[1] using long absorbing paths. They gave vibrational assignments of the observed bands. Most of the bands, whether of perpendicular ($\perp$) or parallel ($\parallel$) type, were found to show the same kind of *PQR* structure. This was understandable, since the molecule CH_3CF_3 is nearly a spherical top. The CH_3 rocking vibration was reported to be split into two close components, and the splitting was tentatively ascribed to the presence of three potential minima separated by low potential maxima. In order to check these interpretations, it appeared to be of interest to study the infrared spectrum of methyl chloroform and to determine its fundamental frequencies. Such a study is the object of the present article.

When this work was started, there were no infrared data available for methyl chloroform but only Raman data[2,3] for the liquid. After the results described in this article were obtained, a spectrum of CH_3CCl_3 in the region 2μ–22μ appeared in the API‡ catalog of Infrared Spectral Data (Serial No. 1032, supplied by the U. S. Naval Research Laboratory). Still more recently, Karplus and Halford[4] reported the infrared spectrum from 700 to 3010 cm^{-1} for gaseous, liquid, and solid CH_3CCl_3, but did not give any vibrational assignments. Their spectrum does not show as many details as the spectrum in the API catalog.

B. EXPERIMENTAL

The spectra underlying the present investigation were recorded on a Perkin-Elmer infrared spectrometer (Model 12C) with a Golay cell detector and a Brown recorder, using NaCl, KBr, and LiF prisms. Absorbing paths of 10 cm and 100 cm with varying pressures (0.5 mm–100 mm) were used for the vapor and the Perkin-Elmer sealed liquid cells of 0.1-mm column were used in the case of the liquid.

The calibration was carried out by determining the positions of the individual fine structure lines of the absorption bands of CH_3OH, NH_3, H_2O, CO_2, CO, HCl, and CH_4. The accuracy of the measurements is estimated to be ± 1 cm^{-1} from 500 to 5000 cm^{-1} and ± 2 cm^{-1} from 5000 to 6000 cm^{-1}.

The methyl chloroform was obtained from the Eastman Kodak Company and was used without further purification.

C. OBSERVED SPECTRUM

The spectrum of gaseous methyl chloroform as determined from the recordings obtained with the Perkin-Elmer spectrometer is shown in Figs. 1 and 2. Compared with the spectrum of Karplus and Halford and that of the API catalog§ the present spectrum shows a good deal more detail and also additional bands.

* National Research Laboratories Postdoctorate Fellow.
† Contribution No. 2325 from the National Research Council, Ottawa, Canada.
[1] Cowan, Herzberg, and Sinha, J. Chem. Phys. 18, 1538 (1950).
[2] G. F. Hull, J. Chem. Phys. 3, 534 (1935).
[3] J. Wagner, Z. physik. Chem. B45, 341 (1939).
‡ American Petroleum Institute Research Project No. 44.
[4] R. Karplus and R. S. Halford, J. Chem. Phys. 18, 910 (1950).

§ The spectrum given in the API catalog agrees very well with the present results except in the region 775–990 cm^{-1}, where it appears to be shifted by about 20 cm^{-1}, probably because of some error in their calibration. A fairly strong band, according to the present results, has its *PQR* branches at 863, 867, and 871 cm^{-1}, respectively, whereas the corresponding values given in the API

TABLE I. Infrared absorption bands of CH_3CCl_3 from 500 to 6100 cm^{-1}.

Experimental data for the vapor						Experimental data for liquid
ν_{vac}(obs) cm^{-1}	Band type[a]	Intensity[b]	Assignment	ν_{vac}(calc)[d] cm^{-1}	ν_{vac}(obs) cm^{-1}
517	b P				
526	b Q	122	$\nu_{11}(e)$		527
535	b R				
549	s	7[c]	$\nu_{11}+\nu_6-\nu_6$		
557	b P				
566	s Q	12[c]	$\nu_5+\nu_{12}(E)$	586	
576	b R				
589	b	5[c]	$\nu_2-\nu_4$	590	
689	b	26[c]	$2\nu_5(A_1)$	690	658
724	vb ⊥	100,000	$\nu_{10}(e)$		712
748	b	15[c]	$3\nu_{12}(A_1, E)$ or $\nu_{10}+\nu_6-\nu_6$	723	
759	s P				763
763	s Q	15[c]	$\nu_{11}+\nu_{12}(A_1, E)$	767	
768	s R				
773	b P?				
796	s Q	80	$\nu_4(a_1)$		791
805	b R				
818	b P				
834	b Q	8[c]	$2\nu_{12}+\nu_6(A_1, E)$	827	828
842	b R				
863	s P				
867	s Q	30	$\nu_3(a_1)$		867
871	s R				
875	h P				
884	b Q	7[c]	$\nu_5+\nu_{11}(E)$	871	883
890	b R				
896	b	7[c]	$2\nu_5+\nu_{12}(E)$ or $\nu_5+\nu_{11}+\nu_6-\nu_6$	931	
953	h P				
962	b Q	21	$\nu_{10}+\nu_{12}(A_1, E)$	965	944
972	h R				
998	h P				
1009	b Q	76	$\nu_4+\nu_{12}(E)$ or $2\nu_{11}(A_1, E)$	1037 1052	1004
1015	b R				
1075	b P				
1088	s Q	2770	$\nu_9(e)$		1080
1095	b R				
1229	b P				
1239	b Q	110	$\nu_{10}+\nu_{11}(A_1, E)$ $\nu_3+\nu_5(A_1)$	1250 1212	1233
1251	h R				
1287	s P				
1293	s Q	20	$\nu_4+\nu_{11}(E)$	1322	1286
1300	s R				
			$\nu_9+\nu_{12}(A_1, E)$	1329	1312
1376	s P				
1386	s Q	203	$\nu_2(a_1)$		1381
1393	s R				
1428	b	61[c]	$2\nu_{10}(A_1, E)$	1428	1422
1447	s P				
1457	s Q	172	$\nu_8(e)$		1449
1465	s R				
2113	b	10[c]	$\nu_2+\nu_{10}(E)$	2110	2092
2133	h P				
2138	s Q	28	$2\nu_9(A_1)$		2128
2143	b R				
2155	h	6[c]	$2\nu_9(E)$	2176	2156
2447	h P				
2452	s Q	20	$\nu_2+\nu_9(E)$	2474	2445
2459	s R				
2509	vb	5	$2\nu_9+\nu_6(A_1, E)$	2521	
2537	vb	4	$\nu_8+\nu_9(A_1, E)$	2545	
2668	vb	2.4	$\nu_7-\nu_5(E)$	2669	
2756	b P				
2762	s Q	1.3	$2\nu_2(A_1)$	2772	
2768	b R				
2828	b P				
2835	b Q	8[c]	$2\nu_8(E)$		2822
2869	b P				
2888	b Q	19	$2\nu_8(A_1)$	2914	2876
2896	b R				
2943	s P				
2951	s Q	59	$\nu_1(a_1)$		2955
2958	s R				
2976	b	1.5	$2\nu_9+\nu_4(A_1, E)$	2972	
2988	b	1.5	$2\nu_2+\nu_{12}(E)$	3013	
3008	b P				
3014	s Q	111	$\nu_7(e)$		3002
3020	b R				
3186	b	4	$\nu_1+\nu_{12}(E)$	3192	3178
3214	b	2	$3\nu_9(A_1, E)$ or $\nu_1+\nu_{12}+\nu_6-\nu_6$	3264	
3254	b	5	$\nu_7+\nu_{12}(A_1, E)$	3255	3247
3295	b	5	$\nu_1+\nu_5(A_1)$	3296	3286
3357	b	12	$\nu_7+\nu_5(E)$	3359	3348
4033	b	14	$\nu_1+\nu_9(E)$	4039	4020
4094	b	18	$\nu_7+\nu_9(A_1, E)$	4102	4086
4191	vb	2	$3\nu_2(A_1)$	4158	
4268	vb	2	$3\nu_8(A_1, E)$	4371	
4396	b	16	$\nu_2+\nu_7(E)$	4400	4384
4443	b	13	$\nu_1+\nu_8(E)$	4408	4427
4461	b	12	$\nu_7+\nu_8(A_1, E)$	4471	4448
5701	b	2	$2\nu_2+\nu_1(A_1)$	5723	5688
5745	b	3	$2\nu_2+\nu_7(E)$	5786	5731
5861	b	8	$2\nu_1(A_1)$	5902	5833
5984	b	6			5968
6027	b	4	$2\nu_7(A_1, E)$	6028	6007

[a] Abbreviations: s = sharp, b = broad, vb = very broad, h = hump (i.e., no distinct maximum), *PQR* refer to peaks that are likely to be due to *PQR* branches, respectively.
[b] The relative intensities in this column are based on the value 100,000, for the strongest band at 724 cm^{-1}. These values are necessarily rough.
[c] The bands whose intensity values are marked '*c*' are measured on the background of a large slope.
[d] Based on the harmonic oscillator approximation.

The wave numbers of the absorption maxima observed in the present recordings for both gaseous and liquid CH_3CCl_3 are listed in Table I along with the relative intensities of the bands which are based on their peak heights. The intensity of the strongest band, at 724 cm^{-1}, is assumed to be 100,000; and the intensities for the other bands are calculated with the assumption that the intensity is proportional to $(1/pl)\log(I_0/I)$, where p and l are pressure and path length and where I_0 and I are the incident and transmitted intensities, respectively. These values will necessarily be rough as the dependence of the peak height on the slit width and the effect of pressure broadening on the peak heights have been neglected.

Most of the absorption bands of gaseous methyl

catalog are 845, 850, and 854 cm^{-1}, respectively. Because of this difference the spectrum of CH_3CCl_3 in the region 775–990 cm^{-1} and the calibration spectrum of ammonia were again taken and the present results were confirmed. Furthermore, the present value of 867 cm^{-1} for the *Q* branch, agrees with the value 866 cm^{-1} given by Karplus and Halford for the band center.

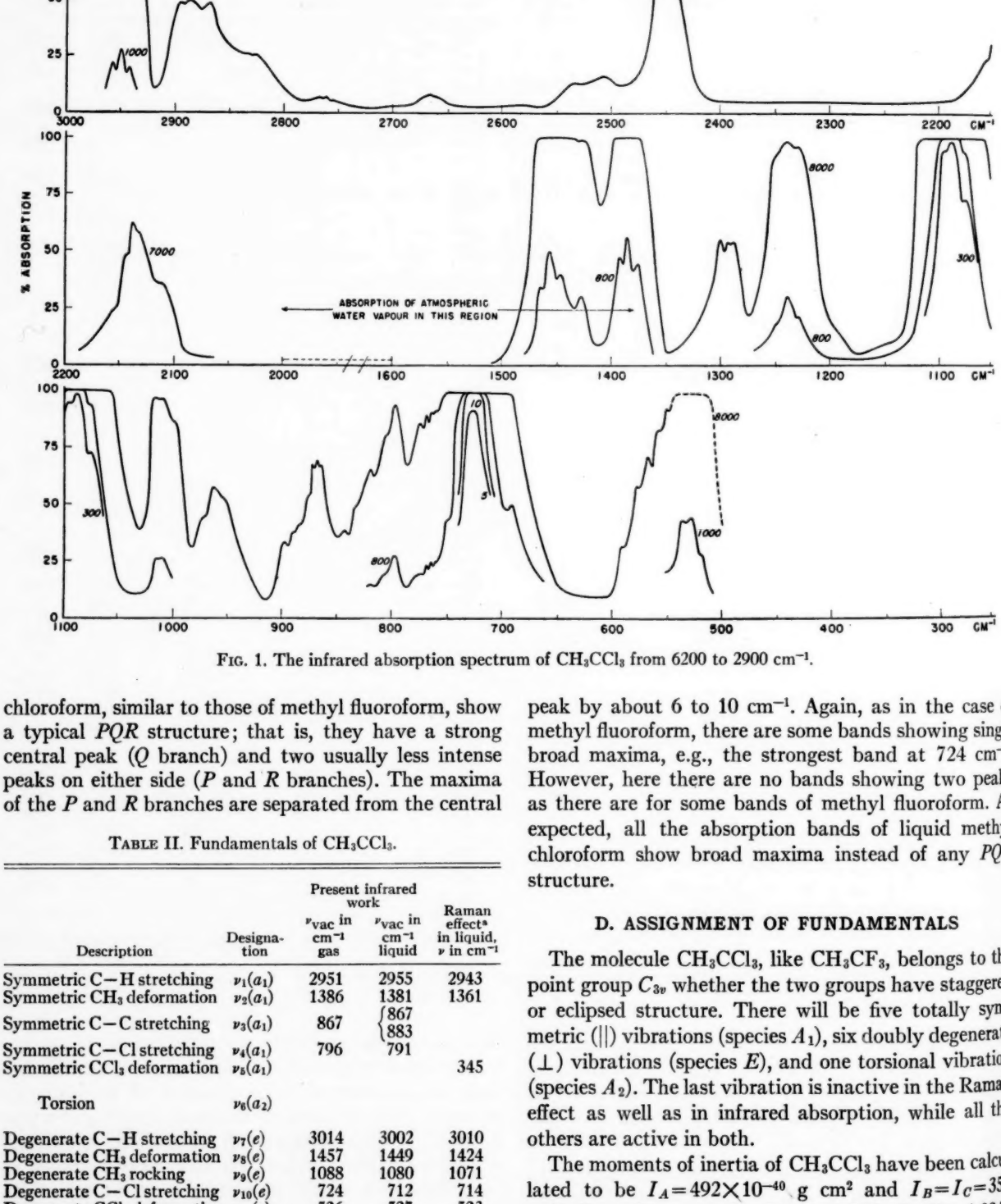

FIG. 1. The infrared absorption spectrum of CH_3CCl_3 from 6200 to 2900 cm^{-1}.

chloroform, similar to those of methyl fluoroform, show a typical *PQR* structure; that is, they have a strong central peak (*Q* branch) and two usually less intense peaks on either side (*P* and *R* branches). The maxima of the *P* and *R* branches are separated from the central peak by about 6 to 10 cm^{-1}. Again, as in the case of methyl fluoroform, there are some bands showing single broad maxima, e.g., the strongest band at 724 cm^{-1}. However, here there are no bands showing two peaks as there are for some bands of methyl fluoroform. As expected, all the absorption bands of liquid methyl chloroform show broad maxima instead of any *PQR* structure.

TABLE II. Fundamentals of CH_3CCl_3.

Description	Designation	Present infrared work: ν_{vac} in cm^{-1} gas	Present infrared work: ν_{vac} in cm^{-1} liquid	Raman effect[a] in liquid, ν in cm^{-1}
Symmetric C—H stretching	$\nu_1(a_1)$	2951	2955	2943
Symmetric CH_3 deformation	$\nu_2(a_1)$	1386	1381	1361
Symmetric C—C stretching	$\nu_3(a_1)$	867	867 883	
Symmetric C—Cl stretching	$\nu_4(a_1)$	796	791	
Symmetric CCl_3 deformation	$\nu_5(a_1)$			345
Torsion	$\nu_6(a_2)$			
Degenerate C—H stretching	$\nu_7(e)$	3014	3002	3010
Degenerate CH_3 deformation	$\nu_8(e)$	1457	1449	1424
Degenerate CH_3 rocking	$\nu_9(e)$	1088	1080	1071
Degenerate C—Cl stretching	$\nu_{10}(e)$	724	712	714
Degenerate CCl_3 deformation	$\nu_{11}(e)$	526	527	523
Degenerate CCl_3 rocking	$\nu_{12}(e)$			241

[a] See reference 2.

D. ASSIGNMENT OF FUNDAMENTALS

The molecule CH_3CCl_3, like CH_3CF_3, belongs to the point group C_{3v} whether the two groups have staggered or eclipsed structure. There will be five totally symmetric (||) vibrations (species A_1), six doubly degenerate ($\perp$) vibrations (species E), and one torsional vibration (species A_2). The last vibration is inactive in the Raman effect as well as in infrared absorption, while all the others are active in both.

The moments of inertia of CH_3CCl_3 have been calculated to be $I_A = 492 \times 10^{-40}$ g cm^2 and $I_B = I_C = 353 \times 10^{-60}$ g cm^2 by assuming C—C = 1.53A, C—H = 1.09A, C—Cl = 1.76A, and tetrahedral angles for the CH_3 and CCl_3 groups. These values give the rotational constants

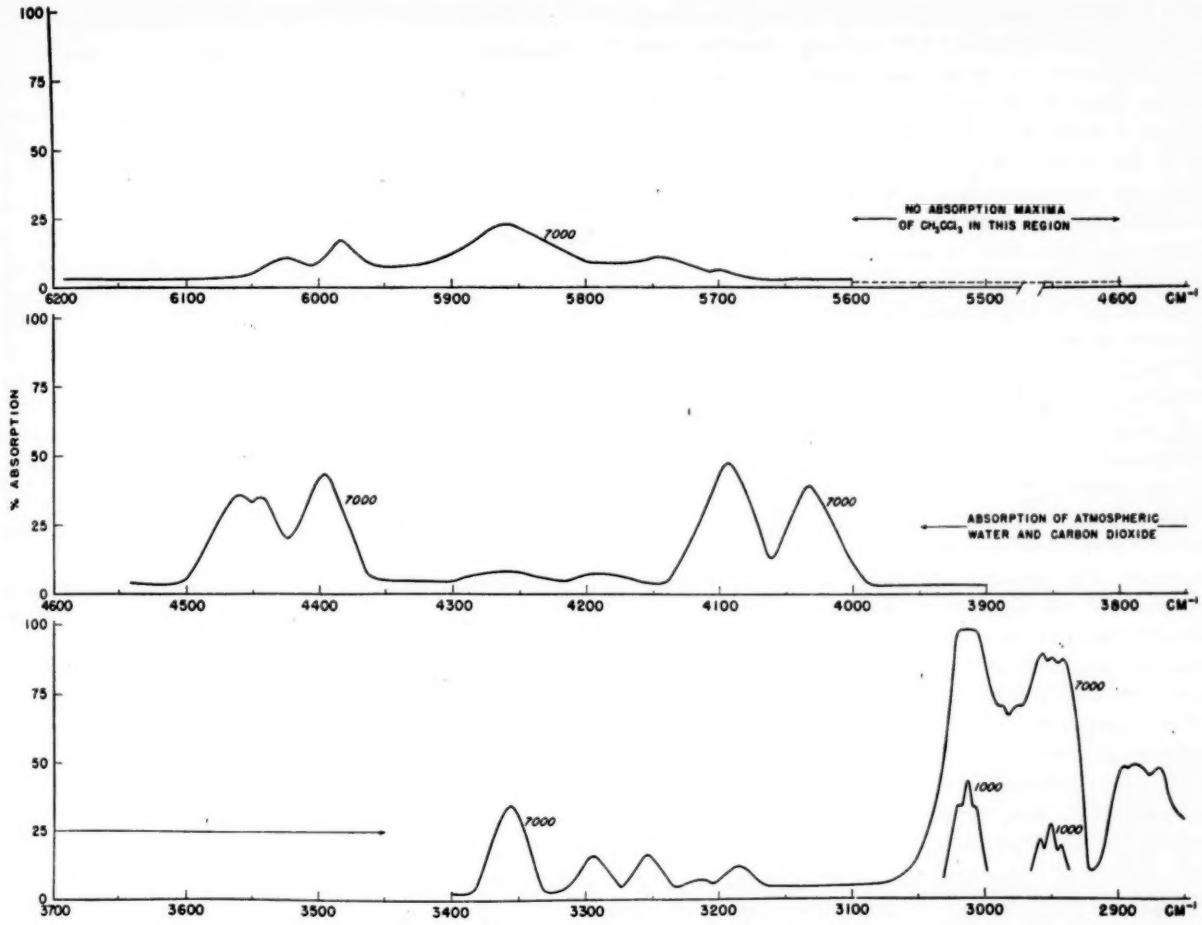

FIG. 2. The infrared absorption spectrum of CH_3CCl_3 from 3000 to 500 cm^{-1}. The italic numbers written on the curves refer to the products of the pressure in mm and the path length in cm of the absorption column used for recording the respective spectra.

as $A=0.0569$ cm^{-1} and $B=0.0793$ cm^{-1}.‖ The separation[5] of the successive subbands (Q branches) of a $\perp$ band for a symmetric top molecule is given by $2[A(1-\zeta_i)-B]$, where ζ_i is the Coriolis interaction constant. As $(A-B)$ is very small for CH_3CCl_3, the separation of the subbands of a $\perp$ band will be small and the band will have the same appearance as a $\parallel$ band provided ζ_i is also small. This seems to be the reason why most of the bands of CH_3CCl_3 have PQR peaks.

If, however, ζ_i is large, the Q branches of the subbands will no longer coincide and a broad maximum will arise. Similarly, the envelopes of superposition of the P and R branches of the subbands show much broader features not separated by minima from the central branch. This appears to be the case for the strongest band of CH_3CCl_3 at 724 cm^{-1} just as for the CH_3CF_3 band at 1235 cm^{-1}. Following the vibrational assignment for CH_3CF_3, the band 724 cm^{-1} of CH_3CCl_3 is attributed to the degenerate C—Cl stretching vibration $\nu_{10}(e)$ (Table II). The second C—Cl stretching vibration $\nu_4(a_1)$ corresponds to the band 796 cm^{-1}, which appears to have a PQR structure. The magnitudes of these C—Cl stretching frequencies agree with those in other molecules[5,6] like $CHCl_3$, CH_2Cl_2, and CF_3CCl_3. However, unlike that in the other molecules, the symmetric C—Cl stretching frequency of CH_3CCl_3 is greater than the corresponding degenerate frequency. This behavior is similar to that of the C—F frequencies in CH_3CF_3.

It is natural to assign the bands 2951 and 3014 cm^{-1} to the symmetric and degenerate C—H stretching vibrations, $\nu_1(a_1)$ and $\nu_7(e)$, respectively (Table II), and similarly the bands 1386 and 1457 cm^{-1} to the CH_3 deformation vibrations $\nu_2(a_1)$ and $\nu_8(e)$, respectively. These assignments are supported[7] by those in CH_3CN, where, unlike those in CH_3CCl_3, the parallel and perpendicular bands can be unambiguously distinguished. The parallel and perpendicular C—H stretching frequencies of CH_3CN are at 2954 and 3009 cm^{-1}, respectively; and the corresponding CH_3 deformation frequencies are at 1388 and 1413 cm^{-1}.

‖ Using this value of B in the formula (reference 5) $\Delta\nu=2.358(TB)^{\frac{1}{2}}$, where $\Delta\nu$ is the separation of the maxima of P and R branches and T is the absolute temperature, one gets $\Delta\nu=10.4$ cm^{-1}, which is of the same order of magnitude as the observed separation.

[5] G. Herzberg, *Infrared and Raman Spectra of Polyatomic Molecules*, (D. Van Nostrand Company, Inc., New York, 1945).

[6] G. Glockler and C. Sage, J. Chem. Phys. **9**, 387 (1941).

[7] P. Venkateswarlu, J. Chem. Phys. **19**, 293 (1951).

The CH_3CCl_3 band at 1088 cm^{-1} corresponds very probably to the degenerate CH_3 rocking vibration $\nu_9(e)$. This assignment is quite reasonable, as the corresponding band in methylcyanide is at 1059 cm^{-1}. The 1088 cm^{-1} band of CH_3CCl_3 shows *PQR* peaks like most of the other CH_3CCl_3 bands, while, as mentioned earlier, the corresponding CH_3CF_3 band, 970 cm^{-1}, shows two peaks instead of three.

Comparing with other molecules having C—C bonds, one concludes that the observed band at 867 cm^{-1} corresponds to the C—C stretching vibration $\nu_3(a_1)$. This frequency is 830 cm^{-1} in the case of CH_3CF_3 and 919 cm^{-1} in CH_3CN.

Besides the eight fundamentals discussed above, there must be three more fundamentals which are active in both the infrared and Raman effect. They are the low frequency CCl_3 vibrations (see Table II). In the Raman spectrum of liquid CH_3CCl_3, Hull[2] observed three low frequency bands at 241, 341, and 523 cm^{-1}. The present observations in the infrared absorption of the vapor show a band at 526 cm^{-1}. The expected infrared bands corresponding to the Raman bands 241 and 345 cm^{-1} fall beyond the region investigated here. The Raman band 241 cm^{-1} can be assigned to the degenerate CCl_3 rocking vibration $\nu_{12}(e)$, since the similar vibrational frequencies in $CHCl_3$ and $CDCl_3$ are at 260 cm^{-1} and 262 cm^{-1}, respectively. The band 345 cm^{-1} can be assigned to one of the CCl_3 deformation vibrations and the band 523 cm^{-1} to the other, but it is surprising that there is such a large difference between the two. It is possible that one of the CCl_3 deformation frequencies is not observed in the Raman spectrum and that 523 cm^{-1} is a combination band. This point cannot be decided definitely until the infrared absorption spectrum of methyl chloroform has been investigated in the region 250–500 cm^{-1}. However, the large intensity of the band 526 cm^{-1} both in infrared absorption and in the Raman spectrum strongly suggests that it corresponds to a fundamental.

In Table II the frequencies of the fundamentals of CH_3CCl_3 and the description of their respective vibrational modes are summarized. For comparison the Raman frequencies of the liquid, according to Hull, are included.

E. OVERTONE AND COMBINATION BANDS

Besides the fundamentals discussed above, there are a large number of overtone and combination bands as shown by Table I. The first overtone of the strongest fundamental 724 cm^{-1} is at 1428 cm^{-1} and is fairly strong. The first overtones of the fundamentals $\nu_7{}^{C-H}(e)$ and $\nu_8{}^{CH_3}(e)$ show the expected splitting into two bands each (species A_1 and E) as observed in the same type of overtones in CH_3I[8] and CH_3CF_3.[1] The two components of $2\nu_8$ lie at 2835 cm^{-1} and 2888 cm^{-1} both showing *PQR* structure. The components of $2\nu_7$ lie at 5984 and 6027 cm^{-1}; but their *PQR* peaks are not separated, because the resolution of the instrument in that region is not high enough. The first overtone of the CH_3 rocking vibration $\nu_9(e)$ is at 2138 cm^{-1} showing *PQR* peaks and is fairly strong. This 2138 cm^{-1} band is probably the A_1 component of $2\nu_9$, the E component being at 2155 cm^{-1}, which is weaker and does not show *PQR* branches.

The band at 1009 cm^{-1}, which could be interpreted as either $2\nu_{11}$ or $\nu_4+\nu_{12}$ is fairly strong and so is the overtone $2\nu_1$ at 5861 cm^{-1}. However, the overtone $2\nu_2$ is extremely weak, $2\nu_5$ is observed only in the liquid and $2\nu_4$ and $2\nu_3$ are not observed in the present recordings.¶

All the other bands are easily interpreted as binary and ternary combinations, the latter usually being very weak. The calculated wave numbers for all overtone and combination bands, based on the adopted vibrational assignment of the fundamentals and neglecting anharmonicity, are included in Table I.

ACKNOWLEDGMENT

The author wishes to express his thanks to Dr. G. Herzberg for suggesting the problem and for his continued interest during the course of the work.

[8] G. Herzberg and L. Herzberg, Can. J. Research **B27**, 332 (1949).

¶ In the region 1500–1910 cm^{-1}, the following bands are recorded in the API catalog: 1543, 1567, 1597, 1730, 1800, and 1910 cm^{-1}, which could be interpreted according to the above Table II as $3\nu_{11}(A_1+E)$, $2\nu_4(A_1)$, $\nu_9+\nu_{11}(A_1+E)$, $2\nu_3(A_1)$, $\nu_9+\nu_{10}(A_1+E)$, and $\nu_2+\nu_{11}(E)$, respectively. However, these bands are not recorded in the present experiments. This might be because of the strong water vapor absorption in this region and because these bands are not strong. The bands 4720, 3860, 3760, 3660, 3560, 3100, 2040, 1170, 1167, and 1161 cm^{-1}, which are also recorded in the API catalog and which are not obtained in the present experiments, are probably due to impurities.

Thermomagnetic Investigations of Promoted and Unpromoted Iron Oxide and Iron Catalysts*

LOUIS R. MAXWELL AND J. SAMUEL SMART
Naval Ordnance Laboratory, Silver Spring, Maryland
AND
STEPHEN BRUNAUER
Bureau of Ordnance, Washington, D. C.
(Received June 19, 1950)

The Curie temperature (θ) and intensity of magnetization of certain unreduced and reduced iron oxide catalysts have been determined. For the singly promoted unreduced systems of Fe_3O_4 containing small amounts of one of the following, Na_2O, K_2O, Cs_2O, BaO, B_2O_3, Al_2O_3, or SiO_2, θ was found to be practically the same as for Fe_3O_4, but large reductions in the saturation intensity of magnetization (I_s) were observed. The doubly promoted unreduced systems studied contained additions to Fe_3O_4 of Al_2O_3 and one of the following (in small amounts): Na_2O, K_2O, BaO, or SiO_2. θ for these materials varied only slightly and was either equal to or less than that for Fe_3O_4. Large reductions in I_s were found. Magnetic measurements on the reduced materials gave values of θ the same as for pure iron. The extent to which the promoters go into solid solution, both for the unreduced and reduced materials, is determined. Additional unreduced unpromoted iron oxides were investigated that had variable ratios (γ) of Fe^{++}/Fe^{+++}. Starting at $\gamma=0.352$, I_s was found to increase with increasing γ to a maximum at $\gamma=0.50$, agreeing with the known value for magnetite, and then to decrease to a small value for large γ. The value found for I_s at $\gamma=0.352$ is in agreement with Néel's theory of "ferrimagnetism" as applied to cubic Fe_2O_3 and Fe_3O_4. θ was found to be constant at about 583°C for γ from 0.352 to 1.276.

I. INTRODUCTION

A KNOWLEDGE of the location of promoters in iron oxide and iron catalysts contributes greatly to the understanding of the nature of promoter action in catalysts. In the case of the singly promoted unreduced iron oxide catalyst, $Al_2O_3+Fe_3O_4$, two questions can be asked: first, where is the Al_2O_3 located before the iron oxide catalyst is reduced to the state of iron; and secondly, where is the Al_2O_3 located after reduction? The significance of the first question comes from the well-known fact that the previous history of a catalyst plays an important role in its catalytic activity.

It has been considered likely that in the preparation of a fuzed oxide catalyst, the Al_2O_3 promoter goes into solid solution with Fe_3O_4. The x-ray diffraction investigation of Wyckoff and Crittenden[1] supported this conclusion.

The second question was studied by Brill[2] who showed that in the reduced catalyst the aluminum is in the form of extremely finely divided Al_2O_3—the crystal size was estimated at probably less than 10^{-5} cm on a side.

Another approach to these problems can be made by thermomagnetic investigations. The way in which the saturation intensity of magnetization varies with temperature can provide information concerning the location of the promoters in these catalysts. The present paper describes thermomagnetic studies of certain catalysts prepared (1919–1926), at the Fixed Nitrogen Research Laboratory of the U. S. Department of Agriculture.

II. EXPERIMENTAL METHOD AND PROCEDURE

A photographic method similar to that described by Dejean[3] was used to record the thermomagnetic data. A small spot of light traversed the surface of a photographic paper which was held stationary. The motion of the spot of light was produced by two mutually perpendicular displacements, one proportional to the intensity of magnetization, the other proportional to the temperature of the sample. The trace, thus formed gives the intensity of magnetization as a function of the temperature, expressed by a curve in a rectangular two-coordinate system.

The ferromagnetic specimens placed in a strong magnetic field H, having a constant $\partial H/\partial x$, were acted upon by a force F, in the x direction of an amount

$$F=(\partial H/\partial x)I_sV, \qquad (1)$$

where V is the volume of the material, I_s the saturation intensity of magnetization. A linear relationship between F and I_s was realized approximately by constructing an electromagnet containing pole pieces that gave a constant $\partial H/\partial x$ in a region where H was large.

Figure 1(a) shows a sketch of a longitudinal cross section taken through the ends of the circular pole pieces used. The nature of the magnetic field obtained by such an arrangement is illustrated in Fig. 1(b). This spacial distribution of magnetic field intensities is in agreement with the data obtained by Buehl and Wulf[4] for similar pole pieces.

Powdered unreduced material was contained in a small platinum capsule,† held between the pole pieces of the electromagnet by means of an alundum tube which was suspended by a small torsion rod. For the reduced catalysts, the material was held in an atmosphere of nitrogen within a glass capsule.

On application of the magnetic field, the resulting

* Supported in part by the ONR.
[1] R. W. G. Wyckoff and E. D. Crittenden, J. Am. Chem. Soc. 47, 2866 (1925).
[2] R. Brill, Z. Elektrochem. 38, 669 (1932).
[3] P. Dejean, Ann. Physik 18, 171 (1922).
[4] R. Buehl and J. Wulf, Rev. Sci. Instr. 9, 224 (1938).
† Demagnetization fields, not amenable to computation, existed so that Eq. (1) is only approximate. Calibration tests, however, made with nickel and iron, showed that Eq. (1) proved to be sufficiently correct for the determination of Curie temperatures.

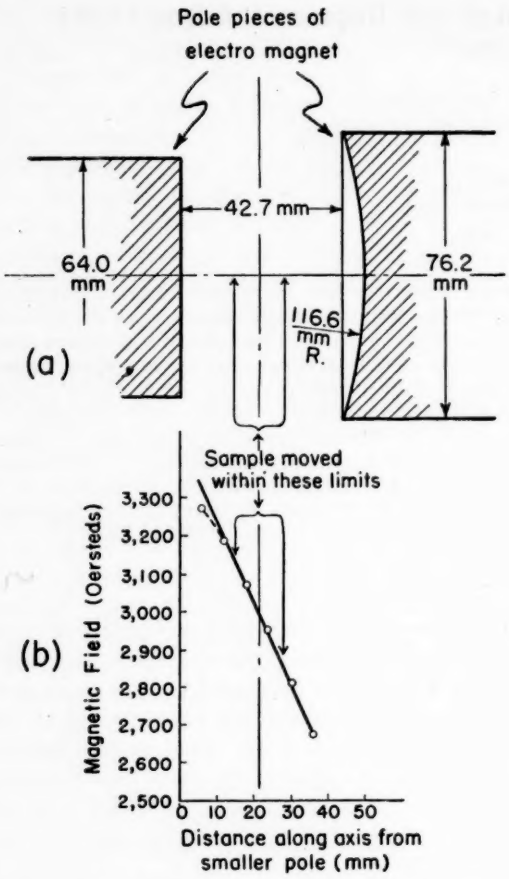

FIG. 1. Diagram illustrating the shape of the pole pieces used and the variation in the intensity of the magnetic field.

torque twisted the torsion rod, thereby rotating a plane mirror (M) mounted on the axis of the rod. The angular displacement of M was directly proportional to the forces acting on the sample.

Specimen temperatures were determined by means of a calibrated thermocouple arrangement with the hot junction held in contact with the capsule. The angle of rotation of a galvanometer mirror (N) in the thermocouple circuit was, therefore, proportional to the temperature of the specimen.

The specimens were heated by a cylindrically shaped furnace noninductively wound with nichrome V wire having a magnetic permeability of about 1.001. Heat insulation was obtained by using radiation shields. This compact furnace with one end open could be slid around the specimen and fitted between the pole pieces. The time required to heat the samples through the Curie temperature varied from 30 to 40 minutes.

The mirrors M and N were arranged in an optical system suitable for tracing out the thermomagnetic curves as described previously.

III. EXPERIMENTAL TESTS OF APPARATUS AND PROCEDURE

Preliminary runs on pure nickel.—A sample of nickel (No. N24), with a total amount of impurities of 0.067 percent, was kindly furnished by Mr. Harold E. Cleaves of the National Bureau of Standards for calibration purposes. Figure 2 shows a typical curve obtained for this material. Six runs were made on a sample held in an atmosphere of nitrogen which gave a Curie point of 369±1°C, while three runs on a second sample in air gave the same value. From Stoner[5] we find the Curie point $(\theta)_H$ of nickel in a field of H (in oersteds) given by

$$(\theta)_H=(\theta)_{H=0}+0.20(H^{\frac{1}{2}}), \qquad (2)$$

where reliable data give $(\theta)_{H=0}$ varying from 357.6°C to 360°C. If we take $(\theta)_{H=0}$ as 359° then from Eq. (2) we have for comparison with the present data a value of $(\theta)_H=370°$ for $H=3000$ oersteds. The agreement is within the experimental error.

Preliminary runs on pure iron.—Two different samples of iron having high purity were also furnished by Mr. Cleaves. One piece was from a quantity identified as No. 1 electrolytic iron ingot 8×, while the other was from ingot No. 9. Total amount of impurities were given as less than 0.009 percent. Eleven runs were made on three different samples of ingot No. 9 in air which, when averaged together, gave a Curie point of 780 ±1.6°C. Three runs in air, one by cooling, were made on a sample from the electrolytic iron which gave a Curie point of 779±1.3°C. Previous determinations, given in the literature, vary from 760 to 780°C (see reference 5) including changes in the Curie point due to existing magnetic fields. Pruess, for example, found a θ_H for iron of 774°C at $H=10{,}000$ oersteds. The present values found for iron appear slightly higher than was expected. The agreement, however, is considered satisfactory since, surprisingly, there appears to be no accurate value for reference in the case of iron.

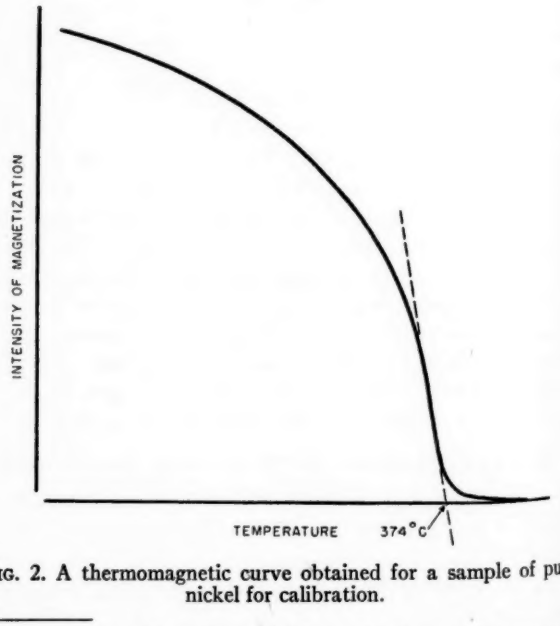

FIG. 2. A thermomagnetic curve obtained for a sample of pure nickel for calibration.

[5] E. C. Stoner, *Magnetism and Matter* (Methuen and Company, Ltd., London, 1934), pp. 383–4.

IV. RESULTS ON UNREDUCED CATALYSTS

Singly Promoted

Figure 3 shows typical records made on Fe_3O_4, Fe_3O_4 containing 20 mole percent Al_2O_3, and Fe_3O_4 containing 35.4 mole percent Al_2O_3. The temperature at which these materials lose their magnetization is roughly the same, but their intensities of magnetization are considerably different. Figure 4 illustrates other runs taken with other types of promoters. The same general behavior exists. For the case of the doubly promoted catalyst containing 6.02 mole percent Al_2O_3 and 0.80 mole percent BaO, the intensity of magnetization is about one-tenth that of Fe_3O_4, but the Curie point has not been greatly changed. It is apparent from these data that these materials show greater variation in their intensities of magnetizations than in their Curie temperatures.

The present apparatus was not designed for quantitative determinations of the intensity of magnetization; however, a procedure was adopted to obtain this information. A number of carefully weighed samples of unreduced catalysts, covering a wide range of intensities of magnetization, were submitted to Mr. R. L. Sanford of the National Bureau of Standards, who furnished accurate values for their intensities of magnetization. This information was obtained at an effective magnetizing field of 3000 oersteds. These samples were then used to calibrate the force deflections of the present apparatus so that the intensity of magnetization could be obtained for all of the remaining materials.

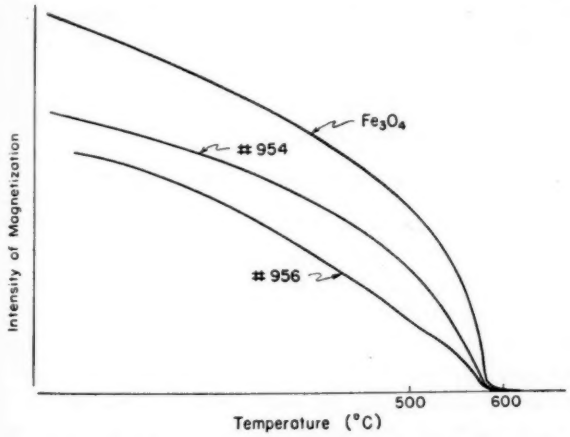

FIG. 3. Typical thermomagnetic curves for Fe_3O_4 and two singly promoted (Al_2O_3) unreduced catalysts Nos. 954 and 956 having 20 and 35.4 mole percent of Al_2O_3 respectively.

A summary of the data obtained for the singly promoted unreduced catalysts is shown in Table I. A number of different oxides have been used as promoters. Catalyst No. 956, containing about 35 mole percent of Al_2O_3, represents the case of the greatest amount of added promoter. The most striking fact shown by Table I is the constancy of the Curie point with corresponding large variations in the intensity of magnetization.

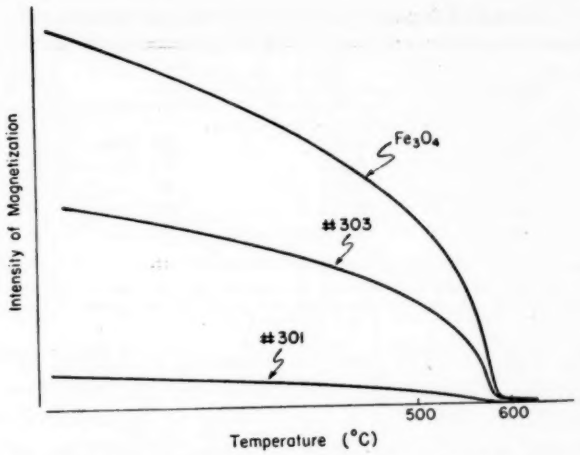

FIG. 4. Thermomagnetic curves for unreduced singly promoted (No. 303, 2.5 mole percent BaO) and doubly promoted (No. 301, 6.02 mole percent Al_2O_3, 0.80 mole percent BaO) catalysts.

Unpromoted

One group of unreduced catalysts studied are identified by the fact that they contain no added promoter. They are distinguishable by the amount of oxidation which occurred during their preparation. As a result, we have a series of iron oxides having various amounts of ferrous and ferric ions. We define γ as the ratio of the number of ferrous to ferric ions. Table II lists the results obtained for the Curie temperatures for a number of these compounds. Data for catalyst No. 973 ($\gamma = 0.50$), s given for comparison. The differences found in the Curie temperatures are not considered to be significant.

Data on the intensity of magnetization, at room temperature, were obtained as a function of the applied field up to about 10,000 oersteds. The measurements were made at the National Bureau of Standards under the direction of Mr. R. L. Sanford. The apparatus used was a high H permeameter.[6] The results are plotted in

TABLE I. Summary of data obtained for singly promoted unreduced catalysts.

Catalyst No.	Composition mole-percent	Curie point (°C)	Intensity of magnetization at room temperature (cgs units)
973[a]	Fe_3O_4	585 (19)[b]±1.3	460
210	5.4 Na_2O bal. Fe_3O_4	583 (4)±0.75	298
930	2.5 K_2O bal. Fe_3O_4	582 (4)±1.0	374
215	0.30 Cs_2O bal. Fe_3O_4	583 (4)±0.5	196
303	2.5 BaO bal. Fe_3O_4	583 (4)±1.25	246
380	2.4 B_2O_3 bal. Fe_3O_4	582 (4)±1.0	264
954	20.4 Al_2O_3 bal. Fe_3O_4	585 (4)±1.0	354
956	35.4 Al_2O_3 bal. Fe_3O_4	585 (4)±1.5	280
232	15 SiO_2 bal. Fe_3O_4	574 (3)±1.25	225

[a] Contains trace of Al_2O_3 that has been neglected.
[b] Numbers within the parenthesis give the number of runs taken. Variations given are the average deviations from the mean without regard to sign.

[6] The apparatus used is described by R. L. Sanford and E. G. Bennett, J. Research Natl. Bur. Standards **26**, January 1941.

TABLE II. Summary of data on Curie temperatures.

Catalyst No.	$\gamma = \frac{Fe^{++}}{Fe^{+++}}$	Curie temperature (°C)
909	0.352	585 (3)*±1.0
973	0.500	585 (19)±1.3
918	0.551	582 (3)±0.6
926	0.774	583 (3)±1.6
928	1.276	582 (3)±1.0

* Numbers within brackets are the number of runs taken. Variations given are the average deviations from the mean without regard to sign.

Fig. 5. It is noticed that saturation sets in at about 3000 oersteds. Figure 6 illustrates how the saturation magnetization varies as a function of γ; the maximum occurring at approximately that value of γ corresponding to magnetite.

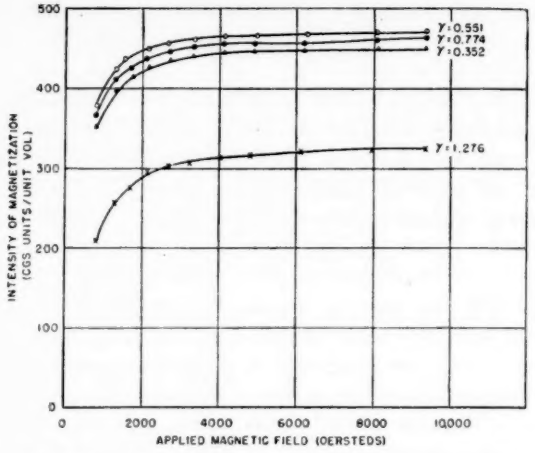

FIG. 5. Relationship between the intensity of magnetization and applied field for various values of $\gamma = Fe^{++}/Fe^{+++}$.

Doubly Promoted

Table III gives the results obtained for the unreduced doubly promoted catalysts, as indicated by the information in the first four and the last columns. These doubly promoted catalysts contained, in all but one case, Al_2O_3 as one component. The second component was one of the single promoters listed in Table I We find in these data a situation somewhat similar to that found for the singly promoted catalysts: small variations in the Curie point but large variations in the intensity of magnetization. Additions of these various oxides, in every instance, reduced the intensity of magnetization—the Curie point either remained constant or decreased slightly.

In the last column of Table III, we have listed the nature of the slope of the intensity of magnetization *vs* temperature curves. This terminology refers to the steepness of the slope of the curves in the neighborhood of the Curie point. The curves for the doubly promoted catalysts are classified as having either a steep, flat, or double slope. Figure 7 illustrates examples of a steep and double slope for Nos. 178 and 952 respectively. This distinction has been made because it shows an important characteristic of the material which is not evident when only values for the Curie temperature are given. Two separate phases with different Curie temperatures may show a resultant thermomagnetic curve that has only an approximately flat slope which does not resolve itself into two abrupt reductions in I_s which could be identified as two Curie temperatures.

V. RESULTS ON REDUCED CATALYSTS

Table IV summarizes the data obtained for the reduced catalysts. The Curie temperature obtained for these materials is close to the value for pure iron. Although no calibration measurements were made of the intensity of magnetization of these materials, it was estimated, from the forces developed on the samples studied, that they did not show as great a variability in the intensity of magnetization as found for the unreduced catalysts.

VI. DISCUSSION

The Curie temperature can be expressed[7] approximately in terms of the exchange energy of interaction J

TABLE III. Summary and calculations of data for doubly promoted unreduced catalysts.

Catalyst No.	Composition mole percent	Curie point (°C)	Intensity of magnetization at room temperature (cgs units)			Nature of slope
	Balance Fe_3O_4		Experimental	Calculated	Expt/Calc	
922	2.35 Al_2O_3 0.61 K_2O	583 (4)*±2.5	446	427	1.04	Steep
178	3.80 Al_2O_3 2.27 K_2O	571 (6)±1.7	342	363	0.94	Steep
951	5.07 Al_2O_3 7.98 K_2O	561 582	290	158	1.83	Double slope
952	14.70 Al_2O_3 11.90 K_2O	583±1.5 560	350	0	—	Double slope
383	1.21 B_2O_3 0.48 K_2O	574 (4)±0.5	380	345	1.10	Steep
401	6.35 Al_2O_3 4.25 Na_2O	579 (4)±1.0	185	300	0.62	Flat
234	1.18 Al_2O_3 6.88 SiO_2	576 (3)±0.3	348	347	1.00	Steep
301	6.02 Al_2O_3 0.80 BaO	569 (4)±1.70	31	363	0.08	Flat

* Numbers within the parenthesis give the number of runs taken. Variations given are the average deviations from the mean without regard to sign.

[7] R. M. Bozorth, Bell System Tech. J. **19**, 1 (1940).

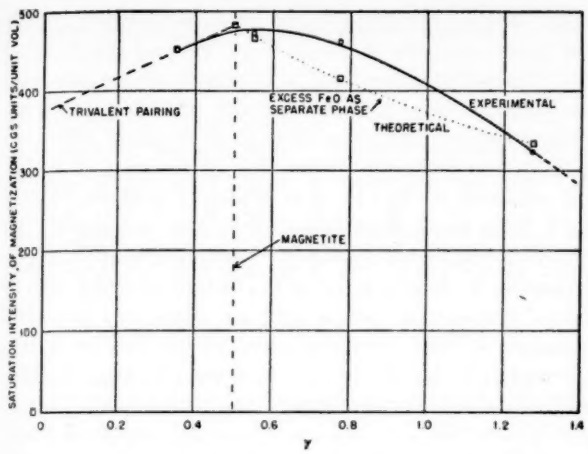

FIG. 6. Variation of saturation magnetization with γ; full curve experimental, broken curve theoretical.

by

$$\theta \sim zJ/k, \tag{3}$$

where z is the number of nearest magnetic neighbors, and k is the Boltzman constant. It is apparent, therefore, that any loss or gain in the number of nearest neighbors, for a completely homogeneous material, should result in a corresponding linear change in the Curie temperature provided that J remained constant.

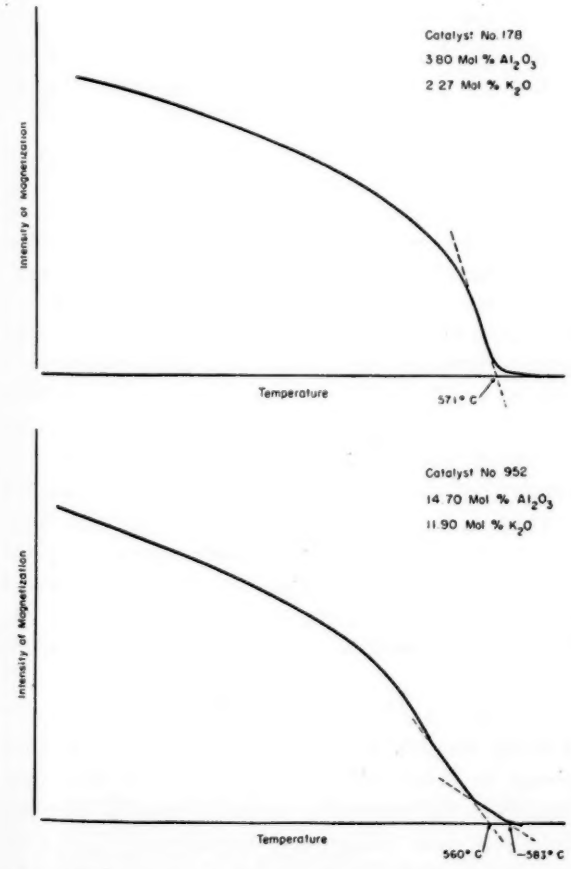

FIG. 7. Thermomagnetic curves of unreduced doubly promoted catalysts illustrating variation of slope with concentration of promoters.

TABLE IV. Summary of data obtained for reduced catalysts.

Catalyst No.	Composition before reduction (mole percent)	Curie point (°C)
973	Fe_3O_4	779 (3)±1.6
954	20.4 Al_2O_3	779 (2)±1.0
930	2.5 K_2O	779 (3)±1.5
178	3.8 Al_2O_3 2.27 K_2O	782 (1)
952	14.70 Al_2O_3 11.90 K_2O	782 (1)
301	6.02 Al_2O_3 0.80 BaO	777 (3)±0.3

From Table I we find that, with the exception of the case of catalyst No. 232 containing 15 mole percent of SiO_2, the Curie temperatures of the unreduced catalysts lie within the range 582 to 585°C. The most surprising case of these is No. 954 containing 20.4 mole percent of Al_2O_3. When the amount of Al_2O_3 was increased to 35.4 mole percent, for No. 956, the Curie temperature remained unchanged but the slope of the thermomagnetic curve, as it approached the Curie temperature, showed an indication of a new phase whose Curie point is considerably below that for Fe_3O_4, see Fig. 3.

An intensity of magnetization I (theor) has been calculated on the assumption that the promoters serve only to reduce the intensity of magnetization in proportion to the volume which they occupy. The results of such a calculation are given by Fig. 8. The ratios of the experimental to theoretical values of the intensity of magnetization are plotted with respect to the ionic radii of the metallic ion as given by Goldschmidt. Considering first the case of the addition of Al_2O_3, we have a point indicated by Al^{+++} which was taken from catalyst No. 954 listed in Table I. The intensity of magnetization was found to be nearly proportional to the volume occupied by the Fe_3O_4. Such a situation was not found for the other ions; the greater the ionic radii differ from those for Fe^{++} and Fe^{+++} the greater is the reduction in the intensity of magnetization.

For the doubly promoted unreduced catalysts, we have calculated an intensity of magnetization on the assumption that each of the promoters act independently

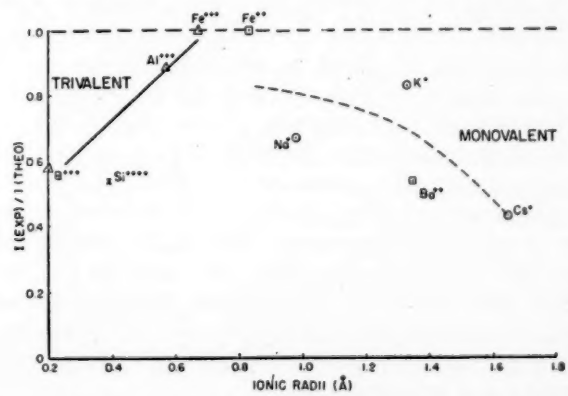

FIG. 8. Correllation of intensity of magnetization with ionic radii for singly promoted catalysts.

in reducing the intensity of magnetization but with the same effectiveness as found when they are used as single promoters. How well such an assumption agrees with the experiment is found in Table III for the values of Expt/Calc listed in the sixth column. We find that this ratio is near unity for catalysts Nos. 922, 178, 383, and 234. For these materials, the slope of the thermomagnetic curve near the Curie point is steep or is a type of curve characteristic of a single magnetic phase. The corresponding Curie points hold near to or slightly less than that for magnetite. When the amounts of Al_2O_3 and K_2O are increased, as for Nos. 951 and 952, the above calculations of the intensity of magnetization are no longer in agreement with the experimental values. The thermomagnetic curves, however, have a double slope, indicating the existence of new phases within these materials. A certain amount of magnetite still persists for Nos. 951 and 952, because the magnetization is not lost until a temperature of 583°C is reached. When K_2O is replaced by Na_2O or BaO, the calculated value of the intensity of magnetization is much greater than the experimental values and the thermomagnetic curve is flat, indicating the existence of at least two magnetic phases.

Catalyst No. 301 was found to have an intensity of magnetization about 8 percent of the calculated value. The presence of BaO in combination with Al_2O_3 has resulted not only in the formation of at least one new phase but also caused a great reduction of the intensity of magnetization at the applied field of about 3000 oersteds.

Wyckoff and Crittenden[1] obtained x-ray diffraction patterns of catalysts Nos. 954 and 955‡ in the unreduced state. For 954 there was an excess of FeO equal to the excess Al_2O_3, while for No. 955 the amount of Al_2O_3 present was sufficient to combine with only one-half of the excess FeO. The x-ray diffraction patterns showed only the magnetite lines for 954, but for 955, lines from FeO were present. The size of the unit cell for 954 was found to be only slightly greater than that for magnetite (918). It was concluded that probably the Al_2O_3 combines with the excess FeO forming ferrous aluminate ($FeO \cdot Al_2O_3$), which goes into solid solution with $FeO \cdot Fe_2O_3$. Failure to find additional lines from $FeO \cdot Al_2O_3$ was explained by the fact that the size of the unit cells of the two materials are nearly equal as estimated from their densities. It was pointed out by Wyckoff and Crittenden, however, that in the case of unreduced magnetite, promoted with silica and zirconia, the promoters are simply finely mixed; and that in the case of the doubly promoted (K_2O, Al_2O_3) unreduced catalysts, potassium aluminate may exist as an "unmixed solid solution." The present thermomagnetic studies of catalyst No. 954 indicate that the promoter, even if it combines to form the aluminate, exists at least partially as a separate phase.

‡ No. 955 was not studied in this investigation.

Michel and Pouillard[8] have made a thermomagnetic and x-ray analysis of Fe_3O_4 with various amounts of Al^{+++} substituted for Fe^{+++}. It was observed that both the Curie temperature and the size of the unit cell decreased linearly, with increasing amounts of Al_2O_3, up to the point where about one ion out of seven of Fe^{+++} was replaced by Al^{+++}. For greater concentrations of Al_2O_3 both the Curie temperature and the size of the unit cell remained constant. The reduction in Curie temperature, proportional to the reduction in number of Fe^{+++} present, is in accordance with Eq. (3). The constancy of both the Curie temperature and the lattice spacing observed by Michel and Pouillard are readily understood as indicating that the additional Al_2O_3 is not held in solid solution but must exist as a separate phase forming an inhomogeneous system.

Since, in the present investigation, the Curie temperature remained constant for the singly promoted unreduced catalysts to within less than one percent of that for Fe_3O_4, with the exception of No. 232, we are lead to believe that for the following catalysts not more than about one mole percent of the promoters are in solid solution with Fe_3O_4:

Catalyst No.	Promoter (mole percent)
210	5.4 Na_2O
930	2.5 K_2O
303	2.5 BaO
380	2.4 B_2O_3
954	20.4 Al_2O_3
922	2.35 Al_2O_3 0.61 K_2O

Catalyst No. 232 is partially in solid solution to the extent of about 2 percent leaving approximately 13 percent SiO_2 existing as a separate phase. While No. 956 apparently has a phase in solid solution with Fe_3O_4, judging from the slope of the thermomagnetic curve.

Of the remaining doubly promoted unreduced catalysts there are Nos. 178, 383, and 234 which have similar thermomagnetic characteristics, as discussed previously in reference to Table III. Their Curie temperatures have shifted to values about 2 percent below that for Fe_3O_4 with a steep slope at the Curie temperature. This indicates that for these materials an appreciable amount of the promoters have gone into solid solution with Fe_3O_4 forming a predominant single phase system. Catalysts Nos. 951, 952, 401, and 301, all containing a greater concentration of the promoter than the above group, indicate that at least two phases exist in solid solution.

Reduced Catalysts

For the reduced catalysts it is concluded, for those reported in Table IV, that the promoters exist separately from the magnetic material after it has been reduced to pure iron, in agreement with the x-ray investigations mentioned above.

[8] A. Michel and E. Pouillard, Compt. rend. **227**, 194 (1948).

TABLE V. Application of the Néel theory to the binary system $FeO-Fe_2O_3$.

Material	$\frac{Fe^{++}}{Fe^{+++}}$	Interstice			Net number of unpaired electrons* per unit cell (at saturation and 0°K)	
		Tetrahedral	Octahedral		Theory	Experiment
Fe_3O_4	0.50	8 $Fe^{+++}\uparrow$	8 $Fe^{+++}\downarrow$	8 $Fe^{++}\downarrow$	32	32.6
No. 909	0.352	8 $Fe^{+++}\uparrow$	9.30 $Fe^{+++}\downarrow$	6.06 $Fe^{++}\downarrow$	30.7	30.6
$\gamma-Fe_2O_3$	0	8 $Fe^{+++}\uparrow$	13.33 $Fe^{+++}\downarrow$	0	26.7	25.6

*On the basis of five Bohr magnetons for Fe^{+++} and four Bohr magnetons for Fe^{++}.

Binary System $FeO-Fe_2O_3$

The magnetic data given for the unreduced catalysts having variable ratios of ferrous to ferric iron, constitute a basis for studying, in effect, the binary system $FeO-Fe_2O_3$. These data, given in Fig. 6 and Table II, are in essential agreement with similar results obtained by Kopp[9] and Snoek,[10] who found the maximum intensity of magnetization at $\gamma=0.50$ although the maximum was considerably sharper than the one found in the present work. Likewise Snoek[10] found a constant Curie temperature of 585°C for specimens containing between 30 and 65 mole percent Fe_2O_3 which is in excellent agreement with the present data.

These results are of interest in connection with a recent model proposed by Néel[11] to explain the magnetic properties of Fe_3O_4 and $\gamma-Fe_2O_3$. For Fe_3O_4 the 8 tetrahedral holes per unit cell are presumable occupied by Fe^{+++} ions and the 16 octahedral holes are occupied by 8 Fe^{+++} and 8 Fe^{++} ions. Néel has suggested that the trivalent ions in the tetrahedral and octahedral interstices have negative exchange coupling energies, and tend to align anti-parallel, so that at 0°K the saturation magnetization of Fe_3O_4 is entirely due to the divalent ions. Assuming that there is no orbital contribution to the magnetic moment of the Fe^{++} ions, Néel's model predicts a saturation magnetization of 32 Bohr magnetons per unit cell for Fe_3O_4; the experimental value is 32.6.[12]

The crystal structure of $\gamma-Fe_2O_3$ is spinel-like with vacancies occurring in the octahedral holes. Specifically, it is believed that for a cell of 32 oxygen atoms, the 8 tetrahedral holes are filled and that an average of $13\frac{1}{3}$ of the 16 octahedral holes are occupied. All of the Fe ions are trivalent in $\gamma-Fe_2O_3$ and Néel's model of anti-parallel coupling would suggest that the saturation magnetization is due to the unequal numbers of oppositely aligned Fe^{+++} ions. Again assuming the ionic magnetic moment to be due to spin only, one obtains a value of 26.7 Bohr magnetons per cell of 32 oxygen atoms for the saturation magnetization of $\gamma-Fe_2O_3$; the experimental value is 25.6.[12]

The catalyst No. 909 has a composition between Fe_3O_4 and $\gamma-Fe_2O_3$, so that it offers an interesting possibility of checking Néel's suggestion. The saturation magnetization of No. 909 at 0°K was estimated by assuming that its I *vs* T curve has the same shape as the corresponding curve for magnetite. The saturation magnetization, computed in this way, is 30.6 Bohr magnetons per unit cell. Néel's model would predict 30.7. Table V summarizes the above correlation, while the dashed portion of the theoretical curve given in Fig. 6 is shown for comparison with the experimental curve for data reduced to room temperature. For values of γ above 0.5, x-ray diffraction measurements[1] indicate that the excess FeO exists as a separate phase. The x-ray pattern of FeO became progressively stronger as γ increased. To explain the reductions of intensity of magnetization with increasing γ, we simply assume that the excess FeO exists as a separate nonmagnetic phase which gives the dotted curve shown in Fig. 6. The agreement with the experimental results, however, is only fair.

Attempts were made to explain, by the Néel theory, the reduction of the intensity of magnetization of the unreduced catalyst, No. 954. The Al^{+++} was assumed to fit into the lattice without distortions. The agreement was unsatisfactory. If one wishes to accept the idea of pairing of the ferric ions to hold when different types of metallic ions are present, then we would conclude that the failure to find agreement with the experimental result for No. 954 was due to the fact that the Al_2O_3 was not in complete solid solution with Fe_3O_4—a conclusion already arrived at from the value found for its Curie temperature. It is felt that more information is needed as to the crystal structure of the unreduced singly promoted catalyst before applying the Néel concept of spin orientation to this type of material.

The authors appreciate receiving helpful criticisms of this work by Dr. Paul H. Emmett and the assistance provided by Miss Katharine Love in securing the information on the composition of the materials studied. We are indebted to Dr. Sterling B. Hendricks for proposing this investigation, the experimental part of which was carried out at the Fixed Nitrogen Research Laboratory.

[9] W. Kopp, doctoral thesis (Eidgenössischen Technischen Hochschule, Zurich 1919).
[10] J. L. Snoek, Physica, III, 463 (1936).
[11] L. Néel, Ann. Physik **3**, 137 (1948).
[12] P. Weiss and R. Forrer, Ann. Physik **12**, 279 (1929).

Conductivities of Strong Electrolytes in Aqueous Solution*

ROBERT L. EVANS
Mathematics and Mechanics Department of the Institute of Technology, University of Minnesota, Minneapolis, Minnesota
(Received September 22, 1950)

The concentration dependence of the conductivities of strong electrolytes is of interest in both theory and application. Older theoretical and empirical equations fail at high concentrations.

This article presents three empirical equations for the concentration dependence of conductivity. The first of these contains only a single fitted parameter ("a" in Eq. (1) and Table I). Each of the other equations contains two parameters and follows the experimental curves up to high concentrations. However, Eq. (3) is the only one that shows the proper exponential concentration dependence at very high concentrations.

Also, a description is given of two anomalies in the behavior of tetramethyl ammonium salts.

IN both theoretical and applied chemistry it is of importance to know about the conductivities of strong electrolyte solutions, and especially about their dependence on concentration. Good treatments, both theoretical and empirical, of the conductivities of concentrated solutions would be interesting and very useful, but such treatments are not yet available. Some empirical approaches are presented here for practical use and as a guide to the desired theory.

The Debye-Hückel-Onsager (henceforth D-H-O) theory[1] agrees with the Kohlrausch square root law[2] and yields a satisfactory limiting law,

$$\Lambda/\Lambda^0=1-A(c)^{\frac{1}{2}},$$

for very low concentrations. However, this theory neglects both the hydration of the ions and the concentration dependence of the average or gross dielectric constant, so it cannot be expected to give satisfactory results at high concentrations. Its limiting law for low concentrations is incorporated in three different empirical expressions presented here for representing conductivities over extended concentration ranges.

ONE-PARAMETER EQUATION FOR MODERATE CONCENTRATIONS

All reported equivalent conductances are decreasing and non-negative functions of concentration. Secondly, Kaneko[3] has suggested that the finite ionic diameters should be taken into account. One possible formulation of these two facts and the limiting law is the empirical equation

$$\Lambda/\Lambda^0=\exp\left(\frac{-A(c)^{\frac{1}{2}}}{1+\kappa a}\right), \qquad (1)$$

wherein the A and κ are familiar and computable terms in the D-H-O theory and the "a" is a fitted constant that may or may not have theoretical significance.

Computations with Eq. (1) are greatly facilitated by the use of *Tables of the Exponential Function.*[4]

In Table I there appear the results that are obtained by fitting Eq. (1) to the experimentally observed conductivities of eight strong electrolyte salts of five different valence types. The tabulated values of "a" are "good" values, but not necessarily "best" values, because they were selected for representation within about 1 percent over greatest possible concentration ranges, and because they were not obtained by least square methods. For each salt, the values used for Λ^0 and A are included for reference. As a measure of "goodness of fit," the greatest relative error is given in terms of percent.

The values of A in Table I are higher for salts of multivalent ions, and the concentration range over which the data are fitted is correspondingly less in these cases. However, it is noteworthy that the range of the fitted relative conductances is practically independent of the valence type of the salt.

Bernal and Fowler discussed the hydration of ions in aqueous solutions,[5] and the variations of "a" in Table I can be at least partially attributed to the hydration factor.

Since Eq. 1 has an asymptote and lower bound at

$$\Lambda/\Lambda^0=\exp(-A(c)^{\frac{1}{2}}/\kappa a)=\text{a constant},$$

it cannot give accurate representation in regions of high concentration, where the experimental findings indicate that zero is the greatest lower bound. Thus, one or more other equations are needed if the representation is to be extended to high concentrations.

TWO-PARAMETER EQUATION FOR HIGH CONCENTRATIONS

Hasted, Ritson, and Collie[6] point out that the equivalent conductances of most strong electrolytes are approximately linear functions of concentration in the range between 2 and 6 molar. An expression that includes both a linear term and the correct limiting law

* The author takes pleasure in thanking the Graduate School of the University of Minnesota for a grant in support of this work.

[1] P. Debye and E. Hückel, Physik. Z. **24**, 185, 305 (1923); L. Onsager, Physik. Z. **28**, 277 (1927).

[2] F. Kohlrausch and L. Holborn, *Das Leitvermögen der Elektrolyte* (B. G. Teubner, Leipzig, 1916).

[3] S. Kaneko, J. Chem. Soc. Japan **58**, 675 (1936); (Chem. Abs. **31**, 8324[6] (1937)).

[4] *Tables of the Exponential Function* (Federal Works Agency, Works Progress Administration for the City of New York, 1939).

[5] J. D. Bernal and R. H. Fowler, J. Chem. Phys. **1**, 515 (1933).

[6] Hasted, Ritson, and Collie, J. Chem. Phys. **16**, 1 (1948).

TABLE I. Representation of relative conductance (Λ/Λ^0) by Eq. (1).

Salt	Temp., °C	Λ^0	A[a]	10^8a	Molar conc. range	Rel. cond. (Λ/Λ^0) range	Greatest rel. error, %	Lit. ref.
KCl	18	129.44	0.61357	3.52	$\leqq 2.0$	$\geqq 0.71$	0.8	I.C.T.[b] (234 and 239)
KBr	25	151.8	0.62204	3.72	$\leqq 2.0$	$\geqq 0.72$	0.6	J. and B.[c]
LiCl	25	115.03	0.74808	2.07	$\leqq 1.0$	$\geqq 0.64$	0.9	I.C.T.[b] (233)
$BaCl_2$	25	140.0	1.8146	3.40	$\leqq 0.5$	$\geqq 0.58$	1.1	J. and D.[d]
$Pb(NO_3)_2$	25	143.4	1.80288	1.345	$\leqq 0.7$	$\geqq 0.40$	0.55	I.C.T.[b] (237)
$(NH_4)_2SO_4$	18	132.3	1.6986	2.65	$\leqq 0.2$	$\geqq 0.64$	1.1	I.C.T.[b] (235)
$AlCl_3$	25	158.8	3.1962	−0.62	$\leqq 0.005$	$\geqq 0.79$	0.65	I.C.T.[b] (233)
$MgSO_4$	25	133.06	3.6211	−3.4	$\leqq 0.005$	$\geqq 0.74$	0.85	I.C.T.[b] (236)

[a] Both A and κ were computed as indicated in the book by H. S. Harned and B. B. Owen, *The Physical Chemistry of Electrolytic Solutions* (Reinhold Publishing Corporation, New York, 1950), second edition, pp. 119, 121, 128–9.
[b] "*International Critical Tables*" (McGraw-Hill Book Company, Inc., New York, 1929), Vol. VI (page nos. in parentheses).
[c] G. Jones and C. F. Bickford, J. Am. Chem. Soc. **56**, 602 (1934).
[d] G. Jones and M. Dole, J. Am. Chem. Soc. **52**, 2245 (1930).

is the empirical equation

$$\Lambda/\Lambda^0 = 1 - Bc - A/D \log_e[1 + D^2c/2 + D/2(4c + D^2c^2)^{\frac{1}{2}}], \quad (2)$$

in which A is computed by the D-H-O theory[1] and "B" and "D" are fitted constants. For conductivities of 1–1 valence-type salts at or near room temperature, the value of "B" usually turns out to be about 0.02 less than the H-R-C (Hasted, Ritson, and Collie—or 2 to 6 molar) slope of Λ/Λ^0. For a given pair of values (Λ/Λ^0 and c) an increase in B can be offset by an increase in D, and similarly, B and D can both be decreased. At large concentrations, say, $c > 0.5$ or $c > 1$ for the cases reported here, Eq. (2) is approximated very closely by the simpler equation

$$\Lambda/\Lambda^0 = 1 - Bc - A/D \log_e(1 + D^2c). \quad (2a)$$

Computation with either Eq. (2) or Eq. (2a) is complicated by the fact that for particular values of Λ, c, and B, it is a transcendental equation in D, so that D must be found by the method of successive approximations.

In Table II, there appear the results that are obtained by fitting Eq. (2) to the data for three salts that are also among those included in Table I. With approximately the same accuracy, Eq. (2)[7] represents the conductivities of these salts up to two to five times higher concentrations than does Eq. (1). Only for lithium chloride do the available data include higher concentrations, because solubility imposes an upper limit on the concentration.

The linear or "Bc" term of Eq. (2) is the one with most dependence on concentration at very high concentrations, and this causes the equation to give inaccurate representation at these concentrations. The same disadvantage is inherent in the best other empirical equation, that of Jones and Dole.[8] (The equation of Jones and Dole is also inaccurate at very low concentrations of the salts to which it has thus far been applied.)

For a specific comparison, it is noted that in the case of KBr the Jones and Dole equation is over 8 percent high at $c = 3.75$ and the Shedlovsky equation[9] is already almost 6 percent high at $c = 0.5$.[6]

At very high concentrations the relative conductance is approximately an exponential function of concentration. For example, the relative conductance of lithium chloride is expressed by the equation

$$\Lambda/\Lambda^0 = 1.1308 \exp(-0.23c)$$

with a greatest relative error of 1.2 percent at concentrations between 7 and 14.04 molar. As a result, this feature must be incorporated in any equation that is to extend the representation to very high concentrations.

SECOND TWO-PARAMETER EQUATION FOR HIGH CONCENTRATIONS

An equation that correctly represents all the general features of the relative conductance curves is

$$\Lambda/\Lambda^0 = (1 + \alpha c) \exp(-A(c)^{\frac{1}{2}} - \beta c), \quad (3)[4]$$

in which α and β are fitted constants and A is still that of the D-H-O theory.

Table III presents the results of fitting Eq. (3) to the data for two salts that are also included in Tables I and

TABLE II. Representation of relative conductance (Λ/Λ^0) by Eq. (2).

Salt*	B	D	Molar conc. range	Rel. cond. (Λ/Λ^0) range	Greatest rel. error, %
KCl	0.017	14.66	$\leqq 3.0$	$\geqq 0.68$	0.65
KBr	0.020	15.6	$\leqq 3.75$	$\geqq 0.65$	1.0
LiCl	0.053	12.0	$\leqq 5.0$	$\geqq 0.35$	1.2

* Additional information on these cases is included in Table I and also, for LiCl, on page 239 in reference b of that Table.

[7] For increasing the accuracy and/or the range of fitting with Eq. (2), one could extend it in a way that is suggested by its origination in the equation:

$$A^2 = (4c + D^2c^2)(d(\Lambda/\Lambda^0)/dc + B)^2.$$

That is, one could obtain an equation with one more parameter by solving the differential equation:

$$A^2 = (4c + D^2c^2 + Ec^3)(d(\Lambda/\Lambda^0)/dc + B)^2,$$

but this is not attempted here because the resulting equation would probably be too complicated to be very useful. It is mentioned only for completeness and as a possible aid to other workers.

[8] T. See Table I, footnote d.
[9] T. Shedlovsky, J. Am. Chem. Soc. **54**, 1405 (1932).

II. In both cases, the range of fitting is the entire available one. The lithium chloride concentration range, 14 molar, shows the great extent of fitting that can be obtained with Eq. (3), while the potassium bromide case shows that over a smaller concentration range the fitting obtained with Eq. (3) is about on a par with that of Eq. (2).

A better equation than either (2) or (3) appears to be needed for good representation, up to high concentrations, of the conductivities of salts containing multivalent ions—or at least of bi-ionic salts whose valence type numbers total four or more units.

TABLE III. Representation of relative conductance (Λ/Λ^0) by Eq. (3).

Salt*			Molar conc. range	Rel. cond. (Λ/Λ^0) range	Greatest rel. error, %
LiCl	0.70	0.19	$\leqq$14.04	$\geqq$0.045	5
KBr	0.57	0.10	$\leqq$ 3.75	$\geqq$0.65	0.9

* Additional information on these cases is included in Table I.

ANOMALOUS BEHAVIOR OF TETRAMETHYL AMMONIUM SALTS

A hydration-like effect in solutions containing tetraalkyl ammonium ions is described by Frank and Evans,[10] so the data for these compounds have also been studied. The available data on tetraalkyl ammonium salts[11] show at least two anomalies in their behavior.[12]

First, the values of Λ^0 at 25° for tetramethyl ammonium iodide and bromide solutions give inconsistent values of the limiting equivalent conductance of the tetramethyl ammonium ion, by about 5 or 6 units.

Secondly, the solutions of both the iodide and the bromide of the tetramethyl ammonium ion appear not to follow the D-H-O[1] theoretical limiting law but rather to have limiting slopes that are at least about 50 percent greater than the theoretical ones.[13] This phenomenon does not arise in the case of tetrapropyl ammonium iodide, and the data for tetraethyl ammonium iodide appear to be indecisive on this point. A possible alternative manifestation of this anomaly is the almost linear concentration dependence of the conductivity of tetramethyl ammonium bromide solution at concentrations between 10^{-5} and 10^{-4} molar. This can scarcely be caused by ionic association because the association constant is only of the order of 10^{-3}.

Because of these anomalies, no attempt has been made to fit any of Eqs. (1) through (3) to the data for the tetraalkyl ammonium salts.

[10] H. S. Frank and M. W. Evans, J. Chem. Phys. **13**, 507 (1945).

[11] See reference b of Table I, pp. 231, 234, and 235.

[12] Dr. A. R. Pray of the University of Minnesota is undertaking a study of these anomalies which will include experimental work.

[13] After this article was written, Kuhn and Kraus, J. Am. Chem. Soc. **72**, 3676 (1950), reported a similar anomaly in the cases of octadecyltrimethyl ammonium chloride and nitrate. Their suggested explanation that ". . . the long chain ions pair up and thus exhibit the behavior of 2-1 salts." appears not to be supported by the tetramethyl ammonium salt cases.

Fischer-Tropsch Reaction Mechanism Involving Stepwise Growth of Carbon Chain

R. B. ANDERSON,* R. A. FRIEDEL,* AND H. H. STORCH†
Synthetic Liquid Fuels Branch, Bureau of Mines, Bruceton, Pennsylvania
(Received May 15, 1950)

Expressions are derived which predict satisfactorily the observed isomer and carbon number distribution of products from iron and cobalt catalysts in the Fischer-Tropsch synthesis. These expressions are based on three schemes of stepwise addition of one carbon atom to the end or adjacent-to-end carbons of the longest carbon chain of the growing group at the catalyst surface. The implications of these schemes to some general aspects of the reaction mechanism are considered.

THE products of the Fischer-Tropsch synthesis are not in thermodynamic equilibrium with respect to the types of molecules, structures of the carbon chains, and possibly carbon number distribution.[1] Hence, the nature of the products is at least partly determined by the reaction mechanism. The extent to which the products of primary reactions are modified by subsequent reactions is difficult to estimate.

This paper considers the formation of Fischer-Tropsch products by the stepwise additions of one carbon atom to the growing chain. It will be shown that simple rules for the stepwise, one-carbon-atom addition satisfactorily predict the available hydrocarbon isomer distribution and carbon number distribution data.

Mechanisms of this general type have been discussed previously. Herington,[2] Beeck,[3] and Friedel and Anderson[4] considered the carbon number distribution of hydrocarbons from cobalt catalysts, and Weller and Friedel,[5] Weitkamp,[6] and Anderson,[7] the isomer distribution of hydrocarbons from iron and cobalt catalysts. In these papers, as well as in the present one, it is assumed that the hydrocracking reactions postulated by Craxford[8] do not occur to a significant extent. The present paper considers a simple kinetic picture of chain growth that predicts the carbon number as well as the isomer distribution. Three sets of rules for addition of one carbon atom will be discussed. In all three cases, addition is postulated to occur *only at end or adjacent-to-end carbon atoms of the longest carbon chain* and does not occur on an adjacent-to-end carbon atom already attached to three carbon atoms. It is assumed that the rate constants for addition to end carbon atoms are equal, i.e., independent of the length and structure of the growing chain. Similarly, rate constants for addition to adjacent-to-end carbon atoms are assumed to be equal, but different in magnitude from those for end carbons.

The three postulated schemes of addition are:

A. Addition may occur at *only one end* of the growing chain on *only one end* carbon atom if two are present or on the adjacent-to-end carbon.[9] This scheme was considered by Weitkamp[6,10] and Anderson.[7]

B. Addition may occur at *only one end* of the growing chain on *any* end or adjacent-to-end carbon.[9]

C. Addition may occur at *either end* of the growing chain on *any* end or adjacent-to-end carbon.[9] This scheme is the same as that postulated by Weller and Friedel.[5]

The process of one-carbon-atom addition starting with a normal- and with an iso-C_5 chain may be illustrated as follows:

Scheme A: [Addition at right end of chain with addition to one end carbon (*) or the adjacent-to-end

---

* Physical chemist, Synthetic Liquid Fuels Branch, Bureau of Mines, Bruceton, Pennsylvania.

† Chief, Research and Development Branch, Office of Synthetic Liquid Fuels, Bruceton, Pennsylvania.

[1] C. B. Montgomery and E. B. Weinberger [J. Chem. Phys. **16**, 424 (1948)] considered disproportionation reactions between paraffin hydrocarbons. Assuming that thermodynamic equilibrium is attained between all normal paraffins, the carbon number distribution was calculated using temperature, methane-to-ethane ratio, and carbon-to-hydrogen ratio as independent variables. With reasonable values for these variables, a typical carbon number distribution for products from cobalt catalysts was approximated. While such a disproportionation equilibrium is not unreasonable for cobalt products where paraffins are the principal product, it is difficult to conceive of such an equilibrium being operative in the synthesis with iron catalysts where the major fraction of products is oxygenated and olefinic molecules.

[2] E. F. G. Herington, Chemistry and Industry **1946**, 347 (1946).

[3] O. Beeck, paper given at Catalysis Conference of A.A.A.S., June, 1949.

[4] R. A. Friedel and R. B. Anderson, J. Am. Chem. Soc. **72**, 1212, 2307 (1950).

[5] S. Weller and R. A. Friedel, J. Chem. Phys. **17**, 801 (1949); **18**, 157 (1950).

[6] A. W. Weitkamp, paper given at Catalysis Conference of A.A.A.S., June, 1949.

[7] R. B. Anderson, paper given at Catalysis Conference of A.A.A.S., June, 1949.

[8] S. R. Craxford and E. K. Rideal, J. Chem. Soc. **1939**, 1604 (1939); S. R. Craxford, Trans. Faraday Soc. **42**, 576 (1946); Fuel **26**, 119 (1947).

[9] Addition to adjacent-to-end carbon atoms is subject to the restriction that this addition does not occur if the carbon atom is already attached to three carbons.

[10] The details of Weitkamp's derivation of expressions for isomer distribution are not the same as those used in reference 7 of this paper.

carbon (+)]

$$\begin{array}{l} \text{C C C C}^{+}\text{ C}^{*} \xrightarrow{2H_2+CO} \text{Intermediates } (I_1 \text{ to } I_n) \rightarrow \text{C C C C C C} + H_2O \\ \qquad\qquad \xrightarrow{2H_2+CO} \text{Intermediates } (I_1' \text{ to } I_n') \rightarrow \begin{array}{l}\text{C C C C C}\\ \qquad\quad \text{C}\end{array} + H_2O \\ \begin{array}{l}\text{C C C C}^{*}\\ \quad\ \text{C}\end{array} \xrightarrow{2H_2+CO} \text{Intermediates } (I_1'' \text{ to } I_n'') \rightarrow \begin{array}{l}\text{C C C C C}\\ \qquad\quad \text{C}\end{array} + H_2O. \end{array}$$

Scheme B: [Addition at right end of chain with addition to any end carbon atom (*).] Same as scheme A for addition to normal chain. For iso-C_5 chain:

$$\begin{array}{l}\text{C C C C}^{*}\\ \quad\ \text{C}^{*}\end{array} \xrightarrow{2H_2+CO} \text{Intermediates } (J_1' \text{ to } J_n') \rightarrow \begin{array}{l}\text{C C C C C}\\ \qquad\quad \text{C}\end{array} + H_2O.$$

Scheme C: [Addition at either end of molecule at any end carbon (*) or adjacent to end carbon (+)]

$$\begin{array}{l} \text{C}^{*}\text{ C}^{+}\text{ C C}^{+}\text{ C}^{*} \xrightarrow{2H_2+CO} \text{Intermediates } (K_1 \text{ to } K_n) \rightarrow \text{C C C C C C} + H_2O \\ \qquad\qquad \xrightarrow{2H_2+CO} \text{Intermediates } (K_1' \text{ to } K_n') \rightarrow \begin{array}{l}\text{C C C C C}\\ \qquad\quad \text{C}\end{array} + H_2O \\ \begin{array}{l}\text{C}^{*}\text{ C}^{+}\text{ C C}^{*}\\ \quad\ \text{C}^{*}\end{array} \xrightarrow{2H_2+CO} \text{Intermediates } (K_1'' \text{ to } K_n'') \rightarrow \begin{array}{l}\text{C C C C C}\\ \qquad\quad \text{C}\end{array} + H_2O \\ \qquad\qquad \xrightarrow{2H_2+CO} \text{Intermediates } (K_1''' \text{ to } K_n''') \rightarrow \begin{array}{l}\text{C C C C C}\\ \qquad\quad \text{C}\end{array} + H_2O \\ \qquad\qquad \xrightarrow{2H_2+CO} \text{Intermediates } (K_1^{IV} \text{ to } K_n^{IV}) \rightarrow \begin{array}{l}\text{C C C C}\\ \qquad\ \text{C C}\end{array} + H_2O. \end{array}$$

The reactivity of these carbon atoms may result from the presence of reactive structures such as an olefin bond, or reactive groups, such as hydroxyl attached to a carbon atom; or it may result from the dissociative adsorption of the growing chain to yield a radical and a hydrogen atom. On addition of carbon monoxide, the growing group passes through a number of intermediate structures indicated by I_i, J_i, or K_i, and eventually forms an intermediate similar to the first but containing an additional carbon atom. From these intermediates, molecules such as aldehydes, alcohols, olefins, or paraffins may desorb and appear as products.

It is assumed that upon addition to an end carbon the rate of growth through intermediates 1 to n may be represented by a first-order rate constant, α, with respect to the concentration of the growing chain on the catalyst surface; and similarly that upon addition to an adjacent-to-end carbon, the rate of growth through intermediates 1 to n may be represented by a first-order rate constant, β. The rate of desorption of the intermediates in both cases is assumed to be characterized by a first-order rate constant, γ, with respect to the concentration of growing chain species. Thus, for chain species n, the rates of growth by addition to an end or an adjacent-to-end carbon and the rate of desorption are given by αC_n, βC_n, and γC_n, respectively, where C_n is the molar concentration of chain n at the catalyst surface.

For schemes A and B, therefore, three typical reactions may be considered, with addition occurring at the right end of the chain (reactions 1, 2, and 3).

1. $\text{C C C C} \rightarrow \underset{(C_4)}{\text{C C C C}} \rightarrow \underset{(C_5)}{\text{C C C C C}} \longrightarrow \begin{cases}\text{C C C C C C}\\ \text{C C C C}\\ \qquad\ \text{C}\end{cases}$

2. $\text{C C C C} \rightarrow \underset{(C_4)}{\text{C C C C}} \rightarrow \underset{(C_5')}{\begin{array}{l}\text{C C C C}\\ \quad\ \text{C}\end{array}} \rightarrow \begin{array}{l}\text{C C C C C}\\ \qquad\ \text{C}\end{array}$

3. $\underset{(C_6')}{\begin{array}{l}\text{C C C C C}\\ \quad\ \text{C}\end{array}} \rightarrow \underset{(C_7')}{\begin{array}{l}\text{C C C C C C}\\ \qquad\ \text{C}\end{array}} \longrightarrow \begin{cases}\text{C C C C C C C}\\ \qquad\quad \text{C}\\ \text{C C C C C C C.}\\ \qquad\ \text{C C}\end{cases}$

In steady-state operation, the concentration of any species of growing intermediate remains constant; therefore, the rate of formation of a given species must equal its rate of removal by growth and desorption. From the definition of γ, the ratio of the rates of appearance of any two chain species equals the ratio of their concentrations at the surface. Hence, for scheme A:

Reaction 1. $C_4\alpha = C_5(\alpha+\beta+\gamma)$

$$C_5/C_4 = \alpha/(\alpha+\beta+\gamma) = R_5/R_4 = a. \qquad (1)$$

TABLE I. Isomer and carbon number distributions in terms of a and f.

	Schemes A		B		C	
	Relative isomer composition	Relative carbon number distribution, moles	Relative isomer composition	Relative carbon number distribution, moles	Relative isomer composition	Relative carbon number distribution, moles
CC	1	1	1	1	1	1
CCC	1	$2a$	1	$2a$	1	a^{*}[a]
CCCC	1	$2a^2(1+f)$	1	$2a^2(1+f)$	1	$a^{*2}(1+f/2)$
CC(C)	f		f		$f/2$	
CCCCC	1	$2a^3(1+2f)$	1	$2a^3(1+3f)$	1	$a^{*3}(1+1.75f)$
CCC(C)	$2f$		$3f$		$1.75f$	
CCCCCC	1	$2a^4(1+3f+f^2)$	1	$2a^4(1+5f+2f^2)$	1	$a^{*4}(1+3.62f+0.87f^2)$
CCCC(C)	$2f$		$3f$		$1.87f$	
CCCC(C)	f		$2f$		$1.75f$	
CCC(C)C	f^2		$2f^2$		$0.87f^2$	
CCCCCCC	1	$2a^5(1+4f+3f^2)$	1	$2a^5(1+7f+8f^2)$	1	$a^{*5}(1+5.56f+4.44f^2)$
CCCCC(C)	$2f$		$3f$		$1.93f$	
CCCC(C)C	$2f$		$4f$		$3.63f$	
CCC(C)CC	$2f^2$		$6f^2$		$3.50f^2$	
CCC(C)C	f^2		$2f^2$		$0.94f^2$	
CCCCCCCC	1	$2a^6(1+5f+6f^2)$	1	$2a^6(1+9f+18f^2)$	1	$a^{*6}(1+7.53f+11.72f^2)$
CCCCC(C)C	$2f$		$3f$		$1.97f$	
CCCC(C)CC	$2f$		$4f$		$3.75f$	
CCC(C)CCC	f		$2f$		$1.81f$	
CCCC(C)CC	$2f^2$		$6f^2$		$3.56f^2$	
CCC(C)CCC	$2f^2$		$6f^2$		$3.69f^2$	
CCC(C)CC	f^2		$4f^2$		$3.50f^2$	
CCC(C)C(C)	f^2		$2f^2$		$0.97f^2$	

[a] $a^{*}=2a$.

Reaction 2. $C_4\beta = C_5'(\alpha+\gamma)$

$$C_5'/C_4 = \beta/(\alpha+\gamma) = R_5'/R_4 = b. \quad (2)$$

Reaction 3. $C_6'\alpha = C_7'(\alpha+\beta+\gamma)$

$$C_7'/C_6' = \alpha/(\alpha+\beta+\gamma) = R_7'/R_6' = a, \quad (3)$$

where R_n is the rate of appearance of species, n, in moles per unit time, and a and b are constants defined by Eqs. (1), (2), and (3).

For scheme B:

Reaction 1. $C_4\alpha = C_5(\alpha+\beta+\gamma)$

$$C_5/C_4 = \alpha/(\alpha+\beta+\gamma) = R_5/R_4 = a'. \quad (4)$$

Reaction 2. $C_4\beta = C_5'(2\alpha^{\ddagger}+\gamma)$

$$C_5'/C_4 = \beta/(2\alpha+\gamma) = R_5'/R_4 = b'. \quad (5)$$

Reaction 3. $C_6'2\alpha^{\ddagger} = C_7'(\alpha+\beta+\gamma)$

$$C_7'/C_6' = 2\alpha/(\alpha+\beta+\gamma) = R_7'/R_6' = 2a', \quad (6)$$

where constants a' and b' are defined by Eqs. (4), (5), and (6). Equations for scheme C are developed in a manner similar to that for scheme B, except that addition is permitted at both ends of the growing chain; these equations may be characterized by constants a'' and b''. For scheme C the expressions for R_{n+1}/R_n in terms of α, β, and γ, for addition to end carbons are not always equal to or multiples of the same expression. Similarly, for addition to adjacent-to-end carbons the expressions for R_{n+1}'/R_n are not identical to or multiples of the same expression. However, for simplicity the expressions for addition to end carbons are assumed equal to or multiples of a constant a'', and similarly all ratios for addition to adjacent-to-end carbons are assumed equal to or multiples of a constant b''. The errors introduced by this assumption are not large. At this point the superscripts will be dropped; but it must be emphasized that the values of the constants according to schemes A, B, and C are different. A new constant, f, defined as $f=b/a$, is introduced. The constant f represents the ratio of the rate of appearance of the isomer formed by addition to an adjacent-to-end carbon to the rate of appearance of the isomer formed by addition to an end carbon atom of a given growing intermediate. In general, for addition to end carbons, $R_{n+1}/R_n = am$, where m is the number of end carbons on which addition can occur; similarly, for addition to adjacent-to-end carbons, $R_{n+1}'/R_n = bm' = afm'$, where m' is the number of adjacent-to-end carbons on which this addition can occur. As discussed in the previous paragraph these expressions do not exactly describe some of the addition steps for scheme C.

Starting with a C_2 intermediate and considering all of the possible chain structures that can be formed according to the addition rules, we may evaluate the number of moles in each carbon number fraction as functions of a and f, and the distribution of isomers as functions of f. Specifically, the number of moles in any carbon number fraction is equal to the number in the C_2 fraction times a function of a and f. For all three schemes it is assumed that both carbon atoms of the C_2 intermediate are effective in end carbon addition, i.e., addition characterized by constant a. In Table I the relative carbon number distributions are computed with respect to the value of 1 for C_2, and the isomer distribution is evaluated relative to the value of 1 for the normal isomer. To illustrate the method of obtaining the values in Table I, these quantities are derived in detail through C_5 for scheme A, in which the addition occurs at the end or adjacent-to-end carbons at the right ends of the chains in the following equation:

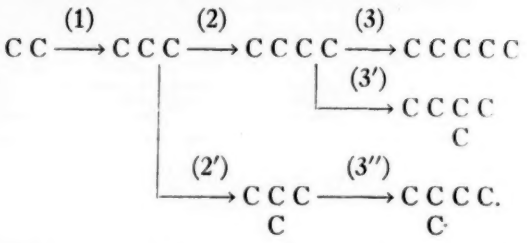

Reaction 1. Both carbons of C_2 are effective in end addition, and R_2 is taken as unity:

$$R_3/R_2 = 2a = R_3.$$

Reaction 2.
$$R_4/R_3 = a$$
$$R_4 = 2a^2.$$

Reaction 2′.
$$R_4'/R_3 = af$$
$$R_4' = 2a^2f$$

$$\text{Total } R_4 = 2a^2(1+f).$$

Reaction 3.
$$R_5/R_4 = a$$
$$R_5 = 2a^3.$$

Reaction 3′.
$$R_5'/R_4 = af$$
$$R_5' = 2a^3f.$$

Reaction 3″.
$$R_5'/R_4' = a$$
$$R_5' = 2a^3f$$

$$\text{Total } R_5 = 2a^3(1+2f).$$

It is evident from Table I that for schemes A and B the molar quantity of C_2 is less than C_3 for values of a greater than 0.5. When $f=0$, the carbon number distributions of all three schemes reduce to that of Friedel and Anderson[4] for n greater than 2.

The isomer distribution of Friedel and Anderson[4] for saturated hydrocarbons obtained from cobalt catalysts and data of Bruner[11] and Weitkamp[6] for hydrocarbons obtained from iron catalysts were used to test the ability of the expressions in Table I to predict isomer distribution. Values of f were chosen that appear to give best approximation, and the calculated and experimental data are compared in Table II. For cobalt products, the average absolute deviations of normal and monomethyl isomers in percent for schemes A, B, and C were 1.2, 0.7, and 0.8, and for products from iron catalysts 1.4, 2.1, and 3.6, respectively. For all cases, the predicted amounts of dimethyl isomers are somewhat greater than those observed. Scheme A predicts most closely the observed isomer distribution; however, schemes B and C predict more accurately the observed ratios of 2-methyl to 3-methyl isomers in the C_6, C_7, and C_8 fractions. In general, the agreement between predicted and observed isomer fractions by all three schemes is satisfactory in view of the simplicity of the postulates and the combined errors that are possible in the production and analysis of the products.

‡ Two end carbons on the right end of the molecule.

[11] F. H. Bruner, Ind. Eng. Chem. **41**, 2511 (1949); also private communication.

TABLE II. Comparison of predicted and observed isomer distributions.

	Isomer distribution, mole percent								
	Products from cobalt catalysts				Products from iron catalysts				
		Predicted by scheme			Observed		Predicted by scheme		
Value of f	Observed[a]	A 0.035	B 0.029	C 0.0275	B[b]	W[c]	A 0.115	B 0.0727	C 0.904
C C C C		96.6	97.9	98.6	89.4	90.0	89.7	93.2	95.7
C C C C		3.4	2.1	1.4	10.6	10.0	10.3	6.8	4.3
C C C C C	95.0	93.4	94.1	95.2	81.2		81.3	82.1	86.3
C C C C C	5.0	6.6	5.9	4.8	18.8		18.7	17.9	13.7
C C C C C C	89.6	90.2	90.4	90.9	78.8	74.2	73.5	73.2	74.9
C C C C C C	5.7	6.4	5.7	4.7	11.2	12.4	16.9	15.9	12.7
C C C C C C	4.7	3.2	3.8	4.4	9.5	11.3	8.5	10.5	11.9
C C C C C C	0	0.1	0.1	0.1	0.4	2.1	0.9	0.4	0.5
C C C C C C C	87.7	87.3	86.9	86.5	66.0	70.4	66.0	64.6	64.3
C C C C C C C	4.6	6.2	5.5	4.6	13.1		15.4	14.0	11.2
C C C C C C C	7.7	6.2	7.3	8.6	19.1	17.3	15.4	18.7	21.2
C C C C C C C	0	0.2	0.2	0.2	1.6		1.7	2.0	1.8
C C C C C C C	0	0.1	0.1	0.1	0.3	1.0	0.8	0.7	0.5
C C C C C C C C	84.5	84.4	83.6	82.4	61.0		60.5	57.1	57.5
C C C C C C C C	3.9	6.0	5.2	4.5					
C C C C C C C C	7.2	6.0	7.0	8.5	36.4		34.7	37.4	38.3
C C C C C C C C	4.4	3.0	3.5	4.1					
C C C C C C C	0	0.2	0.2	0.2					
C C C C C C C	0	0.2	0.2	0.2					
C C C C C C C	0	0.1	0.1	0.0	2.6		4.8	5.4	4.2
C C C C C C C	0	0.1	0.1	0.1					

[a] See reference 4.
[b] See reference 11.
[c] See reference 6.

From Table I, it is evident that the carbon number distribution can be expressed by

$$\phi_n = kF_n a^{n-2} \tag{7}$$

and

$$\log(\phi_n/F_n) = n \log a + \log(k/a^2), \tag{8}$$

where ϕ_n is the number of moles in the fraction containing n carbon atoms, F_n is the function of f in parentheses in the column marked "Relative carbon number distribution" in Table I (i.e., for C_7 of Scheme A, $F_7 = 1+4f+3f^2$), and k is a constant. Equation (8) is suitable for testing experimental data, since a plot of $\log(\phi_n/F_n)$ against n should be linear. Carbon number distribution data are meager, and those used to test

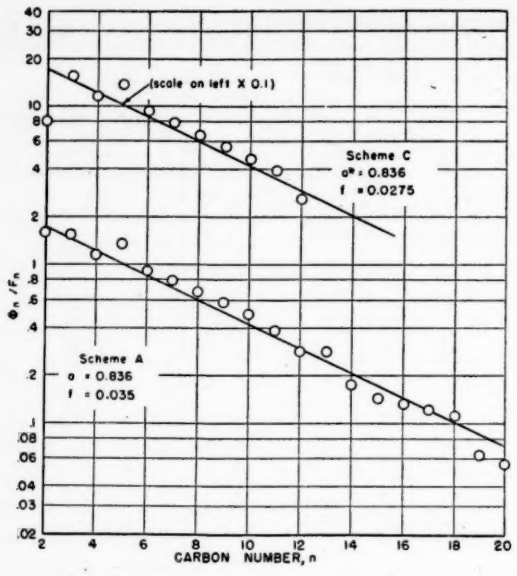

FIG. 1. Plots of Eq. (8) for schemes A and C using carbon number distribution of products from cobalt catalysts.

Eq. (8) were obtained in this laboratory. The product distribution from cobalt catalysts have been described previously.[4] The products from iron catalysts were obtained in a fluidized-bed reactor and are similar to those on which Weitkamp's isomer analyses were made; the carbon number distribution is given on an aromatic- and oxygenated-free basis. Schemes A and C were tested with Eq. (8), as shown in Figs. 1 and 2 for products from cobalt and iron catalysts, respectively. The values of f used in evaluating F_n were those given in Table II. The values of F_n for scheme C were evaluated only to $n=12$. In Figs. 1 and 2, both schemes A and C give essentially linear plots of Eq. (8) with relative deviations of ± 10 percent. For the products from cobalt catalysts (Fig. 1),

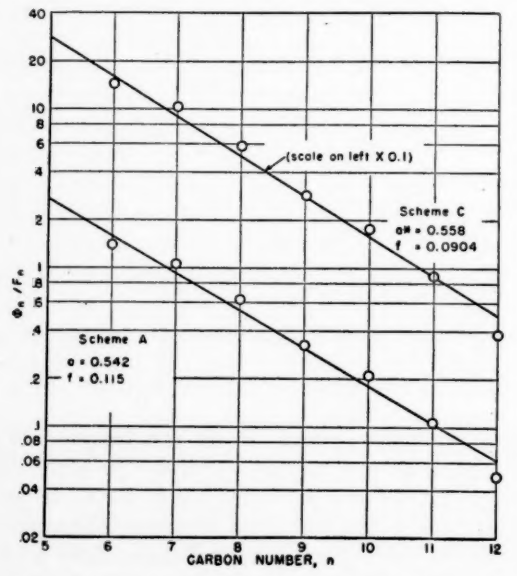

FIG. 2. Plots of Eq. (8) for schemes A and C using carbon number distribution of products from iron catalysts.

scheme A accurately predicts the moles of C_2; but scheme C does not. From the value of constant a and a^* for iron catalyst products, the molar ratios of C_2 to C_3 were predicted to be 0.92 and 1.79 for schemes A and C, respectively. Values of the molar ratio C_2/C_3 of about one are usually observed in fixed bed tests of iron catalysts; for example, the average of the molar ratios C_2/C_3 for the tests in Table I of reference 12 was 1.12.[12] Other than the C_2 to C_3 ratios the available data are predicted equally well by both schemes A and C.

On the basis of our present knowledge of the mechanism of the Fischer-Tropsch synthesis, it seems inadvisable to postulate specific reactions and intermediates at the catalyst surface; therefore, a number of general criteria for the attachment of reactive intermediates will be considered with respect to addition schemes A, B, and C. It appears likely that the intermediate is attached to the surface by carbon-to-metal bonds, possibly of the type found in metal carbonyls; i.e., the carbon atom contributes electrons to unfilled $3d$ and $4p$ electronic shells of the metal. Some reasonable ways in which an intermediate may be attached to the surface are summarized below:

I. Formation of carbon-to-metal bonds at
  i. a carbon-to-carbon double bond of α-olefinic intermediate
  ii. a carbon attached to other atoms such as oxygen
  iii. any carbon atom by bonds similar to those formed in dissociation adsorption involving dissociation of a hydrogen atom.

II. Number of simultaneous points of attachment of the intermediate
  i. at one carbon
  ii. at two adjacent carbons
  iii. at or near both ends of intermediate
  iv. at many or all carbon atoms.

III. The growing intermediate may
  i. desorb and readsorb repeatedly
  ii. remain attached to the surface throughout its growth.

IV. Possible reasons that addition occurs at only end or adjacent-to-end carbons:
  i. Addition occurs at carbons attached to reactive groups located at end or adjacent-to-end carbons (or both in the case of an α-olefinic intermediate).
  ii. Steric hindrance.

V. Possible reasons why addition does not occur on carbon atoms already attached to three carbon atoms:
  i. The carbon atom on which addition occurs must be attached to the surface by a primary valence, thus leaving no valences available for addition.
  ii. Steric hindrance.

Thus, scheme A may be explained by assuming that the growing intermediate is attached at the end or adjacent-to-end carbon atoms because these carbons are also attached to a "reactive" group (I-i or I-ii). This might involve attachment at one carbon atom (II-i) for I-ii, or two carbons (II-ii) for I-i. Since the position of the reactive group determines the position of attachment and of one carbon addition, it is of no consequence if the intermediate remains attached to the surface or desorbs and readsorbs repeatedly (III-i and III-ii). To

[12] Anderson, Shultz, Seligman, Hall, and Storch, J. Am. Chem. Soc. 72, 3502 (1950).

predict adequately the C_2/C_3 ratio, it is necessary to assume that the C_2 intermediate reacts more rapidly than C_3. A C_2 intermediate of the olefinic type (I-i) may be expected to be equally active at each end and thus have a higher reactivity than C_3 and higher intermediates of this type. C_2 intermediates of type I-ii would be expected to have about the same reactivity as C_3 and higher intermediates; i.e., only one carbon of the C_2 chain is reactive in end carbon addition.

Scheme B may be explained by a dissociative adsorption (I-iii) occurring at one end of the chain. It requires that the intermediate remain attached to the surface (III-ii) throughout its growth, or else addition would be possible at both ends of the chain. The postulate that chain growth is limited to end or adjacent-to-end carbons must be explained by steric effects (IV-ii). Similarly, for scheme C dissociative adsorption (I-iii) may be postulated; however, since growth may occur at both ends of the chain, the intermediate must be permitted to desorb and readsorb repeatedly (III-i). In scheme C it is difficult to find a simple way of making the C_2 chain more reactive than C_3 or longer chains as required for adequately reproducing the observed C_2/C_3 ratios.

Thus, considering all of the evidence, the postulates for scheme A appear to explain the available data most adequately, especially when an α-olefinic type intermediate is assumed. However, a mechanism of scheme A involving chain growth at carbon atoms that are also attached to oxygen (I-ii involving, for example, OH groups) has interesting possibilities, even though the C_2/C_3 ratio is not correctly predicted according to our simple addition rules. The discussion of reaction mechanism in this paper, however, should be regarded as tentative, especially in view of the lack of complete carbon number distribution data for products from iron catalysts.

ACKNOWLEDGMENTS

The authors wish to thank Dr. F. H. Bruner of the Texas Company and Dr. A. W. Weitkamp of the Standard Oil Company of Indiana for permission to use unpublished data. Distillation data presented in this paper were obtained by Dr. J. Feldman.

THE JOURNAL OF CHEMICAL PHYSICS VOLUME 19, NUMBER 3 MARCH, 1951

The Mercury ($^3P_1$) Photo-Sensitized Decomposition of Propane at High Temperatures*

S. Bywater† and E. W. R. Steacie
Division of Chemistry, National Research Council, Ottawa, Canada

(Received October 24, 1950)

The mercury ($^3P_1$) photo-sensitized decomposition of propane has been studied from room temperature to 450°C at pressures between 4 and 300 mm. The high temperature results are explained in terms of the decomposition of the propyl radical to form ethylene or propylene, and activation energies of 20 and 38 kilocalories, respectively, are assigned to these reactions. Experiments are also described where propane and propylene were in competition for hydrogen atoms, the relative rates of reaction being found at three temperatures. The difference in the activation energies of the two reactions is 4 kilocalories. The reactions at lower pressures are more complex and only a qualitative description of them can be given.

INTRODUCTION

PREVIOUS investigations of the mercury photo-sensitized deomposition[1,2] of propane have shown that the primary step in the reaction involves a C—H bond split. This adequately explains the experimental fact that at room temperature and at relatively high pressures of propane, the only products are hydrogen and hexanes. However, at pressures of a few millimeters of propane or at high temperatures, methane is produced in considerable quantities. It is the purpose of this work to examine the reactions which lead to methane production, and in particular the high temperature reaction.

EXPERIMENTAL

Propane was obtained in cylinders from the Ohio Chemical Company or alternatively, from the Phillips Petroleum Company (Research Grade). The former was stated to be 99.9 percent pure and the latter better than 99.99 percent pure. No difference in reaction rate could be detected between the two samples. The gas was used without further purification except for a simple bulb to bulb distillation and rigorous degassing. Propylene was similarly "Phillips Research Grade" with a stated purity of 99.7 percent and was used after bulb to bulb distillation. Cylinder hydrogen was purified by passage through a palladium tube.

The reaction was investigated in a conventional static system. A cylindrical quartz-reaction cell was enclosed in a concentric tubular furnace, a small quantity of liquid mercury effectively at room temperature being contained in a side tube below the furnace. In this

---

* NRC No. 2334.
† National Research Council (of Canada) Postdoctorate Fellow.
[1] E. W. R. Steacie and D. J. Dewar, J. Chem. Phys. **8**, 571 (1940).
[2] B. deB. Darwent and E. W. R. Steacie, J. Chem. Phys. **13**, 563 (1945).

TABLE I. Summarized rates of hydrogen and methane production (30 cm pressure).

Temp. °C	Rate of H_2 production (cc NTP/hr)	Δ (chain H_2)	Rate of CH_4 production (cc NTP/hr)
26	0.153	—	—
250	0.223	—	—
300	0.230	—	0.030
350	0.249	—	0.120
400	0.440	0.195	0.440
425	0.780	0.532	0.624
450	1.62	1.37	1.011

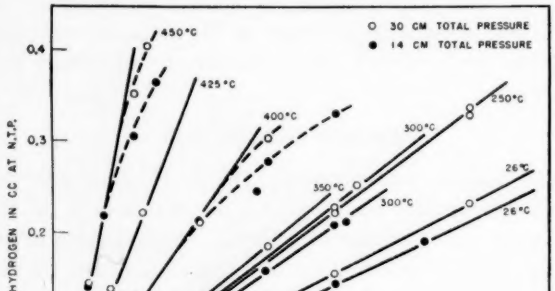

FIG. 1. Rate of hydrogen production at 14 and 30 cm total pressure.

way the mercury vapor pressure was kept constant irrespective of the furnace temperature. The furnace was supplied with current from a voltage stabilizer and was controlled manually to ±1°C. The cell temperature was measured by a chromel-alumel thermocouple in contact with the rear face of the cell.

Unreversed λ2537 was obtained from a low pressure mercury lamp with neon (3 mm) as carrier gas. The light was roughly collimated using diaphragms and a quartz lens. The presence of λ1849 was unlikely due to a large path length in air and passage through several fused quartz windows. The intensity of λ2537 was estimated from the rate of decomposition of uranyl oxalate using the techniques described by Leighton and Forbes,[3] and Forbes and Heidt.[4]‡

TABLE III. Variation of hydrogen production with pressure and intensity at room temperature.

Pressure C_3H_8 (cm Hg)	(dH_2/dt)(cc NTP/hr)
4.0	0.118*
7.0	0.125
14.0	0.142
14.0	0.074†
20.0	0.152
30.0	0.153
40.0	0.155

* Initial rate.
† Light intensity reduced to 0.50 of normal value.

The reaction products were frozen out in liquid nitrogen and the hydrogen and methane taken off by a Toepler pump. Blank experiments showed quantitative removal of both these gases from the propane. The mixture was then passed over copper oxide at 280°C and the hydrogen completely oxidized.

Typical experiments were subjected to complete analysis by fractional sublimation at low pressures in an apparatus of the type described by Ward[5] and modified by Savelli, Seyfried, and Filbert.[6]

In this way, C_1-C_5 hydrocarbons could be separated with an accuracy of ±0.01 cc at NTP. The various fractions were analyzed for unsaturates using the Blacet-Leighton microanalysis apparatus. The hexane fraction was analyzed using a mass spectrometer, standard high purity hexanes from the National Bureau of Standards in Washington being used as reference hydrocarbons.

RESULTS

(a) Experiments at Higher Pressures

The results of experiments at higher pressures are given in Tables I, II, and III and Figs. 1 to 5. Relatively high pressures of propane were used to eliminate side reactions, particularly those caused by quenching of excited mercury by the reaction products, some of which

TABLE II. Ward still analysis on several representative experiments at 14 cm pressure.

Expt. no.	Temp. °C	Time (min)	H_2 cc NTP	CH_4 cc NTP	C_2H_4 cc NTP	C_2H_6 cc NTP	C_2H_2 cc NTP	C_3H_8 cc NTP	C_4H_{10} cc NTP	Residue C_5+ cc NTP
170	27	80	0.189	0.00	0.00	0.00	—	34.9	—	0.198
135	300	79	0.261	0.049	0.034	0.008	—	21.2	—	0.212
141	350	90	0.294	0.174	0.098	0.080	—	22.1	—	0.238
150	400	30	0.211	0.244	0.241	0.050	—	19.5	—	0.128
156	450	5	0.139	0.096	0.112	0.025	—	18.5	—	0.018
157	450	20	0.366	0.338	0.345	0.078	—	18.3	—	0.043

[3] P. A. Leighton and G. S. Forbes, J. Am. Chem. Soc. **52**, 3139 (1930).
[4] G. S. Forbes and L. J. Heidt, J. Am. Chem. Soc. **56**, 2263 (1934).
‡ As in all photo-sensitization experiments, some uncertainty is introduced by inhomogeneity of light absorption. However, this will not be serious so long as it is not largely temperature dependent. The pressure broadening of the absorption line is so large that Doppler broadening will be negligible, and hence no serious error should result.
[5] E. C. Ward, Ind. Eng. Chem. Anal. Ed. **10**, 169 (1938).
[6] Savelli, Seyfried, Filbert, Ind. Eng. Chem. Anal. Ed. **13**, 868 (1941).

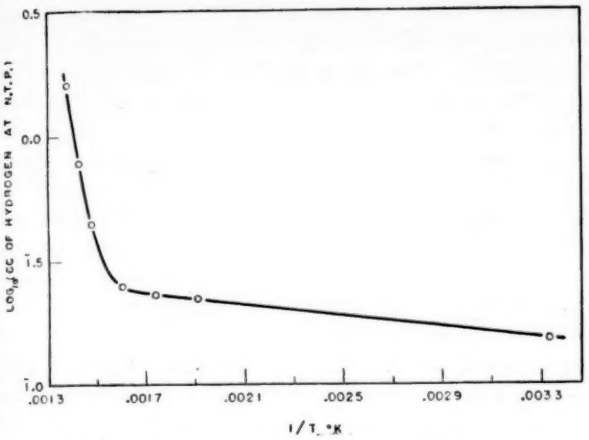

FIG. 2. Activation energy plot for the total hydrogen production at 30 cm total pressure.

have a much larger quenching cross section for mercury than propane itself. These conditions also increase the probability that radicals formed will react with the substrate rather than amongst themselves.

Below 200°C these experiments confirm that hydrogen and hexanes are the only reaction products. This low temperature production of hydrogen is directly proportional to the light intensity and becomes independent of the pressure of propane at the higher pressures (Table III). The quantum yield of hydrogen production is 0.46 at room temperature and 14 cm pressure, rising to 0.50 at high pressures. Hydrogen production is a linear function of time.

Above 300°C appreciable amounts of methane are formed. A roughly equivalent amount of ethylene is produced. The rate of methane production is the same at both 14 cm and 30 cm total pressure. The activation energy for methane formation is 20±1 kilocalories (Fig. 5). This value has been obtained by plotting logarithmically the cc of methane produced at NTP against reciprocal temperature. The experiments were carried out at constant total pressure rather than constant concentration, but since the reaction proceeds

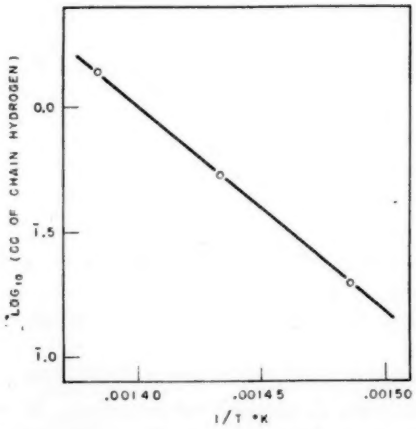

FIG. 3. Activation energy plot for the chain production of hydrogen (30 cm total pressure).

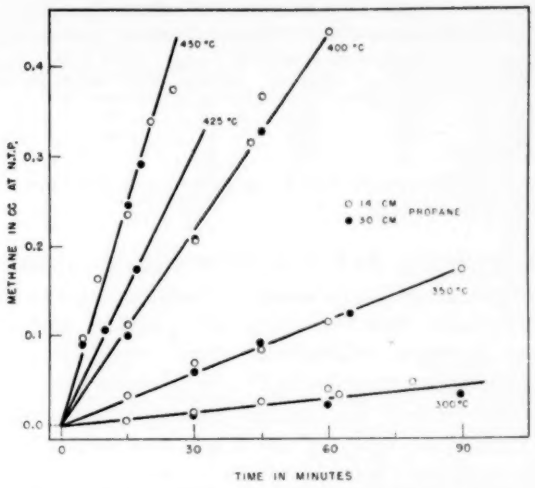

FIG. 4. Rate of methane production at 14 and 30 cm total pressure.

independently of concentration in this range no error results from this procedure. In a similar manner the activation energy for hydrogen formation is 0.5 kilocalorie in the low temperature region (Fig. 2). Above 350°C the formation of hydrogen becomes rapid, quantum yields of above unity being observed. Thus it appears an alternative mechanism involving short chains, is coming into play at the highest temperatures. The activation energy for this step (Fig. 3) has been obtained by subtracting from the total hydrogen produced, the quantity which would have been formed had the non-chain mechanism only been operative. The activation energy of this chain step is 38 kilocalories.

The absence of thermal decomposition of propane was established by blank experiments carried out without ultraviolet radiation. Even at the highest temperature used (450°C) only 0.021 cc of noncondensible gas was produced in twenty minutes—which is negligible compared with the 1.0 cc of noncondensible gas produced by the photo-chemical reaction in the same time.

Mass spectrometer analyses show that the predomi-

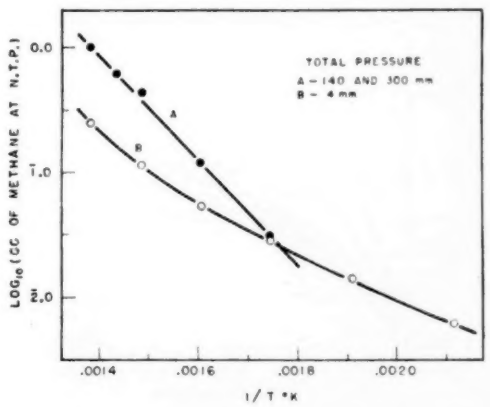

FIG. 5. Activation energy plots for methane formation at various pressures.

TABLE IV. Composition of hexanes.*

Expt. no.	Temp. °C	% di-Me-butane	% 2-Me-pentane	% *n*-hexane	% *n*-propyl radicals
186	450	48	35	17	35
141	350	78	12	10	16
170	27	88	10	2	7

* All figures ±5 percent.

nant product in the hexane fraction of the products is 2,3-dimethylbutane. A secondary hydrogen atom is thus preferentially removed from the propane molecules giving isopropyl radicals at room temperature.[1] At higher temperatures (Table IV), appreciable amounts of 2-methyl pentane and normal hexane appear, until at 450°C the ratio of the three hexanes approaches a value corresponding to equal quantities of normal and isopropyl radicals.

(b) Reactions at Low Pressures

A series of reactions was carried out at pressures of the order of 4 mm of propane. For convenience, these reactions were carried out at constant concentration rather than at constant pressure.

The results are shown graphically in Figs. 6 and 7. It will be seen that the hydrogen production is not a linear function of time, a result which is to be expected since at these low pressures, hydrogen quenches the $^3P_1$ mercury atoms at low concentration. Methane formation is, however, a linear function of time. The apparent activation energy for methane formation (Fig. 5) varies with temperature. Below 300°C a value of approximately 8 kilocalories is obtained whereas at higher temperature the value is seen to approach that value obtained at high pressures of propane.

(c) Reactions at Intermediate Pressures

A series of reactions was carried out at a constant pressure of 2.0 cm of propane. Here hydrogen formation is nonlinear with time and the rate falls off rapidly in the first few minutes of reaction. Addition of a small quantity (0.215 cc) of hydrogen to a series of experiments showed that this is due to the hydrogen produced quenching the $^3P_1$ mercury atoms in competition with the propane, since this curve (Fig. 8) parallels the normal curve (after subtraction of the initial hydrogen added), but does not show the initial higher slope. The simple mercury sensitized reaction of propane with a higher rate of hydrogen production only occurs therefore in the first few minutes of reaction. A further complication is introduced by the fact that the hexanes produced in the reaction are also quenching, as shown by the presence of nonanes in the heavy fraction of the Ward still analysis. The rate of hydrogen production is proportional to the square root of both light intensity and reaction time after an initial period of about one hour. In the unobserved initial period it is reasonable to suppose that the rate is linearly dependent on reaction time and light intensity by analogy with the higher pressure results. Complete Ward still analyses on typical experiments are given in Table V. These show that the only other product of reaction is a small C_2 fraction.

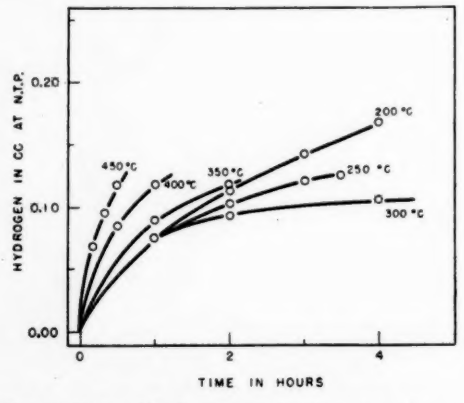

FIG. 6. Rate of hydrogen production at *ca* 4 mm total pressure.

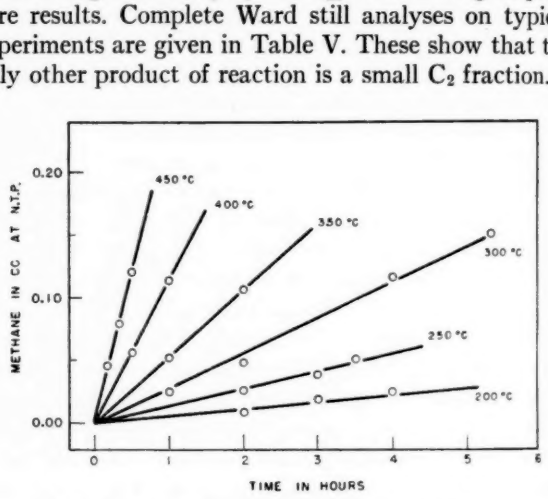

FIG. 7. Rate of methane production at *ca* 4 mm total pressure.

Methane formation occurs above 300°, the amount of methane being linearly dependent on reaction time. An activation energy similar to the values at 4 mm pressure is obtained from an Arrhenius plot, the mean value being about 10 kilocalories. Curvature, however, was noted in the plot.

(d) Experiments Carried Out in the Presence or Propylene

A number of experiments were carried out between room temperature and 200°C to determine the relative reactivity of the hydrogen atoms formed in the system for propylene and propane. For these experiments, a small quantity (0.126 cc) of propylene was mixed with a large excess of propane (14 cm pressure) and subsequently decomposed by a mercury photo-sensitized reaction.

The progress of the reaction, as compared with the normal reaction in absence of propylene, is shown at three different temperatures in Fig. 9. It will be noted that the propylene has a marked inhibiting effect which

TABLE V. Ward still analysis on several representative experiments at 2 cm pressure.

Expt. No.	Temp. °C	Time (min)	H_2 cc NTP	CH_4 cc NTP	C_2H_4 cc NTP	C_2H_6 cc NTP	C_3H_2 cc NTP	C_3H_8 cc NTP	C_4H_{10} cc NTP	Residue cc NTP
28	27	150	0.185	0.010	—	—	—	4.81	—	0.123
29	27	300	0.312	0.008	—	—	—	4.69	—	0.143
95	200	240	0.387	0.017	—	—	—	2.87	—	0.226
105	250	300	0.368	0.096	←	0.048	→	2.65	—	0.231
54	300	240	0.271	0.135	0.025	0.013	0.006	2.72	—	0.216
90	350	240	0.335	0.597	0.113	0.178	0.032	1.91	—	0.291

decreases as the propylene is used up in the reaction. Propylene is a well-known inhibitor of chain reactions since it reacts readily with radicals in the system.

The reaction at room temperature approaches the normal rate of hydrogen production in the uninhibited reaction as the propylene is consumed. The lateral displacement is within the experimental error equal to the amount of propylene initially added to the system.

This fact implies that, at room temperature, the propylene is removed solely by reaction with hydrogen atoms and not by reaction with propyl radicals, for in this case, the lateral displacement would be less than the propylene added. This fact also rules out the formation of molecular hydrogen by recombination of hydrogen atoms either by third body collision in the gas phase or on the wall, since in this case the displacement would be one-half the propylene added. A Ward still analysis on one experiment at 27° revealed no other product except hydrogen and a heavy fraction (probably hexane).

DISCUSSION

(a) Experiments Carried Out at Higher Pressures

The experiments at higher pressures (14 cm and 30 cm) below 300°C are consistent with the mechanism postulated by Darwent and Steacie.[2]

$$Hg(^1S_0)+h\nu \rightarrow Hg(^3P_1) \quad (0)$$

$$Hg(^3P_1)+C_3H_8 \rightarrow Hg(^1S_0)+C_3H_7+H \quad (1)$$

$$H+C_3H_8 \rightarrow C_3H_7+H_2 \quad (2)$$

$$2C_3H_7 \rightarrow C_6H_{14}. \quad (3)$$

This mechanism implies a quantum yield of unity for hydrogen production, whereas the maximum value attained is of the order of 0.64–0.68 at 300°C. This lower quantum yield could be due to the quenching of mercury to the metastable ($^3P_0$) state with subsequent dissipation of energy. Alternatively, reactions

$$H+C_3H_7 \rightarrow C_3H_8 \quad (4)$$

$$H+H \rightarrow H_2 \quad (5)$$

would lower the quantum yield. The absence of reaction (5) has been inferred from the data described previously in the propylene inhibited reactions, and on more general grounds is not likely since at these pressures it would proceed as a three-body collision in the gas phase.

If reactions (4) or (5) were responsible for the low quantum yield, one would expect that the quantum yield would rise continuously with the increasing pressure of propane. Since the rate of hydrogen production reaches a maximum at higher pressure, it seems unlikely that recombination reactions compete for hydrogen atoms at these pressures. Also, the occurrence of reaction (4) or (5), to an appreciable extent, results in the hydrogen production no longer being directly proportional to light intensity contrary to the experimental evidence.

One other cause of inefficiency would be the oc-

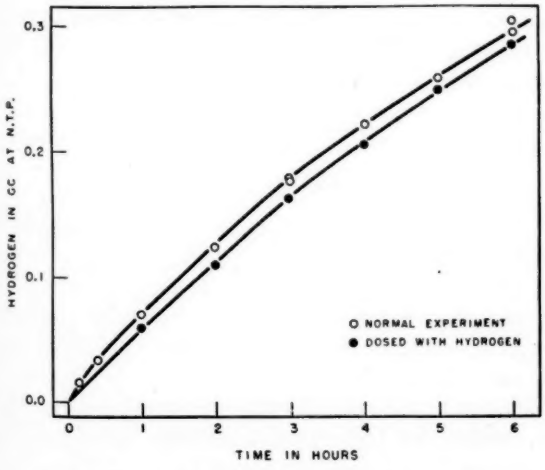

FIG. 8. Rate of hydrogen production at 2 cm total pressure.

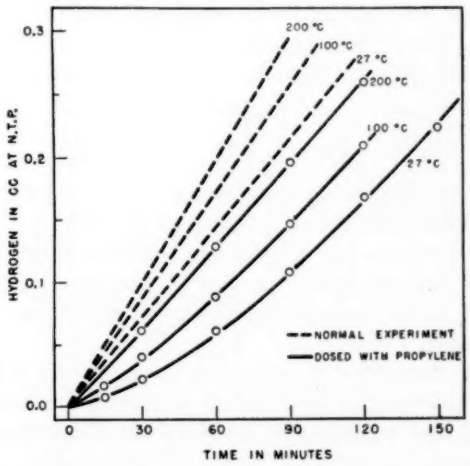

FIG. 9. Rates of hydrogen production in experiments dosed with propylene.

TABLE VI. Infrared analysis of the C_3 fractions from Ward still fractionation.

Expt. no.	Temp. °C	Propylene cc NTP
237	250	<0.04 cc
187	300	<0.04 cc
186	450	0.16±0.04 cc

currence of a disproportionation reaction between two propyl radicals

$$2C_3H_7 = C_3H_6 + C_3H_8. \quad (6)$$

An attempt to check the importance of reaction (6) was made by analyzing the large residual amount of propane for traces of propylene by means of infrared analysis (Table VI) using a strong propylene band at 991 cm^{-1}. The C_3 fraction from Ward still separation was used for this purpose. No propylene could be detected at 250° and 300°, temperatures which are most favorable for the detection of propylene (see below). Propylene was, however, found at 450° but only in amounts corresponding to the decomposition of the propyl radical. However, hydrogen atoms in the system may react rapidly with any propylene, making its detection in the reaction products impossible.

$$H + C_3H_6 = C_3H_7. \quad (7)$$

It is possible to determine the relative rates of reactions (2) and (7) at three given temperatures from the initial rates of reaction in the presence and absence of propylene at each temperature.

Taking reactions 1, 2, 3, 6, and 7 as representing the reaction scheme, then:

$$\frac{\text{rate of hydrogen production}^{(\text{uninhibited})}}{\text{rate of hydrogen production}^{(\text{inhibited})}} = \Phi\ (\text{uninhibited})\left[1+\frac{k_7(C_3H_6)}{k_2(C_3H_8)}\right],$$

where Φ (uninhibited) is the quantum yield of hydrogen in the uninhibited reaction. The experiments then give the following values for the rate constant ratio, k_7/k_2:

27°C	100°C	200°C
3100	860	270

These figures give an activation energy of 4 kilocalories to be identified with $E_2 - E_7$ (Fig. 10). The ratio k_7/k_2 is thus too large for propylene to be stable in the system at low temperatures. At 300°C, however, propylene formed by a disproportionation reaction ought to be detectable.

It is interesting to compare these results with the collision yields for reaction (2) as given by Steacie and Parlee[7] and reaction (7) as given by Robb and Melville.[8] These are 5.0×10^{-8} (mean) at 30°C and 1.4×10^{-4} at 16°C, respectively. Neglecting the small temperature difference, the ratio k_7/k_2 is approximately 2800 in agreement with this investigation. If, in fact, the disproportionation reaction has little importance then the rate constant ratios must be divided by the quantum yield of the uninhibited reaction.

Above 300°C, at high pressures other reaction steps occur leading to methane formation and a large increase in the rate of production of hydrogen. A chain reaction, with hydrogen atoms as chain carriers, is necessary for explaining the latter result. The experimentally observed facts, noted above, make it reasonably certain that we are dealing with the reaction

$$C_3H_7 = C_3H_6 + H. \quad (8)$$

This is the reverse reaction of step (7). Clearly an equilibrium exists between propyl radicals and propylene. Even if the equilibrium is not heavily over on the propylene side at approximately 400°C, removal of hydrogen atoms by reaction with propane rather than propylene will result in the decomposition of the propyl radicals and the stabilization of propylene. It can be easily shown, using the above data on relative rates of hydrogen atom reactions with propane and propylene, that the dominant reaction will be with propane under these experimental conditions.

From the reaction scheme used above

$$\frac{d[H_2]}{dt} = \Phi I_{abs} + k_8\left(\frac{\Phi I_a}{k_3}\right)^{\frac{1}{2}},$$

where Φ is the observed quantum yield at low temperatures. Thus the observed chain hydrogen activation energy obtained as described above is equivalent to

$$E_8 + \tfrac{1}{2}E_\phi - \tfrac{1}{2}E_3.$$

Neglecting the second two terms which should be smaller than the experimental error, $E_8 = 38\pm1$ kilocalories.

Considering the above experimental facts, it seems certain that the methane is produced by reaction (9) at high pressures.

$$C_3H_7 = C_2H_4 + CH_3 \quad (9)$$

followed by

$$CH_3 + C_3H_8 = CH_4 + C_3H_7. \quad (10)$$

Application of the stationary state principle to the scheme of reactions (1)–(10), omitting reactions (4) and (5), shows that the apparent activation energy for methane formation is equivalent to the activation energy of reaction (9), neglecting the two small terms $\frac{1}{2}E_\phi$ and $\frac{1}{2}E_3$.

Reference to Table II shows that the only product not covered by this reaction scheme is ethane. This

[7] E. W. R. Steacie and N. A. D. Parlee, Can. J. Research **B17**, 371 (1939).

[8] J. C. Robb and H. W. Melville, Proc. Roy. Soc. (London) **A196**, 445 (1949).

could be produced by recombination of a small fraction of the methyl radicals or hydrogenation of ethylene. In either case the correction to be applied to the rate of methane formation has a negligible effect on the activation energy of step (9).

Since reactions (8) and (9) are both endothermic, minimum values for the activation energies can be found from thermochemical data. Thus the heat of the reaction

$$C_3H_8=C_2H_4+CH_4$$

is 18 kilocalories.[9] Hence the heat of reaction (9) is numerically equal to the C—H bond strength in methane minus the C—H bond strength in propane plus 18 kilocalories. The present propane bond strength data[10] are quite unreliable. However, on general grounds the C—H bond strength in propane cannot be less than that in ethane. The latter is well established, thus giving a minimum activation energy of 23 kilocalories for reaction (9) and 35 kilocalories for reaction (8). Experimentally, it is difficult to find a mechanism which would give a higher activation energy for reaction (9) in view of the absence of large quantities of side products and the fact that the absolute rate of methane formation is pressure independent. The experimental value for E_8 is satisfactory, and considering the agreement with the thermochemical data for the corresponding reaction of ethane,[11] suggests that Polanyi's C—H bond strengths in propane are rather low, particularly the isopropyl value.

Difficulty arises from the fact that both isopropyl and normal propyl radicals are produced from propane. Our experimental values for E_8 and E_9 probably correspond to some intermediate value between the true values for normal and isopropyl radicals. The present bond strength data are so unreliable that no estimate can be made of the difference between the two.

Since this work was completed, a recent publication[12] has given a preliminary value for the activation energy of reaction (9) of 19 kilocalories in good agreement with this work. This evidence supports the idea that we are measuring E_9 since the methods for C_3H_7 production are widely different.

[9] Selected values of properties of hydrocarbons. U. S. National Bureau of Standards.
[10] E. T. Butler and M. Polanyi, Trans. Faraday Soc. **39**, 19 (1943).
[11] S. Bywater and E. W. R. Steacie, J. Chem. Phys. **19**, 172 (1951).
[12] Durham, Martin, and Sutton, Nature **164**, 1052 (1949).

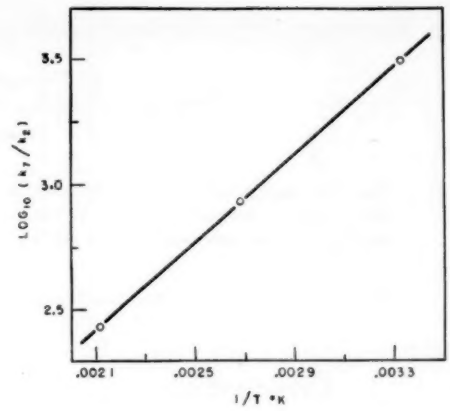

FIG. 10. Activation energy plot E_2-E_7.

(b) Experiments Carried Out at Lower Pressures

A quantitative analysis of the low pressure reactions is not possible due to the complexity of the results.

The results at 4 mm pressure indicate qualitatively, however, that the decomposition of the propyl radical is the main source of methane at high temperatures. Below 300°C this reaction is slow and another mechanism must be sought. It seems likely that reactions

$$H+C_3H_7=C_2H_5+CH_3, \quad (11)$$

and

$$H+C_2H_5=2CH_3 \quad (12)$$

suggested by Darwent and Steacie,[2] are here responsible for methane production. The activation energies have been estimated at less than 5 kilocalories. If methane is produced by reaction (10), which has an activation energy of 8 kilocalories,[13] this will be the rate determining step, and the high activation energy for methane formation observed at high temperatures should drop to 8 kilocalories as is, in fact, observed. The experiments carried out at 2.0 cm total pressure appear to fall in an intermediate range where it is more difficult to separate the two mechanisms leading to methane production.

ACKNOWLEDGMENTS

It is a pleasure to acknowledge our indebtedness to Dr. R. N. Jones and Dr. A. R. H. Cole who carried out the infrared analyses and to Mr. R. Pilon who carried out the Ward still analyses described in Tables II and V. Dr. F. P. Lossing carried out the mass spectrometer analyses in Table IV.

[13] A. F. Trotman-Dickenson and E. W. R. Steacie, J. Chem. Phys. **19**, 169 (1951).

The Mercury ($^3P_1$) Photo-Sensitized Reaction of Ethane at High Temperatures*

S. BYWATER† AND E. W. R. STEACIE
Division of Chemistry, National Research Council, Ottawa, Canada

(Received October 24, 1950)

The mercury photo-sensitized decomposition of ethane has been carried out with particular emphasis on the high temperature reaction. Evidence is given that under these experimental conditions the ethyl radical becomes unstable around 400°C. An activation energy of 39.5 kcal is assigned to the reaction

$$C_2H_5 = C_2H_4 + H$$

on the basis of the proposed mechanism.

INTRODUCTION

THE mercury photo-sensitized reaction of propane at high temperatures and moderate pressures has yielded[1] information on the stability of the propyl radical.

It seemed therefore profitable to investigate the thermal stability of the ethyl radical by producing ethyl radicals at high temperatures by a mercury photo-sensitized reaction of ethane. Various investigations have been carried out[2–4] on the mercury photo-sensitized decomposition of ethane but in no case was the reaction investigated at a sufficiently high temperature that the ethyl radical would be expected to be unstable.

EXPERIMENTAL

Ethane was obtained in cylinders from the Phillips Petroleum Company (Research Grade). This was stated to be 99.9 percent pure and was therefore used without purification except for a simple bulb-to-bulb distillation and rigorous degassing. The reaction was investigated in a static system. The reaction was carried out in a cylindrical quartz cell inside a tubular furnace and the cell illuminated by unreversed λ2537 obtained from a low pressure mercury lamp with neon as carrier gas. Actinometry using uranyl oxalate gave a light input of 1.38×10^{-5} Ein./hr. After reaction the products were frozen out with liquid nitrogen and the hydrogen pumped off and analyzed for traces of methane by combustion over copper oxide. A few typical experiments were completely analyzed using a modified Ward still. The apparatus used was exactly as described by Bywater and Steacie[1] and thus needs no further description.

TABLE I. Rate of hydrogen production.

Temp. (°C)	cc/hr NTP	cc/hr (non-chain)	cc/hr (chain)
27	0.106	...	...
100	0.154	...	...
200	0.202	...	...
300	0.229	...	...
400	0.270	...	...
425	0.380	0.269	0.111
450	0.582	0.277	0.305
475	1.144	0.283	0.861
500	2.184	0.289	1.895

RESULTS

Experiments were carried out at a pressure of 40 cm of ethane. This relatively high pressure was used to eliminate unwanted side reactions, particularly those leading to the formation of methane, and also to eliminate the quenching of excited mercury by the reaction products. Some of these have a much larger quenching cross section than has ethane.

Below 400°C these experiments confirm that hydrogen and butane are the only significant reaction products at high pressures (Tables I and II, Figs. 1 and 2). Between room temperature and 400°C the rate of hydrogen production increases slightly corresponding to an apparent activation energy of 0.9 kcal per M. The quantum yield thus rises from 0.34 at 27°C to 0.87 at

TABLE II. The products of the reaction (cc NTP).

Run	Temp. (°C)	Time (min)	H_2	CH_4	C_2[a]	C_3	C_4	C_5^+
200	200	90	0.299	0.000	72.0	0.00	0.247	0.003
203	400	60	0.270	0.009	55.6	0.007	0.153	0.006
227	425	40	0.262	0.008	55.7	0.000	0.123	0.004
209	450	45	0.402	0.014	53.8	0.000	0.094	0.007
218	500	7.5	0.299	0.002	52.1	0.000	0.073	0.002

[a] C_2 includes unchanged ethane.

* NRC No. 2335.
† National Research Council (of Canada) Postdoctorate Fellow.
[1] S. Bywater and E. W. R. Steacie, J. Chem. Phys. **19**, 172 (1951).
[2] E. W. R. Steacie and N. W. F. Phillips, J. Chem. Phys. **6**, 179 (1938). Can. J. Research **B16**, 303 (1938).
[3] E. W. R. Steacie and R. L. Cunningham, J. Chem. Phys. **8**, 800 (1940).
[4] B. deB. Darwent and E. W. R. Steacie, J. Chem. Phys. **16**, 381 (1948).

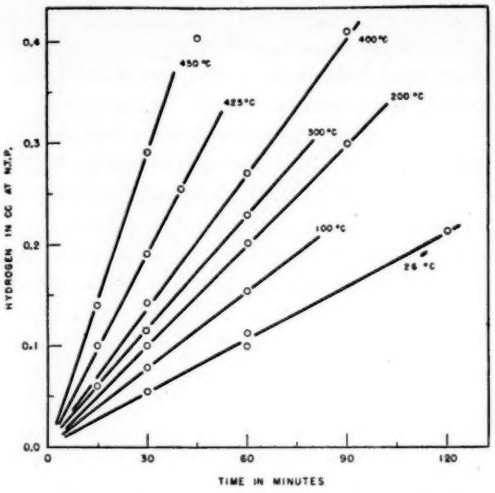

FIG. 1. Rate of hydrogen production at various temperatures.

400°C. This slight rise may correspond to greater efficiency in the quenching of excited mercury by ethane at higher temperatures or to the fact that radical recombination reactions are less likely at higher temperatures or to the occurrence of a disproportionation step between ethyl radicals. In any of these cases it can be easily shown that this is formally equivalent to a primary step with a variable quantum yield, dependent both on pressure and temperature. Most interest attaches to those experiments above 425° where the basic quantum yield is almost unity. It follows that here the other reaction steps are unimportant and in fact can be corrected for by using the rise in quantum yield at low temperatures.

Above 400° the hydrogen production increases rapidly giving quantum yields above unity which indicate a chain mechanism. Such a chain mechanism requires a new elementary reaction which will regenerate a chain carrying hydrogen atom. The apparent activation energy of this step has been calculated from the results (Table I and Fig. 3) by subtracting the amount of hydrogen produced by the non-chain mechanism

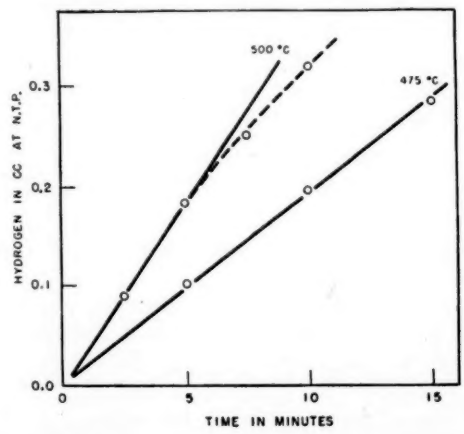

FIG. 2. Rate of hydrogen production at high temperatures.

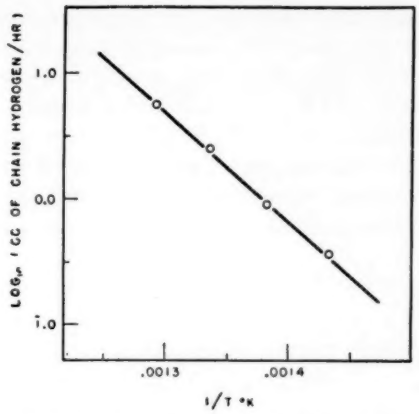

FIG. 3. Activation energy plot for the chain step.

(using an extrapolation from the low temperature experiments (Fig. 4)) from the total hydrogen produced at each temperature. In this calculation quantities of gas evolved were expressed in cc of gas at NTP. In practice the experiments were carried out at constant total pressure rather than constant concentration; since, however, separate experiments showed that at such high pressures the rate of hydrogen production is almost independent of concentration of ethane, the error particularly in a calculation of an activation energy will be negligible. The apparent activation energy for this step is 40±1 kcal.

DISCUSSION

The low temperature measurements are consistent with the mechanism postulated earlier[2,3,4]

$$\mathrm{Hg}(^1S_0)+h\nu = \mathrm{Hg}(^3P_1) \qquad I_a$$

$$\mathrm{Hg}(^3P_1)+\mathrm{C_2H_6}=\mathrm{Hg}(^1S_0)+\mathrm{C_2H_5}+\mathrm{H} \qquad \Phi I_a \qquad (1)$$

$$\mathrm{H}+\mathrm{C_2H_6}=\mathrm{C_2H_5}+\mathrm{H_2} \qquad k_2[\mathrm{C_2H_6}][\mathrm{H}] \qquad (2)$$

$$2\mathrm{C_2H_5}=\mathrm{C_4H_{10}} \qquad k_3[\mathrm{C_2H_5}]^2, \qquad (3)$$

where Φ is a function of temperature. Here the low quantum yield has been attributed to inefficiency in the ethane quenching step. If recombination of hydrogen

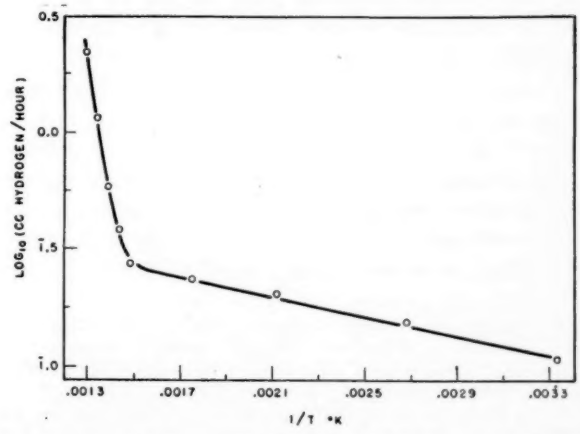

FIG. 4. Activation energy plot for the total hydrogen production.

atoms and ethyl radicals, or disproportionation of ethyl radicals rather than recombination, is responsible for the low Φ value, it is easily shown that the over-all effect is still formally equivalent to a variable primary quantum yield.

At higher temperatures, the only feasible mechanism which will meet the requirements of regeneration of a hydrogen atom and a high activation energy seems to be

$$C_2H_5 = C_2H_4 + H \quad k_4[C_2H_5]. \tag{4}$$

Application of the stationary state hypothesis to this reaction scheme gives for the rate of production of hydrogen

$$\frac{d[H_2]}{dt} = \Phi I_{abs} + \frac{k_4}{(k_5)^{\frac{1}{2}}}(\Phi I_{abs})^{\frac{1}{2}}.$$

It is clear that the low temperature rate is simply equal to ΦI_{abs}. Therefore the activation energy obtained as above is equal to $E_4+\frac{1}{2}E_\Phi-\frac{1}{2}E_3$. $\frac{1}{2}E_\Phi=0.5$ kcal. Making the usual assumption that $E_3=0$, $E_4=39.5$ kcal.‡

The mechanism quoted requires that an amount of ethylene equivalent to the extra chain hydrogen should be produced. Normal methods of analysis are not accurate enough to detect ethylene in the large quantity of unchanged ethane. Attempts were therefore made to detect this small amount of ethylene by infrared analysis using the strong ethylene band at 949 cm^{-1} and using the total C_2 fraction as removed by a Ward still fractionation. The accuracy of these measurements is limited by the low concentration of ethylene and the pressure broadening of the peak caused by the high pressure of ethane present. However, roughly correct amounts of ethylene are present (Table III).

TABLE III. Production of ethylene (cc NTP).

Run	Temp. (°C)	Chain H_2	Measured C_2H_4
203	400	0.024	0.1[0]
227	425	0.088	0.1[5]
209	450	0.248	0.2[0]
218	500	0.242	0.2[0]

Previous experimental evidence for the activation energy of reaction (4) is scanty.

Rice[5,6] assigned a value of 49 kcal to this reaction in order to explain the over-all activation energy for the thermal decomposition of ethane. The activation energy was assessed on a purely speculative basis and so was not claimed to be more than a rough estimate.

Bawn[7] has estimated the activation energy for the decomposition of the ethyl radical by a transition state calculation and has obtained a value of 48–50 kcal.

A minimum value for the activation energy of reaction (4) can be assessed on thermochemical grounds since the reaction is endothermic. Numerically the heat of reaction is equal to the bond strength in hydrogen plus the heat of hydrogenation of ethylene minus the carbon-hydrogen bond strength in ethane. All these values have been established with reasonable certainty giving a heat of reaction of 37.5 kcal. Thus the activation energy of the reaction will be 37.5 kcal plus the activation energy of the reverse reaction. This would suggest an activation energy of 38–43 kcal.[8] The value of 39.5 kcal obtained would require an activation energy of 2 kcal for the back reaction. This value is in agreement with the experimental fact that the back reaction proceeds rapidly at room temperatures. The value 2 kcal can have a large error since it has been obtained by the differences of two large energy terms.

The reaction between hydrogen atoms and various olefins has been investigated at room temperature by Robb and Melville.[9] The value of the collision yield for the reaction of hydrogen atoms with ethylene is given as 8.5×10^{-4} at room temperature. If we assume the usual value (0.1) for the steric factor of this reaction the activation energy corresponds to about 3 kcal. This must be regarded as a maximum value, since there is evidence that similar reactions can have a lower steric factor.

Frost[10] has given thermodynamic arguments why the ethyl radical should be stable even at 600°C. He obtains an equilibrium constant for the reaction

$$C_2H_5 \rightleftharpoons C_2H_4 + H$$

at 900°K expressed as $(P_H \cdot P_{C_2H_4})/P_{C_2H_5}$ and gives a value of 2×10^{-4} at this temperature. The value obtained appears reasonable and has been checked using more recent values of thermodynamic constants. The argument however overlooks the fact that at an elevated temperature the hydrogen atoms produced by decomposition of the ethyl radical will react more readily with ethane than with ethylene under usual reaction conditions. Thus, using the data of Trost and Steacie[11] for the reaction of hydrogen atoms with ethane, and Robb and Melville's collision yield for the reaction of hydrogen atoms with ethylene, and assuming that the activation energy for this reaction is at the most 3 kcal, hydrogen atoms react 6×10^4 times faster with ethylene than ethane at room temperature and standard concen-

‡ Inhomogeneity of light absorption will cause an error here, if it is temperature dependent. However, pressure broadening of the resonance line is so great that Doppler broadening is negligible, and the change in absorption with temperature will be small.

[5] F. O. Rice and K. F. Herzfeld, J. Am. Chem. Soc. **56**, 284 (1934).

[6] F. O. Rice, J. Am. Chem. Soc. **56**, 488 (1934).

[7] C. E. H. Bawn, Trans. Faraday Soc. **31**, 1536 (1935).

[8] E. W. R. Steacie, *Atomic and Free Radical Reactions* (Reinhold Publishing Corporation, New York, 1946).

[9] J. C. Robb and H. W. Melville, Proc. Roy. Soc. (London) **A196**, 494 (1949).

[10] A. V. Frost, Zhur. Fiz. Khim. **8**, 290 (1936).

[11] W. R. Trost and E. W. R. Steacie, J. Chem. Phys. **16**, 361 (1948).

trations. At 850°K, however, this ratio is reduced to about 25 and since the ethane concentration is one to two hundred times greater than the ethylene concentration in the aforementioned experiments, the reaction is weighted at least ten to twenty times in favor of the ethane reaction. Thus the equilibrium will be pushed over by removal of hydrogen atoms from the system, and decomposition products of the ethyl radical will be observed.

ACKNOWLEDGMENTS

We are grateful to Dr. R. N. Jones and Dr. A. R. H. Cole for the infrared analysis, and to Mr. R. Pilon for the Ward still analyses carried out.

THE JOURNAL OF CHEMICAL PHYSICS VOLUME 19, NUMBER 3 MARCH, 1951

The Reactions of Methyl Radicals. IV. The Abstraction of Hydrogen Atoms from Cyclic Hydrocarbons, Butynes, Amines, Alcohols, Ethers, and Ammonia*

A. F. TROTMAN-DICKENSON† AND E. W. R. STEACIE
Division of Chemistry, National Research Council, Ottawa, Canada

(Received September 9, 1950)

The photolysis of acetone in the presence of various compounds has been investigated between 70°C and 340°C. If the reaction

$$CH_3+CH_3=C_2H_6$$

has no activation energy, then the activation energies in kcal for the reactions of the type

$$CH_3+RH=CH_4+R$$

are cyclopropane 10.3, cyclobutane 9.3, cyclopentane 8.5, cyclohexane 8.3, benzene 9.2, toluene 8.3, 1-butyne 9.1, 2-butyne 8.6, methanol 8.2, ethanol 8.7, iso-propanol 7.3, methyl ether 9.5, iso-propyl ether 7.3, monomethyl amine 8.4, dimethyl amine 7.2, trimethyl amine 8.8, and ammonia 10.0. The collision theory steric factors are of the order of 10^{-3} or less for all these reactions.

A table is presented summarizing the results so far obtained on methyl radical reactions by the photolysis of acetone in the presence of other compounds. The accuracy of the method and some of the general implications of the results are discussed.

INTRODUCTION

THIS paper is the fourth of a series describing a quantitative survey of the reactions of methyl radicals. The experiments described here were carried out to determine the rate of abstraction of hydrogen atoms from a variety of compounds by methyl radicals formed in the photolysis of acetone. We have determined the rate constants, k_1, of these reactions of type (1),

$$CH_3+RH=CH_4+R, \qquad (1)$$

relative to the square root of the rate constant, k_2, for the combination of methyl radicals (reaction 2);

$$CH_3+CH_3=C_2H_6. \qquad (2)$$

This was done by two methods: Method I, where the value of $k_1/k_2^{\frac{1}{2}}$ is determined directly using ordinary acetone and Method II, where the ratio is found indirectly using deuterated acetone. These Methods are fully described in the second paper[1] (Part II) of this series.

EXPERIMENTAL

Apparatus

The apparatus was the same as that used in Part II. In the experiments on cyclohexane, cyclopentane, methanol, and methyl ether, which were carried out with ordinary acetone, a chlorine filter five cm long filled with gas at one atmosphere pressure and a light beam collimated with quartz lenses were used. The experiments on cyclopentane using heavy acetone and on toluene, benzene, the butynes, iso-propanol, isopropyl ether, the amines, and ammonia were carried out with a light beam collimated roughly with a polished aluminum cylinder and a 1 mm Corex *D* (also known as 9–53 or 9700) filter. The same method of collimation was employed for the experiments with cyclobutane and cyclopropane, but no filter was used. The experiments with ethanol were carried out using a light beam roughly collimated with a polished aluminum cylinder and a Corex *A* (also known as 9–54 or 7910) filter, with 50 percent transmission at 2450A.

Materials

The acetone was a Mallinckrodt Reagent Grade product which had been refluxed over potassium permanganate, distilled, and dried with drierite.

The heavy acetone, which mass spectrometer analysis showed to be 68 percent acetone-d_6 and 32 percent acetone-d_5, was made for us by Dr. L. C. Leitch of this laboratory.

Cyclohexane, toluene, and benzene were Phillips Petroleum Company (Research Grade) and were stated to have a purity of 99.8 percent or better. Cyclopropane

* N. R. C. No. 2331.
† National Research Council (Canada) Postdoctorate Fellow.
[1] Trotman-Dickenson, Birchard, and Steacie, J. Chem. Phys. 19, 163 (1951).

TABLE I. The reaction of methyl radicals with various compounds by Method I.

Run	Temp. (°K)	[Acetone] (micromole per cc)	[RH] (micromole per cc)	Time (sec)	Products (micromoles) CO	Methane	Ethane	$k_1/k_2^{\frac{1}{2}} \times 10^{3}$
				Methanol				
230	376	1.93	1.86	10,650	10.7	2.20	8.92	1.63
232	404	1.88	1.75	10,930	11.2	4.55	7.49	3.41
229	430	1.90	1.85	10,150	10.7	7.26	5.07	6.25
233	462	1.97	1.89	10,280	11.5	11.7	2.59	12.8
231	492	1.97	1.91	10,290	12.2	15.6	1.33	21.8
				Methyl Ether				
226	381	1.87	1.86	10,670	12.1	3.05	10.3	2.31
224	395	1.88	1.83	10,100	11.1	4.09	8.70	3.42
223	412	1.87	1.85	11,000	12.0	7.32	8.50	6.03
228	433	1.92	1.85	10,900	13.6	10.5	5.88	9.97
227	453	1.88	1.81	9770	12.0	12.1	3.58	15.6
225	471	1.87	1.85	17,680	25.9	30.5	4.72	26.2
				Cyclopentane				
213	339	1.88	1.78	13,000	9.90	1.75	9.25	2.18
211	363	1.99	1.90	10,580	12.4	3.72	9.30	4.51
214	391	1.86	1.82	9730	11.2	6.59	6.40	10.4
210	426	1.70	1.84	8610	10.0	10.2	2.89	24.7
212	469	1.91	1.80	9440	12.00	17.40	1.05	63.3
				Cyclohexane				
217	338	1.89	1.74	12,200	8.69	1.41	8.28	1.88
219	364	2.22	2.07	9870	10.5	3.16	7.95	3.76
215	392	1.92	1.83	10,750	13.1	7.30	7.65	9.52
218	426	1.89	1.76	10,630	13.3	12.9	4.56	21.6
216	462	1.87	1.74	9730	12.2	16.5	1.40	49.7

was obtained from The Ohio Chemical and Manufacturing Company and was 99.5 percent pure. Cyclopentane (2 samples), 1-butyne, and 2-butyne were obtained from the National Bureau of Standards. Their purities were stated to be 99.95±0.02, 99.87±0.07, and 99.93±0.04 percent, respectively. The cyclobutane was made for us by Dr. L. C. Leitch of this laboratory. The exact purity of the cyclobutane is not known, but fractional distillation at low temperatures and mass spectrometric analysis indicated that the purity was of the order of 99 percent. Small amounts of hydrocarbon impurities would have very little effect upon our results.

The methanol was a gift from Drs. Puddington and Stainsby of this laboratory, who had purified it with considerable care by distillations from potassium hydroxide. The ethanol was a gift from Dr. Puddington; it had been stored with sodium and ethylphthallate in vacuum for two years. The iso-propanol was purified by distillation first from potassium hydroxide and then alone on a 32-plate column. The methyl ether was an Ohio Chemical Company product, which was reported to be 99.5 percent pure. The iso-propyl ether was purified by removing the peroxides with acidic ferrous sulfate, washing, drying with sodium, and carefully distilling. The methylamines were Matheson Company products which were reported to be at least 96.5 percent pure. The impurities were probably amines and moisture which would have a very small effect upon our results. The ammonia was also a Matheson Company product; it was reported to be 99.5 percent pure. All these substances were thoroughly degassed before use.

RESULTS

The results obtained by Method I are given in Table I, and those obtained by Method II are given in Table II. Arrhenius plots are given in Figs. 1 to 6. The activation energies, rates, and steric factors deduced from these results are given in Table III. All rate constants are given in molecules, cc, and seconds.

The slight difference between the results found in the two sets of experiments with cyclopentane is within the probable experimental error and probably of no great significance.

We also attempted to determine the activation energy of the reaction of methyl radicals with ethyl ether and with ethylene oxide. An accurate study of the reaction of methyl with ethyl ether could not be made by our experimental procedure. We found that considerable quantities of CH_4 were produced when heavy acetone was photolysed in the presence of ethyl ether. This shows that the ethyl ether radical formed by abstraction of a hydrogen atom is unstable. A reasonable explanation of this fact is that the ether radical is formed by the removal of a secondary hydrogen atom; this radical can then decompose to give acetaldehyde and an ethyl radical. Methyl radicals react very much faster with acetaldehyde[2] than with ethyl ether, so that although the aldehyde is only present in small quantities,

[2] R. E. Dodd, J. Chem. Phys. 18, 234 (1950).

TABLE II. The reaction of methyl radicals with various compounds by Method II.

Run	Temp. (°K)	[RH]/[Acetone]	CD_3H/CD_4	$k_1/k_2^{\frac{1}{2}} \times 10^{13}$
		Cyclopropane		
246	412	1.00	0.87	1.1
250	430	1.03	0.84	1.8
244	454	1.08	0.82	3.1
249	473	1.00	0.77	5.0
245	498	1.00	0.78	8.7
248	532	1.05	0.78	16.2
247	565	1.00	0.80	31.6
		Cyclobutane		
253	427	0.978	5.92	18.6
251	449	1.03	5.54	30.1
257	467	1.02	5.56	47.8
252	497	1.09	5.20	81.2
255	527	1.00	4.71	145
256	571	1.00	4.56	302
258	580	0.994	4.26	355
		Cyclopentane		
A 70	455	1.07	14.5	58.9
A 74	493	1.09	12.3	120
A 71	534	1.02	10.3	234
A 73	569	0.99	9.2	407
		Benzene		
A 69	456	0.955	0.76	2.09
A 67	493	1.00	0.71	4.27
A 64	527	0.946	0.66	7.95
A 68	566	0.964	0.62	13.8
A 65	600	0.988	0.64	24.0
		Toluene		
A 41	393	0.975	8.18	6.03
A 39	411	0.923	7.44	10.2
A 43	445	1.078	7.08	20.4
A 42	473	1.00	6.12	38.9
A 44	512	1.091	5.66	77.7
A 38	551	0.991	4.10	126
A 40	607	1.05	3.86	257
		Ethanol		
299	462	0.98	8.63	45
305	486	0.87	6.87	69
293	532	0.82	5.55	155
302	571	0.83	5.29	269
296	614	0.69	4.25	490
		Iso-propanol		
334	487	0.74	8.43	102
325	533	0.68	6.18	204
337	576	0.67	4.78	323
331	620	0.59	3.72	525
		Iso-propyl ether		
344	452	1.02	16.1	64.6
341	490	1.01	14.2	138
346	535	1.01	10.5	246
340	576	0.95	8.09	400
348	612	0.99	7.38	589
		Monomethylamine		
314	456	0.99	8.78	39
308	486	0.95	6.90	63
317	576	0.98	5.47	257
311	617	0.98	4.95	417
		Dimethylamine		
313	457	1.00	30.5	138
322	463	0.98	28.0	151
319	527	0.98	21.1	430
316	576	1.00	15.2	726
310	614	0.99	11.7	1020
		Trimethylamine		
321	466	1.00	19.0	107
306	487	1.00	17.7	164
318	527	1.03	16.0	316
315	575	1.07	14.7	645
		Ammonia		
345	453	1.01	0.89	2.4
343	487	1.01	0.86	5.0
347	530	0.97	0.78	11.2
349	612	1.01	0.82	43
		1-Butyne		
327	456	1.01	25.1	70.8
324	531	1.00	12.5	275
336	575	1.00	10.9	513
330	620	0.98	10.2	1000
		2-Butyne		
332	486	0.96	13.0	120
323	530	0.97	11.7	257
335	576	0.94	9.66	479
329	619	1.00	9.16	813

The rate constants are expressed in molecules, cc, and sec.

it is attacked, yielding methane and an acetyl radical which rapidly breaks down to give CH_3 and CO. This methyl radical is the source of the CH_4. CH_3 may also be produced by photolysis of the acetaldehyde, but this is likely to be relatively unimportant because of the similar extinction coefficients of acetaldehyde and acetone. A breakdown of radicals similar to that postulated for the ethyl ether radical has been observed in the case of the methyl ether radical and of the methanol radical.[3] It is reasonable to expect that the radical from iso-propyl ether formed by the removal of a tertiary hydrogen atom will break down into acetone and a secondary propyl radical. Similarly, the radical from ethanol and iso-propanol formed by removal of secondary and tertiary hydrogen atoms would at high temperatures break down to hydrogen atoms and acetaldehyde and acetone respectively.

Method I was used to study the reaction of methyl radicals with ethylene oxide but without success. Accurate determinations of the rates of reaction could not be made, because the ethylene oxide radical decomposed readily to give products which interfered with the

[3] Marcus, Darwent, and Steacie, J. Chem. Phys. **16**, 987 (1948). M. K. Phibbs and B. deB. Darwent, J. Chem. Phys. **18**, 495 (1950).

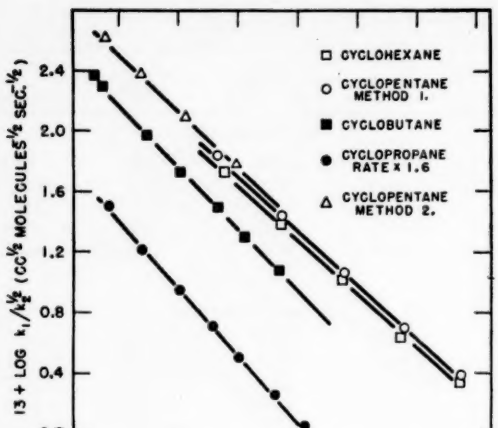

FIG. 1. Reaction of methyl radicals with cyclo-paraffins.

analysis. At high temperatures the radical apparently broke down to give CH_3 and CO as observed by Gomer and Noyes.[4] At temperatures around 200°C, we detected the formation of considerable quantities of acetylene. The gas was first detected by its vapor pressure in the analysis system and subsequently confirmed by mass spectrometric analysis of the C_2 cut. Presumably the ethylene oxide radical can decompose either to give a methyl radical and carbon monoxide or to give acetylene and hydroxyl. The relative importance of the two modes of decomposition appears to be strongly temperature dependent.

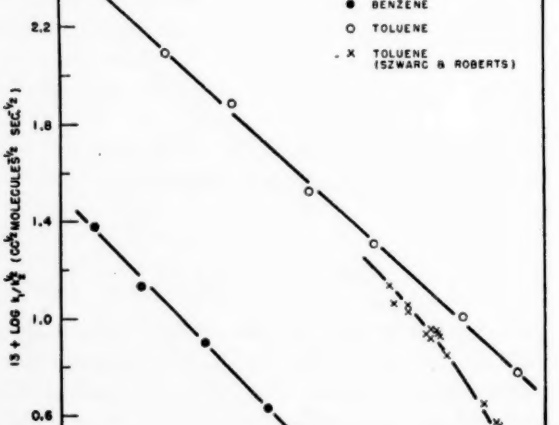

FIG. 2. The reaction of methyl radicals with benzene and toluene.

[4] R. Gomer and W. A. Noyes, Jr., J. Am. Chem. Soc. 72, 101 (1950).

DISCUSSION

Before we consider the results which we have obtained in this investigation as a whole, it seems worthwhile to try to discover the magnitude of the errors involved in the determination of $k_1/k_2^{\frac{1}{2}}$ and of its temperature coefficient.

A striking feature of our results is the very small deviation of the values of $\log k_1/k_2^{\frac{1}{2}}$ from a straight-line relationship when plotted against the reciprocal temperature.

The probable error in the activation energy $E_1-\frac{1}{2}E_2$ for the reaction of methyl with acetone was found by standard methods to be less than ± 0.1 kcal. The error for the analogous reaction with heavy acetone is probably ± 0.2 kcal because of the smaller number of observations made. Not enough observations were made in studying the reactions of methyl with the other hydrogen containing compounds for a proper statistical treatment. But the deviations from linearity are small and in most cases ± 0.2 kcal is a reasonable value to take for the probable error in the activation energies determined by Method I. Method I has the advantage that the activation energies found are not very susceptible to error in the value of $E_1-\frac{1}{2}E_2$ for acetone itself. The faster the reaction studied relative to the reaction of methyl with acetone, the smaller the error. However, the activation energies determined by Method II combine the errors in the determination of the relative rates for the abstraction of hydrogen and deuterium atoms by heavy methyl radicals from the hydrogen containing compound and the heavy acetone with the error in the determination of the rate of abstraction of deuterium from heavy acetone relative to the rate of combination of methyls. So the errors in $E_1-\frac{1}{2}E_2$ are probably of the order of 0.4 kcal when determined by Method II. The values of $E_3^*-E_1^*$, where E_3^* and E_1^*

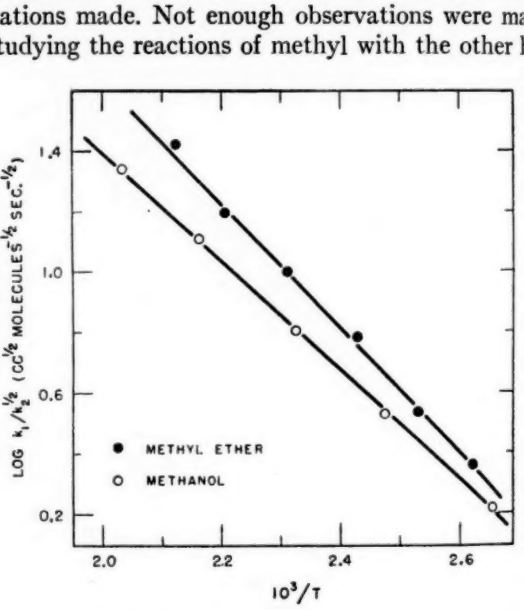

FIG. 3. Reaction of methyl radicals with methanol and methyl ether.

are the activation energies of reactions (3*) and (1*), are only in error by 0.2 kcal

$$CD_3+RH=CD_3H+R, \qquad (1^*)$$
$$CD_3+CD_3COCD_3=CD_4+CD_2COCD_3. \qquad (3^*)$$

Thus, Method II is more suitable for the investigation of small differences in the values of $E_1-\frac{1}{2}E_2$ for the members of a series of compounds than for the absolute determination of $E_1-\frac{1}{2}E_2$ itself. This degree of accuracy is satisfactory in view of the present state of our knowledge of the subject.

The possibility that the results are affected by photolysis of the substance to be investigated other than acetone may be rejected, because the light source used was chosen so that only the acetone was photolysed. Large errors can occur if the reactants are not properly mixed. In some of our early experiments this occurred; afterward, considerable care was taken that mixing was efficient. Many of the compounds investigated have boiling points not very far removed from that of acetone. Then the process of freezing out and rapidly evaporating the reactants effects a satisfactory mixing.

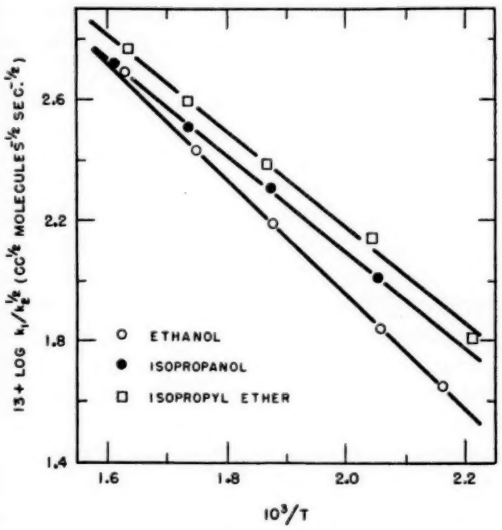

FIG. 4. Reaction of methyl radicals with ethanol, iso-propanol, and iso-propyl ether.

In many cases the possibility that large errors occur due to impurities may be dismissed. Most of the compounds were of a very high state of purity, the most probable impurities being homologues and isomers. As can be seen from our results, small amounts of such impurities would have a negligible effect. At the middle of our temperature range the greatest difference in rates in all the substances we have investigated is between benzene and 2;3-dimethyl butene, where it is a factor of 80. So most impurities present in traces would have little effect. However, it is known[2] that the reaction of methyl radicals with acetaldehyde is very rapid, probably because the steric factor in this case approaches unity. The other aldehydes, with the possible exception

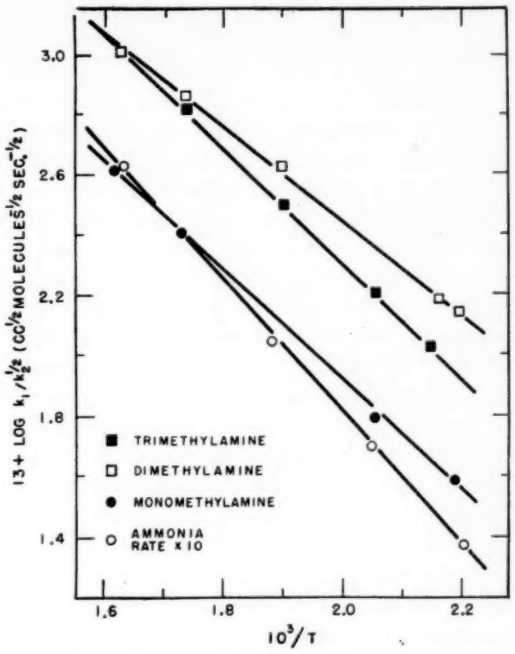

FIG. 5. Reaction of methyl radicals with methylamines and ammonia.

of formaldehyde, will probably also react very rapidly. If traces of acetaldehyde are initially present or are formed during the course of the reaction, the rates found will be too great. This happens when acetone is photolysed in the presence of ethyl ether at high temperatures; the aldehyde is formed by the breakdown of the ether radical.

The quantity of material photolysed was kept as small as was compatible with convenient and accurate analysis of the products. About 2 percent of the acetone present was photolysed in the majority of the experiments. The amount of acetone removed in the formation of biacetonyl and methyl ethyl ketone will vary with temperature and so will the amount of the other

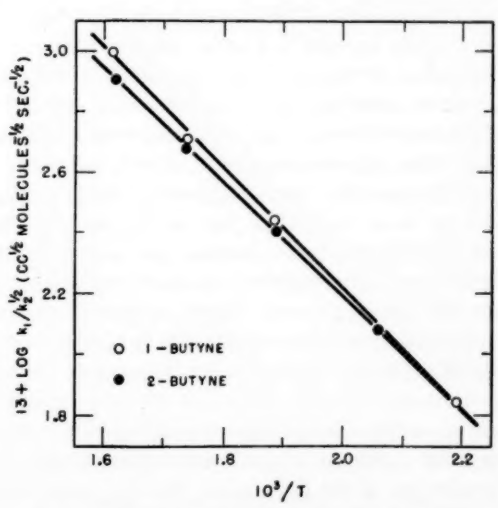

FIG. 6. Reaction of methyl radicals with butynes.

TABLE III. The abstraction of hydrogen atoms by methyl radicals. Summary of results.

Compound	$E_1-\frac{1}{2}E_2$ (kcal)	$k_1/k_2^{\frac{1}{2}}$ $\times 10^{12}$ at 182°C	$P_1/P_2^{\frac{1}{2}}$ $\times 10^4$	Number of "active" H atoms	$k_1'/k_2^{\frac{1}{2}}$ $\times 10^{12}$ per "active" H atom
Ethane	10.4	3.8	6	6	0.6
2,2-Dimethyl propane	10.0	6.3	6	12	0.5
2,2,3,3-Tetramethyl butane	9.5	10.0	7	18	0.6
n-Butane	8.3	21	3	4	4.5
n-Pentane	8.1	27	3	6	4.0
n-Hexane	8.1	33	3	8	3.8
2-Methyl propane	7.6	42	3	1	37
2,3-Dimethyl butane (i)	6.9	68	2	2	31
(ii)	7.8	78	6	2	36
2,3,4-Trimethyl pentane	7.9	65	8	3	20
Ethene	10.0	5.6	9	4	1.4
Propene	7.7	23	3	3	8
2-Butene	7.7	57	7	6	10
2-Methyl propene	7.3	49	4	6	8
2,3-Dimethyl-2-butene	7.8	145	17	12	12
1-Butene	7.6	66	8	2	33
1-Pentene	7.6	68	8	2	34
3-Methyl-1-butene	7.4	102	9	1	102
Cyclopropane	10.3	2.1	4	6	0.4
Cyclobutane	9.3	22	17	8	2.8
Cyclopentane	8.3	47	9	10	4.7
Cyclohexane	8.3	42	8	12	3.7
Benzene	9.2	1.9	1	6	0.3
Toluene	8.3	26	5	3	8.7
Methanol	8.2	11	2	3	3.7
Ethanol	8.7	38	11	2	19
Isopropanol	7.3	60	3	1	60
Methylamine	8.4	36	8	3	12
Dimethylamine	7.2	135	8	6	23
Trimethylamine	8.8	85	30	9	9.5
Ammonia	10.0	2.4	6	3	0.8
Methyl ether	9.5	17	14	6	2.8
Isopropyl ether	7.3	72	3	2	36
1-Butyne	9.1	66	35	2	33
2-Butyne	8.6	64	20	6	11
Acetone	9.7	19	10	6	3.2

reactant which is removed. It is difficult to decide how great an error in the activation energy this will cause. The effect will be much greater on the value of the absolute value of $E_1-\frac{1}{2}E_2$ than on the relative values. This source of error has been disregarded in our calculations, because it is probably negligibly small and we do not know what allowance to make for it.

It has frequently been suggested that energy is carried over from the initial act of the acetone photolysis so that the radicals formed are not in thermal equilibrium with the other components of the reaction mixture but are activated. These activated molecules would presumably react more rapidly than the "normal" radicals. If activated radicals were important, we should expect to obtain curved Arrhenius plots, a variation of activation energy with the over-all pressure in the system, and a dependence of activation energy upon the wavelength of the light used. We find none of these things.

The values of $k_1/k_2^{\frac{1}{2}}$ found differ slightly from the true ratio of the rate constants, because the assumption has been made that the methyl radicals are produced uniformly throughout the reaction cell. This is not true because under the conditions of our experiments about 40 percent of the total incident photo-chemically active radiation is adsorbed. It is not possible to make allowance for this until the absolute values of the rate constants are approximately known so that the leveling effect of diffusion can be treated mathematically. An extensive investigation of the photolysis of acetone, using cells of different length, would provide an alternative method of obtaining the true ratio of the rate constants. However, with acetone under our conditions the uncertainty is small and the deviation of our values of $k_1/k_2^{\frac{1}{2}}$ from the true values, due to this cause, should vary little with temperature. When mercury dimethyl, photolysed by light of wavelength 2537A, is used as a radical source, the importance of this factor will probably be far greater due to the very high extinction coefficient of the compound.

The accuracy of our measurements is certainly sufficiently good that the results can usefully be used to test theories about the factors affecting the rate of reactions involving free radicals.

The reactions of methyl radicals with butane, cyclopropane, methanol, and methyl ether have been studied using radicals from different sources, notably acetone and mercury dimethyl. The results obtained by the two methods are given in Table IV. The agreement is very satisfactory and is better than might have been expected in view of the very high extinction coefficient of mercury dimethyl.

The relative rates found for benzene, toluene, and the alkanes (Part II) are in rough agreement with those found by Taylor and Smith.[5] The agreement is probably

TABLE IV. The reaction of methyl radicals with butane, cyclopropane, and methyl ether.

Compound	Radical source	$k_1/k_2^{\frac{1}{2}}\times 10^{12}$ at 182°C	$E_1-\frac{1}{2}E_2$ (kcal)	Reference
Butane	CH_3COCH_3	21	8.3	a
	$Hg(CH_3)_2$	42	8.2	b
	$Hg(CH_3)_2$	19	9.5	c
Cyclopropane	CH_3COCH_3	2.1	10.3	a
	$Hg(CH_3)_2$	2.8	10.2	d
Methanol	CH_3COCH_3	11	8.2	a
	$Hg(CH_3)_2$	10	8.2	d
Methyl ether	CH_3COCH_3	17	9.5	a
	$Hg(CH_3)_2$	17	8.4	d
	Thermal radicals from decomposition of CH_2CCH_3	23	10	e

[a] This paper, Table III.
[b] R. Gomer, J. Am. Chem. Soc. **72**, 201 (1950).
[c] Recalculation of results from reference b on slightly different basis. See A. F. Trotman-Dickenson and E. W. R. Steacie, paper presented to A.C.S. Symposium on Reaction Kinetics, June 1950, to be published.
[d] M. K. Phibbs and B. deB. Darwent, Can. J. Research, **B28**, 395 (1950).
[e] Marcus, Darwent, and Steacie, J. Chem. Phys. **16**, 987 (1948), calculations corrected as described in reference c.

[5] J. O. Smith and H. S. Taylor, J. Chem. Phys. **7**, 390 (1939). H. S. Taylor and J. O. Smith, J. Chem. Phys. **8**, 543 (1940).

as good as could be expected, seeing that the authors expressed some doubt as to the accuracy of the measurments.

The results obtained with toluene are of particular interest because of the recent work of Szwarc and Roberts[6] on the same reaction. The values for $k_1/k_2^{\frac{1}{2}}$ which they obtained have been taken from Fig. 1 of their paper and plotted in Fig. 2. The methyl radicals used by Szwarc and Roberts were generated by the thermal decomposition of di-*t*-butyl peroxide. There is a big discrepancy between the activation energies found by them and by us. Actually, the scatter of the Szwarc and Roberts results is very great, as may be seen from Fig. 2. The authors attribute this to complications due to a wall reaction. The results show a large and definite curvature and are much better fitted by the dotted curve in Fig. 2 than by a straight line. We do not feel that the Szwarc and Roberts results should be considered seriously. Also, by comparison with a very large number of other reactions, we feel that their value of 12 to 13 kcal for the activation energy of the reaction

$$CH_3+C_6H_5\cdot CH_3=CH_4+C_6H_5\cdot CH_2$$

is most unlikely.

The relative rates and activation energies for the reaction of methyl radicals with methyl and isopropyl ether are of the magnitude which might be expected. They are in accordance with the general rule that tertiary hydrogen atoms react more readily than primary.

The interpretation of the results obtained with the alcohols and amines is difficult because of some uncertainty as to which hydrogen atom is removed in the reaction. The probability that, say, the hydrogen atom attached to the nitrogen atom in dimethylamine is removed when a methyl radical reacts with the compound is increased by the discovery that ammonia reacts rapidly with methyl radicals in comparison with methane. We did some experiments with methane by Method II, but the results were not sufficiently precise for the deduction of an activation energy. However, it could be seen that methane reacts about one-fourth as rapidly as ammonia at 300°C. No information is available on the reaction of methyl radicals with water. Our knowledge is not sufficiently great for us to explain the small differences in the rates and activation energies in the series of alcohols and amines.

The value obtained for the activation energy of the reaction of methyl with ammonia provides an upper limit of 112 kcal for the strength of the N—H bond in ammonia, if the usual value of 102 kcal for the C—H bond in methane is accepted.

In Table III is given a summary of the results we have obtained so far in this survey of methyl radical reactions. The values of $E_1-\frac{1}{2}E_2$ are taken directly from the tables in the papers in which the experimental findings are reported. The values of $k_1/k_2^{\frac{1}{2}}$ at 182°C and of $p_1/p_2^{\frac{1}{2}}$ come from the same source. In the sixth column of the table the values of $k_1/k_2^{\frac{1}{2}}$ are divided by the number of "active" hydrogen atoms in the compound which is being considered. The number of "active" hydrogen atoms is found by a consideration of the results for a series of compounds, such as the alkanes and of their molecular structure. Thus, 2,2-dimethyl propane has twelve and ethane has six hydrogen atoms all of which are equally active. It can be seen from Table III that *n*-butane reacts much more readily than ethane with methyl radicals. This is owing to the presence of the secondary hydrogen atoms of which there are four. *n*-butane is, therefore, said to have four "active" hydrogen atoms. The number of "active" hydrogen atoms in the other compounds has been deduced in a similar manner, and is given in column four of Table III. When it is doubtful whether the methyl radical abstracts a hydrogen atom by the rupture of an O—H or a C—H bond as in the alcohols or an N—H or a C—H bond as the amines, it has been supposed that it is the C—H bond which has been ruptured. In Table III allowance has been made in the paraffin results for the contribution of the primary hydrogen atoms to the over-all rate in a compound containing, say, primary and secondary hydrogen atoms on the assumption that all primary hydrogen atoms react at the same speed. The results are not sufficiently complete in the other series of compounds for the application of such a treatment.

This arrangement of our results for the paraffins and olefins is useful. It can be seen that particular contributions to the over-all rates of reaction are characteristic of the primary, secondary, and tertiary hydrogen atoms. Insufficient results are available for other classes of compound to decide whether the treatment is useful or not.

The steric, or *P* factors, are given in column 4 in the form of $P_1/P_2^{\frac{1}{2}}$. In calculating these, collision diameters were assigned as follows (in A): methyl 3.5, cyclopropane 5.0, cyclobutane 5.3, cyclopentane 5.6, cyclohexane 6.0, benzene 5.5, toluene 5.9, methanol 5.0, ethanol 5.6, isopropanol 6.2, methyl ether 5.0, isopropyl ether 7.0, methylamine 5.0, dimethylamine 5.0, trimethylamine 5.0, ammonia 3.5, 1-butyne 5.7, 2-butyne 5.7. The diameters for the paraffins and olefins are as given in the previous papers.[1,7]

No simple linear relation connects the logarithm of the steric factors with the activation energies found. Such relations have often been found to exist for ionic reactions, and it has been suggested that they also occur in series of free radical reactions studied in solution.

Perhaps, the most important conclusion to be drawn from the data concerns the magnitude of the steric

[6] M. Szwarc and J. S. Roberts, Trans. Faraday Soc. **46**, 625 (1950).

[7] A. F. Trotman-Dickenson and E. W. R. Steacie, J. Chem. Phys. **19**, 169 (1951).

factors of the reactions. From Table III, it will be seen that for almost all the reactions the P values are 10^{-3} or less, if a value of unity is assumed for the steric factor for methyl recombination, or still less if this recombination has a low steric factor. There has been much discussion of these steric factors in the past. It was suggested previously by one of us that the values were probably low.[8] Evans and Szwarc[9] concluded that the steric factors for simple metathetical elementary reactions should be in the neighborhood of 1 to 10^{-2}. Their conclusions were based on two lines of argument; a review of existing data, and a qualitative discussion from the transition state point of view.

From their review of the data they list a number of cases in which the steric factor has been found to be approximately unity. In some of the cases cited, the data are highly doubtful. We agree, however, that a considerable number of cases are cited involving halogens and sodium atoms in which the evidence is strongly in favor of high values of P.

On the other hand, the values which we have determined and those cited by Dorfman and Gomer[10] constitute a list of about 40 well-investigated reactions of free radicals in which the steric factors are 10^{-3} or less. We, therefore, dispute strongly the contention that there is such a thing as a "normal" steric factor. On the basis of presently available data, the steric factors of elementary reactions vary over a wide range and must be determined *experimentally* in each case. However, there does seem to be a tendency for the steric factors to remain of the same order of magnitude for a given type of reaction, and the evidence, thus, favors high values of P for reactions of sodium atoms and low values for reactions of methyl radicals. It seems very dangerous to generalize further with our existing knowledge or to try to fit all elementary reactions into an arbitrary pattern.

Polanyi and his co-workers[11] have suggested that for closely related compounds there will be a linear relation between the activation energies of a series of reactions of type (3)

$$A+BC=AB+C, \tag{3}$$

and the strengths of the bonds B—C. This relation was written as $\Delta E=\alpha\Delta H$, where E is the activation energy of the reaction, and H is the strength of the bond which is broken. To test such an equation the activation energies and the bond strengths must be known with considerable accuracy. Butler and Polanyi[11] tested the relation by comparing the activation energies of the reaction of sodium atoms with chlorides with bond strengths found by the pyrolysis of the iodides. However, the activation energies were obtained in most cases from collision yields, uniform steric factors being assumed and, thus, are quite unreliable. The bond strength values used are very unreliable also, and, hence, it is impossible to check this relationship. The relation which Steiner and Watson[12] claimed to have established depended upon the values of the C—H bond strengths derived from Polanyi's data on the iodides. Also, the activation energies for the reaction of chlorine atoms with paraffins were derived on the assumption that the steric factors of the reactions are constant, and there is no evidence for this.

Bolland[13] has suggested that a Polanyi type relation holds for the activation energy of the metathesis step in the autoxidation of olefins and the strength of the C—H bond in the α-position to the double bond. However, the bond strengths were derived theoretically and are not reliable.

It is very unlikely that all our results could be fitted to a Polanyi type relation, because the order of strengths obtained is not in agreement with what is known about the pyrolysis of hydrocarbons and other compounds. However, a relation might be found for the paraffins when more accurate bond strengths are available, as the members of the series are extremely similar.

ACKNOWLEDGMENT

We wish to thank Miss Frances Gauthier and Dr. F. P. Lossing of this laboratory for the mass spectrometric analyses.

[8] Steacie, Darwent, and Trost, Faraday Soc. Discussion **2**, 80 (1947).
[9] M. G. Evans and M. Szwarc, Trans. Faraday Soc. **45**, 940 (1949).
[10] L. M. Dorfman and R. Gomer, Chem. Revs. **46**, 499 (1950).
[11] E. T. Butler and M. Polanyi, Trans. Faraday Soc. **39**, 19 (1949).
[12] H. Steiner and H. R. Watson, Faraday Soc. Discussion **2**, 88 (1947).
[13] J. L. Bolland, Quart. Rev. **3**, 1 (1949).

New Measurements on the Infrared Spectrum of F_2O*†‡§

E. A. Jones, J. S. Kirby-Smith, P. J. H. Woltz, and A. H. Nielsen¶
K-25 Research Laboratories, Carbide and Carbon Chemicals Division, Union Carbide and Carbon Corporation, Oak Ridge, Tennessee

(Received August 16, 1950)

The infrared spectrum of F_2O has been re-examined from $2-25\mu$ with a prism spectrometer and selected regions further examined with a grating spectrometer. Several bands observed by Hettner, Pohlmann, and Schumacher have been shown to be caused by impurities. Other bands observed by them have been resolved, and an assignment of fundamental modes has been made which is consistent with dimensions of the molecule obtained from electron diffraction data. Two new bands have been observed and assigned to combinations of the fundamentals. The present observed frequencies and their assignments are: $\nu_1=928$ cm^{-1}, $\nu_2=461$ cm^{-1}, $\nu_3=831$ cm^{-1}, $\nu_1+\nu_3$ and $2\nu_2+\nu_3$ at 1731 cm^{-1}, $3\nu_3=2460$ cm^{-1}, $2\nu_1+\nu_3=2643$ cm^{-1}.

I. INTRODUCTION

THE infrared spectrum of F_2O was first observed in 1935 by Hettner, Pohlmann, and Schumacher[1] who suggested two separate interpretations of their observed bands. In 1936, Sutherland and Penney[2] reassigned the bands in an effort to obtain reasonable force constants.

F_2O is a nonlinear triatomic molecule with C_{2v} symmetry. There are three normal modes of vibration; two are totally symmetric, ν_1 and ν_2, and one is antisymmetric, ν_3. The molecular dimensions of F_2O were obtained from the electron diffraction measurements of Maxwell[3] and were used to compute the moments of inertia of the molecule $I_a=15.3\times10^{-40}$ g cm^2, $I_b=73.6\times10^{-40}$ g cm^2, $I_c=88.9\times10^{-40}$ g cm^2. The least axis, I_a, lies perpendicular to the C_2 axis. There are, thus, two vibrations in which the electric moment changes along the intermediate axis of the model giving rise to type B bands, and one vibration in which the electric moment oscillates along the least axis giving rise to type A bands. The envelope of a type B band is a doublet, and for a type A band the envelope has three branches. One would, therefore, expect for this model two doublet bands and one PQR type band for the three fundamentals.

As the band envelopes were not clearly defined in the work of Hettner, Pohlmann, and Schumacher, and as there appeared to be considerable question about the band assignments, it was concluded that a new effort would be worth while.

When the infrared spectrum of carefully purified samples of F_2O, prepared in this laboratory by Mr. Wilbur Simon, was observed, several of the bands attributed to fundamental modes by Hettner, *et al.*, and by Sutherland and Penney were not found. These bands have been ascribed to impurities and a new assignment has been made which conforms to the shape predicted by the electron diffraction data. This paper is a report on this work and includes prism records over the $2-25\mu$ region and grating records over selected regions.

II. EXPERIMENTAL DETAILS

The spectrum of F_2O was examined from $2-25\mu$ with a Perkin-Elmer spectrograph utilizing NaCl, KBr, LiF, and CaF_2 optics. Calibration of the prisms was effected with the aid of well-known infrared spectra. Selected regions were further examined under much greater resolution on the prism-grating spectrograph of the University of Tennessee[4] using a 3600 lines-per-inch grating in several orders. This instrument was calibrated by observing the grating angle of the 1 μ-mercury line in several orders. The F_2O was contained in 10-cm-long absorption cells of fluorothene closed with either NaCl or KBr windows. The windows were sealed to the cell with a lighter polymer of fluorothene. Various pressures of gas in the cell were used for the different bands.

III. EXPERIMENTAL RESULTS

The regions of absorption reported by Hettner, Pohlmann, and Schumacher are discussed separately in the following sections:

20 μ-Region.—Hettner, *et al.*, report a band with one maximum at 492 cm^{-1}. In the present work this band has been resolved into a doublet with its center at 461 cm^{-1}, using a KBr prism. This band has been assigned ν_2.

16 μ-Region.—No band was found in this region in the present sample. The band at 625 cm^{-1} reported by them is attributed to a CF_4 impurity in their sample.

10–12 μ-Region.—In the earlier work, two bands at 833 cm^{-1} and 926 cm^{-1} are listed. In one of their alternative interpretations these bands are called ν_1 and ν_2, respectively, while in the other the two maxima are

---

* This document is based on work performed for the AEC by the Carbide and Carbon Chemicals Division, Union Carbide and Carbon Corporation, at Oak Ridge, Tennessee.

† The results given in this paper were presented at the Symposium on Molecular Structure, The Ohio State University, Columbus, Ohio, in June, 1949, and June, 1950. Prof. R. M. Badger also reported on F_2O at the 1949 meeting.

‡ H. H. Nielsen, Research **2**, 369 (1949).

§ A. H. Nielsen, J. Chem. Phys. **19**, 98 (1951).

¶ The University of Tennessee, Knoxville, Tennessee.

[1] Hettner, Pohlmann, and Schumacher, Z. Physik **96**, 203 (1935).

[2] G. B. B. M. Sutherland and W. G. Penney, Proc. Roy. Soc. (London) **156A**, 678 (1936).

[3] L. R. Maxwell, J. Opt. Soc. Am. **30**, 374 (1940).

[4] A. H. Nielsen, J. Tenn. Acad. Sci. **XXII**, No. 4, 241 (1947).

FIG. 1. Grating record of ν_3.

considered part of one doublet band with its center at 870 cm^{-1}. It is, however, quite clear that there are two bands in this region, one a doublet centered at 928 cm^{-1} and the other a PQR type centered at 831 cm^{-1}. Figure 1 shows a grating record of the band at 831 cm^{-1} which is assigned ν_3. This intense band exhibits PQR structure which is to be expected because, with $I_a \ll I_b \approx I_c$, ν_3 is a parallel band in a very nearly symmetrical top. The Q branch folds toward lower frequencies and the PR spacing is about 30 cm^{-1}. No rotational fine structure is discernible even with the grating. The details appearing in this band, however, repeat from record to record and it may be that it is just on the limit of resolution.

The other band in this region assigned to $2\nu_2$ by Sutherland and Penney has been re-examined under high resolution with the grating instrument. This band, shown in Fig. 2, is type B and is resolved into Q lines with an average spacing of about 3.4 cm^{-1}. An analysis of the rotational structure gives the band center at 928.2 cm^{-1}. The ${}^{R}Q_K$ lines are considerably sharper and better defined than the ${}^{P}Q_K$ lines because the ${}^{P}Q_K$ lines appear to be resolving into further structure with a fairly regular spacing of about 1 cm^{-1}. This band is quite intense and, therefore, it is more reasonable to assign it to ν_1 than to $2\nu_2$. There are, thus, two doublets and one PQR type band conforming to the assumed model.

8–9 μ-Region.—Hettner, Pohlmann, and Schumacher report bands at 1110 cm^{-1} and 1280 cm^{-1}. The band at 1110 cm^{-1}, identified as ν_3 by Sutherland and Penney, was not observed in the present F_2O sample nor was it found in a CF_4 sample. Hettner and co-workers ascribe fundamental status to the 1280 cm^{-1} band, and Sutherland and Penney assign it to $\nu_1+\nu_2$. As this band, too, was not found in the present sample, and as there is an intense CF_4 band at this frequency, it doubtlessly must be attributed to CF_4.

6 μ-Region.—The absorption reported at 1740 cm^{-1}, identified by Sutherland and Penney as $\nu_1+2\nu_2$, has been re-examined both with a CaF_2 prism and a grating. Similar envelopes are obtained with both instruments. Figure 3 shows a percent absorption curve of this band obtained with the CaF_2 prism. The center of the absorption region is at 1731 cm^{-1} and the separation of the two principal maxima is 28 cm^{-1}. This absorption is attributed essentially to $\nu_1+\nu_3$ in this paper.

4–5 μ-Region.—No absorption was observed at 2190 cm^{-1} as reported by Hettner and co-workers. It is suggested that this band too is attributable to the CF_4 impurity in their sample.

Another band, listed by these authors at 2544 cm^{-1}, was not observed even with a pressure of $1\frac{1}{2}$ atmos in a 30-cm cell, and is also ascribed to CF_4. Three grating records across the 2400–2700 cm^{-1} region, shown in Fig. 4, disclose the existence of two type A bands, not previously reported—at 2460 cm^{-1} and 2643 cm^{-1}. Curve (a) shows the background record with the empty cell; curve (b) shows the record obtained with $1\frac{1}{2}$ atmos of F_2O in the 30-cm cell, and curve (c) shows the absorption due to CF_4 at 7 cm pressure in a 10-cm cell.[5] The two new bands are doubtlessly caused by F_2O and have been assigned $3\nu_3$ and $2\nu_1+\nu_3$, respectively. These bands, shown in detail in Fig. 5, have P–R spacings of 27 cm^{-1} and 23 cm^{-1} which is in good agreement with the P–R spacing of ν_3.

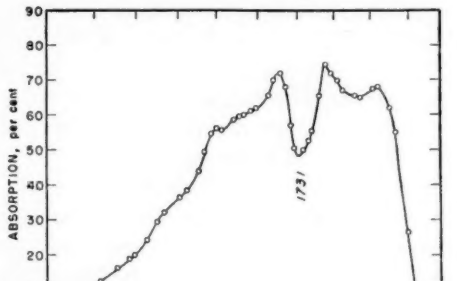

FIG. 3. Percent absorption curve of $\nu_1+\nu_3$, and $2\nu_2+\nu_3$ with a CaF_2 prism.

TABLE I.[a]

Observed frequency cm^{-1}	Calculated frequency cm^{-1}	Band type	$\Delta\nu$ (P–R) cm^{-1}	Assignment: Bernstein and Powling	Assignment: This work
461		(B) Doublet	30	ν_2	ν_2
831		(A) PQR	30	ν_3	ν_3
928		(B) Doublet	30	ν_1	ν_1
1731	1760 1743	(A) 2 PQR Superposed	28	$\nu_1+\nu_3$ $2\nu_1$	$\nu_1+\nu_3$ $2\nu_2+\nu_3$
2460	2493	(A) PQR	27	Not observed	$3\nu_3$
2643	2689	(A) PQR	23	Not observed	$2\nu_1+\nu_3$

[a] Only the bands known to be of F_2O origin are given in this table. The interpretations of Hettner, *et al.*, and Sutherland and Penney are, thus, omitted as they are dependent upon impurity bands.

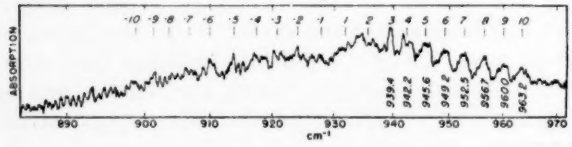

FIG. 2. Grating record of ν_1 showing resolution of the Q lines.

[5] A new band center for the CF_4 band obtained from curve (c) is 2556 cm^{-1} instead of 2544 cm^{-1}.

IV. DISCUSSION

While this paper was being prepared for publication, a paper on F_2O was published by Bernstein and Powling[6] in which they show prism curves of the four most intense bands. They evidently did not observe $3\nu_3$ and $2\nu_1+\nu_3$. Their interpretation is that given here with one exception. These authors suggest that the envelope of the band at 1731 cm^{-1}, which they also attribute to $\nu_1+\nu_3$, is contributed to by $2\nu_1$. This assignment would require an anharmonic term of about 121 cm^{-1} to bring it into the region of 1731 cm^{-1}. A more likely assignment would be that the band, which appears to be a

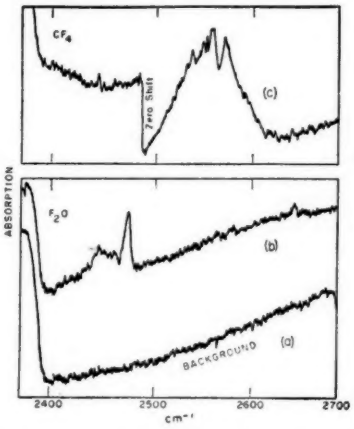

FIG. 4. Grating records of F_2O and CF_4 showing $3\nu_3$ and $2\nu_1+\nu_3$ in the region of the CF_4 impurity.

doublet, is largely composed of $\nu_1+\nu_3$ (1760 cm^{-1}) with a superposition of the weaker $2\nu_2+\nu_3$ (1743 cm^{-1}). These two bands are both type A and it is not difficult to superpose two such bands to obtain an envelope similar to that shown in Fig. 3.

The F_2O frequencies and their assignment are given in Table I.

The asymmetry coefficient for F_2O from the moments of inertia computed from the electron diffraction data is $\kappa=-0.914$. It is, therefore, reasonable to treat the rotational analysis of the band shown in Fig. 2 from the point of view of the symmetrical top. When the moments of inertia I_a, I_b, and I_c of the assumed model are substituted into the relation for the Q-branch separation, $\Delta\nu$ (cm^{-1}) $=(h/4\pi^2c)[1/I_a-1/2(1/I_b+1/I_c)]$, the computed spacing is 2.96 cm^{-1} as compared with the observed 3.4 cm^{-1}. These results are in agreement with Bernstein and Powling. The band center was found to be 928.2 cm^{-1}. It is worth noting in Fig. 2 that the Q branches on the high frequency side of the band center all shade toward low frequencies. On the low frequency side of the band the Q branches are broader and harder to distinguish because of partial resolution. This effect may possibly be explained by the moments of inertia being significantly different in the upper and lower states in such a way as to cause convergence on one side and divergence on the other increasing with K. On the other hand, A″–B″ and A′–B′ appear to be virtually equal from the analysis.

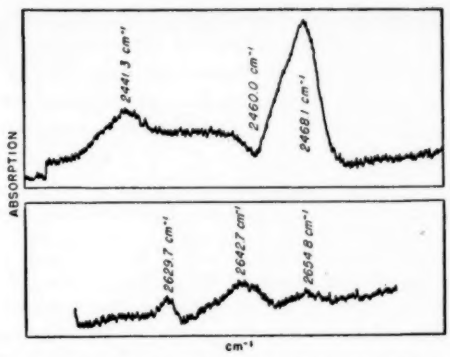

FIG. 5. Detail curves of $3\nu_3$ and $2\nu_1+\nu_3$ obtained with the grating.

The grating record of ν_3, Fig. 1, shows strong convergence in the Q branch which folds toward lower frequencies. It also appears that the P and R branches exhibit strong convergence. Much the same effect may be seen in $3\nu_3$ at 2460 cm^{-1}, Fig. 5. Here the R branch is very intense and sharp while the P branch and the Q branch are broad and of relatively low intensity. $2\nu_1+\nu_3$, however, exhibits three broad branches in contrast.

A grating is not available at the present time with which ν_2 at 461 cm^{-1} could be resolved. It is hoped it can be recorded in the near future.

V. ACKNOWLEDGMENT

The authors wish to express their gratitude to Mr. A. V. Faloon and Mr. W. B. Kenna of the Physics Department for their careful sample preparations and continued interest in the problem.

[6] H. J. Bernstein and J. Powling, J. Chem. Phys. 18, 685 (1950).

Influence of Foreign Gases at High Pressures on the Infrared Absorption Band of Methane at 3.3μ

H. L. WELSH, P. E. PASHLER,* AND A. F. DUNN†
McLennan Laboratory, University of Toronto, Toronto, Canada
(Received October 24, 1950)

An infrared absorption cell for compressed gases was constructed and used at pressures up to 600 atmos. In the cell, which was of the reflection type, the length of the absorbing path could be changed from 5×10^{-4} cm to 4 cm by means of metal spacers placed between the window and the mirror. The influence of high pressures of helium, argon, and nitrogen on the intensity of the methane band at 3.3μ was investigated. It was found that the absolute absorption coefficient for the band increases linearly with the density of the foreign gas. With nitrogen at 600 atmos the absorption coefficient is 20 percent greater than that of the free methane molecule. The magnitudes of the coefficients of induced absorption are compatible with the assumption that the vibrating dipole of the absorbing molecule is increased by the reaction field of the polarizable foreign gas molecules in its neighborhood. The coefficient of absorption for the free molecule was found by extrapolating the measured coefficients to zero density of the foreign gas. The values derived from measurements with the three foreign gases agree closely, and give an average value of 1075×10^{10} sec^{-1} cm^{-1} at NTP.

INTRODUCTION

SPECTROSCOPIC methods can be used in the study of intermolecular forces. When an atom or molecule under the perturbing influence of near neighbors emits, absorbs, or scatters light, the effect of the perturbation is more or less directly evident in the spectrum. In general, the perturbation can change both the frequency of the light emitted or absorbed and the probability of the transition involved. The extreme case of molecular interaction is found in liquids and solids, whose spectra often show significant differences from the spectrum of the corresponding gas at low pressure. However, since the molecular interactions in the condensed phases are very complex, they cannot be correlated easily with the observed changes in the spectrum. It is evident that the investigation of compressed gases will give experimental data which can be interpreted more readily. Changes in the spectrum can be studied as a function of the density of the gas, which can be varied over a wide range. Additional information can be obtained from the continuous variation of other experimental conditions such as the temperature of the gas and the partial pressure of a foreign gas.

The induced infrared absorptions observed in O_2, N_2, H_2, and CO_2[1] are examples of a change in transition probability brought about by intermolecular forces. The vibrations of homonuclear diatomic molecules and the symmetrical vibration of CO_2, normally inactive in infrared absorption, are active in the compressed gas. The absorption, which obeys the Raman effect selection rule for rotation, is induced also by foreign gases. The effect was interpreted as a distortion of the electronic distribution of the absorbing molecule during a close collision with a perturbing molecule. Also, as Mizushima[2] has pointed out, the quadrupole field of the gas can give rise to an induced absorption of the type observed. At least in H_2 the collision effect must predominate, since the absorption can be induced by rare gas molecules which possess no quadrupole moment.

In the present investigation the effect of pressure on the absorption band of an infrared active vibration was studied. From the experimental point of view the simplest case to investigate is the influence of high pressures of foreign gases on the absorption of a gas whose partial pressure is held constant. It is well known that the addition of small partial pressures of foreign gases can cause the observed infrared absorption of a gas to increase, an effect due to the pressure broadening of the individual rotational lines of the band combined with the finite spectral resolution of the detection instrument.[3] In the present experiment the foreign gas pressures were high and the pressure broadening presumably very great, so that the influence of intermolecular forces on the true absorption intensity could be detected. The 3.3μ-band of methane corresponding to the triply degenerate frequency, ν_3, was chosen for the investigation. Helium, argon, and nitrogen were the foreign gases used.

EXPERIMENTAL

The design of an infrared absorption cell for gases at high pressures is complicated by the window which is the weakest part of the system. For retaining pressure the window should be thick and the unsupported area small. On the other hand, the instantaneous detection method used in the infrared requires that the radiation intensity transmitted by the cell be as large as possible. If the cell is to be generally useful the length of the absorbing path must be variable from, say, a few microns to a few centimeters. The short path lengths are necessary for studying infrared active frequencies for which the absorption coefficient can be very large at

* Present address: General Electric Company, Schenectady, N. Y.

† Holder of research scholarships, 1947–1949, under the Ontario Research Council. Present address: Physics Division, National Research Council, Ottawa, Canada.

[1] Crawford, Welsh, and Locke, Phys. Rev. **75**, 1607 (1949); **76**, 580 (1949); **80**, 469 (1950).

[2] M. Mizushima, Phys. Rev. **76**, 1268 (1949).

[3] A review of the literature in this connection is given by Nielsen, Thornton, and Dale, Revs. Modern Phys. **16**, 307 (1944).

high gas densities. The path lengths, especially the very short ones, must be accurately measurable.

It was considered that these requirements could be satisfied most easily in a cell of the reflection type, where the radiation enters and leaves through a single window and is reflected by a mirror within the cell. The emergent beam can be displaced a few degrees from the incident beam by an inclination of the cell. The path length in the cell can be varied by changing the thickness of metal spacers placed between the window and the mirror.

The window, spacer, mirror, and retaining cap were mounted on a hardened steel "lens-ring," as shown in Fig. 1. In the assembled cell the large closing screw applies pressure to the lens-ring which deforms the inner shoulder of the cell and makes a pressure-tight mechanical seal. The lens-ring type of seal was also used for the gas inlet tubing. The window, 2.46 cm in diameter, has a central free area, 0.8 cm in diameter, for admitting the radiation. Both surfaces of the window and the window-sealing surface of the lens-ring were optically polished. Although the window could be contacted to the lens-ring to make a pressure seal, it was found more convenient to use a thermosetting cement (PKR-16)[4] between the polished surfaces. This seal permits evacuation of the cell and holds even when the window is deformed slightly at high pressures.

The mirror in the cell was made of tantalum, chosen for its chemical inertness and because its low reflecting power (about 40 percent) in the visible provides an easy and accurate method of measuring small absorbing path lengths. The light reflected from the mirror combines with the light reflected from the inner surface of the window to give interference fringes of good visibility in the visible region. Thus, path lengths of less than 10^{-2} cm, obtained by metal foil spacers, can be measured accurately with a small glass spectrograph by using the cell as a reflection etalon. In the infrared region the reflecting power of the tantalum is high and the interference fringes have such poor visibility that they do not complicate the reduction of experimental data. Spacers thicker than 10^{-2} cm are measured with a micrometer.

A fused quartz window, 0.38 cm thick, was used in the present investigation in which gas pressures of 600 atmos were reached. In other work, a calcium fluoride window, 1.0 cm thick, has been used up to 300 atmos. The upper limit of safe operating pressure is not yet known for either window.

For gases condensable at liquid air temperature a thermal compressor was used to generate pressures up to 600 atmos. The thermal compressor, a stout-walled stainless steel bottle, was partially immersed in liquid air, and gas from the storage cylinder was condensed in it. The quantity of gas condensed could be regulated by the depth of immersion of the bottle in the liquid air. The bottle was then allowed to warm up to generate the required pressure in the absorption cell. For helium an hydraulic gas compressor was used to fill the thermal compressor with high pressure gas at liquid air temperature. When the temperature of the thermal compressor was allowed to rise, the required high pressures of helium could be obtained. Pressures above one atmos were measured by three Bourdon tube gauges reading to 150, 1500, and 10,000 psi. Pressures below one atmos were measured with mercury or oil manometers.

To insure rapid mixing of the gases the volume of the inlet tube between the admitting valve and the cell was made as small as possible. Mixing in the cell itself was facilitated by cutting slots in the spacer and retaining cap as shown in Fig. 1.

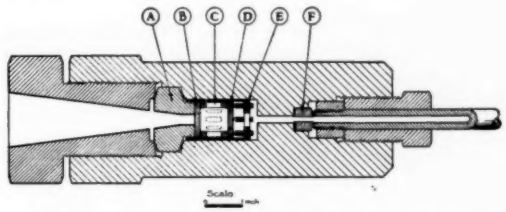

FIG. 1. Infrared absorption cell for gases at high pressures. A, F—"lens-rings" for pressure seals; B—window; C—spacer; D—mirror; E—retaining cap with three adjusting screws.

A Perkin and Elmer Model 12-C infrared spectrometer with a rocksalt prism was used. An aluminized spherical mirror focused a twice-enlarged image of a Nernst filament on the mirror in the absorption cell. A second spherical mirror focused the returning beam at the normal source position of the spectrometer. The wavelength drive mechanism of the spectrometer was geared to the slit adjusting screw in such a way that the resolution of the instrument was constant in the frequency range 2500–3500 cm^{-1}. The intensity of the Nernst filament recorded with the constant spectral slit width did not vary appreciably over this region. An effective slit width of 25 cm^{-1} was used throughout the investigation.

EXPERIMENTAL RESULTS

With a spacer of 1.92 cm in the absorption cell and methane pressures of 2.5, 5, and 10 cm Hg the absorption of the band at 3.3μ could be accurately measured at all foreign gas pressures. The gases were taken directly from commercial cylinders without further purification. Only in the case of argon was an impurity absorption observed of sufficient intensity to reduce the accuracy of the experimental data. The impurity, which was not identified, absorbed so strongly at an argon pressure of 500 atmos that no attempt was made to obtain data at higher pressures. The densities of He, A, and N_2 at high pressures were calculated from isothermals given by Michels and his co-workers.[5,6,7]

[4] Coles, Deuberry, and Curry, J. Opt. Soc. Am. 34, 623 (1944).

[5] A. Michels and H. M. Wouters, Physica 8, 923 (1941).
[6] A. Michels, H. and H. Wijker, Physica 15, 627 (1949).
[7] A. Michels, Physik Z. 35, 97 (1934).

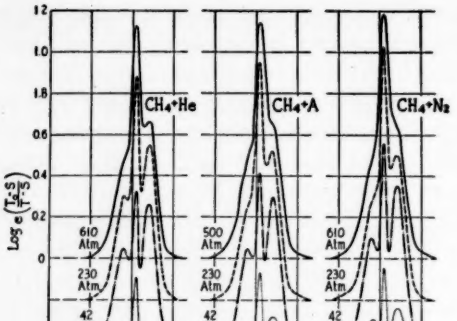

FIG. 2. The effect of various partial pressures of foreign gases on the contour of the 3.3μ-band of CH_4. Absorbing path length, 3.8 cm. Partial pressure of CH_4, 10 cm Hg. For clarity the ordinate scale has been shifted for the various pressures.

The reduction of the experimental data to obtain the true absorption coefficient of the band with various foreign gas pressures followed essentially the extrapolation procedure as developed by Wilson and Wells.[8] The density, $\ln[(T_0-S)/(T-S)]$ was calculated throughout the band from the recorder traces. In this expression T_0 is the intensity recorded by the spectrometer when the absorption cell was evacuated; T is the intensity with the gases in the cell; and S is a correction for stray light, chiefly that reflected from the window of the cell. S was measured in each experiment by observing the recorder deflection at a fixed frequency in the middle of the band as the methane pressure was raised to about 50 atmos. Above about 10 atmos the deflection was constant indicating that the cell was opaque to the radiation. The residual intensity, usually about 5 percent of the incident intensity, was taken as the stray light correction S.

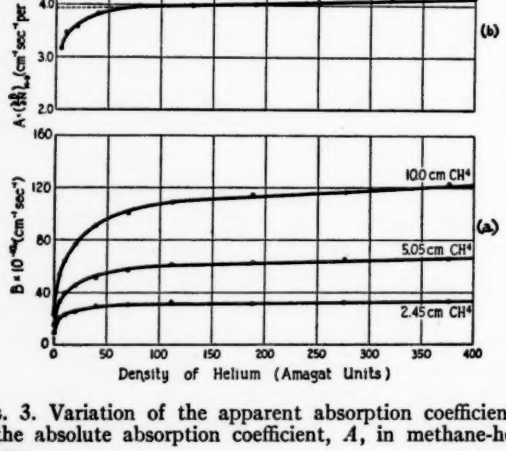

FIG. 3. Variation of the apparent absorption coefficient, B, and the absolute absorption coefficient, A, in methane-helium mixtures.

[8] E. Bright Wilson, Jr., and A. J. Wells, J. Chem. Phys. 14, 578 (1946).

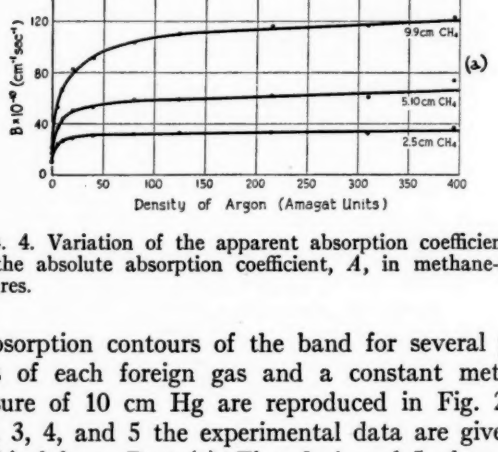

FIG. 4. Variation of the apparent absorption coefficient, B, and the absolute absorption coefficient, A, in methane-argon mixtures.

Absorption contours of the band for several pressures of each foreign gas and a constant methane pressure of 10 cm Hg are reproduced in Fig. 2. In Figs. 3, 4, and 5 the experimental data are given in graphical form. Part (a), Figs. 3, 4, and 5, shows the variation of the integrated apparent absorption coefficient, $B=(1/L)\int \ln[(T_0-S)/(T-S)]d\nu$ with the density of the foreign gas, for three constant partial pressures of methane. From the smoothed curves of these plots the variation of the apparent absorption coefficient with methane pressure was plotted for various densities of the foreign gas. An example of such a plot is shown in Fig. 6. The slope of each of these curves at the origin is, under certain conditions, a measure of the true absorption intensity of the band, $A=\int \alpha(\nu)d\nu$. According to Wilson and Wells,[8] the conditions are that the incident intensity be constant over the range of frequencies covered by the spectrometer slit, that the resolving power be constant over the band, and that the energy curve transmitted by the slit be symmetrical. These

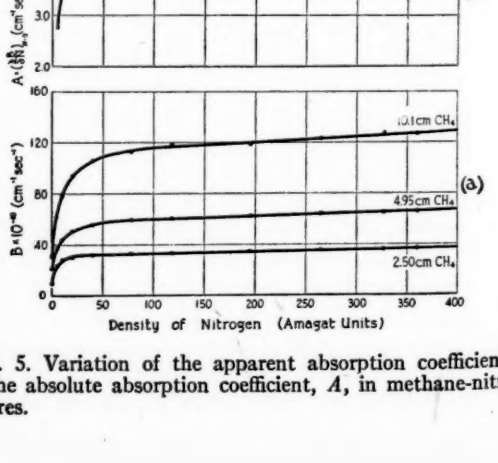

FIG. 5. Variation of the apparent absorption coefficient, B, and the absolute absorption coefficient, A, in methane-nitrogen mixtures.

conditions are satisfied in the present experimental arrangement. The absorption coefficients derived in this way and recalculated on a per molecule basis, $A=(\partial B/\partial N)_{N=0}$, where N is the number of methane molecules per cc, are plotted in part (b) Figs. 3–5.

In each case the absorption coefficient of the band shows a sharp initial rise as the foreign gas density is increased. This is due to the fact that, at low foreign gas pressures, the broadening of the rotational lines is not great enough, and the extrapolation of the apparent absorption coefficient to zero methane pressure is not accurate enough to give a good value for A.

It might be expected that at high foreign gas pressures, the absorption coefficient would have a constant value, the true absorption intensity of the band. However, it is apparent from curves (b), Figs. 3–5, that the absorption coefficient increases linearly with the density of the foreign gas. It must therefore be concluded that there is an absorption induced by the foreign gas and superimposed on the normal absorption of the band. The coefficient of induced absorption, which is proportional to the slope of the linear portion of the curve, is greatest for N_2 and least for He as foreign gases.

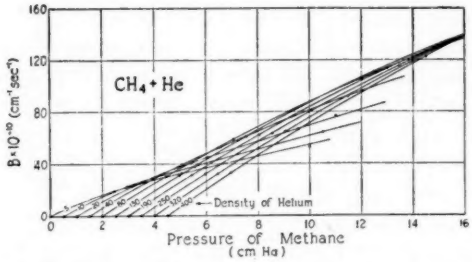

FIG. 6. Variation of the apparent absorption coefficient, B, as a function of the methane partial pressure for various pressures of helium. Each curve goes through the origin; for clarity the abscissa scale has been shifted for successive curves.

The extrapolation of the straight line portion of curves (b) to zero density of the foreign gas gives the absolute absorption coefficient of the free methane molecule. The results for the three foreign gases are given in Table I and show very good agreement. The value found here is some 15 percent greater than that found by Thorndike,[9] who used ammonia as the broadening gas at a pressure of five atmos. In view of this discrepancy the absolute absorption coefficient was measured in the present experimental arrangement with ammonia as the broadening gas up to eight atmos pressure. This gave a value close to that found by Thorndike, but from the shape of the curve corresponding to curves (b) it was clear that the pressure broadening of the widely spaced rotational lines was insufficient to permit an accurate determination of the absolute intensity.

There is considerable variation in the contour of the band with increasing foreign gas pressure, as shown in Fig. 2. The general features of the variation are explicable in terms of the pressure broadening of the rotational lines of the band. At zero foreign gas pressure there is a higher intensity in the P branch than in the R branch, the opposite of the distribution predicted by theory. With a foreign gas pressure as low as five atmos the pressure broadening is sufficient to restore the normal distribution. The anomalous distribution of intensity at low pressures may be due to the wider Coriolis splitting in the P branch which is shown in the high resolution trace obtained by Nielsen and Nielsen.[10] That the broadening action of A and N_2 is much greater than that of He is illustrated by the more rapid disappearance of the maxima in the P and R branches as the pressure is increased. No frequency shift of the maximum of the Q branch greater than ±5 cm^{-1}, the error in the frequency determination, could be detected with increasing foreign gas pressure.

TABLE I. Absolute intensity of the 3.3μ-band of CH_4.

Foreign gas	Absolute absorption coefficient (cm^{-1} sec^{-1} per molecule)	(cm^{-1} sec^{-1} at N.T.P.)
He	3.88×10^{-7}	1060×10^{10}
A	3.98×10^{-7}	1090×10^{10}
N_2	3.96×10^{-7}	1080×10^{10}
Average	3.94×10^{-7}	1075×10^{10}

ORIGIN OF THE INDUCED ABSORPTION

The essential features of the induced absorption are the surprisingly large magnitude of the effect and the persistence of the linear increase to very high foreign gas densities. With nitrogen at 600 atmos, the coefficient of induced absorption is 20 percent of the normal absorption coefficient of the band. At this pressure the density of N_2 is about one-half the density of the liquid at its normal boiling point. The persistence of the linear increase of the absorption to high gas densities indicates that the perturbations produced by the molecules in the neighborhood of an absorbing molecule are additive. The linear portions of graphs (b), Figs. 3, 4, and 5, can be used to calculate absolute values for the absorption induced by the various foreign gases. The calculated absorption coefficients are given in Table II.

It is unlikely that the induction effect observed here can be accounted for by a distortion of the electronic configuration of the methane molecule during collisions

TABLE II. Induced absorption intensity of the 3.3μ-band of CH_4.

Foreign gas	Induced absorption coefficient (cm^{-1} sec^{-1} per molecule CH_4 per molecule foreign gas)	(cm^{-1} sec^{-1} at N.T.P., per Amagat unit of density of foreign gas)
He	2.19×10^{-30}	0.157×10^{10}
A	5.87×10^{-30}	0.438×10^{10}
N_2	7.78×10^{-30}	0.582×10^{10}

[9] A. M. Thorndike, J. Chem. Phys. 15, 868 (1947).

[10] A. H. Nielsen and H. H. Nielsen, Phys. Rev. 48, 864 (1935).

with foreign gas molecules, as was postulated for the induction effect in infrared inactive vibrations.[1] Collision-induced absorption has a magnitude appreciably less than that observed here, and perturbations induced by multiple collisions would be expected to be non-additive, so that the linear law would not persist to high foreign gas densities. If **P** is the vibrating dipole of the methane molecule and **M** is the induced vibrating dipole, assumed to be randomly oriented with respect to **P** in collision-induced absorption, the absorption intensity of the gas as a whole is proportional to $(\mathbf{P}+\mathbf{M})^2=P^2+M^2$. Thus, the intensity is a superposition of the normal intensity and an intensity due to the induction effect. However, the absorption coefficients given in Table II are about twenty-five times greater than those for the absorption induced in hydrogen by He, A, and N_2.[1] Since there is no reason to believe that collision-induced absorption in methane would be much greater than that in hydrogen, some other mechanism must be sought. Induction due to the electric field given by the quadrupole moments of the surrounding molecules, as postulated by Mizushima,[2] can also be dismissed since the rare gas molecules possess no quadrupole moment.

A simple explanation of the induced absorption can be given in terms of the polarizabilities of the molecules. It is apparent that if the induced moment, **M**, is always in the same direction as **P**, the intensity of absorption is proportional to $(\mathbf{P}+\mathbf{M})^2=P^2+2PM+M^2$, where the term $2PM$ can have an appreciable value even when **M** is small compared with **P**. This situation exists when the absorbing and the perturbing molecule are polarizable structures; the vibrating dipole in the absorbing molecule induces dipoles in the surrounding foreign gas molecules, which in turn induce dipoles in the absorbing molecule in phase with and in nearly the same direction as the original dipole.

The order of magnitude of the effect can be easily calculated: Consider the absorbing molecule and a perturbing molecule, both spherically symmetrical with polarizabilities α_1, and α_2, respectively, and with their centers a distance R apart. If the dipole **P** makes an angle θ with the line joining the centers of the two molecules, a simple calculation shows that the resultant moment in the absorbing molecule is

$$\mathbf{P}'\simeq\mathbf{P}[1+(2\alpha_1\alpha_2/R^6)(1+3\cos^2\theta)]^{\frac{1}{2}}.$$

The *fractional increase* in the intensity of the band due to the induction is $(2\alpha_1\alpha_2/R^6)(1+3\cos^2\theta)$. The effect, like the Debye induction effect in intermolecular forces, is approximately additive when the absorbing molecule is in the presence of several perturbing molecules. The fractional increase in the absorption coefficient per molecule in the presence of a foreign gas with N molecules per cm^3 can be estimated by considering the foreign gas molecules to be distributed uniformly outside a sphere of radius R_0 drawn about the absorbing molecule. The fractional increase in absorption is then given by

$$N\int_{R_0}^{\infty}\int_0^{\pi}\int_0^{2\pi}\frac{2\alpha_1\alpha_2}{R^6}(1+3\cos^2\theta)R^2\sin\theta dR d\theta d\varphi$$

$$=\frac{16\pi}{3}\frac{\alpha_1\alpha_2}{R_0^3}N.$$

The polarizabilities of the gases are known from refractive index data, but R_0 the distance of closest approach is more difficult to estimate. If molecular radii as calculated from the Sutherland constant are used,[9] the calculated fractional increase in absorption is from $\frac{1}{5}$ to $\frac{1}{10}$ that observed. The calculated values might be expected to be too small because the formulas used are valid only for point dipoles, and short-range interaction forces are neglected. However, the calculated values are of the right order of magnitude, and it may be concluded that the explanation of the induced absorption in terms of the reaction field of the polarizable foreign gas molecules is essentially correct.

The induction effect which has been shown to give an increased absorption for the 3.3μ-band of methane should of course be observable for the infrared active frequencies of all molecules. The correctness of the explanation given here can be tested by further experiments. For example, the fractional increase in the absorption coefficient due to induction should be independent of the temperature, and should be the same for all infrared active frequencies of a given molecule perturbed by a given foreign gas.

ACKNOWLEDGMENTS

The work in high pressures at Toronto has been made possible by the generous support of the National Research Council of Canada. The authors are also greatly indebted to Professor A. Michels of the Van der Waals Laboratory, University of Amsterdam, for his continued interest and advice.

[9] Trautz, Ann. Physik **15**, 214 (1932).

Remarks on the Interpretation of the CH_2 Vibrational Frequencies of *n*-Paraffins

GORDON M. BARROW*
Department of Chemistry, University of California, Berkeley, California
(Received September 12, 1950)

The infrared and Raman frequencies are calculated for the fundamental vibrations of an infinite *n*-paraffin chain. Valence force constants, chosen to give agreement between the calculated and observed infrared frequencies, give calculated Raman frequencies which are correlated with observed Raman lines. The difference in frequency to be expected for the Raman and infrared bands of the CH_2 out-of-plane rocking vibration is discussed. The CH_2 frequencies of propane are calculated from the infinite paraffin chain force constants and are compared with previous assignments.

AN interpretation of the infrared and Raman spectra of the *n*-paraffins is important not only for the assignment of each paraffin spectra but also for the characterization of the CH_2 group vibrations which is useful for many thermodynamic calculations for hydrocarbons.

Recently the Raman spectra of several solid *n*-paraffins have been reported[1,2] and the infrared spectra of solid polythene is available.[3,4] The spectra of the long chain *n*-paraffins are relatively simple and several attempts,[5–7,2] based on calculations by the method introduced by Whitcomb, Nielsen, and Thomas,[5] have been made to interpret the observed bands. None of these interpretations are entirely satisfactory, since, to various degrees, they are all in serious disagreement with the ranges of frequency generally assigned to the various CH_2 vibrations.

An infinite paraffin chain is admirably suited to a simple valence force field vibrational calculation, since few principal force constants are required to define the hydrogen vibrations and the symmetry classes each contain few vibrations. The calculation has therefore been made using the original method of Whitcomb, Nielsen, and Thomas,[5] but with a valence force field instead of the central force field used by them.

In this method a chain vibration is described in terms of the motions of the individual CH_2 groups, each group vibrating with a particular phase relation to the adjacent groups. In a fundamental vibration the atoms of a CH_2 group of the paraffin chain vibrate in phase with frequency ω and the succeeding group vibrates correspondingly but out of phase with the preceding group by an amount λ, which varies from 0 to π. The frequency of the particular vibration is dependent on this difference in phase with which successive groups vibrate as well as on the force constants and masses involved.

It is necessary to consider for which values of the phase difference λ the vibration will give rise to an infrared or Raman band. Whitcomb, Nielsen, and Thomas[5] have discussed this both for the case of the infinite chain and the more complex case of the finite chain. For an infinite chain, only when the CH_2 groups are moving in phase, $\lambda=0$, or exactly out of phase, $\lambda=\pi$, will the contribution of each unit of the chain to the net change of dipole moment or change of polarizability add to give a non-zero result. Only vibrations corresponding to these values of λ will give rise to an infrared or Raman band. The symmetry of the extended paraffin chain imposes further restrictions on the infrared and Raman activity and the resulting selection rules have been given by Simanouti and Mizushima.[2]

Generally, since the frequency of a hydrogen vibration is quite insensitive to the remainder of the molecule, the band of frequencies permitted for the hydrogen vibrations by the range of phase difference is narrow. The nature of the CH_2 out-of-plane rocking vibration, however, is such that the difference in frequency for $\lambda=0$ and $\lambda=\pi$ is about 400 cm^{-1}; and it is particularly important that neither limit be considered as an average value appropriate for this vibration in thermodynamic calculations.

Nonskeletal force constants for the *n*-paraffin chain were obtained by fitting the frequencies observed in the infrared spectra of polythene for which the assignment is generally accepted. Skeletal force constants were chosen to fit the Raman lines appearing at 890 and 1060 cm^{-1} for the higher *n*-paraffins. In view of the assignment for the skeletal vibrations of *n*-butane and *n*-pentane,[8] these can confidently be taken as C–C stretching frequencies. Only in one class, called B_{1g} by Simanouti and Mizushima,[2] was it necessary to introduce an interaction force constant. The force constants used were, in units of 10^5 dynes/cm,

$f_{H-C-H}=0.42$	$f_{C-H}=4.55$
$f_{H-C-C}=0.61$	$f_{C-C}=3.6$
$f_{C-C-C}=0.2$	$f_{C-C,\ H-C-C}=0.2$.

* Present address: Physical Chemistry Laboratory, Oxford, England.

[1] N. Sheppard and G. J. Szasz, J. Chem. Phys. **17**, 86 (1949).
[2] T. Simanouti and S. Mizushima, J. Chem. Phys. **17**, 1102 (1949).
[3] H. W. Thompson and P. Torkington, Proc. Roy. Soc. (London) **A184**, 3 (1945).
[4] J. J. Fox and A. E. Martin, Proc. Roy. Soc. (London) **A175**, 208 (1940).
[5] Whitcomb, Nielsen, and Thomas, J. Chem. Phys. **8**, 143 (1940).
[6] L. Kellner, Nature **163**, 877 (1949).
[7] T. Simanouti, J. Chem. Phys. **17**, 734 (1949).
[8] D. M. Gates, J. Chem. Phys. **17**, 393 (1949).

TABLE I. Calculated frequencies of the normal vibrations of an infinite (CH_2) chain active in the infrared and Raman spectra and proposed assignment.

Class	Description of vibration	Calculated	Observed
Raman active			
$A1_g$	C−C stretch	950	890
	H−C−H bend	1447	1442, 1471
	C−H stretch	2869	2846, 2878
$A2_g$	CH_2 twist	1242	—
$B1_g$	C−C stretch	1003	1060
	CH_2 wag	1327	1296
$B2_g$	CH_2 rock	1102	1135?
	C−H stretch	2940	2934, 2963
Infrared active			
$A1_u$	H−C−H bend	1465	1475
	C−H stretch	2861	2853
$A2_u$	CH_2 twist	1242	(inactive)
$B1_u$	CH_2 wag	1341	1375
$B2_u$	CH_2 rock	738	728
	C−H stretch	2930	2926

The results of this calculation, together with the proposed assignment of the observed bands, are shown in Table I. This assignment follows, in all but one case, fairly directly from the assignments usually made for the lower paraffins and from the characteristic CH_2 vibrations chosen by most authors.

The Raman line at 1135 cm^{-1} has not previously been attributed to a CH_2 rocking vibration. The *n*-butane Raman line at 1148 cm^{-1}, which might be thought to correspond to the 1135-cm^{-1} line of the longer *n*-paraffins, has been attributed, on the basis of its polarization, to a CH_3 vibration.[9] The 1135-cm^{-1} line appears with relatively undiminished intensity in the spectra of *n*-cetane;[2] and although we cannot completely rule out the possibility that even in a compound of this length the CH_3 vibration persists, it appears most unlikely. That the $B2_g$ CH_2 rocking vibration should appear at about this value, whether or not the 1135-cm^{-1} line is due to this vibration, is further supported by the calculation of Simanouti and Mizushima,[2] who obtain a value of 1112 cm^{-1} for this frequency.

The characteristic frequency for this vibration, suitable for use in thermodynamic calculations, on the basis of our assignment will be given approximately by the average of the two limiting values 728 cm^{-1} and 1135 cm^{-1}, i.e., 930 cm^{-1}. This is in excellent agreement with the value of 940 cm^{-1} chosen by Pitzer.[10] In view of the propane infrared band at 748 cm^{-1} and the longer *n*-paraffin infrared band at 728 cm^{-1}, a considerably lower value has been taken[1,11] as the frequency appropriate to this vibration in thermodynamic calculations. The results obtained here, however, indicate that this infrared band for the long chain *n*-paraffins is the lower limit of the band of frequencies for this vibration rather than the average frequency.

[9] Szasz, Sheppard, and Rank, J. Chem. Phys. **16**, 704 (1948).

TABLE II. Comparison of observed propane frequencies with those calculated for a simplified model X−CH_2−X.

Class	Description of vibration	Observed cm^{-1}	Calculated cm^{-1}
A_1	C−C−C bend	370	362
	C−C stretch	870	876
	H−C−H bend	1460	1460
A_2	CH_2 twist	1278	1264
B_1	C−C stretch	1053	961
	CH_2 wag	1338	1348
B_2	CH_2 rock	748	903
	C−H stretch	2980	2940

The argument given by Rasmussen[11] for the choice of 750 cm^{-1} as the characteristic frequency for this vibration is based, in part, on the occurrence of the CH_2 rocking frequency of propane at 748 cm^{-1}. The results of a vibrational calculation for the simplified propane model, X−CH_2−X, which eliminates from the results the effects of CH_3 interactions, are shown in Table II.† The force constants of the infinite chain calculation have been used. This calculation shows that the CH_2 rocking frequency is to be expected at about 903 cm^{-1} and that its appearance at 748 cm^{-1} is, as suggested by Pitzer,[12] due to the interaction with a CH_3 vibration.

The above results support the characteristic CH_2 rocking frequency of 940 cm^{-1} used by Pitzer. Furthermore, the infrared band observed for *n*-paraffins at 730 cm^{-1}, while indeed due to a CH_2 rocking vibration, represents only the lower limit of the range of frequency for this vibration. The upper limit may be responsible for the 1135 cm^{-1} Raman line in long chain *n*-paraffins and in any case should occur at about this value.

The author gratefully acknowledges the advice and suggestions of Professor K. S. Pitzer during this work.

[10] K. S. Pitzer, Ind. Eng. Chem. **36**, 829 (1944).

[11] R. S. Rasmussen, J. Chem. Phys. **16**, 712 (1948).

† For the same model, Rasmussen calculates the value 761 cm^{-1} for the CH_2 rocking frequency. His calculation, however, gives the CH_2 twisting and the CH_2 wagging frequencies too low by 103 and 133 cm^{-1} respectively. It is to be expected that a better choice of the f_{H-C-C} force constant would raise the calculated CH_2 rocking frequency to near 900 cm^{-1}.

[12] K. S. Pitzer, footnote, page 717, reference 11.

LCAO Self-Consistent Field Calculation of the Ground State of Carbon Dioxide*

JOSEPH F. MULLIGAN
Physics Department, The Catholic University of America, Washington, D. C.
(Received October 16, 1950)

LCAO molecular orbitals and ionization potentials have been calculated for the ground state of CO_2 using Roothaan's LCAO self-consistent field method. The interactions of all electrons have been explicitly considered, and no extra-geometrical empirical data have been used. The calculated molecular orbitals are in general agreement with those predicted by Mulliken and Moffitt from semi-empirical considerations. The calculated ionization energies are 11.5 ev for a $1\pi_g$ electron and 17.9 ev for a $2\sigma_u$ electron, compared with the experimental 13.8 ev, and 18.0 ev, respectively. The evaluation of the large number of integrals over atomic orbitals that occur, is discussed in an appendix. All the larger integrals were calculated exactly, the smaller ones approximated. Useful approximation methods for some of these integrals are considered.

I. INTRODUCTION

SINCE its introduction in 1928 the method of molecular orbitals has been much used for qualitative and semi-empirical descriptions of molecules.[1] This approximation method is essentially an extension of the Bohr theory of electron configurations from atoms to molecules. Each electron is assigned to a one-electron wave function, or molecular orbital, which extends over the whole molecule and is the quantum-mechanical analog of an electron orbit. In practice the molecular orbitals (MO) are usually made up as linear combinations of atomic orbitals[2] (LCAO), though this is not essential to the theory.

Straightforward theoretical calculations by the LCAO MO method have been possible for only a few simple molecules, and for a time it was thought that hope of future success lay in the use of semi-empirical methods.[3] These have been quite successful in explaining the electronic structure and ultraviolet absorption spectra of molecules of considerable symmetry. Recently, however, Roothaan[4] has developed a LCAO self-consistent field (SCF) theory which has shifted the emphasis towards what Mulliken calls "approximate theoretical methods," i.e., methods employing completely theoretical computations, but using approximate LCAO wave functions. This method has been applied by Roothaan to benzene, by Parr and Mulliken[5] to butadiene, and a rather closely related method has been applied by Mulliken[6] to H_2, C_2H_2, C_2H_4, benzene, and graphite, with considerable success.

There has been considerable work done in recent years in developing the theoretical structure of the MO method. The impetus to much of this work was given by Goeppert-Mayer and Sklar's paper[7] on the lower excited states of benzene. Self-consistent field methods analogous to those of Hartree and Fock for atoms have been applied to H_2 and CH_4 by Coulson.[8] A general MO treatment of conjugated systems, based on a number of simplifying assumptions, has been given by Coulson and Longuet-Higgins.[9] Recently Moffitt[10] has applied a SCF LCAO theory similar to Roothaan's to heteromolecules. Moffitt's theory, however, leads to a much more complicated equation for the energy than the usual secular equation, and hence is better adapted to semi-empirical methods than to theoretical calculations. Sir J. Lennard-Jones, *et al.*,[11] in a series of recent papers, have developed a general MO theory of chemical valency, and has shown the importance of "equivalent orbitals" in discussing the properties of chemical bonds.

The importance of Roothaan's contribution to MO theory is that he has introduced self-consistency into the LCAO approximation in such a fashion that the electronic repulsion terms are included in the self-consistent-field hamiltonian from the very beginning, and are not merely added as perturbations at a later stage of the calculation. He has also developed his theory in a matrix form which simplifies the tedious calculations involved, and is completely general in its applicability. Mulliken[6] has also developed a related method, employing an "ionic hamiltonian," which is better suited to calculations on excited states.

Roothaan's theory allows the interactions of all electrons in the molecule to be explicitly included in the calculation. In the applications to hydrocarbons thus

* A dissertation submitted to the Faculty of the Graduate School of Arts and Sciences of The Catholic University of America in partial fulfillment of the requirements for the degree of Doctor of Philosophy.

[1] For an excellent review, bringing molecular orbital theory to 1947 and containing references to the earlier literature, see C. A. Coulson, Quart. Revs. **1**, 144 (1947).

[2] J. E. Lennard-Jones, Trans. Faraday Soc. **25**, 668 (1929).

[3] R. S. Mulliken, Chem. Revs. **41**, 201 (1947).

[4] C. C. J. Roothaan, Ph.D. thesis, University of Chicago, 1950; published in ONR *Technical Report from the University of Chicago* for the period September 1, 1948 to May 31, 1949, Part Two; report for period June 1, 1949 to March 31, 1950, Part Two. Contract N6ori-20, T.O. nine.

[5] R. G. Parr and R. S. Mulliken, J. Chem. Phys. **18**, 1338 (1950).

[6] R. S. Mulliken, J. Chim. Phys. **46**, 497 (1949); **46**, 675 (1949).

[7] M. Goeppert-Mayer and A. L. Sklar, J. Chem. Phys. **6**, 645 (1938).

[8] C. A. Coulson, Proc. Camb. Phil. Soc. **34**, 204 (1938); Trans. Faraday Soc. **33**, 388 (1937).

[9] C. A. Coulson and H. C. Longuet-Higgins, Proc. Roy. Soc. (London) **A191**, 39 (1947).

[10] W. Moffitt, Proc. Roy. Soc. (London) **A196**, 510 (1949).

[11] J. Lennard-Jones, Proc. Roy. Soc. (London) **A198**, 1, 14 (1949); J. Lennard-Jones and G. G. Hall, Proc. Roy. Soc. (London) **A202**, 155 (1950); J. Lennard-Jones and J. A. Pople, Proc. Roy. Soc. (London) **A202**, 166 (1950).

far made, however, only the π-electrons of the carbon atoms have been included explicitly, and the other electrons have been replaced by a smeared-out core potential. A test of the theory in its most general form seemed desirable. For this test carbon dioxide was chosen, both because of its intrinsic interest and because its geometric configuration and interatomic distances are so accurately known. These are the only empirical parameters which go into the calculations. The attempt has been made, then, to calculate the ground state MO's and ionization potentials for CO_2, taking into account all the interactions of the electrons, and using no extra-geometrical empirical data. It is believed that this is the first time such a general attack has been made on a non-hydrocarbon molecule as complicated, from a quantum-mechanical point of view, as CO_2.

II. OUTLINE OF LCAO SCF THEORY

Roothaan's LCAO SCF theory for a closed-shell ground state is based on the Hartree-Fock method for molecules,[12] which is, in turn, an extension of Hartree and Fock's work on atoms.[13]

In the general LCAO SCF method all the electrons of the molecule are represented by LCAO MO's

$$\phi_i=\sum_p a_{ip}\chi_p, \tag{1}$$

where i numbers the MO's, p the AO's, and the a's are undetermined coefficients. The condition that the MO's be orthonormal then reduces to

$$\int \bar{\phi}_i\phi_j dv=\sum_{pq} \bar{a}_{ip}S_{pq}a_{jq}=\delta_{ij}, \tag{2}$$

where the overlap integrals S_{pq} are defined by

$$S_{pq}=\bar{S}_{qp}=\int \bar{\chi}_p\chi_q dv. \tag{3}$$

The total N-electron normalized wave function Φ for the closed-shell ground state is then built up as an antisymmetrized product[7] (AP) of these LCAO MO's, and the ground-state electronic energy is given by

$$E=\int \bar{\Phi}\mathfrak{H}\Phi dv, \tag{4}$$

where

$$\mathfrak{H}=\sum_\mu H^\mu+\tfrac{1}{2}e^2\sum_{\mu\neq\nu}1/r^{\mu\nu} \tag{5}$$

and H^μ is the hamiltonian operator for the μth electron in the field of the nuclei alone.

To obtain the best LCAO MO's, a variation procedure is carried out to minimize the ground-state energy, subject to the orthonormality of the MO's. It can be shown[14] that this variational process leads to the following matrix equation

$$(\mathbf{H}+\mathbf{G})a_i=\epsilon_i\mathbf{S}a_i. \tag{6}$$

Here the column vectors a_i give the coefficients of the AO's in the ith LCAO MO. $\mathbf{S}$ is a hermitian matrix with elements given by (3); $\mathbf{H}$ is the bare-nuclear-field orbital energy matrix with elements

$$H_{pq}=\bar{H}_{qp}=\int \bar{\chi}_p H\chi_q dv \tag{7}$$

and $\mathbf{G}$ is the electronic interaction matrix with elements

$$G_{pq}=\bar{G}_{qp}=\sum_{rt}\bar{a}_{ir}G_{prqt}a_{it}, \tag{8}$$

where

$$G_{prqt}=2J_{prqt}-J_{prtq}$$

and

$$J_{prqt}=e^2\int\frac{\bar{\chi}_p{}^\mu\bar{\chi}_r{}^\nu\chi_q{}^\mu\chi_t{}^\nu}{r^{\mu\nu}}dv^{\mu\nu}. \tag{9}$$

The introduction of the LCAO hamiltonian operator $\mathbf{L}=\mathbf{H}+\mathbf{G}$ leads to the simple equation

$$\mathbf{L}a_i=\epsilon_i\mathbf{S}a_i, \tag{10}$$

which states that the LCAO MO's which give the best AP are obtained as eigenfunctions of the hermitian operator $\mathbf{L}$. This equation differs from the ordinary eigenvalue problem of the hermitian matrix only in the presence of the matrix $\mathbf{S}$. All the important statements about eigenvalues and eigenvectors of the hermitian matrix[15] still hold, however, with but slight modifications, for this generalized case.

The problem of finding the best LCAO MO's for the ground state thus reduces to the solution of the secular equations (10) for the eigenvalues, or LCAO orbital energies, ϵ_i, and the eigenvectors, or undetermined LCAO coefficients, a_i. Since $\mathbf{L}$ depends on the a_i's inasmuch as $\mathbf{G}$ depends on the a_i's, the need of a self-consistent procedure is obvious, hence the name LCAO SCF theory.

III. APPLICATION TO CO_2 GROUND STATE

CO_2 has been treated from a molecular orbital point of view by Mulliken[16] and Moffitt.[17] Mulliken discussed in detail the molecular orbitals, predicted ionization potentials using semi-empirical methods, and reviewed the experimental data, but made no attempt at theoretical calculations. Moffitt considered the bond order

[12] See F. Seitz, *Modern Theory of Solids* (McGraw-Hill Book Company, Inc., New York, 1940), Chapters VI and VII.

[13] For a summary and references to the earlier literature, see N. F. Mott and I. N. Sneddon, *Wave Mechanics and Its Applications* (Oxford University Press, New York, 1948), p. 141.

[14] See reference 4 for details.

[15] E. Wigner, *Gruppentheorie und ihre Anwendung auf die Quantenmechanik der Atomsspektren* (Edwards Brothers, Ann Arbor, Michigan, 1944), pp. 39, ff.

[16] R. S. Mulliken, J. Chem. Phys. **3**, 720 (1935); Revs. Modern Phys. **14**, 204 (1942).

[17] W. Moffitt, Proc. Roy. Soc. (London) **A196**, 524 (1949).

and electron distribution of CO_2 in its ground state $^1\Sigma_g^+$, again from a semi-empirical point of view.

CO_2 is a linear symmetric molecule belonging to the symmetry group $D_{\infty h}$. The C—O equilibrium distance has been given by Herzberg[18] as 1.1615A, in good agreement with the recent electron diffraction value[19] of 1.162±0.010A.

The initial aim of the LCAO calculation was to determine LCAO MO's for the 22 electrons of CO_2, each MO to contain two electrons with paired spins in the ground state. This problem was treated as a full 22-electron one. All the electrons were assigned to MO's extending throughout the molecule. However, in the case of the 1*s* electrons, these MO's were taken as identical with the inner shell AO's, or in the case of the oxygen 1*s* electrons, with simple linear combinations of inner shell AO's required by the molecular symmetry. Originally it was hoped to determine the amount of mixing of inner shell with valence shell AO's in those MO's where such mixing was permitted by symmetry considerations, but the complications introduced in the LCAO SCF procedure by the large number of added coefficients, caused this hope to be abandoned. That this mixing must be small is clear from the large energy difference between the $n=1$ and $n=2$ electrons in the atoms concerned.[8]

a. Atomic Orbitals

The most important, and most difficult, problem in setting up the LCAO MO's was the choice of AO's from which the MO's were constructed. There is evidence that the AO's differ between bonding and antibonding orbitals of the same LCAO family.[20] Even if it was desirable to use different AO's for bonding and antibonding MO's, however, it is impossible to say what the best ones would be. In addition, the introduction of different AO's would have complicated the problem considerably. The best compromise appeared to be to use the AO's that would give the best results for the whole LCAO family. Mulliken's work[6] indicates that these are probably close to free-atom AO's. Of the free-atom AO's, the self-consistent field AO's of Hartree and Fock[21] are the most accurate for atomic calculations, but there is no guarantee that they are the best for molecular calculations. For the latter, the simpler hydrogen-like atomic orbitals of Zener and Slater[22] are most often used. In accordance with the criterion that the AO's to be used in forming the MO's are those of energy close to that of the filled orbitals in the atoms making up the molecule, the following set of Slater atomic orbitals was therefore adopted:

$$\begin{aligned}
(1s) &= (Z_1^3/\pi)^{\frac{1}{2}} \exp(-Z_1 r) \\
(2s) &= (Z_2^5/3\pi)^{\frac{1}{2}} r \exp(-Z_2 r) \\
(2p_z) &= (Z_2^5/\pi)^{\frac{1}{2}} r \cos\theta \exp(-Z_2 r) \\
(2p_x) &= (Z_2^5/\pi)^{\frac{1}{2}} r \sin\theta \cos\phi \exp(-Z_2 r) \\
(2p_y) &= (Z_2^5/\pi)^{\frac{1}{2}} r \sin\theta \sin\phi \exp(-Z_2 r),
\end{aligned} \tag{11}$$

where

$$\begin{aligned}
&\text{for carbon } Z_1=5.70, \quad Z_2=1.625, \\
&\text{for oxygen } Z_1=7.70, \quad Z_2=2.275.
\end{aligned} \tag{12}$$

The atomic orbitals on one atom are normalized and mutually orthogonal, except that the nodeless Slater 2*s* is not orthogonal to the 1*s*. Neglect of such orthogonality can cause serious errors in the simple Hartree method,[23] but in methods employing an AP is not so serious. For consistency in formulation, however, it is convenient to preserve it. Orthogonal 2*s* functions were therefore formed from the original 2*s* and 1*s* in the form:[24]

$$s=\frac{(2s)_o-0.2334(1s)_o}{0.9724} \qquad s_c=\frac{(2s)_c-0.2205(1s)_c}{0.9754}. \tag{13}$$

These normalized orbitals were then orthogonal to all the other orbitals of the same atom. The notation o, s, z, x, y, was adopted for the oxygen 1*s*, 2*s*, $2p_z$, $2p_x$, and $2p_y$ orbitals, with o', s', z', x', y', for the corresponding orbitals of the second oxygen atom. The carbon orbitals were designated by c, s_c, z_c, x_c, y_c. The $2p_z$ orbitals are directed along the internuclear axis, and are all positive in the positive z direction.

b. Symmetry Orbitals

From these 15 atomic orbitals, 15 molecular orbitals were formed according to Eq. (1). These LCAO MO's were chosen so that they belonged in sets to irreducible representations of the symmetry group $D_{\infty h}$ of CO_2, and were all real. To obtain the proper symmetry for these MO's, it was convenient to introduce symmetry orbitals. These were combinations of atomic orbitals of the correct symmetry, from which the MO's were formed. The symmetry orbitals for CO_2 were obtained from the atomic orbitals by the following transformation

$$\sigma_p=\sum_q U_{pq}\chi_q \tag{14}$$

[18] G. Herzberg, Revs. Modern Phys. **14**, 219 (1942).
[19] I. L. Karle and J. Karle, J. Chem. Phys. **17**, 1057 (1949).
[20] C. A. Coulson, Trans. Faraday Soc. **33**, 1479 (1937); C. A. Coulson and W. E. Duncanson, Proc. Roy. Soc. (London) **A181**, 378 (1943); D. P. Craig, Proc. Roy. Soc. (London) **A200**, 272 (1950).
[21] S. Tutihasi, Proc. Phys. Soc. Japan **3**, 135 (1948).
[22] C. Zener, Phys. Rev. **36**, 51 (1930); J. Slater, Phys. Rev. **36**, 57 (1930).
[23] W. Moffitt and C. A. Coulson, Phil. Mag. **38**, 634 (1947).
[24] Mulliken, Rieke, Orloff, and Orloff, J. Chem. Phys. **17**, 1248 (1949).

or, in matrix form,

$$\begin{pmatrix}\sigma_1\\ \sigma_2\\ \sigma_3\\ \sigma_4\\ \sigma_5\\ \sigma_6\\ \sigma_7\\ \sigma_8\\ \sigma_9\\ \sigma_{10}\\ \sigma_{11}\\ \sigma_{12}\\ \sigma_{13}\\ \sigma_{14}\\ \sigma_{15}\end{pmatrix} = \begin{pmatrix} 2^{-\frac{1}{2}} & 2^{-\frac{1}{2}} & 0 & 0 & 0 & 0 & 0 & 0 & 0 & 0 & 0 & 0 & 0 & 0 & 0\\ 0 & 0 & 1 & 0 & 0 & 0 & 0 & 0 & 0 & 0 & 0 & 0 & 0 & 0 & 0\\ 0 & 0 & 0 & 2^{-\frac{1}{2}} & 2^{-\frac{1}{2}} & 0 & 0 & 0 & 0 & 0 & 0 & 0 & 0 & 0 & 0\\ 0 & 0 & 0 & 0 & 0 & 1 & 0 & 0 & 0 & 0 & 0 & 0 & 0 & 0 & 0\\ 0 & 0 & 0 & 0 & 0 & 0 & 2^{-\frac{1}{2}} & -2^{-\frac{1}{2}} & 0 & 0 & 0 & 0 & 0 & 0 & 0\\ 2^{-\frac{1}{2}} & -2^{-\frac{1}{2}} & 0 & 0 & 0 & 0 & 0 & 0 & 0 & 0 & 0 & 0 & 0 & 0 & 0\\ 0 & 0 & 0 & 2^{-\frac{1}{2}} & -2^{-\frac{1}{2}} & 0 & 0 & 0 & 0 & 0 & 0 & 0 & 0 & 0 & 0\\ 0 & 0 & 0 & 0 & 0 & 0 & 2^{-\frac{1}{2}} & 2^{-\frac{1}{2}} & 0 & 0 & 0 & 0 & 0 & 0 & 0\\ 0 & 0 & 0 & 0 & 0 & 0 & 0 & 0 & 1 & 0 & 0 & 0 & 0 & 0 & 0\\ 0 & 0 & 0 & 0 & 0 & 0 & 0 & 0 & 0 & 2^{-\frac{1}{2}} & 2^{-\frac{1}{2}} & 0 & 0 & 0 & 0\\ 0 & 0 & 0 & 0 & 0 & 0 & 0 & 0 & 0 & 0 & 1 & 0 & 0 & 0 & 0\\ 0 & 0 & 0 & 0 & 0 & 0 & 0 & 0 & 0 & 0 & 0 & 2^{-\frac{1}{2}} & 2^{-\frac{1}{2}} & 0 & 0\\ 0 & 0 & 0 & 0 & 0 & 0 & 0 & 0 & 0 & 0 & 0 & 0 & 0 & 1 & 0\\ 0 & 0 & 0 & 0 & 0 & 0 & 0 & 0 & 0 & 2^{-\frac{1}{2}} & -2^{-\frac{1}{2}} & 0 & 0 & 0 & 0\\ 0 & 0 & 0 & 0 & 0 & 0 & 0 & 0 & 0 & 0 & 0 & 2^{-\frac{1}{2}} & -2^{-\frac{1}{2}} & 0 & 0 \end{pmatrix} \begin{pmatrix} o\\ o'\\ c\\ s\\ s'\\ s_c\\ z\\ z'\\ z_c\\ x\\ x'\\ x_c\\ y\\ y'\\ y_c \end{pmatrix},$$

where **U** is a real, orthogonal matrix.

The resultant symmetry orbitals, and the irreducible representations of the group $D_{\infty h}$ to which they belong,[25] are given in Table I. Because of the different convention used here as regards the positive direction of the $2p_z$ orbitals, some of the signs in this table differ from those given by Mulliken. It should also be noted that these symmetry orbitals are not normalized.

There are $5\sigma_g$ symmetry orbitals, $4\sigma_u$, $2\pi_g$, and $4\pi_u$. By taking linear combinations of these, a like number of molecular orbitals of the same symmetry was formed. These MO's were related to the symmetry orbitals σ_n by the transformation

$$\phi_i=\sum_n b_{in}\sigma_n, \tag{15}$$

which reduces to

$$\begin{array}{ll} K(\sigma_g)=\sigma_1 & K^*(\sigma_g)=\sigma_2 \quad K(\sigma_u)=\sigma_6\\ 1\sigma_g=b_{33}\sigma_3+b_{34}\sigma_4+b_{35}\sigma_5 & 1\sigma_u = b_{77}\sigma_7+b_{78}\sigma_8+b_{79}\sigma_9\\ 2\sigma_g=b_{43}\sigma_3+b_{44}\sigma_4+b_{45}\sigma_5 & 2\sigma_u = b_{87}\sigma_7+b_{88}\sigma_8+b_{89}\sigma_9\\ 3\sigma_g=b_{53}\sigma_3+b_{54}\sigma_4+b_{55}\sigma_5 & 3\sigma_u = b_{97}\sigma_7+b_{98}\sigma_8+b_{99}\sigma_9\\ 1\pi_u=b_{10,10}\sigma_{10}+b_{10,11}\sigma_{11} & 1\pi_u^*=b_{12,12}\sigma_{12}+b_{12,13}\sigma_{13}\\ 2\pi_u=b_{11,10}\sigma_{10}+b_{11,11}\sigma_{11} & 2\pi_u^*=b_{13,12}\sigma_{12}+b_{13,13}\sigma_{13}\\ 1\pi_g=\sigma_{14} & 1\pi_g^*=\sigma_{15}. \end{array}$$

The numbering adopted for the MO's is to bring them into agreement with Mulliken's notation, in which the order of increasing number within each symmetry species is the order of increasing energy. The K refers to MO's made up of inner shell electrons only. The π and π^* distinguish the degenerate MO's caused by the linear form of the molecule, one referring to $2p_x$, the other to $2p_y$, orbitals.

c. Determination of LCAO MO's

To determine the best LCAO MO's it was necessary to solve the secular equation (10) for the eigenvectors, or LCAO coefficients, a_i. First the matrices **S** and **L** had to be determined. The elements of the overlap matrix **S** in terms of AO's were easily obtained and are given in Table VII. The matrix **L** is the sum of two matrices, **H**, the bare-nuclear-field orbital energy matrix, and **G**, the electronic interaction matrix. **H** includes the kinetic energy of the electrons, and their potential energy in the field of the three nuclei. The elements of the **H** matrix are given by (7), where the operator

$$H=-\frac{h^2}{2m}\Delta_i-\sum_i\frac{Ze^2}{r_i}, \tag{16}$$

or in atomic units,

$$H=-\Delta_i-\sum_i\frac{2Z}{r_i}. \tag{17}$$

For CO_2 (7) then becomes

$$H_{pq}=-\int\bar{\chi}_p\Delta\chi_q dv-6\int\bar{\chi}_p(2/r_c)\chi_q dv -8\int\bar{\chi}_p(2/r_0)\chi_q dv-8\int\bar{\chi}_p(2/r_{0'})\chi_q dv. \tag{18}$$

On evaluating the necessary integrals, **H** was obtained.

TABLE I. Symmetry orbitals for carbon dioxide.

Symmetry species	σ_g	σ_u	π_u	π_g
Symmetry orbitals	$\sigma_1=2^{-\frac{1}{2}}(o+o')$ $\sigma_2=c$ $\sigma_3=2^{-\frac{1}{2}}(s+s')$ $\sigma_4=s_c$ $\sigma_5=2^{-\frac{1}{2}}(z-z')$	$\sigma_6=2^{-\frac{1}{2}}(o-o')$ $\sigma_7=2^{-\frac{1}{2}}(s-s')$ $\sigma_8=2^{-\frac{1}{2}}(z+z')$ $\sigma_9=z_c$	$\sigma_{10}=2^{-\frac{1}{2}}(x+x')$ $\sigma_{11}=x_c$ $\sigma_{12}=2^{-\frac{1}{2}}(y+y')$ $\sigma_{13}=y_c$	$\sigma_{14}=2^{-\frac{1}{2}}(x-x')$ $\sigma_{15}=2^{-\frac{1}{2}}(y-y')$

[25] H. Sponer and E. Teller, Revs. Modern Phys. **13**, 75 (1941).

TABLE II. H matrix.* ($H_{pq}=\bar{H}_{qp}=\int\bar{\chi}_p H\chi_q dv$.)

		o	o'	c	s	s'	s_c	z	z'	z_c
	o	−73.022	0	—	—	—	—	—	—	—
	o'		−73.022	—	—	—	—	—	—	—
	c			−50.490	—	—	—	—	—	—
	s				−23.135	−0.496	−9.537	−2.093	0.706	11.670
A	s'					−23.135	−9.537	−0.706	2.093	−11.670
	s_c						−21.850	−7.530	7.530	0
	z							−22.845	0.948	7.849
	z'								−22.845	7.849
	z_c									−23.823

		x	x'	x_c	y	y'	y_c
	x	−21.755	−0.140	−5.129	0	0	0
	x'		−21.755	−5.129	0	0	0
	x_c			−20.025	0	0	0
B	y				−21.755	−0.140	−5.129
	y'					−21.755	−5.129
	y_c						−20.025

* Energy in atomic units (1 atomic energy unit = 13.602 electron volts).
— Indicates elements which are not zero, but are not needed since they multiply components of the eigenvectors which have been assumed to be zero.

and is given in Table II, A and B. Here B refers to π AO's, A to non-π AO's, and there is no mixing because of symmetry considerations.

The electronic interaction matrix **G** presented the most difficulty, for its elements are given by (8), and are seen to depend on the values of the undetermined coefficients, a_i, which vary with each cycle of the self-consistent field procedure. The elements G_{pq} of the **G** matrix contain contributions from all the filled orbitals of the closed-shell ground state. Hence the orbitals of highest energy, namely, $3\sigma_g$, $3\sigma_u$, $2\pi_u$, $2\pi_u$*, which Mulliken[16] has shown should be unfilled in the ground state, were omitted from the summation. When G_{pq} was expanded according to (8), and the summation over the filled MO's carried out, the result could be written

$$G_{pq}=\sum_{n=1}^{22} d_n D_{pq}^{(n)}, \tag{19}$$

where the d's are combinations of the a_i's, and the same for all pq. The D_{pq}'s are sums of integrals over atomic orbitals, and of course differ for each different combination pq. It should be noted that the summation (19) is merely one of convenience, and is not a summation over MO's.

The d's are given in terms of the a_i's as

$$\begin{aligned}
d_1&=\tfrac{1}{2} & d_{12}&=a_{74}a_{79}+a_{84}a_{89}\\
d_2&=1 & d_{13}&=a_{77}^2+a_{87}^2\\
d_3&=a_{34}^2+a_{44}^2 & d_{14}&=a_{77}a_{79}+a_{87}a_{89}\\
d_4&=a_{34}a_{36}+a_{44}a_{46} & d_{15}&=a_{79}^2+a_{89}^2\\
d_5&=a_{34}a_{37}+a_{44}a_{47} & d_{16}&=a_{10,10}^2\\
d_6&=a_{36}^2+a_{46}^2 & d_{17}&=a_{10,10}a_{10,12}\\
d_7&=a_{36}a_{37}+a_{46}a_{47} & d_{18}&=a_{10,12}^2\\
d_8&=a_{37}^2+a_{47}^2 & d_{19}&=a_{12,13}^2\\
d_9&=\tfrac{1}{2} & d_{20}&=a_{12,13}a_{12,15}\\
d_{10}&=a_{74}^2+a_{84}^2 & d_{21}&=a_{12,15}^2\\
d_{11}&=a_{74}a_{77}+a_{84}a_{87} & d_{22}&=1,
\end{aligned} \tag{20}$$

where the first subscript refers to the ith MO, the second to the AO, as in (1).

If the notation

$$(pq:rt)=J_{prqt}=e^2\int\frac{\bar{\chi}_p^{\mu}\bar{\chi}_r^{\nu}\chi_q^{\mu}\chi_t^{\nu}}{r^{\mu\nu}}dv^{\mu\nu} \tag{21}$$

is introduced, the D_{pq}'s can be written as

$$\begin{aligned}
D_{pq}^{(1)}&=2(pq:oo)+4(pq:oo')+2(pq:o'o')-(po:qo')-(po':qo')-(po:qo)-(po':qo).\\
D_{pq}^{(2)}&=2(pq:cc)-(pc:qc).\\
D_{pq}^{(3)}&=2(pq:ss)+4(pq:ss')+2(pq:s's')-(ps:qs)-(ps':qs)-(ps:qs')-(ps':qs').\\
D_{pq}^{(4)}&=4(pq:ss_c)+4(pq:s's_c)-(ps_c:qs)-(ps_c:qs')-(ps:qs_c)-(ps':qs_c).\\
D_{pq}^{(5)}&=4(pq:sz)-4(pq:sz')+4(pq:s'z)-4(pq:s'z')-(pz:qs)+(pz':qs)-(pz:qs')\\
&\qquad+(pz':qs')-(ps:qz)-(ps':qz)+(ps':qz)+(ps:qz').\\
D_{pq}^{(6)}&=2(pq:s_cs_c)-(ps_c:qs_c).\\
D_{pq}^{(7)}&=4(pq:s_cz)-4(pq:s_cz')-(pz:qs_c)+(pz':qs_c)-(ps_c:qz)+(ps_c:qz').\\
D_{pq}^{(8)}&=2(pq:zz)-4(pq:zz')+2(pq:z'z')-(pz:qz)+(pz':qz)+(pz:qz')-(pz':qz').\\
D_{pq}^{(9)}&=2(pq:oo)-4(pq:oo')+2(pq:o'o')-(po:qo)+(po':qo)+(po:qo')-(po':qo').\\
D_{pq}^{(10)}&=2(pq:ss)-4(pq:ss')+2(pq:s's')-(ps:qs)+(ps':qs)+(ps:qs')-(ps':qs').\\
D_{pq}^{(11)}&=4(pq:sz)+4(pq:sz')-4(pq:s'z)-4(pq:s'z')-(pz:qs)+(pz:qs')+(pz':qs')\\
&\qquad-(pz':qs)-(ps:qz)+(ps':qz)-(ps:qz')+(ps':qz').
\end{aligned}$$

TABLE III. G matrix.* ($G_{pq}=\bar{G}_{qp}=\sum_{rt}\bar{a}_{ir}G_{prqt}a_{it}$).

		o	o'	c	s	s'	s_c	z	z'	z_c
	o	31.854	0	—	—	—	—	—	—	—
	o'		31.854	—	—	—	—	—	—	—
	c			27.422	—	—	—	—	—	—
	s				20.376	0.374	7.917	1.516	−0.523	−9.958
A	s'					20.376	7.917	0.523	−1.516	9.958
	s_c						19.685	6.236	−6.236	0
	z							21.615	−0.672	−6.842
	z'								21.615	−6.842
	z_c									21.062

		x	x'	x_c	y	y'	y_c
	x	20.894	0.122	4.325	0	0	0
	x'		20.894	4.325	0	0	0
B	x_c			19.504	0	0	0
	y				20.894	0.122	4.325
	y'					20.894	4.325
	y_c						19.504

* As in Table II.

$$D_{pq}^{(12)}=4(pq:sz_c)-4(pq:s'z_c)-(pz_c:qs)+(pz_c:qs')-(ps:qz_c)+(ps':qz_c). \tag{22}$$
$$D_{pq}^{(13)}=2(pq:zz)+4(pq:zz')+2(pq:z'z')-(pz:qz)-(pz':qz)-(pz:qz')-(pz':qz').$$
$$D_{pq}^{(14)}=4(pq:zz_c)+4(pq:z'z_c)-(pz_c:qz)-(pz_c:qz')-(pz:qz_c)-(pz':qz_c).$$
$$D_{pq}^{(15)}=2(pq:z_cz_c)-(pz_c:qz_c).$$
$$D_{pq}^{(16)}=2(pq:xx)+4(pq:xx')+2(pq:x'x')-(px:qx)-(px':qx)-(px:qx')-(px':qx').$$
$$D_{pq}^{(17)}=4(pq:xx_c)+4(pq:x'x_c)-(px_c:qx)-(px_c:qx')-(px:qx_c)-(px':qx_c).$$
$$D_{pq}^{(18)}=2(pq:x_cx_c)-(px_c:qx_c).$$
$$D_{pq}^{(19)}=2(pq:yy)+4(pq:yy')+2(pq:y'y')-(py:qy)-(py':qy)-(py:qy')-(py':qy').$$
$$D_{pq}^{(20)}=4(pq:yy_c)+4(pq:y'y_c)-(py_c:qy)-(py_c:qy')-(py:qy_c)-(py':qy_c).$$
$$D_{pq}^{(21)}=4(pq:y_cy_c)-(py_c:qy_c).$$
$$D_{pq}^{(22)}=(pq:xx)-2(pq:xx')+(pq:x'x')-\tfrac{1}{2}(px:qx)+\tfrac{1}{2}(px:qx')+\tfrac{1}{2}(px':qx)-\tfrac{1}{2}(px':qx')$$
$$+(pq:yy)-2(pq:yy')+(pq:y'y')-\tfrac{1}{2}(py:qy)+\tfrac{1}{2}(py:qy')+\tfrac{1}{2}(py':qy)-\tfrac{1}{2}(py':qy').$$

After the large number of integrals required had been evaluated (see Appendix), the D_{pq}'s corresponding to the atomic orbitals p and q were tabulated. These remained the same throughout the self-consistent procedure. The d's, however, varied depending on the choice of the a_i's. The procedure followed in the calculation was, first, to assume values of the a_i's consistent with the inequalities given by Mulliken and the orthonormality conditions (2). The d's were calculated, multiplied by the corresponding D_{pq}'s, and summed according to (19), to give the element G_{pq}. This was repeated for each combination of p and q to obtain the matrix **G**. **L** was then obtained from $\mathbf{L}=\mathbf{H}+\mathbf{G}$.

With **S** and **L** known, the next step was to solve the secular equation (10). This was in terms of atomic orbitals, but it was much simpler to solve the corresponding equation in terms of symmetry orbitals,

$$\mathbf{L}'b_i=\epsilon_i\mathbf{S}'b_i \tag{23}$$

which was obtained from (10) by applying the transformation

$$b_i=\mathbf{U}a_i. \tag{24}$$

Here a_i and b_i are column vectors, the components of which are the coefficients of the AO's and the symmetry orbitals, respectively, in the MO ϕ_i, and

$$\mathbf{L}'=\mathbf{ULU}\dagger, \tag{25}$$

$$\mathbf{S}'=\mathbf{USU}\dagger. \tag{26}$$

U is the matrix defined in (14), and **U**† is **U** transposed. **S**′ and **L**′ differ from **S** and **L** in that they are evaluated in terms of symmetry orbitals rather than atomic orbitals.

S′ and **L**′ were therefore obtained from **S** and **L** by (25) and (26). The resulting secular equation (23) broke down into two three-by-three, two identical two-by-two, and five one-by-one matrix equations. Three of these latter equations were inner shell equations, one for each atom, and should be nearly identical with the corresponding equations for the free atoms. The other equations were valence shell equations involving all the atoms of the molecule. These were solved for the eigenvectors b_i, from which the coefficients a_i were obtained by (24), and the results compared with the original assumed values. New values were assumed, and the process repeated. In all, seventeen cycles were required before the assumed coefficients agreed with those computed to two places in all cases. When self-

TABLE IV. Overlap matrix* $\mathbf{S}'(S_{mn}' = \int \bar{\sigma}_m(1)\sigma_n(1)dv^1)$.

		σ_1	σ_2	σ_3	σ_4	σ_5	σ_6	σ_7	σ_8	σ_9
	σ_1	1.0000	0.0001	0.0004	0.0655	0.0007	0	0	0	0
	σ_2		1.0000	0.0618	0	0.1008	0	0	0	0
	σ_3			1.0186	0.5746	0.0258	0	0	0	0
	σ_4				1.0000	0.4450	0	0	0	0
A	σ_5					1.0352	0	0	0	0
σ-orbitals	σ_6						1.0000	−0.0004	−0.0007	−0.1090
	σ_7							0.9814	−0.0258	−0.6799
	σ_8								0.9648	−0.4268
	σ_9									1.0000
		σ_{10}	σ_{11}	σ_{12}	σ_{13}	σ_{14}	σ_{15}			
	σ_{10}	1.0054	0.3406	0	0	0	0			
	σ_{11}		1.0000	0	0	0	0			
B	σ_{12}			1.0054	0.3406	0	0			
π-orbitals	σ_{13}				1.0000	0	0			
	σ_{14}					0.9946	0			
	σ_{15}						0.9946			

* The orbitals used in evaluating these integrals are the symmetry orbitals given in Table I.

consistency was attained, the eigenvalues ϵ_i gave the "LCAO orbital energies."

The secular equations (23) were solved using the potentiometric linear equation solver of Filler, Cowan, and Roothaan,[26] which is an improvement of the original model of Frost and Tamres.[27] This instrument gives the eigenvectors and eigenvalues simultaneously for secular equations up to the sixth order, with an accuracy of a few parts in a thousand for a first approximation. For the second- and third-order secular equations solved here, this instrument gave the desired results very rapidly, and with sufficient accuracy for our purposes.

The values of the elements of the **G** matrix, after self-consistency had been obtained, are given in Table III, *A* and *B*. The **S′** matrix and the self-consistent **L′** matrix are given in Tables IV and V.

IV. RESULTS

a. Ground-State Molecular Orbitals

The 11 LCAO MO's of lowest energy obtained by the self-consistent-field procedure, are given in Table VI, a, and are each filled by two electrons with paired spins in the ground state, to yield the known $^1\Sigma_g^+$ ground state of CO_2. The 4 orbitals of higher energy which are obtained from the ground state calculation, but are unfilled in the ground state, are given in Table VI, b, and represent certain approximations to the excited state orbitals. All the orbitals in Table VI satisfy the orthonormality conditions (2).

The orbitals obtained agree rather well with those predicted by Mulliken and Moffitt from semi-empirical evidence. Moffitt[17] showed from an analysis of the π-electron system of CO_2 that the coefficients in $1\pi_u$ should be approximately equal. The LCAO SCF

TABLE V. LCAO hamiltonian matrix **L′** in terms of symmetry orbitals.*

		σ_1	σ_2	σ_3	σ_4	σ_5	σ_6	σ_7	σ_8	σ_9
	σ_1	−41.169	0	—	—	—	0	0	0	0
	σ_2		−23.068	—	—	—	0	0	0	0
	σ_3			−2.880	−2.290	−0.760	0	0	0	0
	σ_4				−2.165	−1.829	0	0	0	0
A	σ_5					−1.506	0	0	0	0
σ-orbitals	σ_6						−41.169	—	—	—
	σ_7							−2.637	−0.394	2.421
	σ_8								−0.954	1.424
	σ_9									−2.761
		σ_{10}	σ_{11}	σ_{12}	σ_{13}	σ_{14}	σ_{15}			
	σ_{10}	−0.878	−1.138	0	0	0	0			
	σ_{11}		−0.521	0	0	0	0			
B	σ_{12}			−0.878	−1.138	0	0			
π-orbitals	σ_{13}				−0.521	0	0			
	σ_{14}					−0.842	0			
	σ_{15}						−0.842			

* As in Table II.

[26] Filler, Cowan, and Roothaan, ONR *Technical Report from University of Chicago* for the period September 1, 1948, to May 31, 1949, Part II; Contract N6ori-20, T.O. nine.

[27] A. A. Frost and M. Tamres, J. Chem. Phys. **15**, 383 (1947).

TABLE VI. LCAO SCF molecular orbitals for the ground state of CO_2.

a. Orbitals occupied by 22 electrons.

$K(\sigma_g)=2^{-\frac{1}{2}}(o+o')$	$K(\sigma_u)=2^{-\frac{1}{2}}(o-o')$
$K^*(\sigma_g)=c$	
$1\sigma_g=0.48(s+s')+0.32s_c+0.21(z-z')$	$1\sigma_u=0.38(s-s')+0.11(z+z')-0.51z_c$
$2\sigma_g=-0.51(s+s')+0.40s_c+0.46(z-z')$	$2\sigma_u=-0.64(s-s')+0.37(z+z')-0.65z_c$
$1\pi_g=2^{-\frac{1}{2}}(x-x')$	$1\pi_u=0.49(x+x')+0.53x_c$
$1\pi_g{}^*=2^{-\frac{1}{2}}(y-y')$	$1\pi_u{}^*=0.49(y+y')+0.53y_c$

b. Unoccupied orbitals.

$3\sigma_g=0.55(s+s')-1.32s_c+0.64(z-z')$	$3\sigma_u=0.85(s-s')+0.84(z+z')+1.55z_c$
$2\pi_u=0.57(x+x')-0.92x_c$	$2\pi_u{}^*=0.57(y+y')-0.92y_c$

values are 0.49 and 0.53, in good agreement with this. Mulliken[16] predicted the signs and relative orders of magnitude of the coefficients for the general linear triatomic molecule. For the symmetric molecule XYX he considered two special cases: A, in which the term value of s_Y is nearly equal to that of (s_X+s_X), and the term value of z_Y nearly equal to that of (z_X+z_X); and B, in which the term value of s_Y is equal to that of (z_X-z_X), and of z_Y is much less than that of (z_X+z_X). The LCAO SCF coefficients agree with his statement that CO_2 falls between case A and B, though, it appears, somewhat nearer to B. The agreement of the calculated coefficients for the π-orbitals with Mulliken's work is again very good for both the ground state orbital $1\pi_u$ and the excited $2\pi_u$. For the σ-orbitals the comparison is not as good. The signs agree in all cases, but the relative magnitudes disagree in a few cases. This is especially true of the lowest valence orbitals $1\sigma_g$ and $1\sigma_u$. Mulliken considers them as made up largely of $2s$ orbitals on the oxygen atoms, with only small contributions from the oxygen $2p_z$ and the carbon orbitals. This would make these orbitals nonbonding. The LCAO SCF results indicate rather large contributions, especially from the carbon orbitals, and, on the basis of the criterion of maximum overlap,[28] would indicate strong bonding properties for these two orbitals. This may partially explain the energy values obtained for $1\sigma_g$ and $1\sigma_u$, which are much lower (higher in absolute value) than Mulliken's predictions.

The MO $2\sigma_u$ is but weakly bonding, since the removal of an electron from this orbital to form the known $^2\Sigma_u{}^+$ state of $CO_2{}^+$ changes the internuclear distance[29] only from 1.1615A to 1.180A, and Moffitt has shown that little reorganization is to be expected after the removal of this electron. Mulliken[30] explains this nonbonding property of $2\sigma_u$ as due to strong $s-p$ mixing in the oxygen orbitals of this MO. The LCAO SCF results verify this prediction, though they would indicate that the oxygen $2s$ orbitals figure more prominently in $2\sigma_u$ than do the $2p_z$ orbitals, which seems unlikely. Very strong $s-p$ mixing in the oxygen orbitals of $3\sigma_g$ and $3\sigma_u$ is also indicated by these calculations, in accordance with Mulliken's predictions. It should be noted that $s-p$ mixing in the carbon orbitals of CO_2 is forbidden by symmetry considerations.

b. Ionization Energies

The "LCAO orbital energies" obtained for the filled ground state MO's of CO_2 are plotted in Fig. 1. As has been shown by Roothaan and others,[31] these orbital energies represent a good approximation to the ionization energies of the corresponding electron shells of the molecule. For comparison purposes, the shell scheme drawn up by Mulliken[16] in 1935 on the basis of the then-known semi-empirical and experimental evidence, is given, along with the two definitely known ionization energies for CO_2.

In 1932 Henning[32] first observed a Rydberg series in the vacuum ultraviolet, leading to an ionization potential for CO_2 of 18.00±0.03 volts, which appeared to correspond to the removal of an inner electron. In 1935 Mulliken identified this as a $2\sigma_u$ electron, and used this and his interpretation of the 2900A emission band of $CO_2{}^+$ as a $^2\Sigma_u{}^+\rightarrow{}^2\Pi_g$ transition, to predict a minimum ionization energy (I) of 13.72±0.03 ev for CO_2, corresponding to the removal of an electron from the topmost filled $1\pi_g$ shell. This value was in exact agreement with the value 13.73±0.01 ev later found by Price and Simpson[33] from an additional Rydberg series, but is slightly less than Honig's[34] recent electron impact value of 13.85 ev. Since the electron impact value corresponds to "vertical ionization," it would be expected to be higher than the 0, 0 spectroscopic potential; but the difference seems rather large to be due to this cause alone. Because of the greater accuracy of the spectroscopic determination, the best value to use for comparison with the LCAO SCF results would seem to be the spectroscopic value increased slightly (perhaps 0.02 or 0.03 ev) to correct for lack of verticality. Hence 13.75 ev can be taken for $I(1\pi_g)$.

[28] L. Pauling, J. Am. Chem. Soc. **53**, 1367 (1931); J. C. Slater, Phys. Rev. **37**, 481 (1931); C. A. Coulson, Proc. Camb. Phil. Soc. **33**, 111 (1937); A. Maccoll, Trans. Faraday Soc. **46**, 369 (1950).

[29] F. Bueso-Sanllehi, Phys. Rev. **60**, 556 (1941).

[30] R. S. Mulliken, Revs. Modern Phys. **14**, 210 (1942).

[31] See reference 4 and Sec. 6 of reference 6; also R. S. Mulliken Phys. Rev. **74**, 736 (1948), and J. Lennard-Jones and G. G. Hall, Proc. Roy. Soc. (London) **A202**, 155 (1950).

[32] H. J. Henning, Ann. Physik (5) **13**, 599 (1932).

[33] W. C. Price and D. M. Simpson, Proc. Roy. Soc. (London) **A169**, 501 (1938).

[34] R. E. Honig, J. Chem. Phys. **16**, 105 (1948).

There is rather strong evidence for the existence of a third I of 17.29 ev in CO_2. This is based on Mrozowski's[35] work on the spectrum of CO_2^+, in which he has conclusively established the location of a $2\pi_u$ state of the ion 3.54 ev above the minimum ionization energy. If this is combined with the minimum I of 13.75 ev, the value 17.29 ev is obtained, which should correspond to the $1\pi_u$ level in CO_2. This value agrees well with Mulliken's prediction of an I slightly greater than 17.1 for $1\pi_u$. Though the experimental evidence for this level is strong, especially in view of Mulliken's successful prediction of the minimum I on the basis of similar evidence, it is indirect and based on experiments on the ion, not on the neutral molecule. For this reason this level is not included among the levels given as experimentally known in Fig. 1, since these were obtained from direct spectroscopic measurements on the neutral molecule.

The results of the LCAO SCF calculation are in fairly good agreement with the experimental data. The LCAO SCF ionization energies are $I(1\pi_g)=11.5$ ev, $I(2\sigma_u)=17.9$ ev, compared with the experimental 13.75 and 18.0 ev, respectively. The agreement for the minimum ionization energy is not too satisfactory; but this may be partially explained by the fact that symmetry considerations require that $1\pi_g$ be $2^{-\frac{1}{2}}(x-x')$, a nonbonding orbital. On the removal of a $1\pi_g$ electron, however, the internuclear distance changes from 1.1615A to 1.177A. Mulliken[16] takes this to mean that $1\pi_g$ is actually somewhat bonding, and explains the bonding properties as due to a slight excitation of carbon $3d$ valence. This might partially explain the high energy value obtained for the $1\pi_g$ orbital from the LCAO SCF calculation. Moffitt,[17] however, has recently shown that there is a considerable rearrangement of the residual π-electrons after the removal of a $1\pi_g$ electron, and has suggested that the increased C—O distance is due to this rather than to any bonding properties of the $1\pi_g$ orbital.

Figure 1 indicates that the LCAO SCF levels fall in the same order as that predicted by Mulliken, except that $2\sigma_u$ and $1\pi_u$ are reversed. Mulliken gives 17.1 ev as a minimum value of $I(1\pi_u)$, and the value of 17.29 ev obtained on the basis of Mrozowski's work seems to be very probably correct. The LCAO SCF value is 18.8 ev for $I(1\pi_u)$. It seems somewhat strange that the Rydberg series corresponding to the removal of this $1\pi_u$ electron has not yet been observed, if it lies between the $1\pi_g$ and $2\sigma_u$ states, whose ionization potentials have been obtained from such series.

The most significant discrepancy is the considerably higher I's obtained for $1\sigma_u$ (42.4 ev) and $1\sigma_g$ (44.9 ev) than Mulliken's predicted values of less than 32 ev. As indicated above, this is due in part to the fact that Mulliken takes these orbitals as nonbonding, whereas

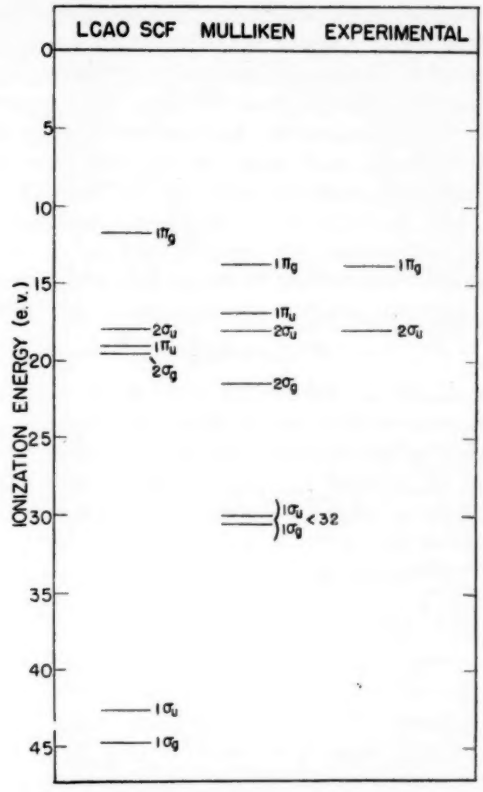

FIG. 1. Ionization energies for the ground state of the carbon dioxide molecule. LCAO SCF = Results of LCAO self-consistent field molecular orbital calculations reported in this paper. Mulliken = Predictions made by Mulliken (reference 16) in 1935 on the basis of the then-known experimental and semi-empirical evidence. Experimental = Values obtained from Rydberg series in the vacuum ultraviolet (references 32 and 33).

the SCF orbitals are strongly bonding. Despite this, however, these levels are still rather low.

The same is true of the inner shell $1s$ electron ionization energies, which would be expected to be very close to the corresponding energies for the isolated atoms. The LCAO SCF values are 560 ev for the I of a $1s$ oxygen electron, and 314 ev for a $1s$ carbon electron, compared with the observed K-shell x-ray absorption limits of 524 and 284 ev, respectively.[36] Of course, this may be to some extent explained by the fact that mixing between these $1s$ orbitals and the outer valence orbitals has been neglected. The contribution to the energy of these orbitals from this source, however, would not be expected to be large.[37]

c. Polarity

It is interesting to compare the present results with Mulliken's and Moffitt's predictions on the polarity

[35] S. Mrozowski, Revs. Modern Phys. **14**, 216 (1942); Phys. Rev. **60**, 730 (1941); **62**, 270 (1942); **72**, 682, 691 (1947).

[36] J. Thibaud, Compt. rend. **186**, 308 (1928).

[37] It should, however, be noted that the overlaps $S(o, z_c)$ and $S(z, c)$ are -0.077 and 0.071, respectively, and hence are not negligible. Mulliken (J. Am. Chem. Soc., to be published) has recently shown that inner shell-valence shell interactions may be of more importance than previously thought, and has discussed their importance in terms of overlap integrals. See also K. S. Pitzer, J. Am. Chem. Soc. **70**, 2140 (1948).

of the bonds in CO_2. Mulliken[16] indicated that CO_2 may be formulated, roughly, as $O^{-\frac{1}{2}}C^{1}O^{-\frac{1}{2}}$, which would correspond to 75 percent homopolar, 25 percent heteropolar, binding. Moffitt,[17] on the other hand, concluded that in the ground state the electron distribution of CO_2 is uniform, each atom having net zero charge. The coefficients resulting from the LCAO SCF calculation lead to $O^{-.2}C^{.4}O^{-.2}$, which corresponds to 10 percent heteropolar, 90 percent homopolar, binding. The LCAO SCF results, therefore, fall between the two predictions, but are in better agreement with Moffitt's.

V. DISCUSSION

The results of the LCAO SCF calculation on the ground state of CO_2 are qualitatively correct, but the numerical values obtained should in no sense be taken as final. An advance has been made over previous MO calculations in that all possible interactions of all the electrons of the molecule have been explicitly included in the calculation. However, this has necessitated approximating a rather large number of integrals (see Appendix). Every effort has been made to insure the approximate values being close to the correct ones, but the fact still remains that they are approximations. Also, because the energies obtained depend on the values of the elements of the **L** matrix, which are obtained as small differences between the large elements of the **G** and **H** matrices, small percentage errors in **G** or **H** result in large percentage errors in the final energies. A program is now in progress at the University of Chicago for a systematic computation of all the integrals needed in MO calculations. When this is completed, both the accuracy and the ease of calculations of this type will be greatly improved.

Even if all the integrals needed were known exactly, there would still be sources of error in the LCAO SCF method. The first of these is the LCAO approximation itself, which replaces the exact wave function for the molecule by an approximate LCAO one. This can only raise the energy. The second is the approximation to the hamiltonian, which reduces to an approximation to the potential energy operator. This operator contains the smeared-out field of the other electrons in which each electron moves, and depending on whether these electrons are bonding or antibonding, the energy is lowered or raised. Usually the energy is lowered, so that these last two errors tend to cancel.

Connected with this error in the potential energy is the form of the atomic orbitals used. As indicated above, in a rigorous treatment different atomic wave functions should be used for bonding and antibonding orbitals. It has been pointed out by Coulson[38] that this is due to the fact that there are two types of screening present in molecules, one due to the nuclei, the other to the electrons as in the atomic case. Slater functions, as used here, allow only for the electronic screening as in atoms. Even in atoms, however, Slater functions cannot be made to fit the true self-consistent field.[39] The use of Slater functions also reduces the electronic interaction between non-neighbors too much, since the Slater functions die down more rapidly than Hartree-Fock SCF orbitals at large distances.[24] It is possible that the LCAO MO method would yield results in better agreement with experiment if Hartree-Fock SCF wave functions were used for the atomic orbitals making up the LCAO MO's. This question of the form of the atomic orbitals to be used in molecular calculations appears to be the most serious one in all LCAO methods.

The simple MO method overemphasizes ionic contributions by allowing a piling-up of electrons on one nucleus.[40] This effect is reduced by the accidental correlation introduced by the Pauli principle provided an AP is used, as in the present case; but there is no guarantee that the correlation is correct. In a more rigorous treatment, correlated MO's should be used.[41]

Another important effect, of special importance for excited states of molecules, is configurational interaction, where states of the same symmetry lie so close together that perturbations must be considered, and one AP cannot be written for each state, but linear combinations of AP's must be used. Craig's work[42] indicates that configurational interaction is of considerable importance for the lower excited states of benzene. It appears that the agreement of Goeppert-Mayer and Sklar's calculations with experiment was partly due to a fortuitous cancellation of errors due to neglect of many-center integrals and errors due to neglect of configurational interaction.[43] For the ground state of a molecule, however, configurational interaction should be of little importance, and in Roothaan's LCAO SCF method it is assumed[4] that there is only one LCAO AP which minimizes the energy of a closed-shell ground state.

These last three sources of error in MO calculations have been considered in detail for H_2 by Coulson and Fischer.[44]

When one considers all these possible sources of error in LCAO MO calculations, in addition to the ever-present possibility of numerical errors in as long and tedious a calculation as attempted here, the results obtained are gratifying. It appears that once the required integrals have been evaluated, Roothaan's LCAO SCF method should be capable of giving very useful results without an incommensurable amount of labor,

[38] C. A. Coulson, Proc. Camb. Phil. Soc. **31**, 244 (1935); Trans. Faraday Soc. **33**, 1479 (1937).

[39] D. R. Hartree and M. M. Black, Proc. Roy. Soc. (London) **A139**, 311 (1933).

[40] C. A. Coulson and G. S. Rushbrooke, Proc. Camb. Phil. Soc. **36**, 193 (1940).

[41] Frost, Braunstein, and Schwemer, J. Am. Chem. Soc. **70**, 3292 (1948).

[42] D. P. Craig, J. Chem. Phys. **17**, 1358 (1949); Proc. Roy. Soc. (London) **A200**, 474 (1950).

[43] C. C. J. Roothaan and R. G. Parr, J. Chem. Phys. **17**, 1001 (1949); see also Parr, Craig, and Ross, J. Chem. Phys. **18**, 1561 (1950).

[44] C. A. Coulson and I. Fischer, Phil. Mag. **40**, 386 (1949).

especially as regards the ground states of molecules of considerable symmetry.

VI. ACKNOWLEDGMENT

The author wishes to thank Dr. Virginia Griffing, who suggested the problem, Dr. Karl F. Herzfeld, and Dr. C. C. J. Roothaan for many helpful discussions, and much assistance and guidance during the course of this work. The author is also indebted to Dr. Robert G. Parr for helpful advice, and for sending him the results of his work on butadiene before publication.

APPENDIX: EVALUATION OF INTEGRALS

The atomic orbitals used in evaluating the large number of integrals required were those given in (11). All results given are for the orthogonal $2s$ functions given in (13), and are in atomic energy units (1 atomic unit $=2.1792\times10^{-11}$ erg $=13.602$ ev). The overlap integrals are of course dimensionless. Since all the AO's used were real, the complex notation was dropped throughout. For simplicity in distinguishing the large number of different types of integrals occurring, a new notation was desirable. Hence α, β, and γ were used to indicate AO's centered on atoms A, B, and C, respectively. The subscripts p, q, r, t were used to indicate that these orbitals might be any of the set (11), and the numbers (1) and (2) were used to indicate the electrons concerned.

I. Overlap Integrals: $S(\alpha_p, \beta_q)=\int\alpha_p(1)\beta_q(1)dv^1$

These two-center overlap integrals were easily evaluated in elliptical coordinates.[45] The introduction of this coordinate system led to integrals of the type:

$$A_n(a)=\int_1^\infty \mu^n e^{-a\mu}d\mu \tag{27}$$

$$B_n(b)=\int_{-1}^{+1} \nu^n e^{-b\nu}d\nu.$$

All the required overlap integrals have been given in terms of these functions by Mulliken, Rieke, Orloff, and Orloff.[24] Useful tables of the A and B functions have been given by Rosen[46] and by Kotani, Amemiya, and Simose.[47] However, it proved simpler and more accurate to calculate the A's and B's for the particular parameters a and b desired than to interpolate in their tables. The A's and B's were obtained very quickly from

$$A_0(a)=e^{-a}/a \tag{28}$$

$$B_0(b)=\frac{1}{b}[e^b-e^{-b}]$$

by use of the recursion formulas

$$A_n(a)=\frac{1}{a}[e^{-a}+nA_{n-1}(a)] \tag{29}$$

$$B_n(b)=\frac{1}{b}[(-1)^n e^b-e^{-b}+nB_{n-1}(b)].$$

Using the WPA tables of exponentials, values of A's and B's were obtained with six-place accuracy. From these the overlap integrals were computed, and rounded off to four places. The results are given in Table VII, and were checked with values obtained from the tables of Mulliken, *et al.*,[24] with excellent agreement.

[45] Eyring, Walter, and Kimball, *Quantum Chemistry* (John Wiley and Sons, Inc., New York, 1944), p. 367.
[46] N. Rosen, Phys. Rev. **38**, 255, 2099 (1931).
[47] Kotani, Amemiya, and Simose, Proc. Phys.-Math. Soc. Japan, **20**, extra number 1 (1938); **22**, extra number 1 (1940).

TABLE VII. Overlap integrals. $S(\alpha_p, \beta_q)=\int\alpha_p(1)\beta_q(1)dv^1$.

$S(o, c)$	0.0001	$S(z, c)$	0.0713	$S(o, o')$	0.0000
$S(o, s_c)$	0.0463	$S(z, s_c)$	0.3147	$S(o, s')$	0.0004
$S(o, z_c)$	−0.0771	$S(z, z_c)$	−0.3018	$S(o, z')$	−0.0007
$S(s, c)$	0.0437	$S(x, x_c)$	0.2409	$S(s, s')$	0.0187
$S(s, s_c)$	0.4063			$S(s, z')$	−0.0258
$S(s, z_c)$	−0.4807			$S(z, z')$	−0.0352
				$S(x, x')$	0.0054

II. One and Two-Center Interaction Integrals

A. *One-Electron Potential and Kinetic Energy Integrals*

1. Bare-nuclear field potential energy integrals:

$$(A:\alpha_p, \beta_q)=\int\alpha_p(1)(2/r_A)\beta_q(1)dv^1.$$

Here r_A is the distance from nucleus A. One-center integrals, which are a special case of this type, were easily evaluated in sperical coordinates. Two-center integrals were evaluated in the same way as the overlap integrals, using elliptical coordinates and the A and B functions. The results are given in Table VIII.

2. Kinetic energy integrals: $(\alpha_p\Delta\beta_q)=-\int\alpha_p(1)\Delta\beta_q(1)dv^1$.—On expansion of the operator Δ in spherical coordinates, these integrals reduced to linear combinations of overlap and one-electron bare-nuclear-field potential energy integrals already calculated. Their values are given in Table IX.

B. *Two-Electron Integrals*

These are particular cases of the integrals $(pq:rt)=J_{prqt}$ defined in Eq. (21). Three basic types occur, usually called coulomb, exchange, and hybrid coulomb-exchange ("ionic") integrals.

1. Coulomb integrals:

$$(\alpha_p\alpha_q:\beta_r\beta_t)=\int\alpha_p(1)\beta_r(2)(2/r_{12})\alpha_q(1)\beta_t(2)dv^{12}.$$

In these integrals each of the interacting electrons belongs wholly to one atom. If they both belong to the same atom, the resulting one-center integral is a special case of the integral defined above. Both the one-center and two-center coulomb integrals were evaluated by integrating over the coordinates of one electron in spherical coordinates to find the potential at any point in space due to this electron, and then evaluating the contribution to the energy from the second electron in this potential field.

For the integration over the coordinates of electron 1, $(1/r_{12})$ was expanded in spherical harmonics about A.[48] The subsequent

TABLE VIII. Bare-nuclear-field potential energy integrals.*

$$(A:\alpha_p, \beta_q)=\int\alpha_p(1)(2/r_A)\beta_q(1)dv^1.$$

$(O:o, o)$	15.4000	$(O:s, z')$	−0.0263	$(C:c, c)$	11.4000
$(O:c, c)$	0.9112	$(O:z, s')$	0.0228	$(C:o, o)$	0.9112
$(O:o', o')$	0.4556	$(O:s, z_c)$	−0.8328	$(C:s_c, s_c)$	1.7915
$(O:s, s)$	2.5271	$(O:z_c, s')$	0.2761	$(C:s, s)$	0.9079
$(O:s_c, s_c)$	0.8851	$(O:s_c, z_c)$	−0.3255	$(C:z_c, z_c)$	1.6250
$(O:s', s')$	0.4555	$(O:z, s_c)$	0.4570	$(C:z, z)$	1.0110
$(O:z, z)$	2.2750	$(O:s_c, z')$	−0.1807	$(C:x_c, x_c)$	1.6250
$(O:z_c, z_c)$	1.0446	$(O:z, z')$	−0.0336	$(C:x, x)$	0.8566
$(O:z', z')$	0.4693	$(O:z, z_c)$	−0.5327	$(C:s, s')$	0.0321
$(O:x, x)$	2.2750	$(O:z_c, z')$	−0.1733	$(C:s, s_c)$	0.4791
$(O:x_c, x_c)$	0.8072	$(O:x, x')$	0.0046	$(C:s, z)$	0.2598
$(O:x', x')$	0.4488	$(O:x, x_c)$	0.3293	$(C:s, z')$	−0.0472
$(O:s, s')$	0.0176	$(O:x_c, x')$	0.1383	$(C:s, z_c)$	−0.5560
$(O:s, s_c)$	0.6167			$(C:z, s_c)$	0.4797
$(O:s_c, s')$	0.2388	$(C:x, x')$	0.0098	$(C:z, z')$	−0.0635
$(O:s', z')$	−0.0667	$(C:x, x_c)$	0.2733	$(C:z, z_c)$	−0.5105

* Values for these and all subsequent integrals are in atomic energy units. The $2s$ functions used are orthogonalized Slater $2s$ functions. The $2p_z$ functions are all positive in the positive z direction.

[48] See reference 45, p. 369.

TABLE IX. Kinetic-energy integrals.

$(\alpha_p \Delta\beta_q) = -\int \alpha_p(1)\Delta\beta_q(1)d\nu^1$.

$(o\Delta o)$	59.2900	$(c\Delta c)$	32.4900	$(s\Delta s_c)$	0.1823
$(s\Delta s)$	6.1738	$(s_c\Delta s_c)$	3.0610	$(s\Delta z_c)$	−0.5376
$(z\Delta z)$	5.1756	$(z_c\Delta z_c)$	2.6406	$(s_c\Delta z)$	0.4506
$(x\Delta x)$	5.1756	$(x_c\Delta x_c)$	2.6406	$(z\Delta z_c)$	−0.8622
$(s\Delta s')$	−0.0207	$(z\Delta z')$	0.0293	$(x\Delta x_c)$	0.2520
$(s\Delta z')$	0.0297	$(x\Delta x')$	−0.0068		

integrations were straightforward, and are not given here, but the resulting expressions for the potential at any point in space due to all possible combinations of AO's on atom A are given in Table X, since they are very useful in all calculations of this type, and are not available in a convenient form in the literature. These potential expressions are all given in atomic units, and the effective nuclear charges for the AO's on atom A to which the electron belongs are designated Z_p and Z_q. If these are the same, simply Z is used. The following quantities can then be defined:

$$\zeta=\tfrac{1}{2}(Z_p+Z_q),\quad \eta=(Z_p-Z_q)/(Z_p+Z_q)\geq 0,\quad x=\zeta r_2 \text{ (or } Zr_2),\quad (30)$$

where r_2, θ_2, ϕ_2 are spherical coordinates of electron 2 with respect to an origin at A.

Many of the coulomb integrals are not independent, because of the relations existing among the angular parts of the potential expressions in Table X. The resulting identities that they must satisfy are given by Kotani, Amemiya, and Simose.[47]

Once these potential expressions were substituted in the corresponding coulomb integrals, the integration over the coordinates of electron 2 could be carried out, in spherical coordinates for one-center integrals, in elliptical coordinates for two-center integrals. In this latter case, of course, the potential expressions had also to be transformed to elliptical coordinates.

One-center coulomb integrals then reduced to simple algebraic expressions, which led to the numerical values given in Table XI, A. Two-center coulomb integrals in which one electron belonged to 1s or 2s AO's only, led to the A and B functions previously considered. For the 2p functions, higher powers of x in the denominator of the potential expressions presented difficulty. Integrals of this type for atoms with equal effective nuclear charges have been evaluated by Sklar and Lyddane,[49] and Parr and Crawford,[50] on the basis of Bartlett's work.[51] However, in our case, coulomb integrals involving the carbon and oxygen atoms, with unequal effective nuclear charges, were needed, in addition to the oxygen-oxygen interactions, where the screening constants were the same. It proved possible to evaluate these carbon-oxygen coulomb integrals in elliptical coordinates by the use of partial fractions, and repeated integration by parts term-by-term. This led to the A and B functions defined in (27), and to the new functions

$$F_n(a,b)=\int_{-1}^{1} e^{-b\nu}\nu^n \int_1^\infty \frac{e^{-a\mu}}{\mu+\nu}d\mu d\nu. \quad (31)$$

Numerical values for these functions were obtained from

$$F_0(a,b)=-A_0(-\delta)[-Ei(-2a)]-A_0(\delta)[-Ei(-2b)] \quad (32)$$

by means of the recurrence formula

$$F_n(a,b)=-Ei(-2a)\frac{e^{\delta}}{\delta}+(-1)^n\frac{e^{-\delta}}{\delta}Ei(-2b)$$
$$-(-1)^n\frac{e^{-a}}{\delta}\sum_{k=0}^{n-1}(-1)^k B_k(b)-\frac{n}{\delta}F_{n-1}(a,b), \quad (33)$$

where $\delta=a-b$, and $-Ei(-2a)$ is the exponential integral defined by

$$-Ei(-x)=\int_x^\infty \frac{e^{-t}}{t}dt. \quad (34)$$

By this method all the carbon-oxygen coulomb integrals were found in terms of rather complicated sums of the functions A, B, and F. The results could then have been simplified by expanding these functions, and combining like terms; but this was such a long and complicated procedure that it was simpler from a computational point of view to obtain the desired numerical results by substituting directly the calculated values of the A's, B's, and F's. The A's and B's needed had already been tabulated, and the F's were obtained using the above recurrence relations, and the WPA tables of exponential integrals.[52]

In this way exact values to four places were obtained for all coulomb integrals. The integrals were calculated individually, and then, where possible, the results checked for consistency by the identities mentioned above. No algebraic expressions are given for these integrals, since they are extremely long, and since they will soon be available in a much neater form due to Roothaan.[53] Numerical values are given in Table XI, B.

The values of the coulomb integrals obtained in this way were compared with those obtained using a geometric mean approximation,[54] and interpolation from Parr and Crawford's tables. The results agreed within one percent in all cases, which was within the accuracy of the interpolation. Hence the geometric mean approximation for coulomb integrals appears to be quite good.

In the course of the evaluation of these coulomb integrals an approximation method was discovered which should be useful in evaluating non-neighbor interactions in other polyatomic mole-

TABLE X. Potentials resulting from various combinations of atomic orbitals.

Atomic orbitals*	Potential†
$(1s)(1s)$	$(2Z/x)[1-(1+x)\exp(-2x)]$
$(1s)(2s)$	$[3(1+\eta)^3(1-\eta)^5]^{\frac{1}{2}}(\zeta/x)[1-(1/3)(3+4x+2x^2)\exp(-2x)]$
$(2s)(2s)$	$(2Z/x)[1-(1/6)(6+9x+6x^2+2x^3)\exp(-2x)]$
$(1s)(2p_z)$	$[(1+\eta)^3(1-\eta)^5]^{\frac{1}{2}}(2\zeta/x^2)[1-(1+2x+2x^2+x^3)\exp(-2x)]\cos\theta_2$
$(2s)(2p_z)$	$(5Z/3^{\frac{1}{2}}x^2)[1-(1/5)(5+10x+10x^2+6x^3+2x^4)\exp(-2x)]\cos\theta_2$
$(2p_z)(2p_z)$	$(2Z/x)[1-(1/6)(6+9x+6x^2+2x^3)\exp(-2x)]$ $+(3Z/x^3)[1-(1/9)(9+18x+18x^2+12x^3+6x^4+2x^5)\exp(-2x)](3\cos^2\theta_2-1)$
$(2p_x)(2p_y)$	$(9Z/x^3)[1-(1/9)(9+18x+18x^2+12x^3+6x^4+2x^5)\exp(-2x)]\sin^2\theta_2\cos\phi_2\sin\phi_2$

* Slater orbitals (non-orthogonal 2s functions) of form given in Eq. (11).
† Atomic units. For the meaning of Z, ζ, η, x, see Eq. (30). Potentials due to all other possible combinations of $n=1$ and $n=2$ atomic orbitals can be found by changing the angular part of these potential expressions to fit the angular part of the AO's desired.

[49] A. L. Sklar and R. H. Lyddane, J. Chem. Phys. **7**, 374 (1939).
[50] R. G. Parr and B. L. Crawford, Jr., J. Chem. Phys. **16**, 1049 (1948).
[51] J. H. Bartlett, Phys. Rev. **37**, 507 (1931).
[52] Works Progress Administration, Mathematical Tables Project, *Tables of the Sine, Cosine and Exponential Integrals* (New York, 1940).
[53] C. C. J. Roothaan, ONR *Technical Report of the Spectroscopic Laboratory of the University of Chicago* for the period June 1, 1949 to March 31, 1950, Part Two; Contract N6ori-20, T.O. nine.
[54] M. Goeppert-Mayer and K. J. McCallum, Revs. Modern Phys. **14**, 248 (1942).

cules. The potential expressions in Table X are seen to contain terms depending on the distance as $1/x$, $1/x^2$, $1/x^3$, and are equivalent to the potentials due to a classical pole, dipole, or quadrupole, decreased by an exponential factor. For large distances the exponential term is so small that the inner bracket can be neglected compared to the leading term. The potential then reduces to a combination of classical pole, dipole, and quadrupole terms, with the corresponding "moments" given by the factors outside the brackets. The same procedure can then be applied to the other electron on the other nucleus, and the integrals evaluated as what would be classically called "dipole-dipole," "pole-quadrupole," etc., interactions, depending on the radial dependence of the potentials, and with $x=\rho=ZR$, its value at the internuclear distance R. The formulas for such interactions are conveniently given by Margenau.[55]

The physical reason why this approximation is valid at large distances is that there is then little overlapping of the charge clouds on the two atoms, and hence each charge cloud can be replaced by a finite number of point charges. The range of validity of such an approximation can be seen by comparing the results it yields with accurate calculated values. Such a comparison is given in Table XII for the first two integrals given by Parr and Crawford.[50] For the first integral, the agreement for $10\leq\rho\leq20$ indicates that this approximation is the same as that used by Sklar and Lyddane,[49] though they give no details of it. The surprising thing is that the error is only a few percent even for $\rho=8.37$, the C—C distance in benzene. For the second integral, the error is even less. For integrals involving σ-functions this approximation is less valid because of the greater overlap, but for $\rho>15$ it is again quite good.

Even when ρ is such that this approximation is not too good, it is always possible to estimate the error by considering the size of the exponential term which has been neglected. This gives a useful criterion for using the approximation. Such an approximation is especially convenient when interaction integrals involving all the electrons on two non-neighboring atoms have to be computed, and for interactions between unlike atoms, for which no tables of integrals yet exist. It was found that all the oxygen-oxygen coulomb integrals for CO_2 could be obtained with four-place accuracy by this method, even integrals of the type $(sx:s'x')$, which vanish when any of the usual approximations in terms of overlaps are tried on them. Of course, the O—O interactions in CO_2 are a particularly good example, since here $\rho\simeq20$.[56] For $1s$ and $2s$ functions this approximation reduces to the familiar point-charge approximation, but for all integrals containing $2p$ functions it is far superior.

A number of the more useful asymptotic formulas of this type are given in Table XIII. They are given for interactions between atoms with the same effective nuclear charge, but, with slight modifications, can be used for different effective nuclear charges.

TABLE XI. Coulomb integrals.

$$(\alpha_p\alpha_q:\beta_r\beta_t)=\int\alpha_p(1)\beta_r(2)(2/r_{12})\alpha_q(1)\beta_t(2)dv^{12}.$$

A. One-center		B. Two-centers			
$(oo:oo)$	9.6250	$(oo:cc)$	0.9112	$(oo:o'o')$	0.4556
$(cc:cc)$	7.1250	$(oo:s_cs_c)$	0.8851	$(oo:s's')$	0.4556
$(oo:ss)$	2.2667	$(oo:s_cz_c)$	−0.3255	$(oo:s'z')$	−0.0664
$(cc:s_cs_c)$	1.6196	$(oo:z_cz_c)$	1.0446	$(oo:z'z')$	0.4693
$(oo:zz)$	2.2594	$(oo:x_cx_c)$	0.8072	$(oo:x'x')$	0.4488
$(cc:z_cz_c)$	1.6149	$(ss:cc)$	0.9079	$(ss:s's')$	0.4556
$(ss:ss)$	1.6078	$(ss:s_cs_c)$	0.8455	$(ss:s'z')$	−0.0664
$(s_cs_c:s_cs_c)$	1.1511	$(ss:s_cz_c)$	−0.2644	$(ss:z'z')$	0.4693
$(ss:zz)$	1.6273	$(ss:z_cz_c)$	0.9476	$(ss:x'x')$	0.4488
$(s_cs_c:z_cz_c)$	1.1640	$(ss:x_cx_c)$	0.7990	$(sz:s'z')$	−0.0193
$(zz:zz)$	1.7809	$(sz:cc)$	0.2598	$(sz:z'z')$	0.0724
$(z_cz_c:z_cz_c)$	1.2721	$(sz:s_cs_c)$	0.1816	$(sz:x'x')$	0.0634
$(xx:yy)$	1.5890	$(sz:s_cz_c)$	−0.0774	$(zz:z'z')$	0.4855
$(x_cx_c:y_cy_c)$	1.1350	$(sz:z_cz_c)$	0.2159	$(zz:x'x')$	0.4612
$(sz:sz)$	0.3499	$(sz:x_cx_c)$	0.1700	$(xx:x'x')$	0.4428
$(s_cz_c:s_cz_c)$	0.2514	$(zz:cc)$	1.0110	$(xx:y'y')$	0.4422
$(xy:xy)$	0.0960	$(zz:s_cs_c)$	0.8918	$(sx:s'x')$	0.0097
$(x_cy_c:x_cy_c)$	0.0686	$(zz:s_cz_c)$	−0.2874	$(sx:z'x')$	−0.0030
$(os:os)$	0.1406	$(zz:z_cz_c)$	1.0117	$(zx:z'x')$	−0.0012
$(cs_c:cs_c)$	0.0937	$(zz:x_cx_c)$	0.8405	$(xy:x'y')$	0.0003
$(oz:oz)$	0.0529	$(xx:cc)$	0.8566		
$(cz_c:cz_c)$	0.0346	$(xx:s_cs_c)$	0.8256	$(xy:x_cy_c)$	0.0102
		$(xx:s_cz_c)$	−0.2579	$(sx:s_cx_c)$	0.0805
		$(xx:z_cz_c)$	0.9235	$(sx:z_cx_c)$	−0.0481
		$(xx:x_cx_c)$	0.7891	$(zx:s_cx_c)$	0.0335
		$(xx:y_cy_c)$	0.7687	$(zx:z_cx_c)$	−0.0206

2. Exchange integrals:

$$(\alpha_p\beta_r:\alpha_q\beta_t)=\int\alpha_p(1)\alpha_q(2)(2/r_{12})\beta_r(1)\beta_t(2)dv^{12}.$$

The important two-center exchange integrals for CO_2 are those involving exchanges between the carbon and oxygen atoms. Exchange integrals involving atoms with unequal effective nuclear charges have been considered by James[57] for $1s$ and $2s$ functions. For the large number of more complicated exchange integrals required here, however, this method was not feasible. As a result an approximation similar to that of Sklar[58] was used. This expressed the exchange integral between atoms with unequal effective nuclear charges in terms of overlap integrals and exchange integrals between atoms with equal effective nuclear charges. For simplicity, the superscripts 1 and 2 were used to indicate atoms of effective nuclear charge Z_1 and Z_2, respectively. The approximation then took the form

$$(\alpha_p{}^1\beta_r{}^2:\alpha_q{}^1\beta_t{}^2)=S(\alpha_p{}^1,\beta_r{}^2)S(\alpha_q{}^1,\beta_t{}^2)\times\left[\frac{(\alpha_p{}^1\beta_r{}^1:\alpha_q{}^1\beta_t{}^1)}{S(\alpha_p{}^1,\beta_r{}^1)S(\alpha_q{}^1,\beta_t{}^1)}\frac{(\alpha_p{}^2\beta_r{}^2:\alpha_q{}^2\beta_t{}^2)}{S(\alpha_p{}^2,\beta_r{}^2)S(\alpha_q{}^2,\beta_t{}^2)}\right]^{\frac{1}{2}}. \quad (35)$$

This was of the same form as that given by Sklar, and justified

TABLE XII. Comparison of exact values and results of asymptotic approximation for coulomb integrals.

$\rho=$	7	8.37	9	10	12	14.5	16.7	20
$Z^{-1}(aa:bb)$								
Parr and Crawford*	0.2367	0.2086	0.1972	0.1806	0.155	0.131	0.115	0.097
Asymptotic approx.	0.2543	0.2138	0.2003	0.1825	0.1554	0.1311	0.1151	0.0972
$Z^{-1}(aa:b_sb_s)$								
Parr and Crawford	0.2273	0.2036	0.1928	0.1774				
Asymptotic approx.	0.2286	0.2033	0.1930	0.1781	0.1537	0.1304	0.1148	0.0971

* The ρ used here is the ρ of Parr and Crawford's paper (reference 50), and is twice the corresponding quantity in Table XIII, since their Z is twice the Z used in the present paper.

[55] H. Margenau, Phys. Rev. **38**, 749 (1931).
[56] ρ here is the ρ of Table XII, and of Parr and Crawford's paper.
[57] H. M. James, J. Chem. Phys. **2**, 794 (1934).
[58] A. L. Sklar, J. Chem. Phys. **7**, 990 (1939).

TABLE XIII. Asymptotic approximations for coulomb integrals.*

$$Z^{-1}(xx:x'x') = (2/\rho - 6/\rho^3 + 81/2\rho^5)$$
$$Z^{-1}(xx:y'y') = (2/\rho - 6/\rho^3 + 27/2\rho^5)$$
$$Z^{-1}(xx:z'z') = (2/\rho + 3\rho^3 - 54/\rho^5)$$
$$Z^{-1}(zz:z'z') = (2/\rho + 12/\rho^3 + 108/\rho^5)$$
$$Z^{-1}(xy:x'y') = 27/2\rho^5$$
$$Z^{-1}(xz:x'z') = -54/\rho^5$$
$$\zeta^{-1}(oz:z'z') = (2/\rho^2)[(1+\eta)^3(1-\eta)^5]^{\frac{1}{2}} + (18/\rho^4)[(1+\eta)^3(1-\eta)]^{\frac{1}{2}}$$
$$Z^{-1}(sz:z'z') = 5/3^{\frac{1}{2}}\rho^2 + 45/3^{\frac{1}{2}}\rho^4$$
$$Z^{-1}(sz:x'x') = 5/3^{\frac{1}{2}}\rho^2 - 45/(12)^{\frac{1}{2}}\rho^4$$
$$\zeta^{-1}(ox:z'x') = -(9/\rho^4)[(1+\eta)^3(1-\eta)]^{\frac{1}{2}}$$
$$Z^{-1}(sx:z'x') = -45/(12)^{\frac{1}{2}}\rho^4$$

* Here o, s, z, x, and y, are $1s$, $2s$ (nonorthogonal), $2p_z$, $2p_z$, and $2p_y$ atomic orbitals on atom A, and the same quantities primed are the corresponding AO's on atom B. $\rho = ZR$ (or ζR), and Z, ζ and η are as defined in Eqs. (11) and (30). The $2p_z$ functions are both positive in the positive z direction, resulting in the minus signs above. Atomic units.

theoretically, except that the geometrical mean was taken, instead of his arithmetic mean. Sklar showed that the quantities being averaged resemble coulomb integrals, and so the geometric mean would seem to be more accurate though the difference is slight in the cases of interest here.

This approximation breaks down for certain integrals involving π-functions, where the overlap integrals are zero. In this case the overlap integrals were replaced by integrals of the form $\int \alpha_p(1)\beta_q(1)x dv^1$, where x (or y) was a coordinate chosen to agree with the π-function occurring in the integral. The "moment" in the x direction of a charge distribution on atom A discussed above under coulomb integrals, can be obtained from an integral of the type $\int \alpha_p(1)\alpha_q(1)x dv^1$. Here this idea was extended to electrons exchanged between two atoms, and resulted in what might be called, for want of a better name, "overlap moments." Calculations indicate that the exchange integrals are roughly proportional to the product of such quantities, just as they are to overlap integrals in the nonvanishing case. Since the approximation used depends on the ratio of such quantities rather than on their absolute values, and since the integrals whose approximations contain vanishing overlaps are small to begin with, such an approximation may be expected to give reasonably good values for these small integrals.

The exchange integrals for equal effective nuclear charges, used in the approximation above, were taken, where available, from Parr and Crawford,[50,59] and from Hirschfelder and Linnett.[60] In all other cases they were computed, using the formulas and tables[61] of reference 47.

[59] The integral $(ab_r:a_rb)$ is wrong in Parr and Crawford's paper, where it is given as the negative of $(ab_r:ab_r)$. Dr. Parr has confirmed this in a private communication. The formula and numerical values for the same integral given by P. J. Wheatley and J. W Linnett, Trans. Faraday Soc. **45**, 897 (1949), are also in error. Some of the numerical values given for the integral $(ab:ab)$ in Wheatley and Linnett's paper also seem to be inaccurate. *Note:* After the work reported here was completed, an article by H. Kopineck [Z. Naturforsch. **5a**, 420 (1950)] appeared, which seems destined to supersede all previous work on molecular integrals. He gives very complete tables for almost all integrals involving $n=2$ AO's with equal effective nuclear charges that are needed in molecular calculations. His values for exchange integrals are in excellent agreement with those calculated here, as was to be expected, since both used the formulas and tables of the Japanese (reference 47).

[60] J. O. Hirschfelder and J. W. Linnett, J. Chem. Phys. **18**, 130 (1950).

[61] Fletcher, Miller, and Rosenhead, *An Index to Mathematical Tables* (Scientific Computing Service, London, 1946), have criticized these Japanese tables because of the large number of errors that had to be corrected in the second part. Once these corrections are made, however, these tables are quite accurate, and extremely useful for molecular calculations. This is indicated by the work of Mulliken, *et al.*, on overlap integrals, and the present calculations on exchange integrals. The same conclusion is reached by Kopineck (see note under reference 59 above).

Exchange integrals between the two oxygen atoms in CO_2 are extremely small. Some of these were available in references 50 and 60. The others were obtained from an approximation suggested by Mulliken,[6] in terms of coulomb integrals and overlaps.

The carbon-oxygen exchange integrals are given in Table XIV. The oxygen-oxygen exchange integrals are so small that no numerical values are given in the tables.

3. Hybrid coulomb-exchange integrals:

$$(\alpha_p\alpha_q:\alpha_r\beta_t) = \int \alpha_p(1)\alpha_r(2)(2/r_{12})\alpha_q(1)\beta_t(2)dv^{12}.$$

These presented the most difficulty of all two-center integrals. In the cases considered here, electron 1 belongs wholly to atom A, while electron 2 is exchanged between atom A and atom B. The same method used for the coulomb integrals was tried here, i.e., integration over the coordinates of electron 1, followed by an integration over the coordinates of the second electron in the potential field of the first. This gave good results when the potential due to electron 1 was spherically symmetrical, i.e., due to $(1s)(1s)$, $(1s)(2s)$, or $(2s)(2s)$. In these cases the integrations over the coordinates of electron 2 were easily carried out in elliptical coordinates, and resulted in the A and B functions previously defined. These integrals were thus obtained exactly to four places for both carbon-oxygen and oxygen-oxygen interactions, and are given in Table XV, A. For nonspherical potentials, however, convergence difficulties arose due to the higher powers of x in the denominator of the potential expressions (Table X). For the coulomb integrals it had been possible to integrate term by term and obtain results in terms of the functions A, B, and F, defined above. For the hybrids, when this was attempted and elliptical coordinates were used, divergent results occurred. It appears that the individual terms in these integrals are divergent, and it is only when they are grouped together properly for the integrations that the infinities cancel and convergent results are obtained. This proved too difficult, and the method was abandoned.

At the time these calculations were carried out,[62] the best method available in the literature for hybrid Coulomb-exchange integrals appeared to be that of Sklar and Lyddane,[49] used also by Parr and Crawford.[50] This differs from the method outlined above in the use of dipolar coordinates instead of elliptical coordinates, and thus avoids the convergence difficulties. This method has the shortcoming that it is extremely tedious, and has been used only for equal effective nuclear charges, though it appears that it can

TABLE XIV. Exchange integrals.*

$$(\alpha_p\beta_r:\alpha_q\beta_t) = \int \alpha_p(1)\alpha_q(2)(2/r_{12})\beta_r(1)\beta_t(2)dv.^{12}$$

$(ss_c:ss_c)$	0.212	$(zs_c:xx_c)$	0.099	$(xx_c:xx_c)$	0.070
$(ss_c:sz_c)$	−0.280	$(zz_c:zz_c)$	0.264	$(xx_c:yy_c)$	0.064
$(sz_c:sz_c)$	0.388	$(zz_c:xx_c)$	−0.116	$(xy_c:xy_c)$	0.003
$(sx_c:sx_c)$	0.023	$(xs_c:xs_c)$	0.031	$(sc:sc)$	0.008
$(ss_c:zs_c)$	0.184	$(xs_c:xz_c)$	−0.043	$(sc:zc)$	0.013
$(ss_c:zz_c)$	−0.219	$(sx_c:zx_c)$	0.024	$(zc:zc)$	0.022
$(ss_c:xx_c)$	0.115	$(xs_c:sx_c)$	0.025	$(xc:xc)$	0.000
$(sz_c:zs_c)$	−0.219	$(xs_c:zx_c)$	0.023	$(os_c:os_c)$	0.013
$(sz_c:zz_c)$	0.294	$(xz_c:xz_c)$	0.063	$(os_c:oz_c)$	−0.021
$(sz_c:xx_c)$	−0.152	$(x_cz:x_cz)$	0.026	$(oz_c:oz_c)$	0.036
$(zs_c:zs_c)$	0.166	$(xz_c:sx_c)$	−0.031	$(ox_c:ox_c)$	0.000
$(zs_c:zz_c)$	−0.193	$(xz_c:zx_c)$	−0.027	$(oc:oc)$	0.000

* Approximate values obtained from Eq. (35).

[62] After the calculations reported here were completed, a paper by C. A. Coulson and N. P. Barnett (to be published) was received, in which a new method of evaluating hybrid coulomb-exchange integrals, equally valid for equal and unequal effective nuclear charges, is proposed. It includes a complete summary of previous work on hybrid integrals, and a criticism of the methods used in their evaluation. Unfortunately, it was not considered feasible to recalculate the large number of hybrid integrals required here by this more accurate method. The author is indebted to Dr. Coulson, and to Dr. Bryce Crawford, Jr., for letting him see a copy of this important paper before publication.

be modified for unequal effective nuclear charges. As used here, for carbon-oxygen interactions, the desired integrals were calculated for equal effective nuclear charges, and then modified by the ratio of the overlaps

$$(\alpha_p^1\alpha_q^1:\alpha_r^1\beta_t^2)=\frac{S(\alpha_r^1,\beta_t^2)}{S(\alpha_r^1,\beta_t^1)}(\alpha_p^1\alpha_q^1:\alpha_r^1\beta_t^1). \quad (36)$$

Here the superscripts 1 and 2 indicate atoms of effective nuclear charge Z_1 and Z_2, respectively. This was a reasonable approximation, since it was to be expected that these integrals were proportional to the amount of exchange, and hence to the overlap integrals. The results obtained by this method were found to agree within three percent with exact values obtained in 10 cases where spherically symmetrical potentials were involved. In most cases the agreement was much better than this.

At the time this work was done there were only a few numerical values for hybrid coulomb-exchange integrals for equal effective nuclear charges available in the literature. Recently Kopineck[63] has given values for six integrals of this type (in his terminology "ionic" integrals) over a wide range of internuclear distances, and has promised similar tables for the remaining integrals, those involving $2s$ functions. For use in Eq. (36) above, hybrids involving all possible combinations of $n=2$ AO's were calculated for equal effective nuclear charges, by the method of Parr and Crawford. Agreement with values interpolated from Kopineck's tables was excellent in the six cases where comparison was possible. Formulas for these integrals are not given, since they are long and tedious, as reference to Parr and Crawford will indicate, and since the completion of Kopineck's tables should make such formulas unnecessary. Numerical values are, however, given in Table XVI for these integrals for $\rho=7.1332$ and 9.9864 (Parr and Crawford's ρ and Z), since no values for many of these integrals have previously appeared in the literature.

TABLE XV. Hybrid coulomb-exchange integrals.

$(\alpha_p\alpha_q:\alpha_r\beta_t)=\int\alpha_p(1)\alpha_r(2)(2/r_{12})\alpha_q(1)\beta_t(2)dv^{12}$.

A. Exact values

$(oo:oo')$	0.0000	$(oo:oc)$	0.0002	$(cc:co')$	0.0001
$(oo:ss')$	0.0177	$(oo:ss_c)$	0.6285	$(cc:s_cs')$	0.4865
$(oo:sz')$	−0.0265	$(oo:sz_c)$	−0.8528	$(cc:s_cz')$	−0.4991
$(oo:zs')$	0.0235	$(oo:zs_c)$	0.4425	$(cc:z_cs')$	0.5553
$(oo:zz')$	−0.0321	$(oo:zz_c)$	−0.5319	$(cc:z_cz')$	−0.5094
$(oo:xx')$	0.0046	$(oo:xx_c)$	0.3290	$(cc:x_cx')$	0.2731
$(ss:oo')$	0.0000	$(ss:oc)$	0.0001	$(s_cs_c:co')$	0.0001
$(ss:ss')$	0.0177	$(ss:ss_c)$	0.5419	$(s_cs_c:s_cs')$	0.4141
$(ss:sz')$	−0.0265	$(ss:sz_c)$	−0.7154	$(s_cs_c:s_cz')$	−0.3941
$(ss:zs')$	0.0235	$(ss:zs_c)$	0.3886	$(s_cs_c:z_cs')$	0.4744
$(ss:zz')$	−0.0320	$(ss:zz_c)$	−0.4463	$(s_cs_c:z_cz')$	−0.3915
$(ss:xx')$	0.0046	$(ss:xx_c)$	0.2921	$(s_cs_c:x_cx')$	0.2361

B. Approximate values

$(zz:ss')$	0.020	$(zz:ss_c)$	0.562	$(z_cz_c:s_cs')$	0.439
$(zz:sz')$	−0.029	$(zz:sz_c)$	−0.769	$(z_cz_c:s_cz')$	−0.408
$(zz:zs')$	0.026	$(zz:zs_c)$	0.421	$(z_cz_c:z_cs')$	0.510
$(zz:zz')$	−0.036	$(zz:zz_c)$	−0.490	$(z_cz_c:z_cz')$	−0.447
$(zz:xx')$	0.005	$(zz:xx_c)$	0.298	$(z_cz_c:x_cx')$	0.241
$(xx:ss')$	0.017	$(xx:ss_c)$	0.523	$(x_cx_c:s_cs')$	0.416
$(xx:sz')$	−0.025	$(xx:sz_c)$	−0.713	$(x_cx_c:s_cz')$	−0.387
$(xx:zs')$	0.022	$(xx:zs_c)$	0.369	$(x_cx_c:z_cs')$	0.446
$(xx:zz')$	−0.030	$(xx:zz_c)$	−0.422	$(x_cx_c:z_cz')$	−0.387
$(xx:xx')$	0.005	$(xx:xx_c)$	0.299	$(x_cx_c:x_cx')$	0.250
$(xx:yy')$	0.005	$(xx:yy_c)$	0.277	$(x_cx_c:y_cy')$	0.227
$(sz:ss')$	0.005	$(sz:ss_c)$	0.114	$(s_cz_c:s_cs')$	0.077
$(sz:sz')$	−0.007	$(sz:sz_c)$	−0.152	$(s_cz_c:s_cz')$	−0.058
$(sz:zs')$	0.007	$(sz:zs_c)$	0.125	$(s_cz_c:z_cs')$	0.167
$(sz:zz')$	−0.009	$(sz:zz_c)$	−0.161	$(s_cz_c:z_cz')$	−0.182
$(sz:xx')$	0.001	$(sz:xx_c)$	0.056	$(s_cz_c:x_cx')$	0.041
$(sx:sx')$	0.001	$(sx:sx_c)$	0.062	$(s_cx_c:s_cx')$	0.051
$(sx:zx')$	0.001	$(sx:zx_c)$	0.044	$(s_cx_c:z_cx')$	0.050
$(sx:xs')$	0.001	$(sx:xs_c)$	0.104	$(s_cx_c:x_cs')$	0.057
$(sx:xz')$	−0.001	$(sx:xz_c)$	−0.152	$(s_cx_c:x_cz')$	−0.065
$(zx:sx')$	0.001	$(zx:sx_c)$	0.023	$(z_cx_c:s_cx')$	0.017
$(zx:zx')$	0.001	$(zx:zx_c)$	0.024	$(z_cx_c:z_cx')$	0.030
$(zx:xs')$	0.001	$(zx:xs_c)$	0.029	$(z_cx_c:x_cz')$	−0.012
$(zx:xz')$	−0.001	$(zx:xz_c)$	−0.040	$(x_cy_c:x_cy')$	0.008
$(xy:xy')$	0.000	$(xy:xy_c)$	0.014	$(z_cx_c:x_cs')$	0.013

[63] H. Kopineck, Z. Naturforsch. **5a**, 420 (1950).

TABLE XVI. Hybrid coulomb-exchange integrals* for equal effective nuclear charges.

Integral	$\rho=7.1332$ $(Z=3.25)$	$\rho=9.9864$ $(Z=4.55)$	Integral	$\rho=7.1332$ $(Z=3.25)$	$\rho=9.9864$ $(Z=4.55)$
$(zz:ss')$	0.5752	0.4197	$(xx:ss')$	0.5455	0.3901
$(zz:sz')$	−0.6244	−0.5353	$(xx:sz')$	−0.5920	−0.4961
$(zz:zs')$	0.5102	0.4481	$(xx:zs')$	0.4467	0.3922
$(zz:zz')$	−0.4070	−0.5179	$(xx:zz')$	−0.3527	−0.4468
$(zz:xx')$	0.3579	0.2036	$(xx:xx')$†	0.3710	0.2045
$(sz:ss')$	0.1006	0.0846	$(xx:yy')$†	0.3380	0.1895
$(sz:zs')$	0.1661	0.1320	$(sx:sx')$	0.0754	0.0407
$(sz:sz')$	−0.0885	−0.1049	$(sx:zx')$	0.0604	0.0378
$(sz:zz')$	−0.1643	−0.1684	$(sx:xs')$	0.0973	0.0597
$(sz:xx')$	0.0604	0.0378	$(sx:xz')$	−0.1230	−0.0847
$(zx:sx')$	0.0261	0.0154	$(xy:xy')$†	0.0158	0.0073
$(zx:zx')$	0.0363	0.0207			
$(zx:xs')$	0.0222	0.0168			
$(zx:xz')$	−0.0222	−0.0223			

* As in Table XIII, except that here ρ and Z are as used in Parr and Crawford's paper. These integrals were used in calculating the hybrid coulomb-exchange integrals with unequal effective nuclear charges in Table XV, B.

† These values are interpolated from Parr and Crawford's tables.

For the smaller oxygen-oxygen hybrids, a method similar to the asymptotic approximation for coulomb integrals given above, was used. A point charge of the amount of oxygen-oxygen overlap was located halfway between the oxygen atoms, and the coulomb interaction between this point charge and the charge cloud belonging wholly to one oxygen atom was calculated. This method was checked against exact calculations, and found to give good results, superior to those obtained by Mulliken's[6] approximation.

The approximate values obtained by these methods for the remaining hybrid coulomb-exchange integrals are given in Table XV, B.

III. Three-Center Integrals

It is well known that neglect of three-center integrals can lead to serious errors in MO calculations.[64] Hence an attempt was made to include all such integrals in this calculation, even though approximations had to be used for many of them.

1. One-electron three-center integrals:

$$(C:\alpha_p,\beta_q)=\int\alpha_p(1)(2/r_C)\beta_q(1)dv^1.$$

The evaluation of these integrals has been considered by Coulson,[65] and by Hirschfelder, Eyring, and Rosen,[66] whose work is based on that of Schuchowitzky and Gordadse. Coulson's method is more general in that it can be applied to atoms with different effective nuclear charges, and to three-centers not in a line. The method results in an infinite series, however, and in the integrals calculated by this method here, the convergence was very slow.

Integrals where the electron was exchanged between the two oxygen atoms in the field of the carbon nucleus were calculated by the method of Hirschfelder, Eyring, and Rosen. The larger three-center integrals are those in which an electron is exchanged between the carbon and one oxygen atom, in the field of the other

[64] C. A. Coulson, Proc. Camb. Phil. Soc. **31**, 244 (1935); A. London, J. Chem. Phys. **13**, 396 (1945); R. G. Parr and B. L. Crawford, Jr., J. Chem. Phys. **16**, 526 (1948).

[65] C. A. Coulson, Proc. Camb. Phil. Soc. **33**, 104 (1937).

[66] Hirschfelder, Eyring, and Rosen, J. Chem. Phys. **4**, 121 (1936); A. A. Schuchowitzky, Acta Physiochim. U.R.S.S. **1**, 901 (1935); G. S. Gordadse, Z. Physik **96**, 542 (1935).

oxygen nucleus. It was found that these could be quite well approximated by considering the interaction between the nucleus and a point charge corresponding to the overlap of the exchanged electron, and located where the overlapping charge cloud takes on its maximum value along the internuclear axis. The reason for the good agreement between exact and approximated values in this case is clear. Because of the greater electronegativity of oxygen, this point is always nearer the oxygen atom. The distance between it and the third nucleus is of the order of 3.5 atomic units, and so the third nucleus is to all purposes outside the overlapping charge cloud, and a point-charge approximation is a valid one.

The best location for the point-charge was found by maximizing the expression for the overlapping charge $\alpha_p\beta_q dv$ along the internuclear axis.[67] For $n=2$ AO's this location was 0.908 atomic units from the oxygen atom, and 1.287 atomic units from the carbon atom.

Values of one-electron three-center integrals calculated in this way are included in Table VIII.

2. Two-electron three-center integrals.—There are two main types of these: (a) in which one electron belongs wholly to one atom, and interacts with an electron exchanged between the other two atoms; and (b) in which both electrons are exchanged between two atoms.

These three-center integrals have been considered by Hirschfelder, Eyring, and Rosen[66] for 1*s* functions. For $n=2$ functions they become much more complicated, and it became clear that approximations would have to be used in the problem reported here, where over 150 integrals of this type occurred.

(a) If the exchanged electron was exchanged between carbon and oxygen atoms, the first type of integral could be well approximated by a combination of the asymptotic approximation considered above under coulomb integrals, and the method used for three-center one-electron integrals. These are the largest integrals of this type, and it is felt that the approximate values obtained for them are rather close to the exact values, for the reasons given above.

If the exchanged electron was exchanged between the two oxygen atoms, and the other electron belonged wholly to the carbon atom, there was no reasonable approximation of the types considered above that could be used. As a result, the approximation given by Mulliken[6] for the many-center case was used. Calculations in the one-electron case did not indicate that this was a very accurate approximation, but these integrals were so small because of the small overlap between oxygen atoms that the errors introduced were not significant.

(b) If both electrons were exchanged between two atoms, a straightforward point-charge approximation was used. These integrals were smaller than in case (a) because of the double overlap involved; and since the point-charge is always located nearer the oxygen atoms, the distance is such that this should be a good approximation.

Since there were over 150 two-electron, three-center integrals required, and since the approximate values used can be obtained very quickly from the above data and tables, no numerical values are given.

In conclusion, it should be noted that all the larger integrals, namely, overlaps, bare-nuclear-field potential energy, kinetic energy, coulomb, and some of the hybrid coulomb-exchange integrals have been evaluated exactly. The remaining hybrid coulomb-exchange, exchange, and three-center integrals have been approximated. Every effort has been made to use as good approximations as possible, but it should be remembered that they are still approximations. An approach of this type in which all interactions are considered, however, and an effort made to evaluate each integral as accurately as possible, seems preferable to one in which some integrals are calculated exactly, and the others completely ignored. Of course, the treatment given here can be much improved, if some day it becomes possible to obtain exact values for the necessary integrals without the unreasonable amount of work that would be required at the present time. The work of Roothaan[53] on coulomb integrals, of Coulson and Barnett[62] on hybrid coulomb-exchange integrals, and of Rüdenberg[68] on exchange integrals, should hasten that day.

[67] This procedure gave better results for these integrals than those obtained by using the point of maximum overlap obtained by maximizing $\alpha_p\beta_q$. The distances obtained in this way also check very well with those obtained using the maxima of the radial probability distribution functions for the individual atoms, and Mulliken's definition of "effective internuclear distance." See R. S. Mulliken, J. Am. Chem. Soc. (to be published).

[68] K. Rüdenberg, see reference 53.

The Diffusion of Thoron Atoms through Photographic Gelatin

G. G. EICHHOLZ AND F. C. FLACK
Department of Physics, University of British Columiba, Vancouver, Canada
(Received October 23, 1950)

Observations have been carried out on the splitting of thorium stars in photographic emulsions. It is found that this process is caused entirely by the Brownian motion of the thoron atoms produced in the course of successive decays. Applying the classical statistical theory, the diffusion coefficient of thoron in gelatin and the viscosity of dry gelatin at room temperature have been deduced. The results are discussed in the light of our present knowledge of the structure of gelatin.

I. INTRODUCTION

A RADIOTHORIUM atom, decaying in a photographic emulsion, produces the well-known five-pronged thorium stars, each prong of which is the track of one of the alpha-particles ejected during the radioactive process. Occasionally events are observed in which two of the prongs radiate from one point, the other three leaving a center some distance away. This apparent shift in the disintegration center or "splitting" of stars was first reported by Taylor and Dabholkar[1] and has since been observed by Demers[2] and Yagoda.[3] The explanation advanced has been that some of the decaying atoms diffused through the gelatin, though little attention seems to have been paid to the actual mechanism involved.

The diffusion of radioactive ions through metallic lattices has been studied very fully by von Hevesy, Seith, and others[4] and has served to explain some of the features of grain boundary diffusion in metals. More recently Flügge and Zimens[5] have incorporated radioactive inert gases into the surface layers of various specimens in an attempt to deduce the size of the molecules from the rate of diffusion. All such experiments depend on an accurate determination of the mean activity of a given layer at a certain instant and, hence, suffer from all the errors imposed by statistical variations of the counting system and lack of definition of the active volume.[6] The application of such radioactive tracer methods to gelatin would, nevertheless, give some valuable information on the viscosity and structure of "dry" gels, supplementing a wealth of data accumulated on the mechanical and elastic properties of aqueous gelatin solutions.[7] Observations on thorium stars make it possible to extend such measurements to dry photographic gelatin and throw an interesting side light on certain phases of the radioactive decay process. They differ from other tracer methods in that they deal with the motion of individual radioactive atoms.

II. EXPERIMENTAL PROCEDURE

Microscopic examination of old nuclear emulsions of the Ilford C2 and Kodak NTB types first drew attention to the apparent splitting of many of the thorium stars found as a "background" effect in these emulsions. The number of such fortuitous events was increased for measuring purposes by soaking some Ilford C2 plates, 100 microns thick, in a thorium nitrate solution, 78 mg/l, for 20 minutes. After drying, these plates were left in a room at a fairly constant temperature of 20°C for two weeks before development. These times and concentrations were found to give the optimum density of events permitting unambiguous correlation of star fragments in the case of large diffusion ranges while keeping the emulsion area to be searched to a minimum. All thorium stars with five prongs were recorded, and detailed measurements were carried out at a magnification of 1420× on all stars showing a perceptible shift of their disintegration centers. The minimum shift detectable was of the order of 0.5 micron. Migration ranges of several microns are quite common with occasional displacements up to 100 microns. Figure 1 shows examples of some typical events. The

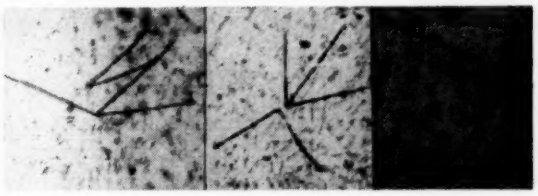

FIG. 1. Typical split thorium stars.

[1] H. J. Taylor and V. D. Dabholkar, Proc. Indian Acad. Sci. A3, 265 (1936).
[2] P. Demers, Phys. Rev. **72**, 536 (1947).
[3] H. Yagoda, *Radioactive Measurements with Nuclear Emulsions* (John Wiley and Sons, Inc., New York, 1949).
[4] J. Groh and G. v. Hevesy, Ann. Physik **65**, 216 (1921). H. Freundlich and H. Neukircher, Kolloid Z. **38**, 180 (1926); v. Hevesy, Seith, and Keil, Z. Physik **79**, 197 (1932); Z. Elektrochem. **37**, 528 (1931). W. Seith, Z. Elektrochem. **39**, 538 (1933). R. F. Mehl, J. Appl. Phys. **8**, 174 (1937). A. W. Adamson, J. Chem. Phys. **15**, 762 (1947).
[5] S. Flügge and K. Zimens, Z. physik. Chem., **B42**, 179 (1939). K. Zimens, Z. physik. Chem. **A191**, 1 (1942); **191**, 95 (1942); **192**, 1 (1943).
[6] W. Lumpe and R. Seeliger, Z. Physik **121**, 546 (1943). G. C. Kuczynsky, J. Appl. Phys. **19**, 308 (1948). A. Gemant, J. Appl. Phys. **19**, 1160 (1948).
[7] E. C. Bingham, *Fluidity and Plasticity* (McGraw-Hill Book Company, Inc., New York, 1922). H. Freundlich, *Colloid and Capillary Chemistry* (Methuen and Company, Ltd., London, 1926). R. C. L. Bosworth, Trans. Faraday Soc. **44**, 308 (1948). S. E. Sheppard and R. C. Houck, J. Phys. Chem. **34**, 273 (1930). R. H. Bogue, J. Am. Chem. Soc. **44**, 1343 (1922). K. Wirtz, Z. Naturforsch. **3a**, 672 (1948). E. K. Rideal, Proc. Roy. Soc. (London) **A200**, 136 (1950).

first hundred stars were measured carefully to establish the identity of the prongs and to detect any angular or momentum correlation that might exist between the star fragments. These measurements established the following facts:

(a) All the stars could be assigned to successive decay of the thorium series starting with radiothorium Th^{228}. The branching ratio of 65:35 for Th C′−C″ was clearly observed.

(b) All the stars were split at the same stage of the decay series; only separation into a 2-prong and a 3-prong star was observed but no other combination.

(c) In no case was there any visible, i.e., ionizing, track linking the two fragments.

(d) Using the range-energy curves of Lattes, Fowler, and Cuer[8] and a shrinkage factor for the emulsion of 2.3, the 2-prong stars were found to consist of the alpha-particles of RdTh (5.42 Mev) and ThX (5.68 Mev), whereas the 3-prong stars consisted of the alpha-particles of Tn (6.28 Mev), ThA (6.77 Mev) and ThC (6.05 Mev) or Th C′ (8.78 Mev), respectively.

(e) The position of the second disintegration center seemed to be entirely at random with respect to the ThX alpha-track showing that the recoil energy of that particle does not contribute appreciably to the subsequent migration of the residual thoron atom. The calculated recoil range is of the order of 0.3 micron and, therefore, barely observable, whereas observed diffusion ranges greatly exceed this value.

From these observations, it seems reasonable to conclude that only the thoron atoms diffuse through the gelatin, presumably because, as an inert atom, thoron does not entɔɹ any structural bond with the gelatin molecules. From observations on the distribution of the effective ranges of the thoron atoms during their life span, it is possible to deduce the diffusion coefficient of thoron in gelatin and the viscosity of the gelatin. To this purpose measurements were extended to 1500 events.

III. THEORY

Three processes of an essentially statistical nature might take place in the splitting of the stars. These are: (1) the activation process liberating the radioactive ions from the gelatin structure, (2) the radioactive decay process, and (3) Brownian motion of the atom, assumed spherical in shape, through the gelatin. Little is known about the forces holding the thorium ions and the other decay products in position in the gelatin. One might assume, for the purpose of discussion, that here, just as in most other materials,[9] an exponential law of the form[10]

$$D=Ae^{-Q/RT} \tag{1}$$

can be used to describe the diffusion coefficient D as a function of temperature T and activation energy Q, though the value of D, as obtained in this experiment, is in no way dependent on the validity of this equation.

It is reasonable to assume that the radiothorium will normally be present as a Th^{4+} ion, having been introduced into the gelatin from a nitrate solution, and it is, therefore, likely to be held in position by molecular forces. Emission of an alpha-particle, transforms it into a bivalent ThX ion, similarly bound, and, therefore, unable to move despite its relatively long half-life of 3.64 days. Since the thoron atoms produced by the next alpha-decay have an inert gas structure, i.e., closed electronic shells, their rate of migration would be determined by thermal forces only. In this respect, this diffusion process differs from the ionic diffusion effects in metals referred to above[4] where the migration energy is largely determined by the lattice field.[10a] The migration must take place during the short lifetime of the thoron atom, which has a half-life of 54.5 seconds. The later disintegration products will presumably again be ions trapped in the gelatin. Even though the bond holding the ions is probably broken by the recoil when an alpha-particle is ejected, the distance traversed is too small to be measured. After the ion is then slowed down, the bond is reformed and the thermal forces alone are insufficient to break it again, thus preventing diffusion at room temperature, though Demers[2] has reported a few cases of diffusion of Th A, B, C, and C′. At higher temperatures such diffusion processes might occur, if the thermal energy exceeds the required activation energy. The thoron atoms, of course, require little energy to free them from the gelatin structure and they diffuse freely at room temperature.

The two other statistical processes are effective simultaneously, and it is best to consider them together. "Dry" gelatin has still enough fluid characteristics[11] to apply Einstein's theory of Brownian motion in liquids.[12]

Taking a single particle, which is placed at the origin of a Cartesian system of coordinates initially, then, with the usual symbols, the mean square displacement in the x direction is given by

$$\overline{x^2}=\frac{kT}{3\pi\eta r_0}t=2Dt, \tag{2}$$

where r_0 is the radius of the diffusing atom. The probability that the particle suffers a displacement between x and $(x+dx)$ in time t is

$$W_{(x)}dx=\frac{1}{2(\pi Dt)^{\frac{1}{2}}}e^{-x^2/4Dt}dx. \tag{3}$$

For random motion in three dimensions x, y, z, this becomes

$$W_{(x,y,z)}dxdydz=\frac{1}{8(\pi Dt)^{\frac{3}{2}}}\times\exp[-(x^2+y^2+z^2)/(4Dt)]dxdydz. \tag{4}$$

[8] Lattes, Fowler, and Cuer, Proc. Phys. Soc. (London) **59**, 883 (1947).

[9] G. Schubert, FIAT Rev., 81 (1948). A. Kochendörfer, Z. Naturforsch. **3a**, 329 (1948).

[10] S. Dushman and I. Langmuir, Phys. Rev. **20**, 113 (1922).

[10a] F. Seitz, *Modern Theory of Solids* (McGraw-Hill Book Company, Inc., New York, 1940). R. M. Barrer, Proc. Phys. Soc. (London) **52**, 58, 1940.

[11] A. Gemant, J. Appl. Phys. **13**, 90 (1942). R. H. Bogue, J. Am. Chem. Soc. **44**, 313 (1922).

[12] A. Einstein, Ann. Physik **17**, 549 (1905). E. H. Kennard, *Kinetic Theory of Gases* (McGraw-Hill Book Company, Inc., New York, 1938). S. Chandrasekhar, Revs. Modern Phys. **15**, 1 (1943).

But the probability of finding a given atom in a given volume element $dx\,dy\,dz$ depends also on its chance of survival. This is governed by the radioactive decay law

$$dN/dt=-\lambda N=-\lambda N_0 e^{-\lambda t}. \quad (5)$$

The number of particles disintegrating in time interval t to $(t+dt)$ is

$$dN=\lambda N_0 e^{-\lambda t}dt, \quad (6)$$

where N_0 is the total number of thoron atoms present initially. Hence, the probability of finding the radioactive atom in the volume interval $4\pi r^2 dr$ during the time interval between t and $t+dt$ is

$$W_{(r,t)}4\pi r^2 dr=\frac{1}{8(\pi D t)^{\frac{3}{2}}}e^{-r^2/4Dt}\lambda e^{-\lambda t}dt\,4\pi r^2 dr, \quad (7)$$

where $r^2=x^2+y^2+z^2$. For all particles observed, diffusion may have taken place during the interval from $t=0$ to a time $t\gg 1/\lambda$ so that the total of particles displaced through a range r out of N_0 original particles is

$$N_{(r)}=\frac{\lambda N_0}{8(\pi D)^{\frac{3}{2}}}4\pi r^2 dr\int_0^\infty \frac{1}{t^{\frac{3}{2}}}e^{(-r^2/4Dt-\lambda t)}dt. \quad (8)$$

Using the substitution $t=u^2$ the integral can be transformed into

$$\int_0^\infty \frac{1}{u^2}e^{-q^2u^2-p^2/u^2}du=\frac{(\pi)^{\frac{1}{2}}}{2p}e^{-2pq}, \quad (9)$$

[12]

where $p^2=r^2/4D$ and $q^2=\lambda$. Hence

$$N_{(r)}=(\lambda N_0/4\pi Dr)e^{-r(\lambda/D)^{\frac{1}{2}}}\cdot 4\pi r^2 dr. \quad (10)$$

If n_r is the number of stars observed with a migration range r per volume element $4\pi r^2 dr$,

$$\begin{aligned}\log_e n_r&=-r(\lambda/D)^{\frac{1}{2}}+\log_e(\lambda N_0/4\pi Dr),\\&=-Ar+\log_e(B/r)\end{aligned} \quad (11)$$

where

$$A=(\lambda/D)^{\frac{1}{2}};\quad B=\lambda N_0/4\pi D=A^2N_0/4\pi. \quad (12)$$

The diffusion coefficient D can then be derived from the constants A or B. It will be noted that according to Eq. (10), the distribution is a function only of $(\lambda/D)^{\frac{1}{2}}$ for the substances involved.

IV. EVALUATION OF RESULTS

The results obtained from the diffusion range measurements are shown in the histogram, Fig. 2. The constants A and B in Eq. (12) were computed numerically as follows. Taking any pair of readings (n_1, r_1 and n_2, r_2) one obtains for A

$$A=\frac{\log(n_1/n_2)+\log(r_1/r_2)}{r_2-r_1}, \quad (13)$$

[12] J. Bierens de Haan, *Nouvelles Tables d'Integrales Definies* (edited by Ritt, Stechert and Company, 1939).

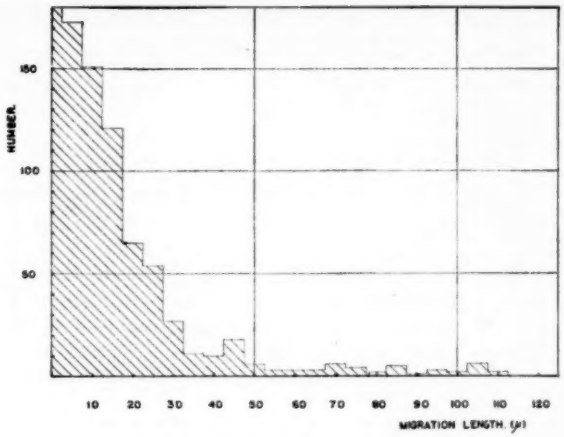

FIG. 2. Distribution of migration ranges.

and

$$\log B=\frac{\log r_1 n_1-(r_1/r_2)\log r_2 n_2}{1-(r_1/r_2)}. \quad (14)$$

The mean value of A, obtained from this computation, was 240 cm^{-1}, the mean value of B 1.4×10^7 cm. For thoron, $\lambda=1.27\times10^{-2}$ sec^{-1} so that from Eq. (12) $D=2.2\times10^{-7}$ cm^2/sec$=1.9\times10^{-2}$ cm^2/day at 22°C. This compares well with Jahn's values[14] for aqueous solutions of gelatin at 16°C as 0.199 and 0.401 cm^2/day for 10 percent and 25 percent solutions respectively.

In order to calculate the coefficient of viscosity from this result, one obtains from Eq. (2)

$$\eta=kT/6\pi Dr_0, \quad (15)$$

which can be assumed to hold fairly well for a viscous medium like gelatine. The only unknown factor in this equation is the effective radius r_0 of the thoron atom. From inspection of a table of atomic radii,[15] one would expect a value of the order of 2.1×10^{-8} cm, whereas the Fermi-Thomas radius $r_0'=A_0Z^{\frac{1}{3}}=0.12\times10^{-8}$ cm. In view of this divergence, it was decided to derive r_0 from published values of the diffusion coefficients for thoron in air and argon together with the measured viscosities of these gases. The latter are[16] $\eta_{\text{air}}=183.3$ micropoises at 23°C; $\eta_{\text{argon}}=221$ micropoises at 23°C. For the diffusion coefficients for thoron, the best values seem to be those of Russ[17]

$$D_{\text{air}}=0.103\text{ cm}^2/\text{sec};\text{ and }D_{\text{argon}}=0.084\text{ cm}^2/\text{sec},$$

which may be supplemented by the results of Hirst and Harrison[18] for radon at 15°C.

$$D_{\text{air}}=0.120\text{ cm}^2/\text{sec};\text{ and }D_{\text{argon}}=0.092\text{ cm}^2/\text{sec}.$$

[14] A. Jahn, thesis, Halle 1914 (quoted in *Handbuch der Physik*), Vol. 22, Part I, p. 276.
[15] E. T. Wherry, Am. Mineralog., **14**, 54 (1929).
[16] *International Critical Tables* (McGraw-Hill Book Company, Inc., New York, 1926–29).
[17] S. Russ, Phil. Mag. **17**, 742 (1909).
[18] W. Hirst and G. E. Harrison, Proc. Roy. Soc. (London) **A169**, 573 (1938).

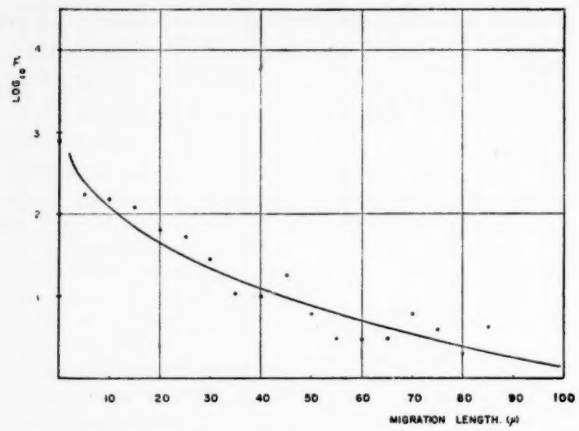

FIG. 3. Comparison of calculated and observed values. The full line was drawn using the computed values of the constants A and B. The dots represent experimental points.

As Stokes' law, Eq. (15), no longer holds precisely for a mixture of gases, these values were inserted into the Langevin equation[19] for the diffusion coefficient of a mixture of gases, using Groth and Harteck's value[20] for the atomic diameter of argon. Solution of this equation leads to an atomic radius $r_0=2.5\times10^{-8}$ cm so that one obtains from Eq. (15) a coefficient of viscosity of dry photographic gelatin (33 percent)

$$\eta=0.40 \text{ poise at } 22°\text{C}.$$

This compares quite well with the results of Mardles.[21] Figure 3 shows a graph of $\log n_r$ against migration range r to compare the fit of the computed constants A and B in Eq. (11) with the experimental points.

Considering the experimental errors in the determination of the constants A and B, the final values for the diffusion coefficient may be in error by a factor 2. The uncertainty in the final value for viscosity depends also on the reliability of the chosen value of the effective atomic radius.

V. CONCLUSIONS

The method described here provides one way of extending diffusion and viscosity measurements to the quasi-solid state and removing the present scarcity of data for colloids near the sol-gel transformation region. There has been a large number of measurements on liquid gelatin solutions,[7,11] and the present experiments lead to results that are clearly of the correct order of magnitude. The method should provide a fairly accurate way of determining the relative viscosity of dry gelatin at different temperatures, different water content and silver halide loading.

Improvement in the absolute value of the diffusion coefficient depends on the clarification of a number of secondary effects. These are:

(a) The presence of silver bromide molecules in the gelatin. The effect of adding various salts to gelatin has been investigated by v. Schroeder,[22] who found that a small addition of halide salts led to a slight increase in viscosity.

(b) Aging of the emulsion. A certain amount of aging of the gelatin may take place and change the structure of the gelatin while drying. This is borne out by a series of measurements reported by Poole[23] and by Gerngross *et al.*,[24] who found that a characteristic crystal structure appeared after several hours. As the addition of silver bromide molecules would probably speed up this process,[19] this effect is relatively unimportant in the present experiments.

(c) Interpretation of the term atomic radius in Eq. (15). This is essentially a thermal collision radius, and the value of 2.5×10^{-8} cm adopted here is not unreasonable though a little higher than the value expected from x-ray measurements of related elements.

The fact that there were no "surplus" events of zero displacement supports the suggestion that thoron atoms do not enter the structure of the gelatin molecule, and it appears that the treatment of the thoron diffusion in terms of classical diffusion theory is fully justified in the case of single radioactive atoms.

The authors are indebted to S. Tabata and G. E. C. Semail for assistance with the observations and to the National Research Council of Canada for a grant for the purchase of microscopic equipment.

[19] E. H. Kennard, *Kinetic Theory of Gases* (McGraw-Hill Book Company, Inc., New York, 1938), equation 166.
[20] W. Groth and P. Harteck, Z. Electrochem. **47**, 167 (1941), quoted in Landolt-Börnstein, Vol. 1, (Springer Verlag, Berlin, 1950).
[21] E. W. J. Mardles, Biochem. J. **18**, 215 (1924).
[22] P. v. Schroeder, Z. physik. Chem. **45**, 75 (1903).
[23] H. J. Poole, Trans. Faraday Soc. **21**, 114 (1925).
[24] Gerngross, Herrmann, and Lindemann, Kolloid Z. **60**, 276 (1932).

Structural Model of Low Pressure "Physical" Adsorption*

MELVIN A. COOK AND DOUGLAS H. PACK†
University of Utah, Salt Lake City, Utah

AND

ALEX G. OBLAD
Houdry Laboratories of the Houdry Process Corporation, Marcus Hook, Pennsylvania

(Received September 22, 1950)

This article describes a proposed new type of adsorption potential associated with surface strain induced in the elimination of unbonded electron orbitals ("first-order strain"), and strain due to surface (chemical) heterogeneities, or surface impurities ("second-order strain"). These surface strains are assumed to give rise to a "semi-chemical" adsorbate-adsorbent attachment in the first layer of multimolecular films. This is termed "structural adsorption" and is considered to be largely responsible, along with ordinary van der Waal's potentials, for the low pressure region of the type II isotherm.

The theory is applied in the calculation of the adsorption isotherms for pure nitrogen, pure oxygen, and mixtures of nitrogen and oxygen on anatase. It is further applied in determining the composition of the adsorbate in mixed gas adsorption and in the computation of the surface pressure of these films over the entire range of relative pressures from zero to $p/p_0=1.0$. Excellent agreement with experimental observations is achieved.

THE experimental adsorption potential relationships in the low pressure region of type II isotherms have not yet been adequately explained. The fundamental arguments of Halsey,[1] in fact, suggest that something aside from normal van der Waal's forces is involved in this region. Likewise the "dual-surface" theories of McMillan[2] and Walker and Zettlemoyer[3] imply other than van der Waal's forces, since as they have emphasized, their dual surfaces must have widely different adsorption potentials for their equations to agree with experimental data. Such selectivity is not consistent with the nonspecific van der Waal's interactions. Smith and Pierce[4] concluded that adsorption resulting in a type II isotherm is really a combination of the type III isotherm and a Langmuir (type I) isotherm. This adds further evidence that van der Waal's forces alone are not responsible for adsorption in the low pressure region of the type II isotherm.

It is interesting to consider the adsorbate-adsorbent and adsorbate-adsorbate interactions separately by the theory of Cook and Pack,[5,6] which is in a convenient form to do this. One finds that the gas-solid component of the adsorption potential (E_1) on the first layer for a nearly completely covered uniform surface is approximately equal to the adsorbate (cooperative) potential (c_1E_L), and $c_1\sim0.75$. For less than this nearly complete coverage of the first layer, on the other hand, the following equations will express the total van der Waal's potentials:

$$E_1{}^1=E_1(\theta)+c(\theta)E_L+T\sigma'(\theta), \tag{1}$$

where $E_1(\theta)$ and $c(\theta)$ may now be considered to vary with the coverage (θ) of the first layer, and $\sigma'(\theta)$ is the "differential net" entropy applying along this layer as a result of such factors as surface heterogeneities. σ_0, the liquid entropy component, is included in the "g" of BET, and of Cook and Pack. In accord with experimental observations[7] and the success of the BET model[5,8] of physical adsorption, we shall assume that σ' is, for all practical considerations, zero for $v/v_m\gtrsim1.0$. Below $v/v_m=1.0$, however, it may not be zero but perhaps appreciably negative.[7] Hence, at zero relative pressure $E_1{}^1\leq E_1(\theta)$ because $c(\theta)=0$ and $\sigma'(\theta)$ is negative or zero. On a homogeneous surface at $v/v_m<1.0$, therefore, the van der Waal's potential will probably always be less than E_L at very low pressures giving a negative "differential net heat" contrary to experimental observations. As far as real heterogeneous surfaces are concerned, the only kind of heterogeneities which would be of much importance in physical adsorption would be the inside corners, edges, and crystal interfaces where the adsorbed gas may experience an increased coordination with the solid.

Brunauer[9] indicated that one might expect values of $E_1(\theta)$ several times larger at inside corners and edges than on a plane surface. This was based on computations by Stranski for ion interactions with ionic crystals. Hence, $E_1(\theta)$ might be as much as $2E_L$ at such points. Since such interactions would represent only a small (perhaps, less than 0.1 percent), portion of the whole surface, they should not be of much significance in

* Presented at the June 3, 1950, meeting of the Catalysis Club of Philadelphia.

† Present address: Kennecott Copper Company, Arthur, Utah.

[1] G. Halsey, J. Chem. Phys. **16**, 93 (1948).

[2] S. McMillan, J. Chem. Phys. **15**, 390 (1947).

[3] S. Walker and A. C. Zettlemoyer, J. Phys. and Colloid Chem. **52**, 58 (1948).

[4] R. N. Smith and C. Pierce, J. Phys. and Colloid Chem. **52**, 1116 (1948).

[5] M. A. Cook, J. Am. Chem. Soc. **70**, 2925 (1948).

[6] M. A. Cook and D. H. Pack, J. Am. Chem. Soc. **71**, 791 (1949).

[7] L. G. Joyner and P. H. Emmett, J. Am. Chem. Soc. **70**, 2353 (1948).

[8] Brunauer, Emmett, and Teller, J. Am. Chem. Soc. **60**, 309 (1938).

[9] S. Brunauer, *Physical Adsorption* (Princeton University Press Princeton, New Jersey, 1945).

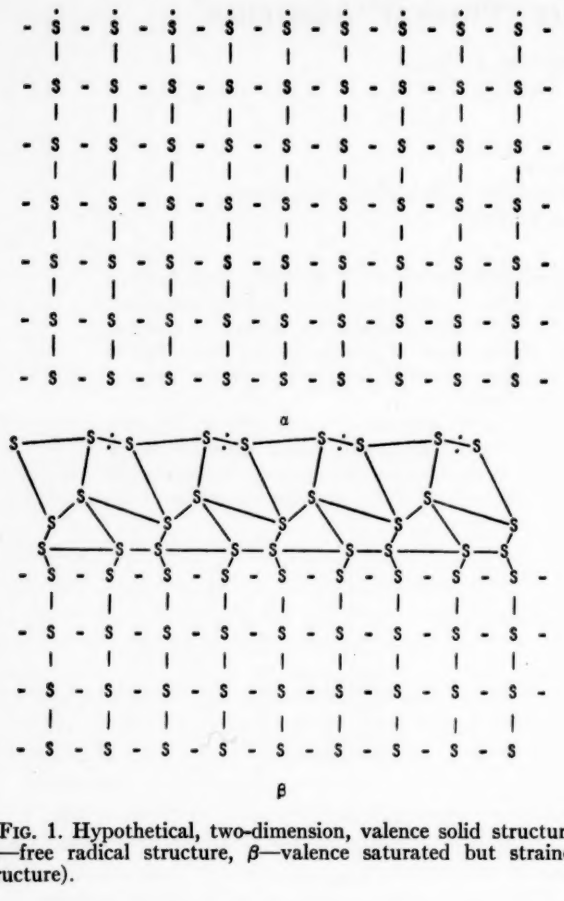

FIG. 1. Hypothetical, two-dimension, valence solid structures (α—free radical structure, β—valence saturated but strained structure).

physical adsorption. On the other hand, one concludes from experimental evidence that high adsorption potentials are required to exist over a large portion, perhaps half, of the surface. Also, E_1^1 for these "hot spots" would be appreciably lower than E_1 because $\sigma'(\theta)$ would be quite negative (the probability of a gas molecule hitting these points would be low). The situation is not improved by cluster-wise adsorption, involving ordinary forces, for although this would allow for an appreciable contribution to the potential from the $c(\theta)E_L$ term, even at $\theta \ll 1.0$, the $E_1(\theta)$ term would drop quickly from the maximum, due to most favorable solid surface coordinations, to the constant E_1 for a plane surface, and $\sigma'(\theta)$ would still be quite negative. (We shall discuss later a type of cluster-wise adsorption that does not possess these difficulties.) All such considerations, in fact, suggest that a physical adsorption isotherm of type II, in which only van der Waal's forces are involved in the low pressure region, is probably nonexistent. Evidently, one requires chemisorption, or a closely related phenomenon, to account for the low pressure region for type II (and IV) isotherms; van der Waal's forces alone, it appears, can account only for type III (and V) isotherms. Rare gases, however, exhibit type II isotherms, and a suitable model must, therefore, be used to explain these isotherms as well as those with gases which may be expected to be chemically active on the bare surface.

"STRUCTURAL ADSORPTION"

We shall introduce the term "structural adsorption" to designate a postulated type of adsorption not previously discussed, and shall define it as adsorption associated with the relief of mechanical strain on the surface of the solid. The following discussion outlines the essential features of the proposed "structural adsorption" model. The basic motions are simple, and can be supported, we believe, by numerous experimental facts pertaining not only to gas adsorption, but also to catalysis, adsorption at the solid-aqueous solution interface, overvoltage, and other phenomena.

FIRST-ORDER STRAINS—PURE SINGLE COMPONENT ADSORBENT—CLEAN SURFACE

Excluding molecular crystals, all solids are held together by primary chemical bonds; a perfect single crystal of a chemically bonded solid (metal, valence crystal, ionic crystal), is a single molecule in the sense that there exists no internal mathematical surface where the particles on either side are not connected by true chemical bonds. All such solids have the property of repeating structure, in the absence of impurities that will interrupt the periodicity of the lattice (e.g., oxygen, hydrogen, nitrogen). The valence crystals and intermediate types (transitions between valence and ionic, and valence and metallic), at least would be free radicals if their bulk structure were to be continued without interruption or distortion right up to the mathematical surface. The free radical nature of the solid may be illustrated by the structure α (Fig. 1) for a hypothetical, two-dimensional, homonuclear solid having sites *S*. Here, the unbonded valence orbitals in α are represented by dots and the bonded ones by lines. Since each bond contains one or more electrons, the dots may also be thought of as either single electrons, combinations of electrons and empty or partly filled orbitals, or both. A free radical structure is always a high energy configuration relative to the bond saturated one, and whenever possible, it will rearrange, e.g., by double- or triple-bond formation (perhaps, of a resonating type), to a valence saturated structure. However, a crystal surface could rearrange to bring about the valence saturation only by undergoing rather drastic distortions from the normal solid lattice configuration as illustrated by the β-structure of Fig. 1. In the process of achieving valence saturation the solid may be pictured, therefore, as attaining a kind of "glass" structure at the surface. By a glass structure we mean an irregular structure in the sense that a glassy state of a substance is irregular in comparison with a more stable crystal structure of the substance. Despite the increased potential associated with strain, the distorted β-structure would still be a lower energy state than the α-structure and would thus represent the stable structure. In other words, valence

forces are usually strong enough to support tremendous mechanical stresses, and a solid surface will, therefore, be expected to undergo whatever distortion from the normal bulk solid lattice structure will be required to eliminate the free radical structure and reduce the surface tension. For a solid possessing no surface impurities the surface tension would be equivalent to the work of strain plus the difference in energy between the surface double-bonded structure (or whatever type of bond eliminates the free radical surface), and the normal cohesive energy of the solid.

For crystal structures held together by ionic bonding, the disarrangement at the surface can be described in the same manner as that previously given for covalent crystal structures. The bonding electrons are correlated about the same way in each type of bonding. The only difference between the ionic bond and the valence bond is the electron symmetry. For the valence crystal the electrons are symmetrically situated between the two bonded atoms. In the true ionically bonded crystal the electrons are asymmetrically situated (toward the electronegative atom), between bonded atoms. In many respects the metallic bond resembles very closely the covalent bond. Hence, what has been illustrated here for the valence crystal also applies to some degree, at least, to ionic crystals and metals.

The free energy $y(\theta)$ of "structural adsorption" according to this model would comprise (1) whatever energy is to be attributed to the adsorbate-adsorbent bond with the solid not under strain, plus (2) the strain relief potential, i.e., the work obtained in removing the surface strain. The latter contribution to the adsorption potential we consider to be sufficient that even gases like argon may be able to form a near, or even true, chemical bond with the adsorbent by donating one of its electron pairs to saturate the surface, for example, as follows:

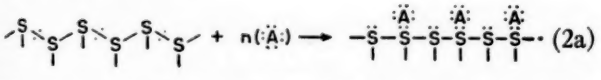

This suggestion carries with it the implication that rare gases would more frequently form chemical bonds with atoms of the solid if the latter were free. The reason chemical bonding with rare gases is not observed more frequently is, perhaps, only that the atoms with which they might otherwise bond form much stronger bonds with themselves. When they are held in the solid surface, however, the ability of the solid constituent atoms, particularly those with empty orbitals, to bond with the rare gas is manifest simply because there is no better means available to saturate the empty orbitals. Comparable with rare gas reactions, we expect that nitrogen would bond with a solid somewhat as follows ("structural adsorption" would not involve atomic nitrogen):

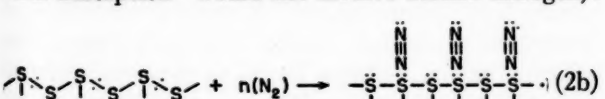

Mechanical strain resulting from the relief of "valence strain" (i.e., the high energy associated with free radical surfaces) would be most pronounced at outside corners, edges, and two-dimensional phase boundaries. For this reason, the adsorbate may tend to adsorb cluster-wise, surrounding these active centers. On the other hand, the entropy of adsorption in this case may be unfavorable, because the effective area of influence of such centers may be excessively small. This would be no handicap, however, for the present model accounts for "active center" like adsorption even on a homogeneous surface (i.e., homogeneous in the sense that the strain-producing and free-radical relieving bonds are uniformly distributed over the entire surface). According to reactions (2a) and (2b), every other site would be a "structural adsorption" site and the alternate sites "physical adsorption" sites. Reactions (2a) and (2b) may be illustrated in the general case (i.e., for the molecule AB) by the reaction:

$$\mathbf{S}+:\ddot{A}:B \rightleftarrows \bar{S}:\ddot{A}:B \tag{2c}$$

where A is the atom donating the (usually unbonding) electron pair, and B is any other atom or radical. This is to be distinguished from normal chemisorption reactions which may take place as follows:

$$\begin{aligned}&\mathbf{S}+AB \rightarrow \bar{S}_1A+\bar{S}_2B\\ &\mathbf{S}+AB \rightarrow \bar{S}AB.\end{aligned} \tag{2d}$$

Here $\mathbf{S}$ represents the strained surface, and $\bar{S}$ the surface upon which strain is partially or entirely relieved depending on θ', the fraction of coverage of the surface associated with "structural adsorption." $\bar{S}_1$ and $\bar{S}_2$ designate different chemisorption sites. Chemisorption, when it occurs, will itself relieve surface strain at least as effectively as the postulated "structural adsorption."

SECOND-ORDER STRAIN—IMPURITY AND MULTICOMPONENT SURFACES

While the present discussion will be restricted to adsorbents which are supposed to have only "first-order (surface) strain," the theory contemplates another type of strain associated with surface impurities, and the use of several strongly interacting components in the adsorbent surface. Strain produced by impurities and interacting components will, in general, be heterogeneously distributed and possibly may give rise to cluster-wise adsorption. Such strain is brought about by "mechanical" distortion of the lattice structure. The induction of structural changes by impurities or component substances are believed to be responsible for (catalytically) "active centers." For example, silica induces structural changes in alumina at the interface between them; a four-six coordination equilibrium is evidently established by this means which is directly responsible for the acid catalyst properties of the silica-alumina system.[10]

[10] Milliken, Mills, and Oblad, *General Discussion on Heterogeneous Catalysis* (Faraday Society, April, 1950). Oblad, Milliken, Mills, Volume III, *Advances in Catalysis* (Academic Press, Inc., New York) (to be published).

The magnitude of the strain potential in "second-order strain" is no doubt considerably larger than in "first-order strain," but the extent of it is much less, i.e., the number of "active centers" in the former is probably seldom more than 0.1 percent of those in the latter type. For this reason, the low pressure region in type II adsorption may depend primarily on "first-order strain" even with catalytically active adsorbents and other impurity and multi-component adsorbents. On the other hand, "second-order strain" effects, we believe, are responsible for many experimental observations not only in heterogeneous catalysis, but in crystal growth, overvoltage, and similar phenomena. In crystal growth "second-order strain" sometimes appears to reach relatively tremendous proportions and is probably directly responsible for the initiation of crystal growth in each layer. The absence or limitation of "second-order strain" on metal surfaces we think is responsible for hydrogen and oxygen overvoltage. Even the completely reversible hydrogen electrode probably has only in the neighborhood of 0.1 percent of its surface "activated" by "second-order strain" and these "active centers" can be destroyed by poisons adsorbing only on the strain sites. We mention these phenomena merely as illustrations of the supposed importance of surface strain. Further discussions in this paper will be confined to the application of the theory to low pressure "physical" adsorption. The detailed manner in which "first- and second-order strains," as defined, are responsible for catalysis, chemisorption, activated absorption, overvoltage, crystal growth, and other surface phenomena will be the subject of future papers.

ENTROPY VARIATIONS IN LOW PRESSURE REGION ON PURE (SINGLE COMPONENT) ABSORBENTS

From the viewpoint of kinetic theory of adsorption ("differential net"), entropy effects in the region $0<\theta<1.0$ will probably be introduced largely in the coefficient of condensation $\alpha(\theta)$ defined by the Langmuir relation:

$$\alpha(\theta)\mu s_0=\nu s_1, \tag{3}$$

where μ is the rate of bombardment of the surface, ν is the rate of evaporation and s_0 and s_1 are the areas of the uncovered and covered surfaces, respectively.

a. Structural Adsorption at Linear Interface

As mentioned previously, the points of maximum free radical relief bonding are the corners, edges, two dimensional phase boundaries [inside corners and edges would be minimum strain points, but points of maximum (solid-gas) van der Waal's interaction]. These are, supposedly, distributed quite irregularly over the surface. They cannot, however, represent a very large portion of the surface; otherwise, the surface energy would be excessive. These may, in other words, be the real structural adsorption "hot spots," but will occupy as an upper limit probably less than 0.1 percent of the surface. The postulated relief bonding will not concentrate the surface strain entirely at the region of the relief bond, but the strain will distribute itself over a much wider area, and even several layers into the crystal as illustrated in structure β. For the sake of evaluating the possible importance of "active centers" in "structural adsorption," let us assume that the strain structure is highly localized around the free radical relief bond, that "structural adsorption" is limited primarily to those points of "adliniation," and that in low relative pressure adsorption gaseous molecules hitting anywhere on the bare surface, except the "hot spots," will rebound, and will condense only on say 0.1 percent of the surface representing these "active centers." In "structural adsorption" orientation probably may be important and, if so, would introduce an additional entropy effect. For an effective "hot spot" area of 0.1 percent of the total surface, the "differential net" entropy of the condensation process would then be $\sigma'\leq R\log_e 0.001$, which at 90°K would lower the adsorption potential more than 1300 cal/mole. Assuming that the heat of adsorption is sufficient to overcome this unfavorable entropy and still leave the boundary a (potential) "hot spot," adsorption would increase by clustering, and the edge of the cluster would be the new "hot spot." The entropy would then increase slowly over the entire range of "structural adsorption," since the effective area of these linear interfaces would remain small. This type and magnitude of entropy variation, however, does not seem to exist along type II isotherms, at least on pure (single component) adsorbents, although Joyner and Emmett found σ' to go as low as -9 E.U. for nitrogen on graphite at $v/v_m\sim 0.9$, increasing rapidly to about ± 2 on either side of $v/v_m\sim 0.9$. It is of particular interest that the value of σ appeared to be about ± 2 over the whole region of supposed "structural adsorption" in this case.

b. Uniform "Structural Adsorption"

The above entropy considerations do not favor the theory of "active centers" (in its usual sense), as applying in adsorption equilibria due to "structural adsorption" on a pure single-component adsorbate, because there is no evidence that the process can involve the very low entropies that it would require. The situation is quite different in regard to "structural adsorption" over a uniform surface. The adsorbate would have a cross section $1/n$ of its average area-of-influence on the surface, i.e., the average area over which each molecule will be effective in relieving its quota of strain. Here n is a small number greater than unity but less than two, or at the most, three. Assuming that other entropy effects associated with "structural adsorption," such as orientation effects, will be of comparable magnitude, the "differential net" entropy in the region of "structural adsorption" would be $\sigma'\sim -9.2\log n$. This probably agrees, within a factor of two, with the real $\sigma'(\theta)$ relations along the very low pressure region for

adsorbents like pure anatase, but of course, does not express them in detail. The important point, however, is that the observed σ' relations are more consistent with uniform "structural adsorption" than with "structural adsorption" associated with irregularly distributed "active centers."

c. Physical Adsorption in Low Pressure Region

The fraction $1/n$ of the area of the solid is associated with "structural adsorption," leaving the fraction $(1-1/n)$ to be associated with pure van der Waal's adsorption. In the region of low $y(\theta)$, i.e., when $\theta' \sim 1.0$, or where $\sigma'(\theta)$ is appreciably negative and $\theta' < 1.0$, physical adsorption would be competive with structural adsorption over the $1/n$ part of the surface. In the present approximation, however, we shall neglect this competition and treat the $1/n$ part of the first layer as "structural adsorption" and the $(1-1/n)$ part as purely physical adsorption. The potential of "structural adsorption" will, of course, always be augmented by the van der Waal's forces; one would simply add $E_1{}^1$ to $y(\theta)$ to obtain the total adsorption potential on the $1/n$ part of the surface. Except for van der Waal's "active centers," $\sigma'(\theta)$ would be zero, if it were to be attributed entirely to the condensation coefficient. Since, according to the above discussion, the homogeneous (strained) surface would be quite predominant in adsorption equilibria, $\sigma'(\theta)$ will thus be taken to be effectively zero. All "differential net" entropy effects in type II adsorption will thus be associated with "structural adsorption" in the present discussion. In other words, $y(\theta)$ and E_1' are component free energy functions; E_i and $c_i E_L$ are component enthalpy functions.

The adsorbate-adsorbate van der Waal's term $c'(\theta)E_L$ for the first layer will be assumed to vary linearly with the total coverage on each type of surface, i.e., $c'\theta E_L$, for both the "structural" and "physical" surfaces. Such a condition should also apply approximately to the other layers of multimolecular adsorption, i.e., $c_i(\theta)_i = c_i\theta_i$. The constant values employed in reference 5 and 6 were tacitly regarded as average values, but, in fact, one cannot justly so regard them. However, we shall not here introduce a more accurate treatment of $i \geq 2$ layers than that given in references 5 and 6.

THE FUNCTION $y(\theta)$ FOR "FIRST-ORDER STRAIN"

It is suggested above that the strain would not be localized, but rather would be broadly distributed over the entire surface. This suggests that each molecule adsorbing on the surface would lower the strain, not only at the position of adsorption, but over a much broader area; in fact, effectively over the whole surface, since the adsorbate would go on the surface uniformly (but not randomly). This model, in which each adsorbed atom or molecule relieves its quota of strain over the whole surface, rather than entirely at specific sites, corresponds, in a sense, to the free electron model of a metal in which the energy gain in a single electron excitation is supposedly distributed throughout the metal, and will therefore affect the energy level of each site of the whole crystal as much as the site of origin. In other words, we assume that the surface (and bulk) mobility of the atoms and radicals of the solid is as large as the binding forces require it to be; a surface will adjust to strain loading or unloading as rapidly as the strain pulses can be carried through the solid. The strength of the "structural adsorption" bond would be proportional to the total strain on the surface, if one were to neglect any gradients of strain and to assume that each particle going on the surface were to remove strain over the whole surface. It seems plausible, therefore, that the "strain potential" would drop in direct proportion to the "structural adsorption." On this assumption $y(\theta)$ would have the simple linear form:

$$y(\theta) = y_0(1-\theta'/\epsilon). \tag{4}$$

Here ϵ is chosen so that $y(\theta)$ in Eq. (4) will reduce to the "structural adsorbate" solid bond energy for an unstrained surface at $\theta' = 1.0$ ($\epsilon \geq 1.0$). Not only does this $y(\theta)$ law for uniform surface strain relief seem logical for adsorption on a homogeneous (strained) surface, but it may also apply to "structural adsorption" induced by "second-order strain," although in the latter case one may need to take into account the gradient of strain from the most active part of the surface—the "catalytic" "active centers"—to the unstrained or "first-order strain" part of the surface. It should be pointed out that Eq. (4) can be deduced on the basis of other models. For the model proposed, Eq. (4) seems to the authors intuitively to be the most logical. Definite proof of the model proposed will only come from critical experiments.

THE ADSORPTION ISOTHERM

The complete isotherm for the proposed model may now be developed by combining in the usual BET manner the appropriate Langmuir equations as follows:

$$xs_0' \exp(\psi_1' - E_L)/RT = s_1'$$
("structural adsorption" part of first layer) (5a)

$$xs_0'' \exp(\psi_1'' - E_L)/RT = s_1''$$
("physical adsorption" part of first layer) (5b)

$$s_i = Z_2 Z_3 \cdots Z_i s_1' \quad (i>1)$$
(Z's defined in reference 5), (5c)

where

$$s_0' = s_0'' = s_0; \quad \text{and} \quad s_1' + s_1'' = s_1. \tag{5d}$$

Proceeding as in reference 5, one obtains

$$v/v_m = \sum_1^\infty i x^i \delta_i / (1 + \sum_1^\infty x^i \delta_i) \tag{6}$$

where

$\delta_i = \delta_1 d_i/d_1$ (d_i and d_1 are defined in references 5 and 6).

And

$$\delta_1=\frac{1}{n(1-\theta)}\{(1-\theta')\exp(\psi_1'-E_L)/RT + (1-\theta'')(n-1)\exp(\psi_1'-E_L)/RT\}=\frac{1}{n(1-\theta)}\left\{(1-\theta')\exp\left(\frac{y_0(1-\theta'/\epsilon+E_1+(c'\theta'-1)E_L}{RT}\right) + (1-\theta'')(n-1)\exp\left(\frac{E_1+(c'\theta-1)E_L}{RT}\right)\right\}. \quad (7)$$

Here s_0 and s_i have been expressed in terms of the θ's by the relation

$$s_0'/s_0=\frac{1-\theta'}{n(1-\theta)}; \quad s_0''/s_0=\frac{(1-\theta'')}{n(1-\theta)}(n-1). \quad (8)$$

So that the curve for $v/v_m<1$ will fit smoothly into that for $v/v_m>1$, using the equations of reference 6 for $v/v_m>1.0$, it is necessary that $\delta_1(\theta_1)=d_1$ (θ_1 is the total first-layer coverage at $v/v_m=1$). As was mentioned in reference 5, one would expect $c_1=0.5$ for a filled monolayer, but in order to obtain a satisfactory fit of the curve in the region $v/v_m>1.0$, it was found necessary in references 5 and 6 to employ larger values of c_1, and this was attributed to compensating errors brought about by certain "neglected adsorbate-adsorbent interactions." The nature of these neglected interactions are now evident, and there is no reason, therefore, not to revert to the use of physically significant c_i values. In fact, since the adsorbate-adsorbate interaction term is θ dependent where the E_1 (van der Waal's gas-solid) term is not, one would obtain a better description of the low pressure region by setting, $c_1=0.5$ (its theoretical value), and computing E_1 from the relation $\delta_1(\theta_1)=d_1$. That is, errors in E_1 cannot be compensated in c_1 for $v/v_m<1.0$ because of the θ dependence of adsorbate-adsorbate interactions. We shall employ the value $c'=0.5$ in this study and adjust E_1 to make $\delta_1(\theta_1)=d_1$ for $v/v_m<1.0$. Later, we shall undertake the problem of adjusting the c_i's in the high pressure region to be consistent with theory. For a given θ, one may compute θ', θ'', and x using the equations:

$$\theta'+(n-1)\theta''=n\theta \quad (9a)$$

$$\frac{\theta'}{1-\theta'}\exp\frac{-y_0(1-\theta'/\epsilon)}{RT}=\frac{\theta''}{1-\theta''} \quad (9b)$$

$$x=\frac{\theta'(1-v_2/v_m\theta)}{1-\theta'}\exp\frac{-y_0(1-\theta'/\epsilon)+E_1+(c'\theta-1)E_L}{RT} \quad (9c)$$

$$\frac{v'}{v_m\theta}=\frac{\sum_2^\infty(i-1)x^{(i-1)}d_i/d_1}{1+\sum_2^\infty x^{(i-1)}d_i/d_1}=\frac{\sum_1^\infty ix^id_i-\sum_1^\infty x^id_i}{\sum_1^\infty x^id_i} \quad (9d)$$

$$1-\frac{v_2}{v_m\theta}=1-\frac{\sum_2^\infty x^{(i-1)}d_i/d_1}{1+\sum_2^\infty x^{(i-1)}d_i/d_1}=\frac{d_1x}{\sum_1^\infty x^id_i}. \quad (9e)$$

Here the factor $(1-v_2/v_m\theta)$ in Eq. (9c) is a correction factor accounting for the effect of the second adsorbed layer on the rate of evaporation from the first.

A possible configuration of a layer of absorbate molecules as they might appear in structural and physical adsorption in the first layer is represented for one of several types of surfaces by Fig. 2. The top layer of atoms of the 100 face of anatase are shown partly dotted. The large dotted spheres represent oxygen while the small dotted spheres represent titanium. The large solid lined circles represent the adsorbate molecules. Those large circles which cover the titanium atom represent "structural adsorption," the remainder represent the physical adsorption in the first layer. Molecules in second and higher layers are not shown. While this diagram indicates one adsorbate molecule for each titanium atom as "structural adsorption," this is simply because all surfaces are not shown. On the average only half of the titanium atoms that appear on the surface would be adsorption sites for "structural adsorption."

The data of Arnold[11] has been used as a test for the model. The agreement between experiment and theory is shown in Fig. 3. The empirical constants obtained from the above data for the isotherms of pure nitrogen and of pure oxygen will be used in the later part of this paper to calculate adsorption isotherms of a mixture of these two gases.

In a six-coordinated solid such as anatase, the "structural adsorption" model would require one electron pair for every two $-TiO_2$-units on surface to saturate the surface. While the relative (effective) densities of the adsorbate and anatase are uncertain, one would expect a value of $1/n$ for nitrogen and oxygen on anatase somewhere between 0.6 and 0.75, the lower value corresponding roughly to solid oxygen and nitrogen The value $n=5/3$ was used in initial calculations for oxygen, and gave satisfactory results. Since y_0 and ϵ are relatively small in this case the transition between "structural" and physical adsorption is not as sharp as in nitrogen. The latter, as expected from the model, showed a sharp discontinuity in the log x *vs* θ curve (Fig. 3) at roughly the expected value of n. Because of this sharp transition for N_2 the results are very critical to the value of n employed in the region $\theta=0.6-0.7$. One can easily see that the value $1/n=2/3$ is too large. The value 0.6 was thus employed and gave good results, although evidence indicates that this may be slightly low. The results for $1/n=0.6$ are presented, and no effort was made to establish it more closely.

The "structural" adsorption constant y_0 is obtained empirically. Equation (9c) may be placed in the form:

$$-\ln x+\ln\left(1-\frac{v_2}{\theta v_m}\right)-\ln\frac{1-\theta'}{\theta'}=\frac{y_0}{RT}+\frac{E_1-E_L}{RT}.$$

As $v/v_m\to 0$, $[1-(v_2/\theta v_m)]\to 1$, and $\theta=n(v/v_m)$, thus

[11] J. R. Arnold, J. Am. Chem. Soc. **71**, 104 (1949). Detailed data (of reference 10) were kindly supplied to us by Arnold.

$(y_0+E_1-E_L)/RT$ may be obtained by an extrapolation (straight line in this case), to $v/v_m=0$ of a plot of $-\ln x-\ln[(1-nv/v_m)/nv/v_m]$ *vs* v/v_m. The constant ϵ is evaluated empirically by use of a suitable point on the experimental curve.

SURFACE PRESSURE

The differential surface pressure $\pi(0.05-1.0)$ between $x=0.05$ and $x=1.0$ was obtained analytically by Cook and Pack.[6] This eliminated a difficult graphical extrapolation to $x=1.0$. The theory was inadequate in that development to carry out the corresponding low pressure extrapolation, which we shall now proceed to do. The differential pressure due to adsorption on top of the first layer in the region $0<x<0.05$ will be very small, and for practical applications we may compute $\pi(0$ to $.0.5)$ from the equations:

$$\pi(0-0.05)=\pi'(0-0.05)+\pi''(0-0.05) \quad (10a)$$

$$\pi'(0-0.05)=\frac{RTv_m}{V\Sigma'}\left\{\int_0^{\theta_2'}\frac{\theta'}{n}\frac{dx}{x}+\int_0^{\theta_2'}(n-1)\frac{\theta''}{n}\frac{dx}{x}\right\} \quad (10b)$$

$$=\frac{RTv_m}{V\Sigma'}\left\{\frac{-2.3}{n}\log(1-\theta_2')-\frac{2.3(n-1)}{n}\log(1-\theta_2'')+\frac{y_0(\theta_2')^2}{2nRT}-\frac{c'E_L}{2RT}\left(\frac{(\theta_2')^2}{n^2}+\frac{(\theta_2'')^2(n-1)^2}{n^2}\right)+2.3\left(\frac{\bar\theta'}{n}+\frac{n-1}{n}\bar\theta''\right)\log(1-v_2/v_m\theta_2)\right\} \quad (11)$$

where θ_2' and θ_2'' are the values of θ' and θ'' at $x=0.05$, Σ' is here the total surface area per gram of the solid, and $\bar\theta'$ and $\bar\theta''$ are average values applying in the integration taking care of second layer effects. In evaluating $\int_0^{\theta_2'}\theta'/x dx$ we have assumed $c'\theta\approx c'\theta'/n$, and in the second integral $\int_0^{\theta_2''}\theta''/x dx$, the approximation $c'\theta\approx c'\{1/n+[(n-1)/n]\theta''\}$ was employed. (This assumes that $\theta''=0$ until θ' is nearly unity.) These approximations will introduce no significant errors in cases where the potential of "structural adsorption" is appreciable. For the second term in Eq. (10a)

$$\pi''(0-0.05)=\frac{RTv_m}{V\Sigma'}\int_0^{.05}\frac{v'}{v_m}\frac{dx}{x}=\frac{2.3RTv_m}{V\Sigma'}\left(\bar\theta\log 1+\sum_2^\infty(0.05)^{i-1}\frac{d_i}{d_1}\right). \quad (12)$$

TABLE I. Comparison of surface pressure of films on anatase.

	Graphical[a]	Calculated[b]	Graphical	Calculated
Nitrogen on anatase				
$\pi(0-0.05)$	23.2		32.9[c]	32.5[d]
$\pi(0.05-1.0)$	32.3[e]	30.0		27.7[e]
$\pi(0-1.0)$	55.5	53.2		60.2
Oxygen on anatase				
$\pi(0-0.05)$			20.4[c]	20.1[d]
$\pi(0.05-1.0)$				30.5
$\pi(0-1.0)$				50.6

[a] Taken from Fig. 8 of reference 12.
[b] Taken from Table II of reference 6.
[c] Graphically integrated from data furnished by Arnold (reference 11).
[d] Calculated by Eq. (10a).
[e] Calculated by methods of reference 6.

Finally

$$\pi(0-0.05)=\frac{RTv_m}{V\Sigma'}\left\{-\frac{2.3}{n}\log(1-\theta_2')-\frac{2.3(n-1)}{n}\log(1-\theta_2'')+2.3\left(\bar\theta\log 1+\sum_2^\infty 0.05^{(i-1)}\frac{d_i}{d_1}\right)+\frac{y_0(\theta_2')^2}{2nRT}-\frac{c'E_L}{2RT}\left(\frac{(\theta_2')^2}{n^2}+(\theta_2'')^2\frac{(n-1)^2}{n^2}\right)+2.3\left(\frac{\bar\theta'}{n}+\frac{n-1}{n}\bar\theta''\right)\log\left(1-\frac{v_2}{v_m}\theta_2\right)\right\}. \quad (10c)$$

The values of surface pressure of oxygen on anatase and of nitrogen on anatase as calculated from Arnold's[11] data are presented in the last column of Table I. The low pressure values were calculated by Eq. (10a), while the high pressure values were calculated by the methods of Cook and Pack.[6] The discrepancy in $\pi(0-0.05)$ for nitrogen on anatase between the values of Harkins and Jura[12] and those calculated from Arnold's data is due largely to the small differences in the experimental data.

MIXED ADSORPTION

We shall confine the further application of the theory in the present discussion to an interpretation of the data of Arnold[11] for "mixed adsorption" of oxygen and nitrogen on anatase.

Arnold found that pure oxygen and pure nitrogen yielded type II isotherms which were remarkably similar (Fig. 2 and Fig. 3, reference 11). In the high pressure region nitrogen showed slightly less adsorption at a given relative pressure than oxygen. In the very low pressure region, on the other hand, differences became apparent only in the region below $x=0.003$ and could be seen only by a hundredfold increase in the x scale. When the oxygen-nitrogen mixtures were used, Arnold found that the total isotherms were still practically

[12] G. Jura and W. D. Harkins, J. Am. Chem. Soc. **66**, 1356 (1944).

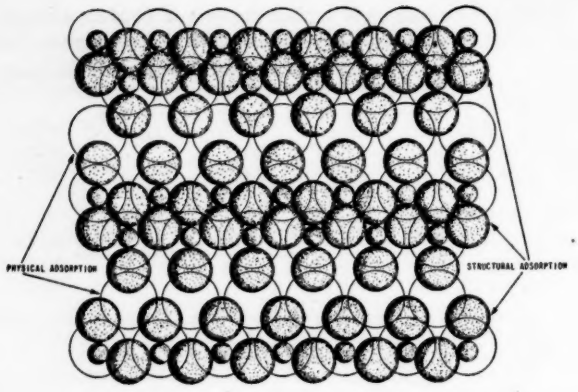

FIG. 2. The 100 face of anatase (small spheres T_0, large spheres oxygen, large circles represent a possible structure of "structurally" and "physically" adsorbed N_2 molecules).

identical with those for pure oxygen and nitrogen, but the mole fraction ($N_{a\alpha}$) of nitrogen in the adsorbate was sharply increased above that in the gas at low relative pressure, but was equally sharply decreased at high relative pressures. The data in Table II computed from Arnold's data illustrate this effect.

Qualitatively, the explanation of this effect is simple on the basis of the present theory. The van der Waal's adsorption potential is appreciably greater for oxygen than for nitrogen. Since these forces predominate at high relative pressures, a decrease in the ratio $N_{a\alpha}/N_\alpha$ is expected at high pressures. For "structural adsorption" however, the more basic substance, i.e., the one which can more easily donate an electron pair, will have the higher "structural adsorption" potential, (y_0). Because of its electronic structure, it is likely that nitrogen will have a greater tendency to "coordinate" with the atoms in an unsatisfied crystal surface than does oxygen. It should predominate in a reaction of the type expressed in Eq. (2a) at low pressures. The experimental data show nitrogen to be more strongly adsorbed at low pressures. (More experimental work is necessary to give greater substance to this explanation.)

We shall introduce the subscript α to designate one component and β the other of the binary mixture (N_α = mole fraction of one component and N_β that of the other gas, $N_{a\alpha}$ and $N_{a\beta}$ the corresponding mole fractions in the adsorbate). Also, we assume the validity of Raoult's law for the adsorbate. The first layer Langmuir equations are then:

$$\begin{aligned} x_\alpha s_0' &= s_{1\alpha}' \exp(-(\psi_{1\alpha}' - E_{L\alpha})/RT) \\ x_\beta s_0' &= s_{1\beta}' \exp(-(\psi_{1\beta}' - E_{L\beta})/RT) \end{aligned} \tag{12a}$$

$$\begin{aligned} x_\alpha s_0'' &= s_{1\alpha}'' \exp(-(\psi_{1\alpha}'' - E_{L\alpha})/RT) \\ x_\beta s_0'' &= s_{1\beta}'' \exp(-(\psi_{1\beta}'' - E_{L\beta})/RT). \end{aligned} \tag{12b}$$

For the ith layer ($i \geq 2$), we have

$$\begin{aligned} x_\alpha s_{i-1} &= s_{i\alpha} \exp(-(\psi_{i\alpha} - E_{L\alpha})/RT) \\ x_\beta s_{i-1} &= s_{i\beta} \exp(-(\psi_{i\beta} - E_{L\beta})/RT). \end{aligned} \tag{12c}$$

The composition of the ith layer may be found by dividing one of the two equations (12c) by the other, and since $x_\alpha = N_\alpha p/p_{0\alpha}$ and $x_\beta = N_\beta p/p_{0\beta}$, we obtain

$$\frac{s_{i\alpha}}{s_{i\beta}} \approx \frac{N_{a\alpha i}}{N_{a\beta i}} = \frac{N_\alpha p_{0\beta}}{N_\beta p_{0\alpha}} \exp \frac{\psi i_\alpha - \psi i_\beta}{RT} - \frac{E_{L\alpha} - E_{L\beta}}{RT} \tag{13}$$

for molecules of approximately the same size.

The composition on both the "structural" and "physical" portions of the first layer varies with θ and we are, therefore, interested in average value for each θ. The "differential" composition may be found as in Eq. (13). On the other hand, the average (or integral) composition is:

$$\frac{N'_{a\alpha 1}}{N'_{a\beta 1}} = \int_0^{\theta'} \frac{s'_{i\alpha}}{s'_{i\beta}} d\theta' \Big/ \int_0^{\theta'} d\theta' \tag{14}$$

with a corresponding equation for ($N''_{a\alpha 1}/N''_{a\beta 1}$). Sub-

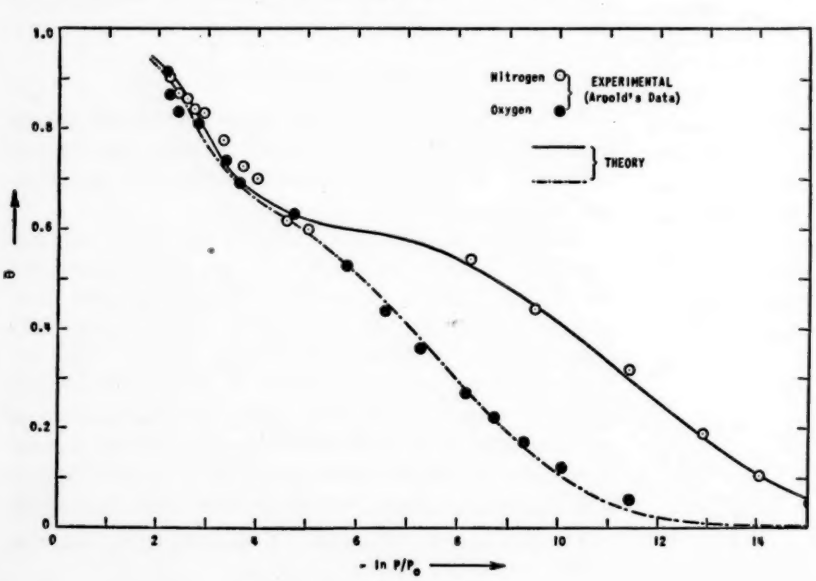

FIG. 3. Comparison of "structural" adsorption theory with experimental data of Arnold.

stituting into Eq. (14) the values $s_{1\alpha}'/s_{1\beta}'$ and $s_{1\alpha}''/s_{1\beta}''$ from Eqs. (12a) and (12b), and integrating, one obtains:

$$\frac{N'_{a\alpha}}{N'_{a\beta}}=\frac{N_\alpha}{N_\beta}\frac{p_{0\beta}}{p_{0\alpha}}\exp\frac{(E_1-E_L)_\alpha-(E_1-E_L)_\beta+(y_{0\alpha}-y_{0\beta})}{RT}\Big/\left\{\left(\frac{-y_0}{\epsilon}+\frac{c'E_L}{n}\right)_\alpha-\left(\frac{-y_0}{\epsilon}+\frac{c'E_L}{n}\right)_\beta\right\}\frac{\theta'}{RT}\left\{\exp\left[\frac{\left(\frac{-y_0}{\epsilon}+\frac{c'E_L}{n}\right)_\alpha-\left(\frac{-y_0}{\epsilon}+\frac{c'E_L}{n}\right)_\beta}{RT/\theta'}\right]-1\right\} \quad (15a)$$

$$\frac{N''_{a\alpha 1}}{N''_{a\beta 1}}=\frac{N_\alpha}{N_\beta}\frac{p_{0\beta}}{p_{0\alpha}}\exp\frac{(E_1-E_L)_\alpha-(E_1-E_L)_\beta+[(c'E_L/n)_\alpha-(c'E_L/n)_\beta]}{RT}\Big/\frac{\theta''}{RT}\{[(n-1/n)c'E_L]_\alpha-[(n-1/n)c'E_L]_\beta\}\frac{\theta''}{n}\left\{\exp\left[\frac{\theta''}{RT}\left(\frac{n-1}{n}(c'E_L)_\alpha\frac{n-1}{n}c'E_{L\beta}\right)\right]-1\right\}. \quad (15b)$$

Here again (as in the surface pressure extrapolation to $x=0$), we have employed the assumption $c'\theta=c'\theta'/n$ during filling the "structural adsorbed" part of the first layer and $c'\theta=c'1/n+[\theta''(n-1)/n]$ for the filling of the second. Since the coordination of "structural adsorbate" increases as "physical" adsorbate builds up, the calculations of π and composition are in error by the failure to take this into account. This small error will probably be compensated approximately by the effect of multilayer adsorption in this region.

The average composition of the whole film may now be found by means of the equation

$$\langle N_{a\alpha}\rangle_{Av}=\frac{v_m}{v}\sum_i^\infty \varphi i\langle N_{a\alpha i}\rangle_{Av} \quad (16)$$

where

$$\varphi_i=1-\sum_0^{i-1}s_i/\sum_0^\infty s_i; \qquad (i\geq 1) \quad (16a)$$

and

$$\varphi_1\langle N_{a\alpha 1}\rangle_{Av}=\frac{\theta'}{n}\langle N'_{a\alpha 1}\rangle_{Av}+\left(\frac{\bar{n}-1}{\bar{n}}\right)\theta''\langle N''_{a\alpha 1}\rangle_{Av}. \quad (16b)$$

The evaluation of $\langle N_{a\alpha}\rangle$ will usually be simple because $\langle N_{a\alpha i}/N_{a\beta i}\rangle_{Av}$ will be nearly $N_\alpha/N_\beta(p_{0\beta}/p_{0\alpha})$ for $i\geq 2$. Moreover, Eq. (16b) may be evaluated within reasonably accurate limits by separate unimolecular adsorption isotherms. It remains to express the total isotherm for mixed (binary) adsorption. This may be done simply by the equation

$$v/v_m=\frac{1}{n}\theta'+\frac{n-1}{n}\theta'+\frac{\theta\sum_2^\infty(i-1)\bar{x}^{(i-1)}\lambda_i}{1+\sum_i^\infty\bar{x}^{(i-1)}\lambda_i}, \quad (17)$$

where

$$\lambda_1=\prod_2^i\left\{\frac{N_\alpha p_0}{p_{0\alpha}}\exp\left(\frac{\psi_{i\alpha}-E_{L\alpha}}{RT}\right)+\frac{N_\beta p_0}{p_{0\beta}}\exp\left(\frac{\psi_{i\beta}-E_{L\beta}}{RT}\right)\right\}, \quad (17a)$$

and $\bar{x}=p/p_0$ with p_0 = saturation pressure of the bulk liquid mixture. Here θ' and θ'' may be found by the methods outlined in evaluating the single component adsorbate problem.

Employing values for ψi for N_2 and O_2 determined from the separate N_2 on anatase and O_2 on anatase isotherms in Eq. (13), one finds that $N_{a\alpha i}/N_{a\beta i}$ is essentially the same for all layers for $i\geq 2$. Similarly, $N''_{a\alpha 1}/N''_{a\beta 1}$ is found to be essentially constant and independent of θ''. Under these circumstances Eq. (16) becomes

$$\langle N_{a\alpha}\rangle_{Av}=\frac{\langle N_{a\alpha 1}\rangle_{Av}+N_{a\alpha i}\cdot(v'/v_m\theta)}{1+v^1/v_m\theta} \quad (18)$$

where

$$\langle N_{a\alpha 1}\rangle_{Av}=\frac{(\theta'/\bar{n})N'_{a\alpha 1}+[1-(1/\bar{n})]N''_{a\alpha 1}}{(\theta'/\bar{n})+[1-(1/\bar{n})]\theta''}. \quad (18a)$$

(Here we have neglected the difference in size of the molecules and have taken $\bar{n}=0.6$ since most of the "structural adsorption" will be nitrogen.) Since the "structural adsorption" sites are essentially all filled at $\bar{x}=0.02$, we may very readily calculate the average mole fraction $\langle N_{a\alpha}\rangle_{Av}$ of component α in the adsorbed phase from Eqs. (18) knowing $(v'/v_m\theta)$ as a function of $\bar{x}$. We shall define d_i's for the mixture by $\lambda_i=(d_i/d_1)_{mix}$, and the equation

$$\left(\frac{d_i}{d_1}\right)_{mix}=\exp\left[\left(\frac{E_1}{RT}\right)_{mix}\sum_2^i a/i^3+B_{mix}\sum_2^i 1/i\right]. \quad (19)$$

TABLE II. Comparison of mole fractions of nitrogen (N_α) in gas and adsorbate phases for mixtures of nitrogen and oxygen on anatase (data from Arnold[11]).

					$N_{a\alpha}$(adsorbate)*	
N_α(gas)	x=0.05	0.1	0.3	0.5	0.7	0.9
0.851	0.88	0.86	0.79	0.77	0.73	0.67
0.702	0.81	0.77	0.67	0.61	0.55	0.45
0.498	0.70	0.64	0.53	0.46	0.38	0.30
0.298	0.60	0.53	0.42	0.33	0.26	0.18
0.147	0.48	0.41	0.30	0.24	0.17	0.12

* $N_{a\alpha}$ = mole fraction of nitrogen in the adsorbate.

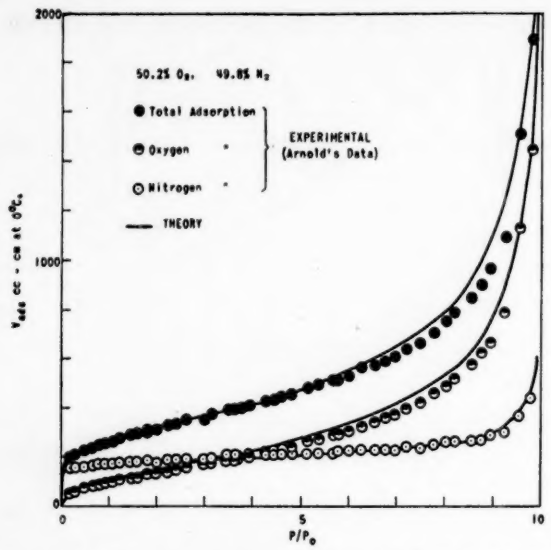

FIG. 4. Comparison of experimental and calculated isotherms for "mixed adsorption" (of nitrogen and oxygen) on anatase.

One may then show that

$$\left(\frac{E_1}{RT}\right)_{\text{mix}}=\frac{\ln\lambda_i-2\ln\lambda_2\sum_2^i 1/i}{\sum_2^i a/i^3-0.25a\sum_2^i 1/i}$$

$$\equiv 14.40[5/3\ln\lambda_2-\ln\lambda_3] \quad (20a)$$

(for $a=1.50$) and

$$B_{\text{mix}}=2\ln\lambda_2-0.25a(E_L/RT)_{\text{mix}}. \quad (20b)$$

This allows one to carry out the calculations to $\bar{x}=1.0$; up to $\bar{x}=0.7$ one could use Eq. (17a) directly. However, Eqs. (20a) and (20b) are more convenient and easier to apply even at low $\bar{x}$. Eq. (17) becomes

$$\frac{v}{v_m}=\left[\frac{1}{n}-\theta'+\frac{n-1}{n}\theta''\right]\frac{\sum_1^\infty i x^i(d_i)_{\text{mix}}}{\sum_1^\infty x^i(d_i)_{\text{mix}}}, \quad (17b)$$

where

$$(d_i)_{\text{mix}}=\exp\left[\left(\frac{E_1}{RT}\right)_{\text{mix}}(1+\sum_2^i a/i^3)+B_{\text{mix}}\sum_1^i 1/i\right]. \quad (17c)$$

TABLE III. Comparison of models with experiment.

Mole fraction nitrogen in gas phase (N)	p/p_0	Average mole fraction nitrogen in adsorbed phase $\langle N_{a\alpha}\rangle_{Av}$: Experimental[a]	'Structural' model	Liquid entropy model[b]	Extended BET model[b]
0.147	0.02	0.54	0.54		
	0.20	0.35	0.33		
	0.50	0.24	0.23		
	0.90	0.12	0.12		
0.298	0.02	0.66	0.71		
	0.20	0.46	0.45		
	0.50	0.33	0.32		
	0.90	0.18	0.19		
0.502	0.02	0.76	0.81	0.71	0.29
	0.20	0.59	0.55	0.48	0.24
	0.50	0.46	0.42	0.38	0.21
	0.90	0.30	0.28	0.26	
0.702	0.02	0.85	0.88		
	0.20	0.72	0.67		
	0.50	0.61	0.55		
	0.90	0.45	0.43		
0.851	0.02	0.92	0.93		
	0.20	0.84	0.79		
	0.50	0.77	0.71		
	0.90	0.67	0.62		

[a] Experimental data of Arnold (see reference 11).
[b] From Arnold (see reference 11).

The value of v_m for the mixtures was evaluated in the usual BET manner. Aside from v_m all the constants used for the isotherms of the mixtures were obtained from the pure N_2 and O_2 isotherms.

Using Arnold's data, the isotherms for a mixture of 49.8 percent nitrogen and 50.2 percent oxygen were calculated by means of the above equation. The results are shown in Fig. 4. A rough comparison of these results with those of the "liquid entropy" model and extended BET model as calculated by Arnold[11] shows a maximum difference between experiment and theory (expressed as mole fraction in adsorbed phase) of 0.05 for the present model, 0.10 for the "liquid entropy" model and at least 0.5 for the extended BET model. (Table III.)

ACKNOWLEDGMENT

The authors wish to thank Dr. P. J. Blatz for presenting this paper at the June 3, 1950, meeting of the Catalysis Club of Philadelphia.

Letters to the Editor

THIS section will accept reports of new work, provided these are terse and contain few figures, and especially few half-tone cuts. The Editorial Board will not hold itself responsible for opinions expressed by the correspondents. Contributions to this section should not exceed 600 words in length and must reach the office of the Managing Editor not later than the 15th of the month preceding that of the issue in which the letter is to appear. No proof will be sent to the authors. The usual publication charge ($8.00 per page) will not be made and no reprints will be furnished free.

Isotopic Exchange Rates as Criteria of Surface Heterogeneity

R. P. EISCHENS
Beacon Laboratories of The Texas Company, Beacon, New York
January 5, 1951

CARBON monoxide, chemisorbed on reduced iron, will exchange with carbon monoxide which is in the gaseous phase.[1] This exchange is being studied by means of radioactive $C^{14}O$. The kinetics of an isotopic exchange can be expressed by the equation[2,3]

$$-\ln(1-X/X_\infty)=Rt(a+b)/ab.$$

In the experiment to be discussed here, X is the fraction of the gaseous phase which is $C^{14}O$ at time, t, X_∞ is the fraction which would be $C^{14}O$ at infinite time, R is the rate of exchange, and a and b are the fractions of the gas in the chemisorbed and gaseous phases, respectively. Physically adsorbed CO is included in the gaseous phase.

Figures 1 and 2 show data obtained by plotting $-\ln(1-X/X_\infty)$ *versus* time for runs at −78°C. Initially, the iron was covered with a monolayer of chemisorbed $C^{14}O$ and the gaseous phase was normal CO at about 1 atmos. The amount of $C^{14}O$ in the gaseous phase was measured continuously.

These data are of interest because they show that the exchange data can be represented by a relatively few straight lines. The percentage of chemisorbed CO involved in the exchange at any time may be calculated from the values of X/X_∞. In Fig. 1, the percentages of chemisorbed CO represented by the straight line portions are O–A, 4 percent; A–B, 43 percent; B–C, 22 percent; C–D, 9 percent. In Fig. 2, the percentages are O–A, 22 percent; A–B, 54 percent; B–D, 8 percent. In Fig. 1 the data end at 78 percent and in Fig. 2 they end at 84 percent. The failure to make measurements past 84 percent is due to the fact that the final rate at −78°C is so slow that inconveniently long times are required to measure small increases. There is no reason to believe that this portion could not be measured.

It is necessary to consider the effect of the separate rates of exchange on each other before the R for any particular portion can be determined. After any of the separate exchanges reaches equilibrium with the gaseous phase, the chemisorbed gas, which is involved in such an equilibrated exchange, will behave as though

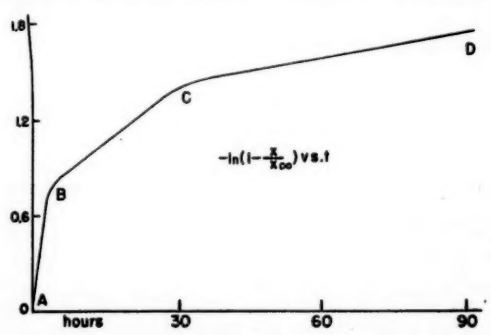

FIG. 1

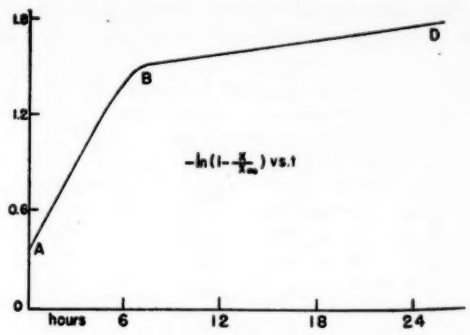

FIG. 2.

it were in the gaseous phase as far as its effect on the slower exchanges is concerned. Thus, in determining the R for any particular section, it is necessary to change the quantities a and b to correct for the effects of the previously equilibrated exchanges. When this factor is taken into account, the rates, relative to the slowest in Fig. 1, are O–A, ∞; A–B, 89; B–C, 7; C–D, 1. In Fig. 2 these values are O–A, ∞; A–B, 60; B–D, 1. The actual R's for the A–B portions in Figs. 1 and 2 are 0.0006/min and 0.0007/min. It should be emphasized that the specific numbers are approximate and are given only to acquaint the reader with the general magnitude of the values. No attempt will be made to discuss the possible reasons for the quantitative differences between the two runs.

A simple explanation of these data is that each rate of exchange is constant over a relatively large portion of the surface because the Fe−CO bonds on this part are equivalent. Each portion may be considered to be homogeneous within itself. However, since the rate of exchange for each portion is different, the surface is heterogeneous from the over-all viewpoint. If the surface were completely heterogeneous, in the sense that there is a gradual transition between the extremes, one would expect the plotted data to give a smooth curve without any straight sections.

[1] J. T. Kummer and P. H. Emmett, *Brookhaven Conference Report, Conference on Isotopic Exchange Reactions and Chemical Kinetics* (December 1–3, 1948).
[2] H. A. C. McKay, Nature **12**, 997 (1938).
[3] R. B. Duffield and M. Calvin, J. Am. Chem. Soc. **68**, 557 (1946).

A Vibrational Analysis of the Fluorescence Spectrum of Formaldehyde

J. C. D. BRAND
The University of Glasgow, Scotland
December 26, 1950

THE ultraviolet fluorescence spectrum of HCHO[1] and DCDO will be shown to develop from two progressions from the upper state to levels in the ground state in which 2, 4···10 and 1, 3···11 quanta of the vibration $\nu_6''(\beta_2)$ are excited. Each band so formed is the origin of a negative progression with the frequency interval ν_2'' and sometimes also of a short positive progression of the same vibration in the excited state (ν_2'). The bands are perpendicular, and some can be shown to be Type B,[2] a result which is probably general. All the important transitions can be assigned, using the vibrations ν_2', ν_2'', and ν_6'', although the nature of the fluorescing levels is not unambiguous. Because the lower state levels involving an even and an odd number of quanta of ν_6'' are, respectively, of species A and B with respect to the rotational sub-group C_2, the spectrum consists of two virtually independent systems, no connecting bands (Type A) being observed. The assignments, vibrational frequencies, and anharmonicity constants are collected in Table I. They are consistent with the infrared

$$\text{HCHO: } \nu=(28312.7-113.2p)+\{(1191.8-11.4p)n_2'-9.4n_2'^2\}$$
$$-(1165.9n_6''-2.3n_6''^2)-(1755.0n_2''-10.3n_2''^2)+6.5n_2''n_6''.$$
$$\text{DCDO: } \nu=(28378-67p)+\{(1173.5+4.1p)n_2'-8n_2'^2\}$$
$$-(937.8n_6''-3.1n_6''^2)-(1713.1n_2''-9.0n_2''^2)+7.0n_2''n_6''.$$
$$p=\begin{cases}1, & \text{if } n_6'' \text{ is odd,}\\ 0, & \text{otherwise.}\end{cases}$$

spectrum and confirm, in particular, the identification of the 1166

TABLE I. Band centers in the fluorescence spectrum of HCHO and DCDO.

Assigt.			HCHO			DCDO		
				Frequency, cm^{-1}			Frequency, cm^{-1}	
n_2'	n_2''	n_6''	Int.	obs	calc	Int.	obs	calc
1	0	0	*a*	29495	29495	*a*	29553	29552
2	0	1	0	29359	29359	0	29715	29715
0	0	0	*a*	28313	28313	*a*	28380	28378
1	0	1	2	28207	28207	3	28550	28553
1	0	2	5	27173*	27173	4	27690	27689
0	0	1		27036	27036	5	27376	27376
0	1	0	1	26569*	26568		—	
1	1	1		26470	26469		—	
1	0	3		—		5	26704	26703
0	0	2	4	25990	25990	6	26515	26515
1	0	4		—		4	25848	25849
0	1	1	6	25297	25298	5	25679	25679
0	0	3	4	24721	24722	7	25524	25525
0	1	2	6	24258	24258	6	24824	24825
0	0	4	10	23687*	23686	9	24675	24676
0	2	1		23579	23580	3	24003*	24000
0	1	3	5	22997	22997	9	23840	23842
0	0	5		—		10	23698	23699
0	2	2	3	22547	22547	3	23154	23154
0	1	4	4	21970*	21967	9	22999	23000
0	3	1		21881*	21883	3	22344*	22339
0	0	6	2	21393*	21400	10	22863	22863
0	2	3		21294	21293		22174*	22177
0	1	5		—		6	22029	22030
0	0	7		—		6	21899	21898
0	3	2		—		2	21499	21499
0	2	4		—		3	21340	21342
0	4	1	0	20207*	20207		—	
0	1	6		—		5	21201	21201
0	0	8	0	19125*	19133	4	21075	21074
0	3	3	1	19613	19609	2	20528	20530
0	2	5		—		2	20375	20379
0	1	7		—		2	20243	20243
0	0	9		—		1	20122	20122
0	2	6		—		0	19552	19557
0	3	5		—		0	18750	18746
0	2	7		—		0	18609	18606
0	1	9		—		0	18479	18481
0	0	11		—		0	18366	18370
0	1	10		—		0	17672	17676

Intensities are visual estimates on a scale of 10. Band centers marked * were overlapped by other transitions. Weak bands were measurable only to within a few cm^{-1}. *a*. Band observed in the absorption spectrum only.

and 938 cm^{-1} frequencies with the ν_6 vibration of HCHO and DCDO, respectively.[3]

$\{\omega_6^{0\prime\prime}(\text{HCHO})/\omega_6^{0\prime\prime}(\text{DCDO})\}^2=1.546$; calc (product rule), 1.569.

On this basis, the symmetry of the complete wave function of the two principal fluorescing levels (which lie at 28378 and 28311 cm^{-1} for DCDO) is, respectively, B_1 and A_2. The assignments do not explain directly the relation of these levels to one another, and no hypothesis regarding them seems entirely free from objection. If the levels are singlet, however, the observation of the β_2 vibration is evidence that at least one of them belongs to an $^1A_2$ state, arising from the $\mathbf{2b_1}\rightarrow\mathbf{2b_2}$ forbidden electronic transition discussed by Mulliken.[4] The appearance of strong bands involving a change by several quanta of the β_2 vibration raises an interesting point. The minimal requirement for an $^1A_1\rightarrow{}^1A_2$ transition in a molecule of C_{2v} symmetry is that it must be accompanied by a one-quantum change of ν_6, because this vibration mixes the $^1A_2$ state with (principally) a higher $^1B_1$ state and thus contributes a non-vanishing component to the transition probability.[5] It is usually assumed that the perturbing vibration will be found to change by one quantum only, greater changes being increasingly forbidden by the Franck-Condon principle. In this spectrum, however, ν_6 changes by up to 10 or 11 quanta, presumably because the square of the amplitude of the vibration determines the coefficient of $\psi(B_1)$ in the expanded wave function for the $^1A_2$ state, and the degree to which the transition thus becomes allowed (i.e., the amount of B_1 character in the A_2 level) increases sufficiently with changes of ν_6 in excess of one quantum to postpone the incursion of the normal Franck-Condon effect, allowing progressions to form in the β_2 vibration. Moreover, the perturbing effect per quantum of this mainly hydrogenic vibrational mode will, because of the relative amplitudes, be larger for HCHO than for DCDO, and the greater development of the ν_6 progression in the latter case can also be accounted for.

I should like to thank Dr. A. G. Gaydon for encouragement and advice.

[1] G. Herzberg and K. Franz, Z. Physik. **76**, 720 (1932); S. Gradstein, Z. physik. Chem. **B22**, 384 (1933); H. Schüler and A. Woeldike, Physik. Z. **44**, 61 (1944).
[2] J. C. D. Brand, Trans. Faraday Soc. **46**, 805 (1950).
[3] E. S. Ebers and H. H. Nielsen, J. Chem. Phys. **6**, 311 (1938); Stevenson, Luvalle, and Shomacher, J. Am. Chem. Soc. **61**, 2508 (1939).
[4] R. S. Mulliken, J. Chem. Phys. **3**, 564 (1935).
[5] G. Herzberg and E. Teller, Z. physik. Chem. **B21**, 410 (1933).

Radiotracer Study of Cationic Surface-Active Agents by Measurement of Gegenion Adsorption

CHARLES M. JUDSON, ANN A. ARGYLE, J. K. DIXON, AND D. J. SALLEY
Stamford Research Laboratories, American Cyanamid Company, Stamford, Connecticut
January 12, 1951

A RADIOTRACER method of measuring the adsorption of a soluble surface active agent at the solution-air interface has been described in reports from this Laboratory.[1-3] Using a soft beta-emitter as a label, the radiation above a solution of a surface active agent is greater than that above a solution in which no surface adsorption occurs. This method, originally used to measure the adsorption of an anionic agent (di-*n*-octyl sodium sulfosuccinate) labelled with S^{35}, has now been extended to the study of cationic agents by measuring the adsorption of radiosulfate gegenions.

Solutions of stearamidopropyldimethyl-2-hydroxyethyl ammonium sulfate (Aerosol SE sulfate) were labelled with tracer amounts of high specific activity $Na_2S^{35}O_4$. The radiosulfate was prepared from irradiated KCl allocated by the U. S. Atomic Energy Commission.

The measured surface adsorption of the sulfate anions increased nearly linearly with the concentration of the cationic agent over the entire range of concentrations measured (Fig. 1). At low concentrations the adsorption was considerably less than that calculated for a monolayer by Gibbs' equation from surface tension measurements (Du Nüoy tensiometer). For example, at a concentration of 5×10^{-5} equiv./liter, which is below the critical micelle concentration but considerably above the point where the monolayer of long-chain ions is supposedly complete, the number of equivalents of sulfate adsorbed was less than one-tenth of the calculated number of equivalents of long-chain ion adsorbed. Evidently, the agent was adsorbed in the form of its hydroxide at low concentrations, with the sulfate replacing hydroxyl as the total concentration was increased. This parallels the previous suggestion[2] that anionic agents may be adsorbed at low concentrations in the form of the acid rather than the salt. At the highest concentration measured, 0.032 equiv./liter, the adsorption of sulfate was about 10 times the long-chain ion adsorption calculated for a monolayer, thus indicating the presence of multilayers.

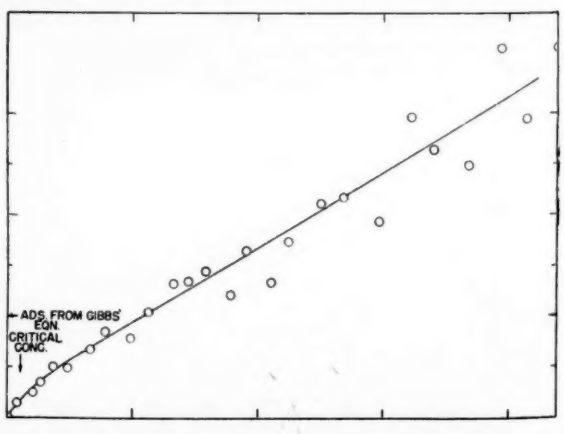

FIG. 1. Adsorption of sulfate from Aerosol SE sulfate solutions.

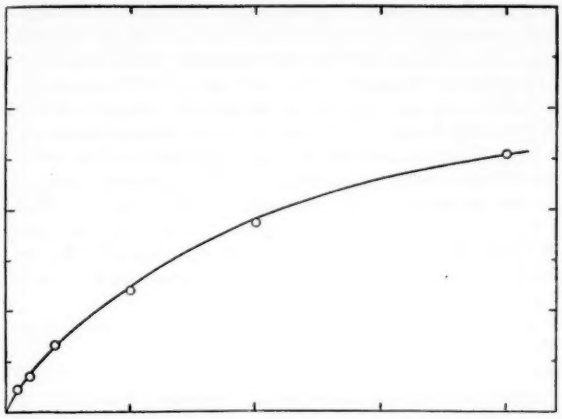

FIG. 2. Adsorption of sulfate from Aerosol SE chloride—Na_2SO_4 solutions (0.001 mole/liter Aerosol SE chloride with varying Na_2SO_4 concentrations).

Measurements made using Hutchinson's[4] radiotracer method of determining adsorption were in qualitative agreement with the above results.

With mixtures of Aerosol SE chloride and $Na_2S^{35}O_4$ at a constant concentration of cationic agent, adsorption of sulfate increased with the sulfate concentration, apparently tending toward a saturation value dependent upon the cation concentration (Fig. 2). Qualitatively similar results were obtained for mixtures of cetyl pyridinium chloride and $Na_2S^{35}O_4$. These results suggest that the sulfate does not completely replace hydroxyl or chloride unless relatively high concentrations of sulfate exist. The assumption made by Reichenberg[5] that the chloride at the surface would be completely displaced by trace amounts of sulfate does not hold for these compounds.

The present results suggest that multilayers of considerable depth may form at the interface in solutions of cationic agents and that the gegenion adsorbed may be, at least in part, the hydroxyl ion rather than the gegenion introduced with the agent. Clearly, the adsorption of the long-chain ions and the adsorption of the gegenions must both be measured in order to obtain a complete picture of the adsorption phenomenon.

[1] Dixon, Weith, Argyle, and Salley, Nature **163**, 845 (1949).
[2] Salley, Weith, Argyle, and Dixon, Proc. Roy. Soc. (London) (A) **203**, 42 (1950).
[3] Judson, Argyle, Salley, and Dixon, J. Chem. Phys. **9**, 1302 (1950).
[4] Hutchinson, J. Colloid Sci. **4**, 599 (1949).
[5] Reichenberg, Trans. Faraday Soc. **43**, 467 (1947).

Note Concerning the Paper on F_2O

ALVIN H. NIELSEN
The University of Tennessee, Knoxville, Tennessee
November 6, 1950

ELSEWHERE[1] in this issue there is published a paper on the infrared spectrum of F_2O. The contents of this paper do not in any way constitute a duplication of a paper by Bernstein and Powling,[2] as the data and assignments in their paper were given by us nearly a year earlier at the June, 1949, Symposium on Molecular Structure at Ohio State University. This paper was cited in a review of the papers presented at this meeting by H. H. Nielsen.[3] Our paper includes grating measurements on the observed bands as well as on two bands not observed by Bernstein and Powling.

The work reported[1] was begun at the K-25 Laboratories in November, 1948, and the measurements were carried on during the winter months. The new data were at variance with those of Hettner, Pohlmann, and Schumacher[4] because of the lack of purity of their sample. It was clear that a new interpretation of the fundamental frequencies other than that of Sutherland and Penney[5] was required. The only reasonable interpretation of the new measurements was to assign the intense bands at 461 cm^{-1}, 831 cm^{-1}, and 928 cm^{-1} as ν_2, ν_3, and ν_1. Although the experimental work was not complete, we reported the new data and the new interpretation at the 1949 Symposium as part of a larger paper on fluorine compounds. While these new results were being prepared for publication, the paper on F_2O[2] by Bernstein and Powling was published in May, 1950. The work published by them was parallel with and independent of our work presented the previous June at the Symposium. As Bernstein and Powling omitted making any reference to our prior discussion and interpretation of these bands, the omission was discussed with Bernstein at the June, 1950, meeting, where we had intended to give a complete discussion of the problem. We informed him that we intended to submit our paper for publication. He concurred that it would be proper and that a statement should be made with regard to our previous report. This letter has, therefore, been written to correct the impression left by their paper as to the priority on the data and interpretation of the spectrum of F_2O.

[1] Jones, Kirby-Smith, Woltz, and Nielsen, J. Chem. Phys. **19**, 337 (1951).
[2] H. J. Bernstein and J. Powling, J. Chem. Phys. **18**, 685 (1950).
[3] H. H. Nielsen, Research **2**, 369 (1949).
[4] Hettner, Pohlmann, and Schumacher, Z. Physik **96**, 203 (1935).
[5] G. B. B. M. Sutherland and W. G. Penney, Proc. Roy. Soc. (London) **156A**, 678 (1936).

Ultraviolet Absorption Spectrum of Gaseous Hydrogen Fluoride

E. SAFARY, J. ROMAND, AND B. VODAR
Laboratoire de Physique (Enseignement) Sorbonne, Paris, France
January 22, 1951

HYDROGEN fluoride gas is known as a strongly associated substance, and it was to be expected that we would find an absorption spectrum entirely different from that of the other hydrogen halides particularly studied by one of us.[1]

The gas, contained in silver or stainless steel cells with aluminium oxide windows and clean "teflon" gaskets mechanically pressed, was studied down to 1500A. The general apparatus has been described elsewhere.[1,2]

We first found that the bands in the near ultraviolet (maxima at $\lambda=2050$A and $\lambda=2800$A, approximately)[2] disappear when the gas is sufficiently pure; from direct and recent experiments, we can say that the responsible impurity is sulfur dioxide, SO_2. Then, in our experimental conditions there are no other bands down to 1650A, where a continuous absorption starts. Figure 1 shows the absorption curves A, B, C, and D obtained for temperatures of 16.5°C, 53°C, 100°C, and 165°C. We have plotted the logarithm of the molecular extinction coefficient $\epsilon=(d/l)\times 22.4\times(M/M_1)$ against the wave number ν; d being the optical density, l the path length (5.8 cm), M the normal molecular mass (No. 20), and M_1 the apparent molecular mass in the experimental conditions. Because of the weakness of the absorption, the pressure was kept constant at the maximum value (about 640 mm Hg). Curves C and D have a maximum for $\nu=62.000$ cm^{-1} of approximately (λ No. 1612A).

In correlation with this we have recently begun the study of the absorption spectrum of liquid hydrogen fluoride. In spite of the preliminary character of our actual results, we can say that the liquid, having a 10-mm path length, is approximately transparent down to 2.200A (limit of our measurements); there are only some fluctuations, their optical density remaining $\leqslant 0.3$.

It is difficult to attempt an interpretation of these results, but we can make the following remarks.

The fact that there are no discrete bands in the whole spectrum down to 1500A for the gas and to 2200A for the liquid is a good reason to think that there are no, or very few, cyclic F_6H_6 molecules in the associated vapor and in the liquid. This supports the conclusions obtained from other measurements, such as those of dielectric constants.[3]

On the other hand, the increase of absorption when the gas is heated shows clearly the effect of association. From the density measurements,[4,5] it is known that there is no possibility of existence for stable associated molecules above approximately 100°C. Therefore, we can make, provisionally, the assumption that the

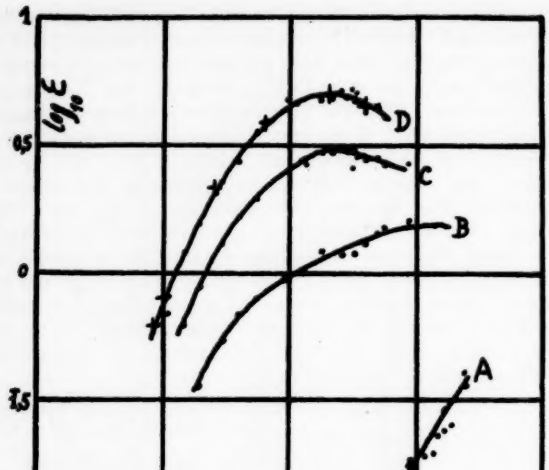

FIG. 1. Logarithm of the molecular extinction coefficient *vs* the wave number for temperatures of 16.5°C (A), 53°C (B), 100°C (C), and 165°C (D).

curves for the highest temperatures (C and D) represent the absorption of the monomer $(FH)^1$, while the curve A would represent the absorption of the associated molecule $(FH)_n$. With this assumption, some remarks can be made. (1) There is no discontinuous spectrum, contrary to the conclusions drawn from the theoretical potential energy curves,[6] whose calculation should be done again. (2) The spectrum limit on the long wavelength side seems in good agreement with the dissociation energy value given by Gaydon,[7] $E_d=6.1\pm0.3$ ev No. 49.200±2.400 cm^{-1}. (3) The reflection method[8] applied to $(FH)_1$ gives good results (dot+for curve D).

However, this assumption is not entirely satisfactory; indeed, the explanation of the spectrum variations above 100°C is difficult because of the high value of the vibrational frequency ($\omega_e=4141$ cm^{-1}). An alternative possible explanation would take into consideration an interaction between two weakly bound FH molecules, this perturbation existing even at temperatures where the density is normal. The potential energy curve would have a very flat minimum, the corresponding vibrational energies being so low that the temperature effect is noticeable, even for our weak increase of temperature. In conclusion, it may be said that it is necessary to work at higher temperatures.

[1] J. Romand, Ann. phys. **4**, 529 (1949).
[2] E. Safary and J. Romand, Compt rend. **229**, 1003 (1949).
[3] H. A. Benesi and C. P. Smyth, J. Chem. Phys. **15**, 337 (1947).
[4] J. Simons and J. H. Hildebrand, J. Am. Chem. Soc. **46**, 2179, 2183 (1924).
[5] Long, Hildebrand, and Morrell, J. Am. Chem. Soc. **65**, 182 (1943).
[6] L. Pauling, *The Nature of the Chemical Bond* (New York, 1948), p. 43.
[7] *Dissociation Energies and Spectra of Diatomic Molecules* (London, England, 1947), p. 188.
[8] J. Romand, Ann. phys. **4**, 576 (1949).

A Reply to a Letter to the Editor Entitled, "Concerning the Steric Factor of Free Radical Reactions" by Gomer and Dorfman

MICHAEL SZWARC
Department of Chemistry, University of Manchester, Manchester, England
December 20, 1950

I HAVE to make the following comments in reply to the Letter by Gomer and Dorfman.[1]

I do not think that there is any real discrepancy between our statement and the statement by the above authors. Our intention was to emphasize the fact that the behavior of radicals in chemical processes is "normal"; i.e., the rates of their reactions are governed by the same factors as the rates of reactions involving molecules only. Hence, we should not expect that the temperature independent factors for the reactions involving radicals would be much different from those which involve molecules only. This point was stressed in the summary of the paper by Roberts and myself when we said ". . . steric factors of this reaction $(CH_3C_6H_5\cdot CH_3)$ as well as that of the reaction $CH_3CH_3C_2H_6$ is 'normal,' i.e., *the collision frequency of these reactions is of the order* 10^{11}–10^{12} *cc/sec moles.*"

It is most unfortunate that the whole discussion shifted the emphasis to the "steric factors" when the real point of issue is connected with the collision frequency. I admit that the title of our paper with Roberts added to the confusion. It was stressed in the paper by Evans and myself[2] that the P factors are based on the Z and the latter value is uncertain, since it depends on the type of interaction which is investigated. If one calculates Z on the basis of $\sigma=5$A or 10A one *must* get lower values for the P factor.

In our calculations, the value 10^{12} was chosen arbitrarily, and s was *defined* by $k=s\cdot10^{12}\exp(-E/RT)$. The purpose was to calculate the temperature independent factor, which came out at 10^{11}–10^{12} cc/sec moles; i.e., it is of the order which would be expected for a reaction involving molecules of similar complexity. This is the essential point which was pointed out by Evans and myself.

The discrepancy between our finding and those of Steacie and his colleagues is due to a different estimation of activation energies. This makes the PZ factor in our estimates higher than that obtained by Steacie by a factor of about 60. The problem of activation energy of these reactions is again under investigation in our laboratories.

[1] Gomer and Dorfman, J. Chem. Phys. **19**, 136 (1951).
[2] M. G. Evans and M. Szwarc, Trans. Faraday Soc. **45**, 941 (1949).

Isotope Effect in Hydrocarbon Flame Spectra*

GEORGE M. MURPHY AND L. SCHOEN
Research Division, University Heights and Chemistry Laboratories of Washington Square College, New York University, New York, New York
January 18, 1951

THE spectra of the low pressure flame of atomic oxygen and deuterated acetylene (C_2D_2) have been photographed (Fig. 1) in the first and second orders of a Jarrell-Ash three meter grating spectrograph using type 103 *a-o* Eastman film. Comparison with the spectra of the normal acetylene flame recorded under similar conditions leads to an isotopic displacement in those bands caused by hydrogen containing molecules from which it is theoretically possible to obtain information concerning the identity and structure of the emitter.

The experimental arrangement was somewhat similar to that employed by Geib and Vaidya.[1] Deuterated acetylene was prepared by means of the reaction between heavy water (99.8 percent) and calcium carbide of high purity.[2] Oxygen atoms were obtained from a water cooled discharge tube operated at several thousand volts and carrying a current of about 650 milliamperes. The reaction with acetylene was carried out in a Pyrex glass chamber fitted with quartz windows and maintained at a total

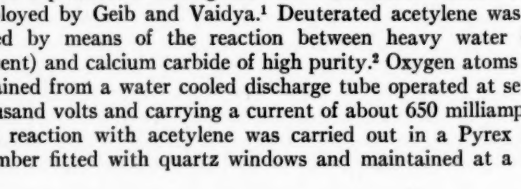

FIG. 1. Spectra of the low pressure flame of atomic oxygen and (a) dideutero acetylene and (b) acetylene.

pressure of about one millimeter. Several wire grids placed between the reaction vessel and the liquid nitrogen trap served to prevent ignition of the explosive material in the condensate.

A reproduction of the first order spectra in the region 2800–4050A is shown in the accompanying figure, where the results for both deuterated and normal acetylene appear. Bands of CD, CH and OD, OH molecules form the most prominent features of the photograph in addition to which appear the hydrocarbon flame bands of Vaidya[3] which have been tentatively attributed to the HCO radical.[4,5]

It had been our purpose to test the validity of the assignment of HCO as the emitter by measuring the magnitudes of the isotopic shifts in the vibrational bands of this system. As may be seen from Fig. 1, however, the hydrocarbon flame bands in the spectra of the C_2D_2 flame, besides being badly overlapped and somewhat more diffuse than their C_2H_2 counterparts, are disposed in such an irregular fashion that the matching of corresponding bands of the two systems is far from obvious.[6] The occurrence of a definite shift, however, does provide conclusive evidence that one or more hydrogen atoms are involved in the structure of the emitter.

* The work described in this paper was done with the support of the Office of Naval Research, Department of the Navy, and the Office of Air Research, Department of the Air Force, under Contract N6ori-11, Task Order 2, as part of Project Squid.

[1] K. H. Geib and W. M. Vaidya, Proc. Roy. Soc. (London) **A178**, 351 (1941).

[2] Supplied through the courtesy of R. J. Niebanck of the National Carbide Corporation.

[3] W. M. Vaidya, Proc. Roy. Soc. (London) **A147**, 513 (1934).

[4] A. G. Gaydon, *Spectroscopy and Combustion Theory* (Chapman & Hall, London, 1948).

[5] Herman, Hornbeck, and Laidler, Science **112**, 417 (1950).

[6] We have recently been informed by Drs. R. C. Herman and G. A. Hornbeck of the Applied Physics Laboratory, Johns Hopkins University, that they have obtained photographs, under high dispersion, of an oxygen-deuterated acetylene flame burning at atmospheric pressure, using a large excess of oxygen or employing CO_2 as a diluent. Under their conditions, the diatomic spectra in this region are highly suppressed. However, the nature of the shift is similar and appears to be of extreme complexity.

The Thermal Decomposition of Nitromethane*

L. J. Hillenbrand, Jr., and Mary L. Kilpatrick
Department of Chemistry, Illinois Institute of Technology, Chicago, Illinois

January 5, 1951

Cottrell and Reid[1] have recently reported the results of a study of the thermal decomposition of nitromethane, carried out by the static method. We have made a study of the reaction using the flow method, with nitrogen as carrier gas, and have obtained results in general agreement with those of Cottrell and Reid.

Two modes of introducing nitromethane into the unit were employed by us: saturation of the nitrogen with nitromethane, and injection of nitromethane from a motor-driven syringe into the nitrogen stream. After mixing, the gases passed at atmospheric pressure through the reactor, a long tube of Pyrex glass packed with Pyrex beads and set in a furnace maintained at a selected temperature between 420 and 480°C. The effluent was analyzed polarographically for nitromethane. When carefully dried nitrogen was used, the rate of disappearance of nitromethane became erratic. The erraticalness is believed to be caused by secondary reactions taking place in the outlet tube between the furnace and the cold trap, where a resinous deposit accumulated. It was found possible to inhibit the secondary reactions and obtain reproducible results by passing wet nitrogen through the unit before the kinetic run.

The decomposition was found to follow the first-order law, the same specific rate being obtained with mole fractions of nitromethane of 0.06, 0.12, and 0.18. Experiments were carried out at seven temperatures between 420 and 480°C. The results may be represented by the equation

$$k = 10^{13.61} e^{-50,600/RT}$$

as compared with the equation

$$k = 10^{14.36} e^{-52,700/RT}$$

Table I. The thermal decomposition of nitromethane at 420°C.

Investigators	Method	Initial pressure, mm Hg CH_3NO_2	Initial pressure, mm Hg N_2	k sec^{-1}
Cottrell and Reid	Static	200 to 350	0	0.0053
Taylor and Vesselovsky	Static	27 to 198	0	0.0034*
Present	Flow	45 and 135	700 and 610	0.0048

* Calculated from the average value of the quarter-life.

given by Cottrell and Reid. To facilitate comparison of results, the values of the specific rate at 420° are shown in Table I; this temperature is common to the investigations of Cottrell and Reid, Taylor and Vesselovsky,[2] and the writers. The specific rate obtained by the flow method is intermediate between the two values obtained by the static method and is considerably closer to that of Cottrell and Reid than it is to that of Taylor and Vesselovsky.

Cottrell and Reid suggest that the initial step in the decomposition is the fission of the C–N bond, of energy 52–53 kcal, which is the value they found for the energy of activation and is also the value of $\Delta H_{298}°$ for the reaction

$$CH_3NO_2(g) \rightarrow CH_3(g) + NO_2(g)$$

as calculated from the heats of formation, using

$$\Delta H_f(CH_3NO_2) = -12.2,^3$$
$$\Delta H_f(CH_3) = 32.0,^4$$
$$\Delta H_f(NO_2) = 8.1^4 \text{ in kcal/mole.}$$

If the values chosen by Szwarc[5] for the two latter quantities are employed, namely, 31±1 and 7.4 kcal/mole, $\Delta H_{298}°$ is lower by one or two kilocalories.

The results of the present investigation thus support the suggestion of Cottrell and Reid that the first and rate-determining step in the thermal decomposition of nitromethane is the fission of the C–N bond. The details of the investigation will be reported later.

* Work done under contract with the ONR, Research Contract N7onr-329, Task Order III.

[1] T. L. Cottrell and T. J. Reid, J. Chem. Phys. **18**, 1306 (1950).

[2] H. A. Taylor and V. V. Vesselovsky, J. Phys. Chem. **39**, 1095 (1935).

[3] D. E. Holcomb and C. L. Dorsey, Ind. Eng. Chem. **41**, 2788 (1949).

[4] *Tables of Selected Values of Chemical Thermodynamic Properties* (National Bureau of Standards, 1949).

[5] M. Szwarc, Chem. Rev. **47**, 75 (1950).

Kinetics of the Ammonia-Deuterium Exchange by a Microwave Method

Joseph Weber* and Keith J. Laidler
U. S. Naval Ordnance Laboratory, White Oak, Maryland, The Catholic University of America, Washington, D. C.

January 11, 1951

The surface exchange reaction between ammonia and deuterium has been interpreted on the basis of two different types of mechanism. In the first, the Langmuir-Hinshelwood mechanism,[1] the ammonia and deuterium are adsorbed on neighboring sites, while in the second, the Rideal mechanism,[2] only one of the molecules is adsorbed, exchange taking place between an adsorbed molecule and a gaseous one. The rate laws corresponding to these two mechanisms have been formulated and compared,[3] and it has been pointed out that a study of the variation of rate with ammonia and deuterium pressure enables a decision to be made as to the mechanism involved.

We have accordingly made such a study, using a singly promoted iron catalyst (#631) kindly supplied by Dr. P. H. Emmett. The rate of disappearance of NH_3 was followed using microwave spectroscopy; samples were taken from the reaction vessel, the ammonias frozen out in a cold trap, the hydrogen was pumped off, and the mixture of ammonias allowed to enter a wave guide. The collision diameter of NH_3 in a mixture of deuterated ammonias was measured, and this value, together with the absorption coefficient of the mixture at the center of the 3-3 line of the ammonia inversion spectrum, enables the mole fraction of ammonia to be determined.

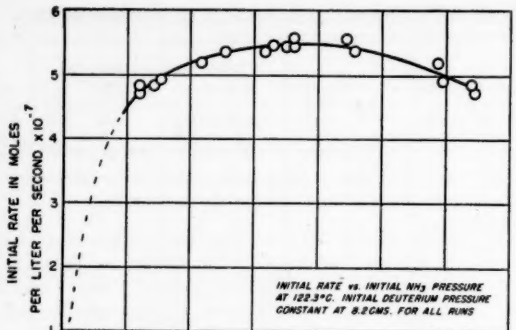
INITIAL RATE IN MOLES PER LITER PER SECOND x 10⁻⁷
INITIAL NH₃ PRESSURE (CM OF HG)
INITIAL RATE vs. INITIAL NH₃ PRESSURE AT 122.3°C. INITIAL DEUTERIUM PRESSURE CONSTANT AT 8.2 CMS. FOR ALL RUNS

FIG. 1.

Farkas[4] has reported that on a pure iron catalyst the rate of exchange is proportional to $p_{D_2}^{\frac{1}{2}}$ and is independent of p_{NH_3}. We have confirmed the $p_{D_2}^{\frac{1}{2}}$ law at deuterium pressures to 150 mm, but find a greater dependence at higher ones, the dependence above 300 mm being almost exactly linear. With regard to the variation with p_{NH_3}, we find only a small change over a fivefold pressure range, as observed by Farkas, but a careful study revealed a well defined maximum. This has been confirmed at three temperatures from 122°C to 164°C; the results at 122.3°C are shown in Fig. 1. The maximum moves in the direction of lower pressures as the temperature is raised. At the highest pressures investigated the activation energy is ~13 kcal.

The falling-off of the rate at higher ammonia pressures was found to be entirely reproducible, and is considered by us to indicate that the mechanism is not of the Rideal-Eley type, since only if both species are adsorbed is the falling-off to be expected. Reaction must, therefore, involve the interaction between adsorbed species. The deuterium is adsorbed atomically, and the square root law implies that only one deuterium atom goes into the activated state. At higher deuterium pressures, however, when the rate varies as p_{D_2}, the activated state apparently involves two deuterium atoms.

A full account of the experimental procedure and results with a detailed kinetic discussion is being prepared for publication in the near future.

* Now at University of Maryland, College Park, Maryland, Electrical Engineering Department.

[1] I. Langmuir, Trans. Faraday Soc. **17**, 621 (1921); C. N. Hinshelwood, *Kinetics of Chemical Change* (Oxford University Press, New York, 1926), p. 145; p. 187 (1940).

[2] E. K. Rideal, Proc. Camb. Phil. Soc. **35**, 130 (1939); Chem. and Ind. **62**, 335 (1943); compare also D. D. Eley, in *Advances in Catalysis* (Academic Press, New York), p. 157; Quart. Revs. **3**, 209 (1949).

[3] K. J. Laidler, *Chemical Kinetics* (McGraw-Hill Book Company, Inc., New York, 1950), pp. 162–166.

[4] A. Farkas, Trans. Faraday Soc. **32**, 416 (1936).

Infrared and Raman Spectra of Vinylidene Cyanide

M. L. DANNIS AND J. J. SHIPMAN
The B. F. Goodrich Research Center, Brecksville, Ohio
November 9, 1950

VINYLIDENE cyanide is a recently synthesized vinyl monomer of a very reactive nature.[1] The infrared and Raman spectra of vinylidene cyanide were obtained in the general study of its properties, because this material is of interest, due to its similarity to the other polymerizable vinyls, and also because of its differences.

The infrared spectrum was obtained on a Perkin-Elmer spectrometer with a NaCl prism. The Raman spectrum was obtained on a spectrometer similar to that described by M. R. Fenske,[2] modified to use pen recording rather than photographic.

TABLE I. Spectra and vibrational frequencies of vinylidene cyanide.

Line No.	Infrared spectrum Wavelength (microns)	Relative intensity	ν cm^{-1}	Raman spectrum $\Delta\nu$ (from Hg 4358)	Relative intensity
1				210	10
2				340	?
3				390	5
4				420	?
5				460	3
6				510	5
7				670	20
8	13.85	50	722	720	?
9	13.20		758	775	20
10	11.75	30	852	820	15
11	11.20		894	880	7
12	10.6	50	940		
13	10.1	90	990	970	7
14				1020	10
15	9.2		1090	1060	5
16				1140	7
17	8.15		1225		
18	7.97	60	1250	1290	15
19	7.4		1350	1350	?
20	7.22	80	1385	1380	?
21	6.85		1460	1440	60
22	6.70		1510		
23	6.55		1530		
24	6.45		1550		
25	6.33		1580	1570	5
26	6.13		1630	1630	70
27	5.95	10	1680		
28	5.4		1850		
29	5.3		1880		
30	5.1	50	1960		
31				2050	?
32				2210	15
33	4.45	45	2250	2260	100
34	4.42	20	2370		
35	3.9		2560		
36	3.8		2640		
37	3.5		2850		
38				2980	7
39	3.22		3110		
40	3.20	60	3120		
41	3.10	60	3200		
42	2.85	10	3500		

The spectra presented in Table I were obtained on the liquid at room temperature. The fundamental frequencies have not been assigned in a satisfactory manner as yet, but it is believed that further study on the vapor state will permit that assignment.

[1] A. Ardis, *et al.*, J. Am. Chem. Soc. **72**, 1305 (1950).

[2] M. R. Fenske, *et al.*, Anal. Chem. **19**, 700 (1947).

Carrier-Free Radioisotopes from Cyclotron Targets XV. Preparation and Isolation of Mn^{52} from Chromium*

HERMAN R. HAYMOND, WARREN M. GARRISON, AND JOSEPH G. HAMILTON
Crocker Laboratory, Radiation Laboratory, and Divisions of Medical Physics, Experimental Medicine, and Radiology; University of California, Berkeley, and San Francisco, California
December 4, 1950

DEUTERON bombardment of chromium produces[1] three radioisotopes of manganese (46-min Mn^{51}, 6.5-day Mn^{52} and 21-min Mn^{52}, and 310-day Mn^{54}) by (d, n) and $(d, 2n)$ reaction. This paper describes a radiochemical procedure used in isolating carrier-free radio-manganese (6.5-day Mn^{52}) from a chromium target which had been bombarded with 19-Mev deuterons in the 60-in. cyclotron at Crocker Laboratory. The Mn^{51} and Mn^{52m} had decayed prior to chemical separation. The 310-day period of Mn^{54} was not observed, presumably due to the low abundance of $Cr^{53,54}$. Other possible concurrent reactions include the formation of radio-vanadium by (d, α) reaction and radio-titanium by $(d, \alpha p)$ reaction. A quantitative separation from vanadium is obtained with the procedure described here. Radio-titanium, Ti^{51}, was not detected.

Spectrographically pure[2] chromium powder, supported on a water-cooled aluminum target plate by 0.25-mil platinum foil, was bombarded for 20 μa-hr at a beam intensity of 10 μa. After bombardment, the chromium powder (approx. 1 g) was dissolved in a minimum volume of 12*N* hydrochloric acid, and the resultant solution was evaporated to incipient dryness. Twenty milligrams

of ferric chloride were added, and the chromic chloride containing the carrier-free radio-manganese was redissolved in 50 ml of 1*N* hydrochloric acid. This solution was then added with stirring to 200 ml of 2.5*N* sodium hydroxide solution previously saturated with bromine. Under the conditions, the carrier-free radio-manganese, presumably in the quadritetrapositive state, is quantitatively carried on the ferric hydroxide precipitate.[3] Chromium and vanadium are retained in the supernatant. Two additional reprecipitations were made to insure complete separation. The ferric hydroxide was washed, dissolved in 6*N* hydrochloric acid, and iron was extracted with ethyl ether. The solution of carrier-free radio-manganese in 6*N* hydrochloric acid was evaporated to dryness after the addition of 5 ml of isotonic saline solution. The activity dissolved quantitatively with the addition of 5 ml of water.

The decay curve was followed for eight half-lives and showed a single period of 6.2 days which agrees closely with the reported[4] value for Mn^{52}. Absorption measurements in aluminum showed the assigned[5] 0.6-Mev positron. The activity was further identified by chemical separations using manganese, chromium, vanadium, and titanium carriers. Over 99 percent of a sample of the activity was recovered in the manganese fraction.

We wish to thank Mr. T. Putnam, Mr. G. B. Rossi, and the crew of the 60-in. cyclotron for bombardments, and Professor G. T. Seaborg for his continued interest in this work.

* This document is based on work performed under Contract No. W-7405-eng-48-A for the AEC.

[1] G. T. Seaborg and I. Perlman, Revs. Modern Phys. **20**, 585 (1948).
[2] Manganese was not detected by spectrographic analysis.
[3] Maxwell, Gile, Garrison, and Hamilton, J. Chem. Phys. **17**, 1340 (1949).
[4] J. J. Livingood and G. T. Seaborg, Phys. Rev. **54**, 391 (1938).
[5] W. C. Peacock and M. Deutsch, Phys. Rev. **69**, 306 (1946).

Evidence of Nuclear Transmutation in the Course of Explosion of Shaped Charges with Lined Cavity

ZYGMUNT FONBERG
Los Angeles, California
June 9, 1950

THE appearance of electromagnetic radiation, generally at the range of x-rays, during chemical reactions, when the chemical compound entering the reaction contains hydrogen, has been observed by several research workers and the author of this short note. This effect appears particularly during detonation of a mixture of hydrogen and air and of gaseous hydrocarbons in mixture with air or oxygen.

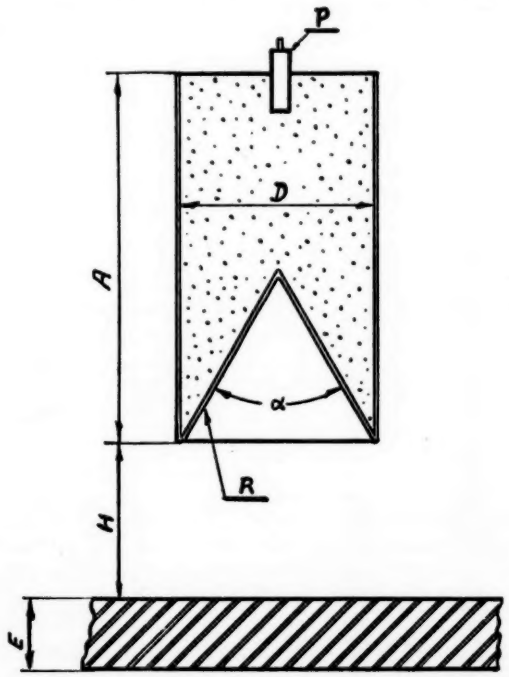

FIG. 1. *A*—20 to 30 cm, *D*—6 to 15 cm, α—20° to 90°, *H*—0 to 30 cm, *E*—2 to 20 cm, *P*—detonator, *R*—retainer.

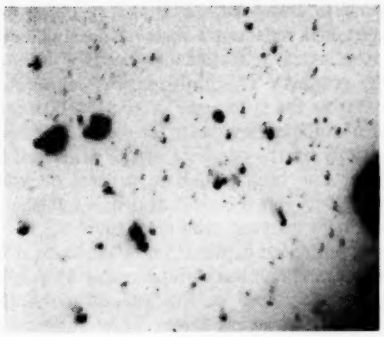

FIG. 2. Impression made by intensive radioactivity, probably from isotope Ag^{108}, immediately after the exposure of the sample to the action of shaped charge composed from ammonium nitrate (60 percent) and nitroglicerin (40 percent). Cavity lined with brass sheet 0.1 mm thick. Weight of charge approximately 2.2 lb, diameter 10 cm. Sample located 20 cm from the charge.

During the detonation of shaped charges composed of certain nitro compounds, with lined cavity, the radiation phenomenon seems to be intensified to the extent that evidence of nuclear transmutation has been observed. Metal plates of silver, copper, zinc, and iron have been exposed to the action of shaped charges (see Fig. 1). The exposure of a remaining splinter to a Geiger-Müller Counter indicated an increase in radioactivity, especially in the case of silver, giving strong indication that due to the explosion, isotope Ag^{108} has been formed.

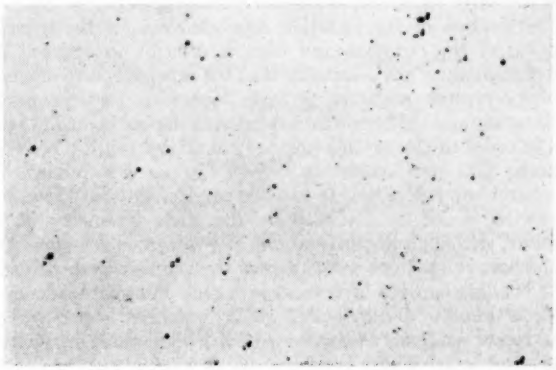

FIG. 3. Impression made by exposure of splinters after action of shaped charge. Time of exposure was 24 hr. Condition of experiment similar to case of Fig. 2.

Splinters of different metals have been superimposed on photographic plate, which was insulated from them by a layer of paper about 0.1 mm thick, and in nearly every case evidence of radioactivity has been observed (Figs. 2 and 3). Experiments have been repeated several hundred times. So far no quantitative measurements have been made.

The observed effect is difficult to explain due to the apparent insufficient energy of electromagnetic waves generated during the explosion.

On the Possible Identity of Rhombohedral and Orthorhombic Graphite

JOSEPH S. LUKESH
Knolls Atomic Power Laboratory, General Electric Company, Schenectady, New York*
January 5, 1951

IN a recent contribution[1] the writer has discussed x-ray evidence for the existence of an orthorhombic superstructure in

graphite. No mention was made at that time of a possible relation between the satellite reflections observed in single-crystal photographs and the extra reflections frequently found in powder photographs of graphite. This omission was deliberate, based on a desire to emphasize the symmetry of the satellite reflections and also on a lack of sufficient evidence for complete understanding of the causes underlying the presence of the satellites. Lately, however, the writer has been asked on several occasions about a possible relation between the two; and it is felt the subject is of sufficient interest to warrant brief discussion.

The presently accepted explanation of the extra reflections seen in powder photographs is that of Lipson and Stokes,[2] who showed that they could be indexed on the basis of a rhombohedral cell three normal graphite layers thick. They suggested a stacking sequence in which the layers followed *ABCABC . . .* rather than *ABAB. . . .* The evidence on which they base their conclusions seems adequate and the structural relations logical. However, the discovery of the satellite reflections suggests an identity between them and the rhombohedral lines. The latter could be superstructure reflections not yet found on single crystal photographs, possibly on levels unattainable with radiations so far used. No attempt has been made, as yet, to assign orthorhombic indices to the rhombohedral reflections. To do so would be of little value in the present discussion, since the complexity of the supercell ($a_0=4.254kx$, $b_0=36.840kx$, $c_0=6.696kx$) results in such a large choice of possible indices that undoubtedly fortuitous agreement could be found for all. That the superstructure reflections could not be due to the rhombohedral form is clear from their twofold distribution.

A further point of interest is the report by Taylor and Laidler[3] that the extra reflections of powder photographs can be removed by purification of the material. A mechanism for the selective removal of the rhombohedral form is difficult to deduce. The writer mentioned[1] the possibility that the superstructure observed in single crystals might result from impurities. Experiments on purification and deliberate introduction of impurities are in progress in order to clarify this point. Preliminary results, however, indicate that purification at ~3000°C does not remove the superstructure reflections. It must be emphasized that location of impurities would be governed by the basic symmetry of the graphite. Although impurity atoms often degrade the symmetry of the host crystal, one would expect that, in a crystal with such loose bonding between layers and with such a normal tendency to twin, as graphite displays, an impurity stabilized superstructure would occur randomly associated with each of the three hexagonally equivalent axes. Thus, every hexagonally equivalent reflection should have satellite reflections associated with it. Since this has never been observed, it seems reasonable to conclude that the orthorhombic character is inherent in the graphite structure, possibly as a result of a localization of a bond of order one-half.[1,4] Observations of twinning[1] also support this view.

* The Knolls Atomic Power Laboratory is operated by the General Electric Company for the AEC. The work reported here was carried out under Contract No. W-31-109 Eng-52.

[1] Joseph S. Lukesh, Phys. Rev. **80**, 226 (1950).
[2] H. Lipson and A. R. Stokes, Proc. Roy. Soc. (London) **A181**, 101 (1943).
[3] A. Taylor and D. Laidler, Nature **146**, 130 (1940).
[4] Linus Pauling, Proc. Roy. Soc. (London) **A196**, 23 (1949).

Infrared Spectrum of Stibine

D. C. SMITH
Naval Research Laboratory, Washington, D. C.
January 2, 1951

COLD dilute H_2SO_4 was dropped from a burette into an evacuated flask containing lathe turnings of 20 percent Sb–80 percent Zn alloy. There was generated a 2.7 percent concentration of stibine (SbH_3) in hydrogen which was passed through a calcium chloride drying tube into a 10-cm evacuated absorption cell (with NaCl windows) to a total pressure of about 830 mm Hg.

Two strong regions of absorption between 2 and 15 mμ were found (Fig. 1) using a spectrometer[1] equipped with NaCl prism.

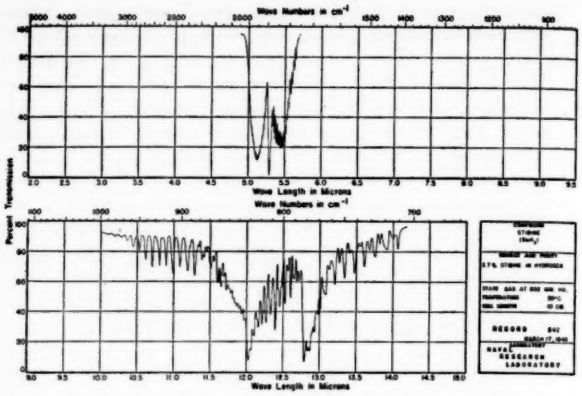

FIG. 1. Infrared absorption of stibine (NaCl prism).

The first has the appearance of a parallel band with strong Q branch at 1890 cm^{-1}, but is probably a superposition of $\nu_1(A_1)$ upon a weaker perpendicular band $\nu_3(E)$, both of which are stretching vibrations. The second region extends from about 700 to 1000 cm^{-1}, with the strongest maxima occurring at 781.5 and 831 cm^{-1}, and evidently consists of overlapping bands corresponding to the two bending vibrations $\nu_2(A_1)$ and $\nu_4(E)$. The positions of all observed maxima (unresolved "shoulders" not included) are listed in Table I.

If it is assumed that the rotational lines in the higher frequency band are those of ν_1, a plot of the equation

$$R(J-1)+P(J)=2J^2(B'-B'')+2\nu$$

yields tentative values of 1893.1±0.5 cm^{-1} for ν_1, and −0.024 cm^{-1} for $(B'-B'')$. Values of the order of 24.5 cm^{-1} are obtained for B' and B'' by similar well-known equations.

These preliminary results on stibine indicate the necessity for more accurate measurements under higher resolution. If such measurements were made, it might be possible to identify the individual lines of the higher perpendicular band and to treat the vibration-rotation problem in detail.

Stibine should be handled with caution and without undue delay, since it is both toxic and chemically unstable. When placed in a new, clean, Pyrex cell the concentration of stibine in the

TABLE I. Observed absorption maxima of stibine.

10–14 mμ region (cm^{-1})		5–6 mμ region (cm^{-1})	
710	822	1772	1874
714	826	1778	*Q* 1890
718	829	1785	1906
723	831	1792	1912
727	835	1798	1918
731	838	1806	1923
734	840	1812	1929
738	842	1818	1935
742	846	1825	1941
746	848	1830	1945
750	853	1837	1952
753	855	1843	1957
757	858	1848	1961
761	860	1855	1966
764	862	1861	1971
769	865	1868	1977
770	868		1982
773	869		
777	873		
779	875		
781.5	878		
786	881		
788	883		
789	886		
791	891		
793	893		
796	902		
798	910		
801	918		
803	928		
807	934		
811	942		
814	950		
818	958		

original sample decreased to half its initial value in slightly over five days, with deposition of antimony upon the cell walls and windows. When the cell was filled a second time (without cleaning), the concentration decreased to half its original value in less than three days.

[1] Nielsen, Crawford, and Smith, J. Opt. Soc. Am. **37**, 296 (1947).

Markoff Chains and Chain Molecules

KEIZO SUZUKI
Masaoka, Toyokawa, Aichi, Japan
August 29, 1950

MONTROLL has treated the volume effect of polymer chains as a problem of Markoff chains;[1] but the use of transition probability is doubtful to me. An example of this doubt will be shown below.

Take a Montroll's model molecule which lies on a square lattice and bends rectangularly at every junction. Any pair of monomers of the polymer is forbidden to occupy the same lattice point unless the monomers are linked by more than 11 bonds. If we take up 2 consecutive bonds as a unit, no trouble will occur; but if we take up more than 3 bonds as a unit, some false results will be given. The 3-bond unit has two forms, *cis*-form, C, and *trans*-form, T (Figs. 1 and 2). Each form has its mirror image. If ith unit is C-form, $(i+1)$th unit can take a C-form and two T-forms (Fig. 3). If ith is T, $(i+1)$th can take two C and three T (Fig. 4).

FIG. 1.

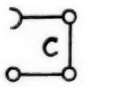

FIG. 2.

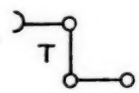

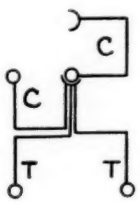

FIG. 3.

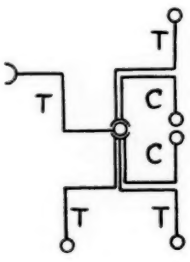

FIG. 4.

Then the matrix p of transition probability must be written as

$$P=\begin{pmatrix} p_{CC} & p_{CT} \\ p_{TC} & p_{TT} \end{pmatrix}=\begin{pmatrix} \frac{1}{3} & \frac{2}{5} \\ \frac{2}{3} & \frac{3}{5} \end{pmatrix}.$$

Let q_{iC}, q_{iT} be the probability that the ith unit takes the C-form or T-form, respectively; then we have

$$\begin{pmatrix} q_{iC} \\ q_{iT} \end{pmatrix}=P^i\begin{pmatrix} q_{0C} \\ q_{0T} \end{pmatrix}.$$

Solving this equation for the molecule with $n+1$ units ($3n+3$ bonds) under the symmetrical conditions

$$q_{0C}=q_{nC}, \quad q_{0T}=q_{nT},$$

we get a value of q independent of i:

$$q_C=\tfrac{3}{8}=0.375, \quad q_T=\tfrac{5}{8}=0.625.$$

However, this is a false result.

Now we count the number of configurations in the case of three units ($n=2$) and show it in Table I. (Each numeral must be multiplied by 2 if we count mirror images separately.) The total is 34. The number of configurations with the zeroth unit of C form is 13. The number of those with the middle (first) unit of C form is 9. Therefore,

$$q_{0C}=13/34=0.3824, \quad q_{iC}=9/34=0.2647.$$

Thus, the failure of the method of transition probability is revealed.

We must use the matrix of transition weight W, e.g., for the model above,

$$W=\begin{pmatrix} w_{CC} & w_{CT} \\ w_{TC} & w_{TT} \end{pmatrix}=\begin{pmatrix} 1 & 2 \\ 2 & 3 \end{pmatrix}$$

TABLE I.

Form	Number
TTT	$3\times3=9$
TTC	$3\times2=6$
TCT	$2\times2=4$
TCC	$2\times1=2$
CTT	$2\times3=6$
CTC	$2\times2=4$
CCT	$1\times2=2$
CCC	$1\times1=1$

If $W=kP$, where k is a scalar, we can use P, but this is not the case. The numbers 34, 13, 9 are obtained by

$$(1 \quad 1)\begin{pmatrix} 1 & 2 \\ 2 & 3 \end{pmatrix}\begin{pmatrix} 1 \\ 1 \end{pmatrix}=34, \quad (1 \quad 1)\begin{pmatrix} 1 & 2 \\ 2 & 3 \end{pmatrix}\begin{pmatrix} 1 \\ 0 \end{pmatrix}=13,$$

$$(1 \quad 1)\begin{pmatrix} 1 & 2 \\ 2 & 3 \end{pmatrix}\begin{pmatrix} 1 & 0 \\ 0 & 0 \end{pmatrix}\begin{pmatrix} 1 & 2 \\ 2 & 3 \end{pmatrix}\begin{pmatrix} 1 \\ 1 \end{pmatrix}=9.$$

Generally, for a molecule with n units we have

$$q_{iC}=(1 \quad 1)W^{n-i}\begin{pmatrix} 1 & 0 \\ 0 & 0 \end{pmatrix}W^i\begin{pmatrix} 1 \\ 1 \end{pmatrix}\Big/(1 \quad 1)W^n\begin{pmatrix} 1 \\ 1 \end{pmatrix}.$$

Some values of q_C are shown in Table II. When n is large enough, q_{iC} becomes almost independent of i, unless i is near 0 or n; but

TABLE II.

n	$i=0$	1	2	3	4	5
0	0.5000	...	...	...	...	...
1	0.3750	0.3750	...	...	...	...
2	0.3824	0.2647	0.3824	...	...	...
3	0.3819	0.2708	0.2708	0.3819	...	...
4	0.3820	0.2705	0.2770	0.2705	0.3820	...
5	0.3820	0.2705	0.2767	0.2767	0.2705	0.3820
...	...	...	...	...	...	...
∞	0.3820	0.2705	0.2767	0.2764	0.2764	0.2764

the result of transition probability method does not cease to be false. The correct limiting value is obtained as

$$q_C=(CC \text{ element of } W^n)/\text{trace } W^n$$
$$=(5-5^{\frac{1}{2}})/10=0.2764\cdots.$$

In a similar way some results on paraffine on diamond lattice have been obtained and are already published in Japanese.[2] I hope they will soon be published in a more international language.

[1] E. W. Montroll, J. Chem. Phys. **18**, 734 (1950).
[2] Y. Suzuki and K. Suzuki, Busseiron-Kenkyu **9**, 37 (1947); K. Suzuki, *ibid.* **16**, 39 (1947).

Orbital Perturbation Effects in Beta-Decay*

H. M. SCHWARTZ AND R. R. EDWARDS
Institute of Science and Technology and Departments of Physics and Chemistry, University of Arkansas, Fayetteville, Arkansas
December 19, 1950

A SUBJECT of continuing interest in the field of hot-atom chemistry is that concerned with atomic excitation and ionization resulting from nuclear transformations within the atom.[1] Some progress has already been made in the experimental and theoretical studies of the degree of internal ionization associated with neutron capture and internal conversion processes,[2] but little attention has been given to the corresponding problem in beta-decay. In examining this problem, we have been led to consider one

aspect related to a question in the theory of beta-spectra. Since this question appears to have independent interest, this communication is being submitted before the completion of our investigation.

In the published theoretical studies of beta-decay-induced internal ionization, two possible causes of this ionization have been considered:[3] (1) the sudden perturbation arising from the change in Z; and (2) the direct perturbation of the atomic electrons due to the coulomb field of the departing beta-particle. Of these, the latter is relatively negligible,[4] while the probability of the former is proportional to $1/Z^2$. The sudden perturbation effect is, therefore, of importance for light nuclei, but for such nuclei, it is also necessary to consider the effect of nuclear recoil, especially in the study of excitation which may involve only a few volts. In order to study the problem in question without the complication of nuclear recoil, it is desirable to consider heavy atoms. Since for these the probability of the sudden perturbation effect is also relatively small, it becomes of interest to investigate other possible causes of ionization which, while negligible for low Z, may assume relative importance at high Z.

A possible source of energy for atomic excitation and ionization in heavy atoms is the excess atomic binding energy which is liberated in a negative beta-decay. This energy[5] is of the order of 25 to $50Z^{4/3}$ ev and thus reaches a value of some 10 kev or more at the highest Z values. The disposition of this excess binding energy is a problem which has also been studied very little. Hebb[6] discusses it briefly and concludes that this energy is carried away by the beta-particle. On the other hand, Jean[7] states categorically that this energy is dissipated in electromagnetic radiation. Hebb's arguments are not entirely conclusive, while Jean adduces no proof for his statement.

Our theoretical investigation of this problem is not yet complete, but we wish to call attention to possibilities of experimental investigation. The direct experimental study of ionization and excitation processes accompanying beta-decay is extremely difficult; however, it is now becoming feasible to test the various hypotheses regarding the excess binding energy insofar as these affect the low energy end of the beta-spectrum, by the use of gaseous sources in proportional counter spectrometry. If Hebb's conclusion is correct, for instance, one expects a pronounced deficiency of beta-particles with energy values below that of the excess binding energy. Waltner and Rogers[8] report, on the basis of cloud chamber studies, a sharp cut-off in the RaE beta-spectrum at about 15 kev; however, because of the inherent uncertainties in cloud chamber energy measurements, this result must be accepted with reservations. Investigation of the low energy end of the RaD spectrum is now in progress in our laboratories, using gaseous tetramethyl lead as the source in photographic proportional counter spectrometry.

* This work is supported in part by the AEC.

[1] R. R. Edwards and T. H. Davies, Nucleonics 2, No. 6, 44 (1948).
[2] S. Wexler and T. H. Davies, J. Chem. Phys. 18, 376 (1950); AECD-2374 (1948).
[3] A. Migdal, J. Phys. (USSR) 4, 449 (1941); E. L. Feinberg, *ibid.* 4, 423 (1941).
[4] E. L. Feinberg, J. Phys. (USSR) 4, 423 (1941). The case of low energy beta-particles, however, requires further study.
[5] E. U. Condon and G. H. Shortley, *The Theory of Atomic Spectra* (Cambridge University Press, Cambridge, 1935), p. 339.
[6] M. H. Hebb, Physica 5, 701 (1938).
[7] M. Jean, Rev. optique 180 (1949).
[8] A. Waltner and F. T. Rogers, Jr., Phys. Rev. 75, 1445 (1949).

The Infrared Spectrum of Boron Trichloride

R. E. Scruby,* J. R. Lacher, and J. D. Park
University of Colorado, Boulder, Colorado
January 22, 1951

THE infrared absorption spectra of boron trichloride has been measured in the region from 3 to 15μ. The work confirms and extends that due to Cassie. Assignments have been made for the fifteen fundamental, combination and overtone bands observed.

In connection with the calorimetric work being carried on at the University of Colorado it was found necessary to determine the infrared spectrum of boron trichloride. The spectrum was obtained with a Perkin-Elmer Infrared Spectrometer, Model 12C. Ten-cm gas cells fitted with NaCl windows were used to hold the gaseous sample. The spectrum was obtained in the region from 3 to 15μ using a NaCl prism.

The spectrum of the boron trichloride as received from the Matheson Company indicated the presence of hydrogen chloride, phosgene, and other unidentified impurities. In order to remove these impurities the boron trichloride was distilled in an efficient column packed with glass helices. The distillation removed most of the hydrogen chloride and unidentified impurities; but, owing to the proximity of the boiling points of boron trichloride and phosgene, the phosgene content was reduced only slightly. A comparison of the intensity of the two strong phosgene peaks with the intensity of these peaks in the spectrum of pure phosgene[1] showed that the distilled boron trichloride contained about 1.5 percent phosgene.

TABLE I. Infrared spectrum of boron trichloride.

Peaks observed cm^{-1} Cassie	cm^{-1} μ This work		Intensity	Assignment	Calc cm^{-1}
1995	1948	5.04	m	$2\nu_3^{10}$	1990
1912	1916	5.22	m	$2\nu_3^{11}$	1912
	1672	5.98	w	$\nu_1+\nu_3^{11}+\nu_4^{11}$, $2\nu_3^{11}-\nu_4^{11}$	1670, 1669
	1464	6.83	m	$\nu_1+\nu_3^{10}$	1466
1429	1420	7.04	s	$\nu_1+\nu_3^{11}$, $3\nu_3^{10}$	1427, 1440
	1395	7.17	s	$2\nu_1+\nu_3^{10}$	1402
1387	1376	7.27	s	$3\nu_3^{11}$	1380
	1241	8.06	w	$\nu_3^{10}+\nu_4^{10}$	1239
1206	1203	8.31	m	$\nu_3^{11}+\nu_4^{11}$	1199
996	995	10.06	vs	ν_3^{10}	995
958	955	10.47	vs	ν_3^{11}	956
	735	13.60	m	$3\nu_4^{10}$	732
	728	13.74	m	$3\nu_4^{11}$	729
	722	13.86	m	$\nu_1+\nu_4^{11}$ and $10?$	714, 715
714	715	13.99	m	$\nu_3^{11}-\nu_4^{11}$	713

The only infrared spectrum of boron trichloride which was found in the literature was that reported by Cassie.[2] Table I, column 1, lists the peaks found by Cassie. A peak was also reported at 11.81μ, but this was undoubtedly due to phosgene.

Since the boron trichloride molecule has been shown to be symmetric and planar, it belongs to point group D_{3h}. The symmetry species of the components of the dipole moment of molecules belonging to point group D_{3h} are E' and A_2'', while the species of the components of the polarizability are A_1', E', and E''. There are four fundamental modes of vibration in boron trichloride, two of which are doubly degenerate. Adopting the nomenclature used

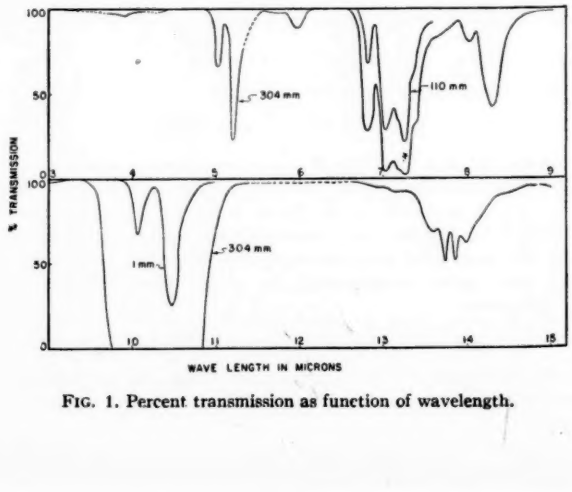

FIG. 1. Percent transmission as function of wavelength.

by Herzberg,[3] ν_1 is the completely symmetric boron-chlorine stretching vibration of symmetry species A_1'. ν_1 is therefore active in the Raman but not in the infrared. This fundamental has been observed by Anderson, Lassettre, and Yost[4] in the Raman spectrum. ν_2, of symmetry species A_2'', may be associated with the boron-chlorine bending vibration. It is inactive in the Raman but

TABLE II. Fundamental modes of vibration of boron trichloride.

Vibration	Symmetry species	Active in	$B^{11}Cl_3$	$B^{10}Cl_3$
ν_1	A_1'	R.	471	471
ν_2	A_2''	I.	460	480*
$\nu_3(2)$	E'	R., I.	956	995
$\nu_4(2)$	E'	R., I.	243	244*

* Calculated from Teller-Redlich product rule. R. Raman. I. Infrared.

should be active in the infrared. Since this vibration does not occur in the region of the infrared investigated, it was not observed. However, the first overtone is Raman active and was observed by Anderson, Lassettre, and Yost; and the second overtone is infrared active and was observed in this work. Both ν_3 and ν_4 are doubly degenerate vibrations of symmetry species E' and are therefore active in both Raman and infrared. Anderson, Lassettre, and Yost have observed ν_3 and ν_4 in the Raman spectrum. ν_3 was observed in the infrared, but ν_4 was not in the range of the infrared investigated. The frequencies of the fundamentals are given in Table II.

The infrared spectrum of boron trichloride is shown in Fig. 1. The two phosgene peaks (5.47 and 11.84μ), the weak doublet due to hydrogen chloride (3.42 and 3.55μ), and the atmospheric carbon dioxide doublet (4.32μ) have been deleted from the spectrum as shown by the dashed lines in these regions.

One of the most interesting features of the spectrum of boron trichloride is the isotopic doubling observed due to the boron 11 and boron 10 isotopes. The boron 11 isotope is about four times as abundant as the boron 10 isotope. The absorption peaks due to boron 11 are thus about four times as intense as those due to boron 10. For example, the peaks at 10.47 and 10.05μ are the fundamentals, ν_3, due to the two isotopes. Isotopic doublets are also observed for the first overtone of ν_3, the second overtone of ν_4, and the combination bands $\nu_2+\nu_4$ and $\nu_1+\nu_3$.

The assignments of Anderson, Lassettre, and Yost based on their Raman data and Cassie's infrared data have been extended to conform with the more detailed infrared spectrum obtained in this work. This assignment is given in Table I, and values have been calculated from the assignment of fundamentals given in Table II.

* Gerard Swope Fellow, General Electric Company. This work has been supported in part by the ONR.

[1] C. R. Bailey and J. B. Hale, Phil. Mag. **25**, 98 (1938).
[2] A. B. D. Cassie, Proc. Roy. Soc. (London) **148**, 87 (1935).
[3] G. Herzberg, *Molecular Spectra and Molecular Structure. II. Infrared and Raman Spectra of Polyatomic Molecules* (D. Van Nostrand Company, New York, 1945).
[4] Anderson, Lassettre, and Yost, J. Chem. Phys. **4**, 703 (1936).

Activation of a Solid Nickel Catalyst for the Hydrogenation of Ethylene by Heat Treatment in a High Vacuum*

R. K. SHERBURNE† AND H. E. FARNSWORTH
Physics Research Laboratory, Brown University,‡ Providence, Rhode Island
December 18, 1950

SOME previous experiments[1-3] indicate that contact catalysis depends on the atomic spacing in the surface. As a preliminary to an investigation of the catalytic activities of individual faces of metal single crystals, we are reporting results on the hydrogenation of ethylene at a small, smooth, nickel surface which has previously received various amounts of outgassing in a range of low pressures.

The main components of the apparatus are a Pyrex glass system for purifying and handling gases, a Pyrex tube reaction chamber of 200-cc volume, and a mass spectrometer of the Nier type[4] for analyzing the gas mixture as the reaction proceeds.[5] Cold traps are inserted in all gas lines leading from the reaction chamber. Since the hydrocarbon molecules are partially decomposed by the ionizing electron beam, corrections to the observed collector currents at masses 27 and 30 are made in order to obtain the relative amounts of ethane and ethylene.[6]

Commercial hydrogen and ethylene are purified separately before they are mixed in a one-to-one volume ratio at equal pressures in a Pyrex glass storage flask. A disk of sheet nickel, 15 mm in diameter and 0.25 mm in thickness, which has been electropolished, is used for the catalyst in the activation tests. The resulting nickel surface is very smooth with no sharp edges or points.

The following steps are included in a single test. (1) The nickel is heated at dull red in the evacuated reaction chamber by induction. (2) The induction coil is replaced by a furnace and the chamber brought to 135°C. (3) A large stopcock between the diffusion pumps and the cold trap is closed, and hydrogen and ethylene are admitted into the reaction chamber. (4) The reaction rate is determined by successive analyses of the gas mixture with the mass spectrometer.

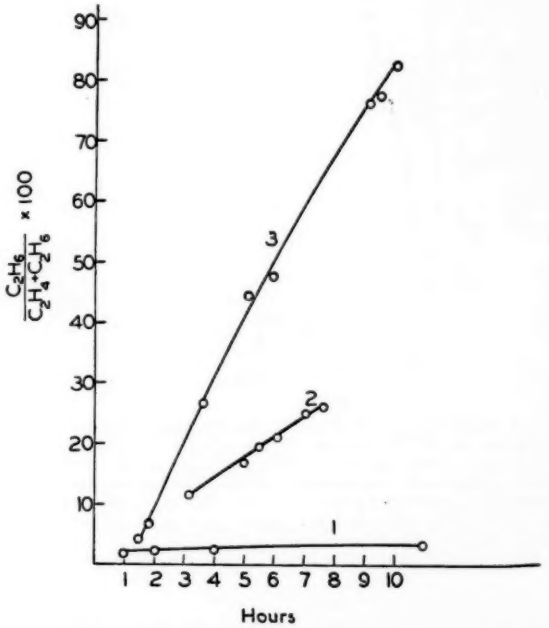

FIG. 1. Percentage of ethane present as a function of reaction time. Minimum pressure in the reaction chamber during outgassing is 10^{-4} mm Hg. Pressure during the activity tests is 16 mm Hg. The slopes of the curves determine the activity. Heat treatments of the nickel specimen at dull red heat, in addition to the preliminary baking at 400°C, which preceded the activity tests, are as follows: curve 1—none; curve 2—20 minutes; curve 3—3.5 hours.

Figure 1 shows the effect of outgassing at the pressure of 10^{-4} mm Hg. Practically no activity is observed after the preliminary baking at 400°C. The largest activity is obtained after 3.5 hours of heating at dull red heat. Further heating produces no additional change. The same behavior is observed at each of two other pressures, 10^{-5} and 2×10^{-7} mm Hg. However, as the vacuum is improved, the limiting activity is increased as shown in Fig. 2. A

total outgassing time of 27.25 hours produces the limiting activity at 2×10^{-7} mm Hg, with a half-time for the reaction of 16 minutes. After the specimen has reached its greatest activity at each of the three pressures, it is possible to reproduce the same activity for later reactions during the same day without intermediate outgassing of the specimen. Hence, one can make comparisons of specimens by outgassing each under similar conditions until their highest activity is obtained. On the other hand, after allowing the specimen to remain overnight at room temperature with the pumping line closed (at pressures of 10^{-5} to 10^{-6} mm Hg), the activity is decreased to approximately one-half its former value by readsorbed gas.

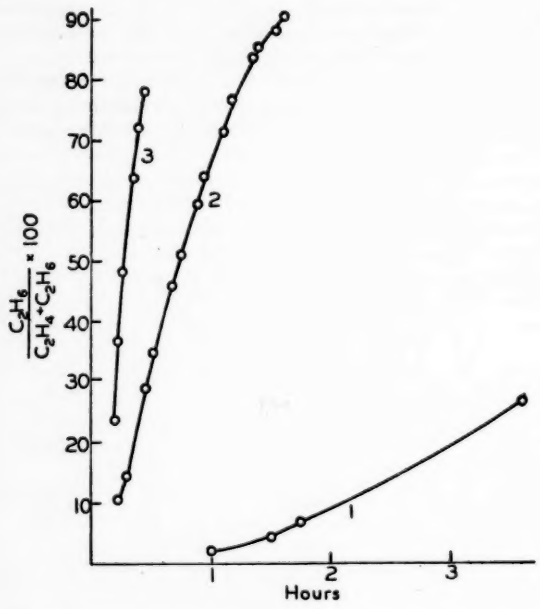

FIG. 2. Percentage of ethane present as a function of reaction time. Pressures during the activity tests are 16 mm Hg for curve 1 and 6 mm Hg for curves 2 and 3. The slopes of the curves determine the activity. The curves show the highest activities obtained by heating the nickel specimen at dull red heat, just preceding the activity tests, with the following residual gas pressures in the reaction chamber: curve 1—10^{-4} mm Hg; curve 2—10^{-5} mm Hg; curve 3—2×10^{-7} mm Hg.

These results indicate that a clean, gas-free nickel surface is necessary for highest catalytic activity per unit area and that this can be obtained only by heating at temperatures considerably above the usual baking temperature. These results may appear in contradiction with the generally held view that sintering reduces the activity of solid catalysts because of the smoothing effect, and consequent decrease in surface area, in the sintering process. However, in the present experiments the surface of the specimen is smooth initially, so that the primary effect of the heat treatment is to produce a more nearly gas-free surface.

* Part of a thesis submitted by R. K. Sherburne in partial fulfillment of the requirements for the Ph.D degree at Brown University.
† Now at New Mexico College of Agriculture and Mechanic Arts, State College, New Mexico.
‡ Assisted by the ONR and Research Corporation of New York.
[1] Beeck, Smith, and Wheeler, Proc. Roy. Soc. (London) **A177**, 62 (1941).
[2] O. Beeck, Revs. Modern Phys. **17**, 61 (1945); **20**, 127 (1948); Rec. Chem. Progress (Kresge-Hooker Sci. Libr.), July–October (1947).
[3] R. Leidheiser, Jr. and A. T. Gwathmey, J. Am. Chem. Soc. **70**, 1200 (1948).
[4] A. O. Nier, Rev. Sci. Instr. **11**, 212 (1940).
[5] S. A. Landeen, Ph.D. thesis, Brown University (1950).
[6] Mass Spectral Data issued by the American Petroleum Institute Research Project 44 at the National Bureau of Standards.

Entropy of Crystalline Benzene Calculated from Molecular Data

ISAO ICHISHIMA AND SAN-ICHIRO MIZUSHIMA
Chemical Laboratory, Faculty of Science, Tokyo University, Bunkyoku, Tokyo, Japan
January 23, 1951

WE have recently reported in this Journal the assignment of the lattice frequencies of crystalline benzene.[1] This enables us to calculate the entropy of crystalline benzene based on molecular data.

The anharmonic intermolecular forces of molecular crystals to which the large values of thermal expansion coefficient and considerable temperature dependence of lattice frequencies are due[2] are also responsible for the characteristic distribution of normal frequencies of these crystals. The exact derivation of this distribution function would be very difficult, but the qualitative feature would easily be seen from the following argument.

From the equation of motion of an anharmonic oscillator,

$$m\ddot{x}+ax-bx^2=0, \quad (a>0, b>0),$$

we can calculate approximately the difference in frequency between the harmonic (ν_0) and the anharmonic (ν) oscillators as

$$\nu^2=\nu_0^2-5b^2C^2/24\pi^2am,$$

where C is the amplitude for $b=0$. We see that the frequency decreases more markedly for normal vibrations with higher frequencies or with shorter wavelengths, since in such vibrations the relative displacements between the neighboring molecules becomes larger and the effect of the anharmonicity will be more pronounced. In consequence, the frequency *vs* wave number curve in the higher frequency region becomes much flatter in the case of anharmonic oscillator than in the case of harmonic oscillator: in other words, the greater part of normal frequencies of molecular crystals tend to converge into a narrow frequency region in which the optically active frequencies lie. Therefore, we may calculate

TABLE I. Molecular and thermal entropies of crystalline benzene.

T (°K)	40	80	120	160	200	240	260
S_{mol}	2.8	8.9	13.9	18.3	22.5	26.5	28.6
S_{ther}	3.5	9.5	14.4	18.6	22.6	26.7	28.8

the approximate values of the entropy of crystalline benzene, using these frequencies instead of those spread in the whole vibrational spectrum. This conclusion is compatible with our model for the vibration of molecular crystals in which we considered the motions of a molecule moving in a potential field formed by surrounding molecules in their equilibrium positions.[2]

Now the assignment of the normal frequencies of single benzene molecule was made by Pitzer and Scott[3] and that of the lattice frequencies was made by us as follows:[1]

$69-0.100T$ cm^{-1} →(translational vibrations)
$89-0.083T$ cm^{-1}, $112-0.127T$ cm^{-1} →(rotational oscillations about the axes in the molecular plane)
$141-0.128T$ cm^{-1} →(rotational oscillation about the hexagonal axis).

Using these frequencies, we have calculated the entropy of crystalline benzene from the usual formula:

$$S=R\sum_n\left[-\ln(1-e^{-h\nu_n/kT})+\frac{h\nu_n/kT}{e^{h\nu_n/kT}-1}\right].$$

As shown in Table I the calculated values of entropy (S_{mol}) are in good agreement with those obtained from thermal data (S_{ther}).[4]

[1] I. Ichishima and S. Mizushima, J. Chem. Phys. **18**, 1686 (1950).
[2] I. Ichishima, Rep. Rad. Chem. Res. Inst. (Tokyo Univ.), **4**, 9 (1949); I. Ichishima and S. Mizushima, J. Chem. Phys. **18**, 1420 (1950).
[3] K. S. Pitzer and D. W. Scott, J. Am. Chem. Soc. **65**, 803 (1943). See also Herzfeld, Ingold, and Poole, J. Chem. Soc. **1946**, 316 (1946).
[4] Calculated from the specific heat data of Oliver, Eaton, and Huffman, J. Am. Chem. Soc. **70**, 1502 (1948).

Near-Ultraviolet Absorption Spectrum of Benzaldehyde Vapor

SUNAO IMANISHI
Chemical Laboratory, Faculty of Science, Kyushu University, Fukuoka, Japan
January 8, 1951

IN view of recent achievements in the analysis and interpretation of substituted benzene spectra, F. Almasy's[1] analysis of the absorption bands of benzaldehyde vapor in the 2970–2480A region appears to need a revision; and we have made a new observation of the spectrum, using the vapor in a 40-cm quartz cell at pressures from 0.3 to 300 mm Hg (Figs. 1(a) and 1(b)). The

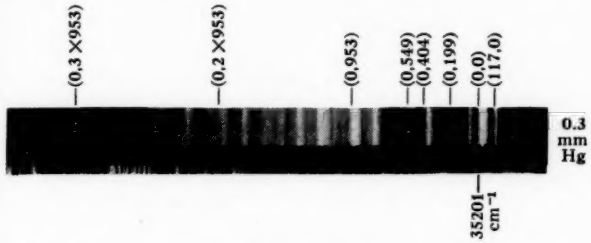

FIG. 1(a). Spectrum of benzaldehyde vapor at 0.3 mm Hg.

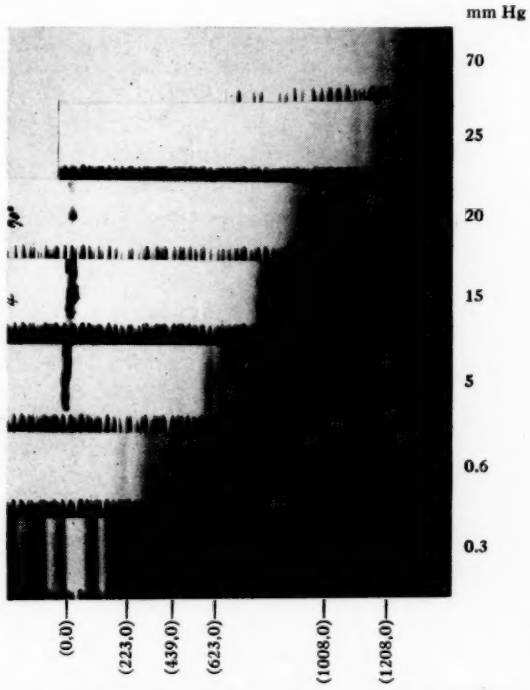

FIG. 1(b). Spectrum of benzaldehyde vapor at various pressures.

quartz prism spectrograph employed had a dispersion of 5.0A (at 2840A)~8.0A (at 2970A) per mm.

On the shorter wave side of the strongest 0,0 (35201 cm^{-1}) band, 51 bands at 0.3-mm vapor pressure were observed; and on the longer wave side, 17 additional bands at various higher pressures.[2] They are all degraded towards the red with more or less sharp single heads. All the observed wave numbers can be expressed quite accurately in terms of the fundamentals listed in the first two columns of Table I, and the 0,0 wave number. The 223″(199′)-cm^{-1} or the 623″(549′)-cm^{-1} frequency is always excited with a single quantum, while the 404′-cm^{-1} and the 953′-cm^{-1} frequencies are excited to any quanta (up to 13 for the 404′ cm^{-1}), making various progressions of bands starting from the 0,0 and the 117,0 (35084 cm^{-1}) bands to appear.

The close resemblance of the vibrational structure of this system to those of toluene and halogen mono-substituted benzenes, involving an "allowed" (substitution) and a "forbidden" (benzene) type vibrational subspectra, suggests that the electronic transition is likewise of the A_1-B_1 type, conforming to the C_{2v} molecular symmetry. The effect of the resonance,

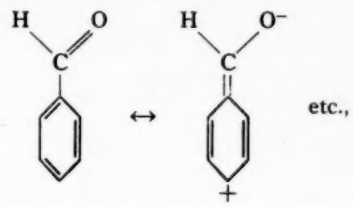

etc.,

is therefore slight as far as the vibrational spectrum is concerned;[3] and the free rotation of the −CHO group around the C−C axis may be assumed approximately. Mr. M. Anno of this laboratory has calculated the six α_1-type C, C normal vibration frequencies, taking the CHO group as a mass point, and has obtained good agreements with those values indicated in Table I.

TABLE I. C_6H_5CHO fundamental vibration frequencies (cm^{-1}).

Vapor, U. V. absorption		Liquid, Raman effect K. W. F. Kohlrausch: "Ramanspektren," 1943		Type
Ground electronic state	Excited electronic state	$\Delta\tilde{\nu}$	ρ	
117		126(3*b*) +140(3*b*)	0.71	Non-totally symmetric
223	199	225(2*b*) +237(2*b*)	*dp*?	α_2 or β_1
324				
439	404	437(5)	0.4	α_1 *
550(117 +439?)				
623	549	614(6*s*)	0.80	β_1 *
656		649(4)	0.54	
737		744(1/2)		
799		828(5)	0.14	α_1
869		852(0)		
913(117 +799?)				
1008	953	1000(14*s*)	0.08	α_1
1115		1160(3*b*) +1166(4*b*)	0.36	
1208		1204(8)	0.25	α_1
1307		1311(00)		
1434		1453(2)	0.33	α_1
		1489(1)	0.49	
		1583(1)		
		1595(12)	0.44	
		1698(10*b*)		α_1
		2735(1)		
		3065(4*b*)	0.87	Non-totally symmetric

* Components arising from splitting of the degenerate 606″-cm^{-1} e_g^+ vibration in C_6H_6 (D_{6h} symmetry).

The writer is much indebted to Professor H. Sponer of Duke University for valuable suggestions and information, for which the writer expresses his hearty thanks.

[1] F. Almasy, J. chim. phys. **30**, 528, 634, 713 (1933).
[2] Wave number table and other details will be published elsewhere shortly.
[3] It causes, however, a large red shift of the 0,0 band (2888 cm^{-1}) relative to the forbidden 0,0 band of C_6H_6 (38089 cm^{-1}).

The Vapor Pressure of Mercury from 40°C to 240°C: (5 microns to 6 cm) Measured by the Streaming Method*

T. M. DAUPHINEE
Physics Department, University of British Columbia, Vancouver, Canada
January 8, 1950

ALTHOUGH accurate knowledge of the vapor pressures of metals has been of considerable interest to both physicist and chemist for some time, very few measurements have been

made in the pressure region 10 to 10^{-3} mm of Hg. Most of the methods of measurement do not apply in this region, high pressure methods failing because of fundamental limits of sensitivity and low pressure methods failing because the gas theory on which they are based is no longer applicable.

The "streaming" or "transpiration" method, in which a known volume of carrier gas (say argon) is saturated with metallic vapor at the temperature of the measurement and the vapor condensed out at some other point in the system, does not suffer from theoretical limitations at low pressures, but the amount of metal carried over at pressures below 1 mm is normally rather small for accurate titration. The writer has, however, found it possible to build an apparatus on the "streaming" principle with which accurate measurements can be made over the relatively wide range of pressures from 10^2 mm to 5×10^{-3} mm. To accomplish this the following procedures were adopted: (1) the flow of carrier gas was considerably increased so that more metal was transported, (2) the surface area over which saturation took place was made very large by using a condenser column filled with beads, (3) the carrier gas was brought to saturation by condensing out an excess of metallic vapor (instead of depending on evaporation), thus insuring a large fresh surface area with low reflection coefficient, (4) the gas was recirculated and purified in a closed system, (5) the temperature was controlled very precisely, (6) provision was made to check the effect of flow, temperature gradients, degree of oversaturation, efficiency of trapping, total pressure, etc., (7) a continuous flow technique was used, equilibrium being reached during a long balance run which preceded the measurement.

In the present experiment the vapor pressure of mercury was measured at 10°C intervals over the pressure range 60 to 5×10^{-3} mm. The results of the experiment are in excellent agreement with high pressure measurements where overlapping of ranges occurs and are consistent with the calculated experimental error of $\Sigma(E_{\text{systematic}})=0.8$ percent and $(\Sigma E_{\text{random}}{}^2)^{\frac{1}{2}}=1$ percent. The results are appreciably higher than previous measurements[1] at the low end of the range but are in complete agreement with the equation for the variation of vapor pressure of mercury with temperature, $\log p=10.3735-(3308/T)-0.8\log T$ (T = Absolute temperature), which was proposed by Ditchburn and Gilmour[2] in 1941. The mean deviation of the present measured values from the Ditchburn and Gilmour equation is less than 0.35 percent. Equations for the vapor pressure of mercury that have been suggested by Kelly[3] and Dushman,[4] and values for temperatures below 140°C (2 mm) given by the *International Critical Tables* (also in the *Handbook of Chemistry and Physics*) differ from these measurements by considerably more than the experimental error. The Ditchburn and Gilmour equation appears to be the only current expression for the vapor pressure of mercury that is suitable for temperatures below 140°C. It is probably correct to better than ±2 percent at 70°C and ±4 percent at the freezing point.

A complete report of the experiment is being prepared for publication.

* This work has been supported by a research grant from the National Research Council of Canada.

[1] K. Neumann and E. Volker, Z. physik. Chem. **161**, 33 (1932).
[2] R. W. Ditchburn and J. C. Gilmour, Revs. Modern Phys. **13**, 310 (1941).
[3] K. K. Kelly, U. S. Bureau of Mines Bulletin 383 (1935).
[4] S. Dushman, *Scientific Foundations of Vacuum Technique* (John Wiley and Sons, Inc., New York, 1949), p. 781.